Final Report

ESTIMATING DRIVEN PILE CAPACITIES DURING CONSTRUCTION

FDOT No.: 99700-3600-119
UF No.: 4910450460312
WPI No.: 0510852
Contract No.: BB-349

Principal Investigator: Michael C. M^{c} Vay
Researchers: Victor Alvarez
Limin Zhang
Ariel Perez
Andrew Gibsen

University of Florida
Civil and Coastal Engineering
PO Box 116580
Gainesville, FL 32611-6580

Submitted to: FDOT

August 2002

TABLE OF CONTENTS

Page

LIST OF FIGURES

LIST OF TABLES

CHAPTER 1

INTRODUCTION

Dynamic testing has been used for estimating pile capacities and hammer suitability since 1888 when the first driving formula, i.e., the Engineering News formula, was published. Up to the early seventies, most if not all-driving formulas adopted into codes were derived from the principles of impulse-momentum conservation. In the late sixties, research focused on predicting both stresses and pile capacities based on wave mechanics. The results were the creation of programs such as WEAP (GRL, 1993), PDA (Pile Dynamics Inc., 1992), and CAPWAP (GRL, 1996). More recently, energy approaches based on both wave mechanics and energy conservation (Paikowsky, 1992) have been developed to determine the pile capacity. However, until recently the accuracy of the older versus the newer methods was unknown, especially for Florida soils conditions.

Recently, the American Association of State Highway and Transportation Officials (AASHTO) and FDOT has changed from the Allowable Stress Design (ASD) to the newer Load Resistance Factor Design (LRFD). The latter method allows the resistance factor, ϕ, to be computed in terms of the probability of failure (i.e., reliability index). In order to determine accurate resistance factors (ϕ), a database to assess mean and standard deviation of measured versus predicted is required. Once the resistance factor, ϕ, and the bias (ratio of measured to predicted) for a given method is known, then its percentage of Davisson capacity available for design may be determined. The latter may be subsequently used to compare all of the current and past prediction methods based on a predetermined risk (i.e., failure probability).

Based on the FDOT (at University of Florida) pile database (242 piles), AASHTO's recommended reliability index, and live to dead load ratios, the resistance factors (LRFD) and

equivalent safety factors (ASD) were developed for many of the current and past dynamic pile prediction methods. The latter included four stress wave and energy approaches (CAPWAP, PDA, Paikowsky Energy, and Sakai Energy) as well as four driving formulas (ENR, modified ENR, FDOT, and Gates). In the case of the older driving formulas, the database was broken into both small (i.e., Davisson capacity less than 1779 kN [200 tons]) and large (Davisson capacity larger than 1779 kN) capacity piles. It was found that on the whole, the newer methods were more accurate and higher percentage of Davisson's capacity is available for design; however, for smaller piles and lower capacities (i.e., capacities less than 1779 kN [200 tons]), a few of the older methods (i.e., Gates) did quite well.

Since 1994, the Florida Department of Transportation (FDOT) construction specification (A455) recommends the use of a Wave Equation approach to assess the suitability of driving systems, as well as estimate pile capacity. In the case of pile capacities, a two step approach is generally employed. First the PDA (Pile Driving Analyzer) collects data (strain and acceleration) and performs a field estimate of pile capacity based on a user supplied Case Damping Coefficient, J_c. The latter is usually selected on the site based on soil type. Subsequently, CAPWAP (Case Pile Wave Analysis Program) is performed in the office on the recovered data to assess distribution of skin and tip resistance, as well as determine an improved capacity prediction (i.e., over PDA). CAPWAP will also estimate a J_c value, which may be used in PDA pile capacity assessment. However, a review of the FDOT database, revealed that over seventy percent of the PDA pile capacity predictions was computed from J_c values estimated from soil type, not CAPWAP. It was also determined that a thirty percent change in J_c resulted in only a ten percent change in estimated pile capacity.

Since the CAPWAP program requires very experienced users and may not result in a unique solution (total capacity, skin and tip resistance), this research focused on estimating J_c, and skin and tip resistance real time (in the field). It was found that the static tip to skin resistance ratio was approximately equal to the measured PDA dynamic value, and that the J_c value was proportional as well. The latter allowed for a field assessment of total pile capacity and corresponding breakdown of skin and tip resistance. The latter was compared with measured (FDOT database) field values, as well as CAPWAP predictions. The proposed method was found as accurate as CAPWAP and allows for immediate assessment of pile capacity and its distribution automatically (no user input required) in the field.

The focus of the research mainly consisted of improving the field instrumentation. A number of different technologies were investigated: laser, optical, and radio. Given the economical constraints, location of the needed information (i.e., pile tip), the radio option (wireless) was pursued. The effort started from initially transmitting an analogue signal from embedded strain gauges and accelerometers cast in the pile. The latter had significant noise interference, resulting in very poor signal recovery. Next, a frequency approach was tried. However, due to limited bandwidth of the transmitters, the approach resulted in a limited the number of channels, which could be broadcasted. Finally, multiple analogue (i.e., multiple gauges) signals were converted to a single digital signal which was transmitted through one transmitter (wireless) which was picked up by a receiver and decoded (recover multiple channels). Also, due to cost constraints (gauges, transmitters, etc. were not reusable, i.e., lost with pile), a new accelerometer was required. Using new technology, a piezoelectric accelerometer was developed for this application with an estimated mass production cost of thirty dollars.

For each of the three generations of instrumentation development, model piles were constructed to test the instrumentation. In the case of the final system, i.e., digital, two full-scale twenty-four inch piles were tested. These piles were production piles in SR-54 (north of Tampa) new bridge over Cypress Creek. One of the piles was instrumented on the top and the other was instrumented on the top and bottom in the casting yard (SCG). During the driving, the new wireless system and PDA system were employed. The wireless analysis of a pile (WAP) employed a standard laptop computer, labview software running a vi (virtual interface--i.e., program), and a receiver/decoder, along with the cast insitu transmitter and gauges. The results (accelerations, strains) at the top of the piles compared very favorably between the PDA and WAP systems. Also, the WAP system gave a real-time assessment of pile capacity (skin, tip and total).

The report is arranged as follows. First, a discussion of LRFD, phi factors, and ASD safety factors along with pile capacity assessment methods is presented. Next, a comparison of the accuracy of pile capacity methods is presented. Then the development of tip, skin and total capacity from PDA dynamic measurements is given. Finally, the new wireless instrumentation package is discussed, along with field trials. The report recommends the further development of the new wireless technology for the installation of pile foundations.

CHAPTER 2

REVIEW OF FLORIDA PILE DRIVING PRACTICES

In this chapter, a review of pile driving practices in the state of Florida will be presented. Because the Florida Department of Transportation (FDOT) uses a large percentage of driven piles compared to the private industry, the information presented herein is based on the former recommendations. Both the current driving practice together with the most relevant changes through the years are presented. This discussion is focussed on such aspects as bearing requirements, and methods to determine pile capacity.

CURRENT FLORIDA PRACTICE

The information presented is in relation to the current Florida practice, which was obtained from the FDOT Standard Specifications for Road and Bridge Construction of 1999. For more details, the reader is referred to the latest FDOT specifications.

Bearing Requirements

As a general criterion the engineer in charge of the driving process may accept a driven pile if it has achieved the minimum penetration, the blow count has a tendency to increase and the minimum bearing capacity is obtained for 2 ft (600 mm) of consecutive driving. The engineer may also accept a driven pile if the minimum penetration was reached and the driving has achieved practical refusal in firm strata. Aspects such as practical refusal and others driving criteria will be discussed in detail in the following sections.

Blow count criteria.

Using the Wave Equation Analysis for Piles (WEAP) the engineer can determine the number of blows per specific penetration to reach a design pile capacity. The blow count has to be averaged for every 12 inches (250 mm) of pile penetration or through the last 10 to 20 blows

of the hammer. It should be noted that the driving equipment must be selected in order to provide the required resistance at a blow count ranging from 36 blows per foot (36 blows for 300 mm) to 120 blows per foot (120 blows per 300 mm).

Practical refusal.

Practical refusal is defined as a blow count of 20 blows per inch (20 blows per 25 mm) for 2 inches (50 mm) of driving. The FDOT specifications recommend that driving cease after driving to practical refusal conditions for 12 inches (300 mm). If the required penetration can not be achieved by driving without exceeding practical refusal, other alternatives should be considered such as jetting or Preformed Pile Holes.

Set-checks and pile redrive.

Set-checks - Set checks are performed in the event that the Contractor has driven the pile up to the point that the pile top elevation is within 300 mm of the cut-off elevation and the pile has not reached the required resistance. Prior to a set check, the driving process is interrupted for 15 minutes. Then, the engineer is provided with a level or other suitable equipment to determine elevation in such a way that the pile penetration during the set-checks could be determine in a very accurate manner. If the initial set-check results are not satisfactory, additional set-checks could be performed. The pile is then accepted if the pile has achieved the minimum required pile bearing.

Pile redrive.

Pile redrive consists of redriving the pile after 72 hours from original driving. The pile redrive is considered when time effect is important in the pile capacity. Other considerations include the pile heave.

Pile heave.

Pile heave is defined as the upward movement of a pile from its originally driven elevation. In occasions, driving a pile can cause excessive heave and/or lateral displacement of the

ground. The previously driven pile should be monitored, and in the event of pile heave (6 mm or more), all piles must be redriven unless the engineer has determined that the heave is not detrimental to the pile capacity.

Piles with insufficient bearing.

In the event that the pile top has reached the cut-off elevation without achieving the required bearing resistance, the FDOT specifications recommends:

1. Splice the pile and continue driving.
2. Extract the pile and drive a pile of greater length.
3. Drive additional piles until reducing the adjusted required bearing per pile to the bearing capacity of the piles already driven.

Methods to Determine Pile Capacity

The FDOT Specifications recommend the use of Wave Equation to determine pile capacity for all structures or projects. The use of static load tests or dynamic load tests, or both, is recommended to verify the capacity estimated from Wave Equation predictions. Nevertheless, the prediction by the Wave Equation (blow count criteria) could be adjusted to match the resistance determined from the static or dynamic load tests, or both.

Wave equation.

The FDOT Specifications recommends to use the WEAP program to predict the pile capacity. This program allows the engineer to evaluate other aspects of the driving process. In the following paragraphs, a description of these aspects will be presented.

Evaluation of driving system. Evaluate the suitability of the driving system (including hammer, follower, capblock and pile cushions. The driving system must be capable of driving the pile to a resistance of 3.0 times the design load, plus the scour and down drag resistance or the ultimate resistance, whichever is higher.

Determine pile driving resistance. The pile driving resistance, in blows per 300 mm or blows per 25 mm are to be determined. The required driving resistance is defined as the design load multiplied by the appropriate factor of safety plus the scour and down drag resistance or the ultimate bearing capacity, whichever is higher.

Evaluate pile driving stresses. The engineer must evaluate the driving system to avoid overstressing the pile at any moment during the driving. If the Wave Equation analyses show that the hammer will overstress the pile, the driving system has to be rejected. The FDOT Specifications 455-5.11.2 presents the allowable stresses for piles made out of concrete, steel and timber. Equation 2-1, 2-2, and 2-3 give the maximum allowable tensile and compression stresses for prestressed concrete piles.

The allowable compressive stress is,

$$s_{apc} = 0.7\ f_c^1 - 0.75\ f_{pc} \tag{2-1}$$

For piles length less than 15 meters the allowable tensile stress is given by

$$s_{apt} = 0.54\left(f_c^1\right)^{0.5} + 1.05 f_{pc} \tag{2-2a}$$

For piles length less than 50 m,

$$s_{apt} = 6.5\left(f_c^1\right)^{0.5} + 1.05\ f_{pc} \tag{2-2b}$$

And for piles length greater than 15 meters

$$s_{apt} = 0.27\left(f_c^1\right)^{0.5} + 1.05 f_{pc} \tag{2-3a}$$

For piles length greater than 50 feet,

$$s_{apt} = 3.25\left(f_c^1\right)^{0.5} + 1.05\ f_{pc} \tag{2-3b}$$

where S_{apc} Maximum Allowable Pile Compressive Stress, MPa/psi

S_{apt} Maximum Allowable Pile Tensile Stress, MPa/psi

f_c' Specified Minimum Compressive Strength of Concrete, MPa/psi

f_{pc} Effective Prestresses at Time of Driving.

For steel piles the maximum allowable compression and tensile stresses are equal to ninety percent (90 %) of the yield strength (0.9 f_y) of the steel.

Dynamic load tests.

Dynamic load testing consists of predicting pile capacity from blows of the hammers during drive and/or redrive of an instrumented pile. Chapter 3 includes more details of how the dynamic load test is performed (see PDA and CAPWAP sections).

Static load tests.

Static load testing consists of applying a static load to the pile to determine its capacity. The FDOT recommends the Modified Quick Test. For more details about the static load test, the reader is referred to the FDOT specification 455-2.2.1. Some general information about this test, and the procedure to obtain the pile capacity are explained in Chapter 3.

EVALUATION OF FLORIDA PRACTICE CHANGES

In the following sections the most relevant changes in the Florida practice (i.e., bearing requirements and proposed methods to determine pile capacity) for the last 10 years approximately will be discussed. For this purpose, the actual practice will serve as a reference for any comparison. To facilitate the comparison process, only the changed criteria will be discussed. The latter does not mean that the aspects not mentioned within this document did not vary (i.e., only the topics related to this report will be investigated). Because the largest change in FDOT specifications in regards to pile foundation were found in the 1994 version versus 1991 version specifications, the discussion will be based on these two references. To simplify the comparison,

the FDOT specifications of 1991 and prior to 1991 will be called “old specifications” and any other specification after 1991 will be called the “new specifications”.

Bearing Requirements

In general, there was a great change in the FDOT specifications of 1994 in comparison to the older FDOT specifications. In the old specifications the piles were allowed to be driven to grade. Even if the practical resistance had not been reached at that point, the engineer was able to drive the pile below grade and build up. After driving 12 inches (0.305 m) below grade, a set-check could be performed after 12 hour of initial driving. The latter criterion differs from the new practice in the elevation at which the set-check is recommended. The new practice recommends the set-check to be performed at approximately 10 inches above the cut-off elevation.

Another important difference is related to the bearing formulas. In the old specifications, the FDOT recommend the use of bearing formulas to determine the pile bearing capacity for piles made out of timber, concrete, composite concrete-steel and steel. Then, from 1994 to date the specifications limited the use of bearing formulas to timber piles driven with power hammers only.

Methods to Determine Pile Capacity

It was noted that in the older specifications no requirement for the use of Wave Equation programs to determine the pile capacity was given. The same observation applies to the use of dynamic testing as a method to determine the pile capacity. Prior to 1994, the FDOT recommended the use of static load test to determine the pile capacity of any pile that did not reach the required resistance at the end of drive or as directed by the engineer. The new specifications recommend the use of Pile Driving Analyzer (PDA), the Wave Equation Analysis for Pile

(WEAP), and the static load test separately or in a combination of each, as recommended by the engineer (the safety factor for design depends upon type of test performed).

Other difference were noted in the criterion for determining pile capacity from the static load test. In the old specifications, the failure criteria is given by either or both conditions shown below:

1. One and one-half times the yield load settlement develops. The yield load is defined as that load beyond which the total additional settlement exceeds 0.03 inch per ton, for the last increment applied.
2. The total permanent settlement of the top of the pile is greater than ¼ of an inch.

The new specifications present two criteria to determine the static pile capacity. Those criteria are:

1. Davisson – for shafts with diameter up to 24″ (600 mm), the load that causes a shaft top deflection equal to the calculated elastic compression, plus 4 mm, plus $^{1}/_{120}$ of the shaft diameter in millimeters.
2. FHWA – for shafts with diameter larger than 24″ (600 mm), the load that causes a shaft top deflection equal to the calculated elastic compression, plus $^{1}/_{30}$ of the shaft diameter.

The changes in criteria for selecting the failure load reflect, first, an increase in the use of larger piles in the construction field, and second, the FDOT recognizes that for larger piles (diameter larger than 24″ (600 mm)) the capacity according to Davisson's criterion is conservative.

As a general observation, the FDOT has abandoned the old methods to determine the bearing capacity of piles (i.e., bearing formulas, based on momentum conservation). At the same

time, the FDOT has adopted other prediction methods such as Wave Equation, PDA, and CAPWAP, which are based on wave propagation through the pile to estimate static pile capacity. Other old methods such as Gates, ENR, and Modified ENR are not considered as alternates in estimating the pile capacity, neither are the relatively new methods such as Paikowsky's method and Sakai et. al. method.

It was proposed by the FDOT to investigate the new FDOT specifications in relation to the older methods based on momentum conservation (i.e., FDOT, Gates, ENR, Modified ENR). Another important consideration was to evaluate the older methods for large capacity piles, which are prevalent today, separately from small capacity piles (i.e., piles with capacity up to 2000 kN approximately). The latter reflects the magnitude of design loads for which piles were designed in the past in comparison to the present practice.

CHAPTER 3

PILE CAPACITY ASSESSMENT USING STATIC AND DYNAMIC METHODS

The Florida Department of Transportation (FDOT) under contract No. BB-349 required UF to evaluate the older empirical methods for determining pile capacity and compare them to the modern instrumented methods. In order to perform the latter, the Davisson's capacity served as the measured capacity for each case. In the following sections, a brief description of the Davisson criterion together with the description of the dynamic methods investigated will be presented.

DAVISSON'S CAPACITY

The Davisson method (Davisson, 1972) is one of many methods developed to determine the pile capacity based on a static load test results. Davisson defined the pile capacity as the load corresponding to the movement which exceeds the elastic compression of the pile by a value of 4-mm (0.15 inches) plus a factor equal to the diameter of the pile in millimeter divided by 120. Figure 3-1 presents the load-displacement curve resulting from a static load test. From this curve, the Davisson's pile capacity can be obtained. The steps to obtain the Davisson's capacity are as follow:

Plot a line with slope representing the elastic deformation of the pile

(Slope m):

$$m = \frac{AE}{L} \tag{3-1}$$

where: A Cross-sectional Area of the Pile

E Elastic Modulus of the Pile Material

L Pile Length

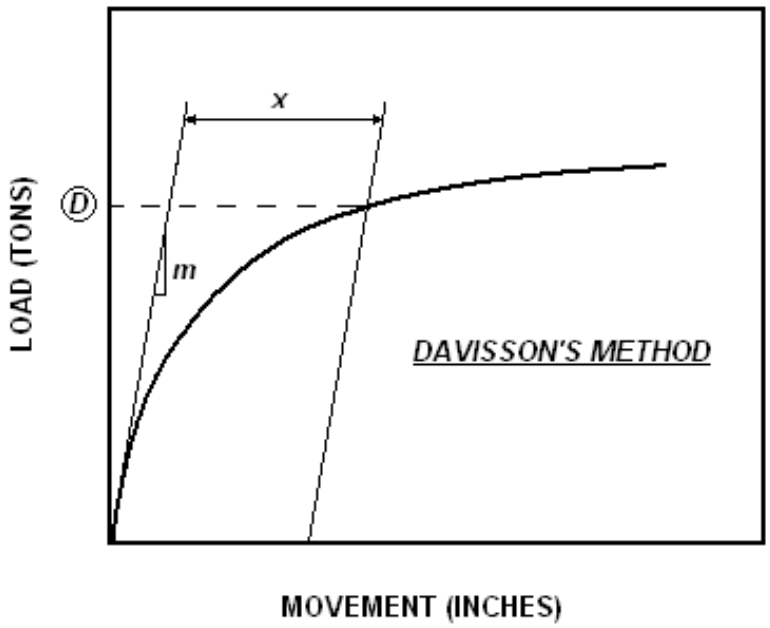

Figure 3-1. Construction of Davisson's Pile Capacity

Draw a line parallel to the elastic deformation line with an intercept, x, on the settlement (movement) axis given as

$$x = 4.0 + \frac{D}{120} \tag{3-2}$$

where: D Diameter of Pile in millimeters

x horizontal displacement of elastic deformation line in millimeters

The Davisson's capacity (point D on Figure 3-1) is defined as the intersection point between the load-settlement curve and the elastic deformation line.

DYNAMIC METHODS REVIEW

Eight methods were considered in this study, which are subdivided in three categories: momentum conservation, combined wave mechanics with energy conservation, and wave mechanics alone. The methods are the Engineering News Record (ENR), Modified ENR,

FDOT, Gates, Paikowsky, Sakai (Japanese), Pile Driving Analyzer (PDA) and the Case Pile Wave Analysis Program (CAPWAP). In the following sections, a brief description of each method is presented.

Momentum Conservation

ENR

One of the older formulas developed to estimate the driven pile capacity was the formula published in the Engineering News Record (ENR) (Coduto after Wellington, 1994). It has since become known as the Engineering News Record formula:

$$P_a = \frac{W_r h}{F(s+0.1)} \tag{3-3}$$

where: P_a Allowable Pile Load

W_r Hammer Ram Weight

h Hammer Stroke (the distance the hammer falls)

F Factor of Safety

s Pile Set (penetration) per Blow in Inches

Wellington (1888) recommended using a Safety Factor of 6.0.

Modified Engineering News Record Formula

In 1961, the Michigan Highway Department (Housel, 1966) performed a series of pile driving tests with the objective of evaluating the accuracy of the ENR formula. After evaluating 88 piles, the investigators found that the ENR formula overpredicted the pile capacities by a factor of 2 to 6. The findings mean that piles designed with a SF of 6 will have a real factor of safety of 1 and 3. Based on their results, the Michigan Highway Department developed the Modified Engineering News Formula:

$$P_a = \frac{0.0025E(W_r + e^2 W_P)}{(s + 0.1)(W_r + W_P)} \quad (3\text{-}4)$$

where: P_a Allowable Pile Load (kips)

E Rated Hammer Energy Per Blow (ft-lb)

W_P Weight of Pile plus Driving Appurtenances (lb)

W_r Weight of Hammer Ram (lb)

s Pile Set (in/blow)

e Coefficient of Restitution

FDOT

The Florida Department of Transportation under specification 455-3.3 (1991) recommends the following bearing formula (FDOT, 1991).

$$R = \frac{2E}{S + 0.1 + 0.01P} \quad (3\text{-}5)$$

where: R Safe Bearing Value in Tons

P Weight of Pile as Driven, in Tons

S Average Penetration per Blow, in Inches

E Energy per Blow of Hammer, in Foot-Tons

The last formula was used for concrete piles, composite concrete-steel piles and steel piles. The bearing capacity obtained using the latter FDOT approach either coincided or exceed the design capacity (suggested FS = 1.0).

Gates method.

The method was the results of a research performed by Marvin Gates, J.M (1957). The basic assumption is that the resistance is directly proportional to the squared root of the net hammer energy. This relationship is presented by:

$$P_u = a\sqrt{e_h E_h}\left(b - \log s\right) \tag{3-6}$$

where: P_u Static Pile Resistance

e_h Hammer Efficiency (0.85 used for all Cases)

E_h Hammer Energy

a, b 27 and 1.0 Respectively (English units)

s Point Permanent Penetration per Blow - Set

A suggested safety factor equal 3.0 is recommended.

Combined Wave Mechanics and Energy Conservation

Sakai et al. Japanese energy method.

Sakai's pile driving formula was developed based on stress-wave theory. According to Sakai, this consideration introduced two advantages, it is theoretically accurate as well as easy to use (Sakai et al., 1996). For a blow by an elastic hammer Sakai recommends

$$R_u = \frac{AE}{L_P}\left(\frac{M_P}{2M_H}\right)\left(D_{\max} - s\right) \tag{3-7}$$

where: A Pile Cross Sectional Area

E Young's Modulus of Pile Material

L_P Length of the Pile

M_P Mass of the Pile

D_{max} Maximum Penetration of Pile per Blow

s Permanent Set

Paikowsky's method.

The Paikowsky method or "Energy Approach" is a simplified energy approach formulation for the prediction of pile resistance based on the dynamic measurements recorded during

driving. The basic assumption of the method is an elasto-plastic load displacement pile-soil reaction. The Paikowsky method uses as input parameters the maximum calculated transferred energy and maximum pile displacement from the measured data together with the field blow count. Equation 3-8 presents the solution for the dynamic pile capacity R_u (Paikowsky, 1994).

$$R_u = \frac{E_m}{Set + \frac{(D_{\max} - Set)}{2}} \tag{3-8}$$

where: R_u Dynamic Pile Capacity

E_m Maximum Energy Entering the Pile

D_{max} Maximum Pile Top Pile Movement

Set Point permanent penetration per blow

The static pile resistance P_u can be obtained by

$$P_u = K_{sp} R_u \tag{3-9}$$

where: K_{sp} 'Static Pile' Correlation Factor Accounting for all Dynamic Energy Looses.

For easy driving of piles with small area ratios, Paikowsky recommends a value of K_{sp} smaller than 1.0, while for hard driving cases with large area ratios, the recommended K_{sp} value must be larger than 1.0. A value of K_{sp} equals 1 was used in our calculations.

Wave Mechanics

PDA method.

In the 1960's a new method to determine the pile capacity was developed at the Case Institute of Technology in Cleveland, Ohio. This new method called Pile Driving Analyzer (PDA) is based on electronic measurements of the stress waves occurring in the pile while driving. Some advantages of dynamic pile testing are (GRL, 1996):

Bearing Capacity – The bearing capacity can be found at the time of testing. For the prediction of a pile's long term bearing capacity, measurements can be taken during restriking (Beginning of Restrike – BOR)

Dynamic Pile Stresses – While the pile is driving the stresses within the pile can be monitored. This avoids any possibility of pile damage due to compression or tension stresses. Bending stresses caused by asymmetry of the hammer impact can be also monitored.

Pile Integrity – To detect any existing damage within the pile.

Hammer Performance – The performance of the hammer is monitored for productivity and construction control purpose.

The PDA is considered as field equipment for measuring the forces and accelerations in a pile during driving. The methodology is standardized and is described in ASTM standard D4945.

The equipment includes three components (Coduto, 1994):

1. A pair of strain transducers mounted near the top of the pile on each side.
2. A pair of accelerometers mounted near the top of the pile.
3. A pile driving analyzer (PDA).

The main purpose of the PDA is to compute the static resistance of the pile using the Case method as it is driven. To perform the latter, the dynamic capacity has to be separated from the static capacity by mean of a damping value J_c, or Case damping value. In the following paragraph a summary of the basic equations used by PDA is presented.

The pile wave speed, c, can be determined prior to pile installation while the pile is still on the ground. The accelerometers are installed and the pile is hit with a hammer. Knowing the pile length and the wave travel time, the wave speed can be calculated using Equation 3-10.

$$c = \frac{2L}{t} \tag{3-10}$$

where: L Length of the Pile

t Time Required for the Pulse to Travel Twice the Pile Length

The dynamic modulus of the pile material, E, is presented in Equation 3-11. The mass density of the pile material is represented by ρ and the wave speed c.

$$E = \rho c^2 \tag{3-11}$$

Equation 3-12 presents the impedance, Z, of a pile as a function of the dynamic modulus, E, the wave speed, c, and the pile cross-sectional area, A.

$$Z = \frac{EA}{c} \tag{3-12}$$

The force within the pile can be obtained from the strain transducers and knowing the elastic modulus of the pile material and cross-sectional area, according to Equation 3-13.

$$P = \varepsilon\ EA \tag{3-13}$$

The velocity is obtained from the integration of the acceleration signal acquired by the accelerometers. It should be noted that the force and velocity used in the PDA calculation is the result from the average of the two strain transducers and the two accelerometers. The velocity is then converted to force units by multiplying by the pile's impedance (Z). The result of the force and velocity are then plotted in a graph versus time for a given blow. Figure 3-2 shows an example of the force and velocity traces for a given hammer blow.

The main equation used by PDA to determine static pile capacity was derived assuming that the pile is linearly elastic with constant cross sectional properties along its length. This equation is based on the force and velocity records at time T_1, time T_2 equal to T_1 plus 2L/c, and the Case damping constant, J_c. Equation 3-14 presents the PDA equation for determining the static pile capacity. The reader is referred to the PDA manual for detailed information and more thorough derivation.

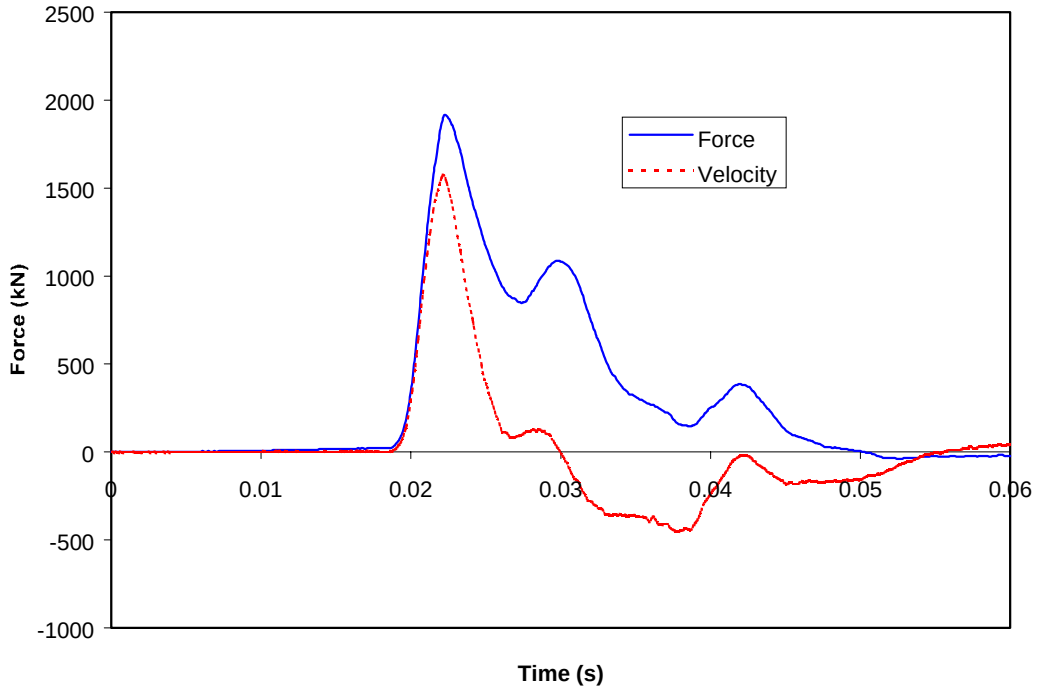

Figure 3-2. Typical Force and Velocity Traces from PDA

$$RSP = (1 - J_c)\frac{[P_1 - ZV_1]}{2} + (1 + J_c)\frac{[P_2 - ZV_2]}{2} \qquad (3\text{-}14)$$

where: RSP Total Static Capacity

J_c Case Damping Constant

P_1,P_2 Force at Time T_1 and T_2 Respectively

V_1,V_2 Velocities at Time T_1 and T_2 Respectively

Z Impedance

CAPWAP program.

The Case Pile Wave Analysis Program (CAPWAP) is a computer program that combines the wave equation's pile and soil model with the Case method of forces and velocities from PDA. The CAPWAP solution includes the static total resistance, skin friction and toe bearing of

the pile, in addition to the soil resistance distribution, damping factors, and soil stiffness. The program calculates acceleration, velocities, displacements, waves up, waves down and forces at all points along the pile.

The procedure used by CAPWAP includes inputting the force trace obtained from PDA and adjust the soils parameters until the velocity trace obtained from PDA can be recreated. It should be noticed that the opposite procedure (i.e., input velocity trace and generate the force trace) can also be performed. When the match obtained is unsatisfactory, it is necessary to modify the soil parameters, until satisfactory match results. Consequently, the process of running CAPWAP is considered an iterative one.

CHAPTER 4

FLORIDA DEPARTMENT OF TRANSPORTATION PILE DATABASE

GENERAL INFORMATION AND HISTORY

The University of Florida in conjunction with the Florida Department of Transportation (FDOT) maintains a database on driven piles inside and outside the state of Florida. The database, originally called PILEUF, began with the collection of driven pile load tests to study pile failure (Davisson, Fuller-Hoy, Debeer, etc.) in mid 1980s. Since then, the database has expanded to H piles, pipe piles and drilled shafts with conventional load tests, Osterberg tests and Statnamic tests. Recently, efforts are under way to collect data on cylinder piles (soil properties and conventional load test data).

Originally, the database was in a Lotus 123 format (spreadsheet) and recently it was transferred to Microsoft's Access (Geotech.mdb) in 1998. For this research, the database information was transferred to a Microsoft Excel format for data analysis. New pile information (driving data) was obtained from the original Geotechnical reports for this research.

For this study, a total of 242 piles were in the database. Out of these, 198 were concrete piles (both square and round), 21 were steel pipe piles, and 9 were H-Piles. Table 4-1 summarizes the number of piles, classification and diameter for the Florida cases while Table 4-2 summarizes the same information for the Non Florida cases.

The total in state piles (Table 4-1) includes 175 piles obtained from 60 sites and represents 218 cases. The difference between the number of piles and cases is due to the multiple attempts to determine the same pile's capacity (i.e., multiple piles on same site). The Non-Florida total from Table 4-2 represents 22 sites. For the latter, the number of cases is equal to the number of piles.

Table 4-1. Classification of Florida Driven Piles

Pile Diameter (inches)	Number of Piles		Sub-Total
	Squared Concrete	Pipe Piles	
10	4	3	7
12	14	2	16
14	26	8	34
18	34	0	34
20	12	0	12
24	44	0	44
30	26	0	26
36	2	0	2
Sub-Total	162	13	175

Table 4-2. Classification of Non-Florida Driven Piles

Pile Diameter (inches)	Number of Piles				Sub-Total
	Squared Concrete	Round Concrete	Pipe Piles	H-Piles	
10	3	0	1	6	10
10.75	2	0	0	0	2
12	15	2	0	1	18
12.75	3	0	0	0	3
14	2	0	3	2	7
16	5	0	0	0	5
18	2	0	0	0	2
24	2	0	0	0	2
59.06	0	0	4	0	4
Sub-Total	34	2	8	9	53

It should be noted that for the Non-Florida information in Table 4-2, the total number of piles does not include 14 piles, which had unspecified diameter.

The following sections describe briefly the information gathered in the database for this study.

PILE INFORMATION

General

Each pile record contains general description of the site location, together with pier or bent number (if available). Four pile types were selected to describe the piles within the data-base based on shape and materials. The four categories were:

1. Square concrete pile
2. Round concrete pile
3. Pipe pile
4. H-pile

The geometry of the piles was described by the pile width, total length, embedded length, and cross sectional area. In addition, the dates when the piles were driven and tested were recorded.

Soil Classification

The soil information includes the soil stratigraphy (description and properties) with in-situ tests such as SPT, CPT, etc. Nine soil types were used to allow consideration of several combinations of cohesive and non-cohesive soil. The nine soil categories were presented according to the following numbering:

1. Plastic clay
2. Silt-sand-clay, silts and marls
3. Clean sand
4. Limestone, very shelly sands
5. Clayey sand
6. Sandy Clay
7. Silty clay
8. Rocks
9. Sandy gravel, tills

The original database combined the side and tip soil number to form a two-digit code, in which the first digit is the side soil type and the second digit is the tip soil type.

Driving Information

The driving information includes the driving system type, hammer and pile weight and manufacturer's rated energy together with the efficiency of the hammer. Additional information includes the dynamic modulus, wave speed and the pile impedance. If the impedance was not available from CAPWAP or other results, it was calculated as EA/c. The average set for EOD (End of Drive) and BOR (Beginning of Restrike) was taken as the inverse of the blow counts as near as possible to the blow used in PDA or CAPWAP analysis. The latter may represent an average of the last foot of driving in some cases, if inch-by-inch information was not available. A record of the depth of penetration and blows per foot (calculated for penetration intervals less than one foot) facilitated the determination of set, knowing the tip depth at the time of the blow.

Dynamic Data (CAPWAP and PDA)

The CAPWAP and PDA results were sometimes available only for EOD or BOR. Furthermore, not all CAPWAP analyses have complete PDA results available or vice versa. Having both results was not a requirement during the construction of the database.

The PDA results include date, RMX (maximum Case Static Resistance calculated during the blow analysis) or other PDA calculated capacity as listed in the source report. The database also presents the PDA Case damping used for calculating the Total Static Resistance.

CAPWAP results include date, tip and friction capacities, total capacity, and Case and Smith damping factors for side and tip, where the Case damping factors were calculated from the Smith damping factors. The latter was performed by dividing the Smith damping value by the impedance and multiplying the result by the side or tip resistance.

Load Test Results

The database contains load test information, measured at the top of the piles. It includes the load in tons and settlements in inches at failure for a given criterion. The failure criteria presented in the database are:

1. Davisson
2. Fuller-Hoy
3. DeBeer
4. FDOT

The database also includes the maximum load in tons from the static load test, in addition to the date at which the load test was performed.

SPT97 Capacity

SPT97 is a pile capacity prediction program based on the original Research Bulletin 121 (RB-121), "Guidelines for use in the Soils Investigation and Design of Foundations for Bridge Structures in the State of Florida". The latter has under a number of changes (1989) and recently with the inclusion of "Design of Steel Pipe and H-piles" by McVay et al in 1994. The method calculates pile capacity based on N values obtained from the Standard Penetration Test. SPT97 is capable of evaluating round and square concrete piles, H-piles, and steel pipe piles (open or close end). It calculates an Estimated Davisson capacity by summing the Ultimate Side Friction and 1/3 of the Ultimate End Bearing (Mobilized End Bearing) capacity of the pile.

SPT97 predictions presented in the database include the Ultimate Side Friction, Ultimate Tip Capacity, Mobilized Tip Capacity, Ultimate Total Capacity, and Davisson's Capacity.

Other related information presented in the database is the input data for SPT97 program. It includes the layering and the soil properties (i.e., unit weight and SPT blow count).

GATHERING NEW INFORMATION

During the course of evaluating the eight dynamic methods (Chapter 3), some extra information was necessary. The latter required that the original Geotechnical reports on many of these sites be found and catalogued. A discussion on the new information follows.

Additional Information

Two parameters that were not found in the original database were the maximum displacement and the maximum energy transfer to the pile. They were essential to obtain the Paikowsky and Sakai capacities (Chapter 3). Both, the maximum energy transfer to the pile and the maximum displacement were obtained from the CAPWAP output printout in the geotechnical reports.

Criteria for New Entries in Database

As a general criterion for this research, new entries should be from within the State of Florida. Also, because the evaluation of the dynamic methods was performed in correlation to the Davisson's capacity, any new entries should have the Load Tests carried to the point for which Davisson's capacity could be determined. Other information needed depends on the method, which is to be evaluated. The more information obtained for a particular record will assure a larger number of dynamic methods which may be evaluated, as well accurate statistical analysis (bias, standard deviation, etc.).

CHAPTER 5

ASD AND LRFD CONCEPTS

Over the years, multiple design procedures have been developed which provide satisfactory margins of safety. Safety in design is obtained when the material properties exceed the demand put on them by any load or loads combination. Another way to describe the same principle is that the resistance of the structure must exceed the effect of the loads, i.e.:

$$\text{Resistance} \geq \text{Effect of Loads} \tag{5-1}$$

When a specific loading condition reaches its limit, failure occurs. Two general states of interest to engineers are Strength and Service Limit. Strength Limit State involves the total or partial collapse of the structure (i.e., bearing capacity failure, sliding, and overall instability). On the other hand, Service Limit State only affects the function of the structure under regular service loading conditions (i.e., excessive settlement and/or lateral deflection, structural deterioration, etc).

ALLOWABLE STRESS DESIGN (ASD) METHOD

In Geotechnical engineering, the ASD has been the primary method used in U.S.A. ASD procedures are different for Service Limit and Strength Limit States. For the Strength Limit State, safety is obtained in the foundation elements by restricting the ultimate loads to values less than the ultimate resistance divided by a factor of safety, (FS):

$$\frac{R_n}{FS} \geq \sum Q_i \tag{5-2}$$

where: R_n Nominal Resistance

ΣQ_i Load Effect (Dead, Live and Environmental Loads)

FS Factor of Safety

For the Service Limit State, the deformations (i.e., settlements) are calculated using the unfactored loads, and the values obtained are compared to the allowable deformation for that structure.

LOAD RESISTANCE FACTOR DESIGN (LRFD) METHOD

The LRFD specifications as approved by AASHTO in 1998 recommend the use of load(s) factors to account for uncertainty in the load(s) and a resistance(s) factor to account for the uncertainty in the material resistance(s). This safety criterion can be written as:

$$\phi R_n = \eta \sum \gamma_i Q_i \tag{5-3}$$

where: ϕ Statistically Based Resistance Factor

R_n Nominal Resistance

0 Load Modifier to Account for Effects of Ductility, Redundancy and Operational Importance

γ_i Statistically Based Load Factor

Q_i Load effect

Even though the LRFD method differs from the accustomed ASD procedure, it has been widely approved by the Geotechnical engineers. Some of the advantages and disadvantages of the LRFD method over the ASD method are as follows (Withiam et al., 1997).

Advantages of LRFD Over ASD

- Account for variability in both resistance and load.
- Achieves relatively uniform levels of safety based on the strength of soil and rock for different limit states, foundation types, and design methods.
- Provide more consistent levels of safety in the superstructure and substructure when the same probabilities of failure are employed.

- Using load and resistance factors provided in the code, no complex probability and statistical analysis is required.

Limitation of LRFD

- Implementation requires a change in design procedures for engineers accustomed to ASD.
- Resistance factors vary with design methods and are not constants.
- The most rigorous method for developing and adjusting resistance factors to meet individual situations requires availability of statistical data and probabilistic design algorithms.

CALIBRATION OF LRFD

Calibration is defined, as the process of assigning values to resistance factors and load factors, required for the LRFD approach. This process can be performed by use of engineering judgement, fitting to other codes (e.g. ASD method), use of reliability theory, or a combination of them. In the following sections these approaches will be discussed.

Engineering Judgement

The calibration of a code using engineering judgement requires experience. Such experience is usually obtained through years of engineering practice. Sometimes, using such an approach results in certain level of conservatism with little validation. Also under varying conditions where no experience exist both excessive conservatism or ever unconservatism may develop.

Fitting ASD to LRFD

Fitting ASD to LRFD is the selection of LRFD resistance factor, ϕ, that will result in equivalent physical dimensions of a substructure or superstructure as given by ASD. It does not

provide a better or more uniform margin of safety. In order to calibrate the ASD method, the first step is to rewrite equations 5-2 and 5-3 as:

$$\frac{R_n}{FS} \geq Q_D + Q_L \tag{5-4}$$

$$\phi R_n \geq \gamma_L Q_L + \gamma_D Q_D \tag{5-5}$$

It should be noted that the loads only include dead and live loads. Environmental loads (i.e., wind, earthquake, etc) were not taken into consideration for the derivation of the ASD fitting equation herein. Solving both equations for R_n gives:

$$R_n \geq FS\left(Q_D + Q_L\right) \tag{5-6}$$

$$R_n \geq \frac{\left(\gamma_L Q_L + \gamma_D Q_D\right)}{\phi} \tag{5-7}$$

Setting Equation 5-6 equal to Equation 5-7 and solving for ϕ results in:

$$\phi = \frac{\gamma_L Q_L + \gamma_D Q_D}{FS\left(Q_L + Q_D\right)} \tag{5-8}$$

Dividing both the numerator and the denominator of Equation 5-8 by Q_L:

$$\phi = \frac{\frac{Q_D}{Q_L}\gamma_D + \gamma_L}{FS\left(\frac{Q_D}{Q_L} + 1\right)} \tag{5-9}$$

Equation 5-9 is the resulting calibration equation for LRFD based on ASD factor of safety, FS, dead load/live load ratio, (Q_D/Q_L), and load factors (γ_D and γ_L). For deep foundation design, the values of γ_D and γ_L recommended by LRFD Highway Bridges Design Specifications (AASHTO, 1994) are 1.25 and 1.75 respectively. The Q_D/Q_L definition and values will be presented in more detail in latter sections. Calibration by fitting is recommended when there is insufficient measured and predicted data to perform a more sophisticated calibration by statistical

analysis. When measured and predicted data is available, reliability theory is strongly recommended.

Reliability Calibration

Statistical data.

In order to perform a reliability calibration for deep foundations (obtain resistance factor, ϕ), such as piles and drilled shafts, the designer must have available statistical data for the method of interest. This statistical data is based on the real or measured capacities and the estimated or nominal capacities of individual piles. First, the bias is defined as:

$$\lambda_{Ri} = \frac{R_m}{R_n} \tag{5-10}$$

where: λ_{Ri} Bias Factor for an individual pile

R_m Measured Resistance for an individual pile

R_n Predicted (nominal) Resistance for an individual pile

After the biases for all cases are determined for the database for a given method, its mean, standard deviation and coefficient of variance are found. Equations 5-11, 5-12 and 5-13 (Withiam et al., 1997) identify the process.

$$\lambda_R = \frac{\sum \lambda_{Ri}}{N} \tag{5-11}$$

$$\sigma_R = \sqrt{\frac{\sum (\lambda_{Ri} - \lambda_R)^2}{N-1}} \tag{5-12}$$

$$COV_R = \frac{\sigma_R}{\lambda_R} \tag{5-13}$$

where: λ_R Average Resistance Bias Factor

N Total Number of Χασεσ in Database

σ_R Resistance Standard Deviation

COV_R Resistance Coefficient of Variance

It should be noted that the measured resistance, R_m (Eq. 5.10) was obtained from the computed Davisson's capacity from the individual field load test. The nominal resistances (R_n) were obtained from the various dynamic equations under study (Chapter 3).

Probability density function.

For the LRFD design, the probability of failure to occur for a given load and resistance distribution is of fundamental importance. The latter is calculated with the "probability density function" which is defined as the probability that X occurs in the interval x to x + d_x as $f_x(x)dx$ (See Figure 5-1). The total area under the curve $f_x(x)$ must be equal to unity because a probability of 1 includes all possible outcomes.

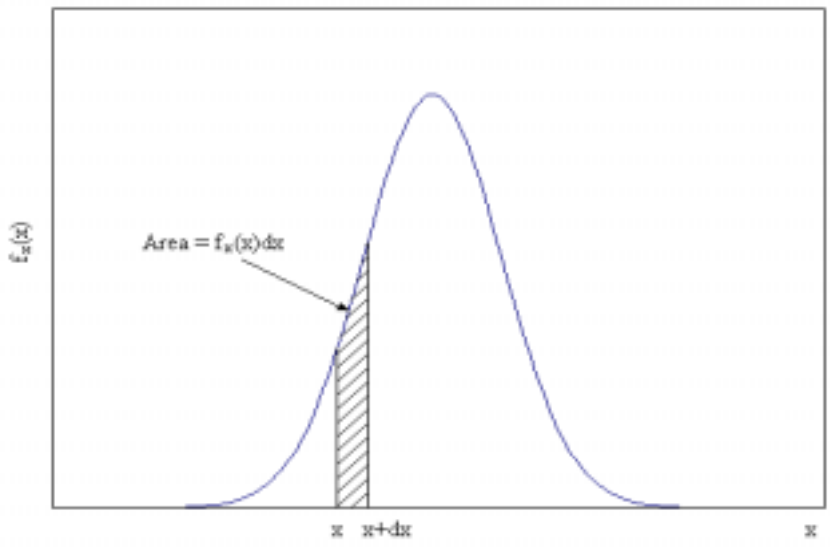

Figure 5-1. Lognormal Probability Density Function

Based on the distribution of the resistance data, a lognormal probability distribution was recommended for the resistance data by the AASHTO Specification. A normal function was used to represent the observed distribution of load data. Equation 5-14 presents the lognormal probability density equation.

$$f_x(x) = \frac{1}{\sqrt{2\pi}\xi x} \exp\left[-\frac{1}{2}\left(\frac{\ln x - \theta}{\xi} \right)^2 \right] \tag{5-14}$$

In Equation 5-14 the values of θ and ζ are the lognormal mean and lognormal standard deviation respectively,

$$\xi^2 = \ln\left(1 + \frac{\sigma_R^2}{\lambda_R^2} \right) \tag{5-15}$$

$$\theta = \ln \lambda_R - \frac{1}{2}\xi^2 \tag{5-16}$$

Where σ_R and λ_R are the standard deviation and the mean of the resistance as defined earlier.

LRFD Approach

Probability of failure.

The LRFD approach defines the probability of failure of a structure based on the load and resistance distribution curves. Figures 5-2 shows the probability density functions for normally distributed load and resistance. The shaded area represents the region of failure where the resistance is smaller than the loads. For the load and resistance curves, the margin of safety can be defined in terms of the probability of survival as:

$$p_s = P(R > Q) \tag{5-17}$$

And the probability of failure, p_f may be represented as

$$p_f = 1 - p_s = P(R < Q) \tag{5-18}$$

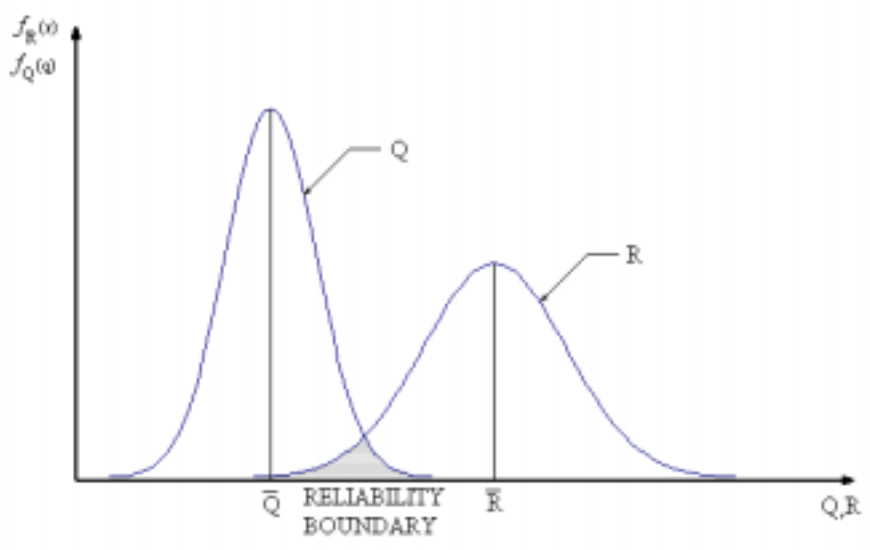

Figure 5-2. Probability Density Functions for Normally Distributed Load and Resistance

Where the right hand of Equation 5-18 represents the probability, P, that R is less than Q.

It should be noted that the probability of failure can not be calculated directly from the shaded area in Figure 5-2. That area represents a mixture of areas from the load and resistance distribution curves that have different ratios of standard deviation to mean values. To evaluate the probability of failure, a single combined probability density curve function of the resistance and load may be developed based on a normal distribution, i.e.,

$$g(R,Q) = R - Q \tag{5-19}$$

If a lognormal distribution is used, the limit state function g(R,Q) can be written as:

$$g(R,Q) = \ln(R) - \ln(Q) = \ln(R/Q) \tag{5-20}$$

For both Equation 5-19 and 5-20, the limit state is reached when R=Q and failure will occurs when g(R,Q)<0.

Reliability index.

The reliability index is a simple method of expressing the probability of failure using function g(R, Q) (Eq. 5-20). The frequency distribution of g(R,Q) looks similar to the curve shown in Figure 5-3.

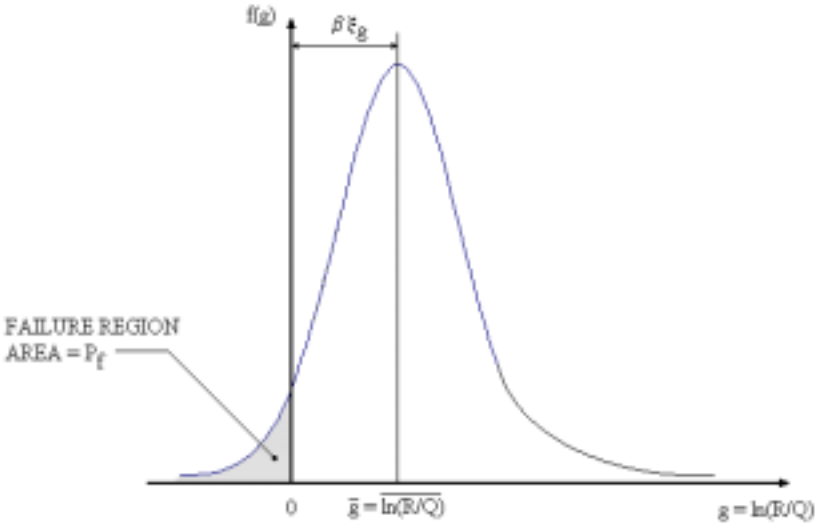

Figure 5-3. Definition of Reliability Index, β for Lognormal Distributions of R and Q

Evident from the curve is that if the standard deviation is small or the mean value is located further to the right, the probability of failure will be smaller. The reliability index β, is defined as the number of standard deviations, ξ_g, between the mean value, g (average), and the origin, or:

$$\beta = \frac{\bar{g}}{\xi_g} \tag{5-21}$$

If the resistance, R, and load, Q, are both lognormally distributed random variables and are statistically independent, it can be shown that the mean values of g(R, Q) is:

$$g = \ln\left[\frac{\bar{R}}{\bar{Q}}\sqrt{\frac{1+COV_Q^2}{1+COV_R^2}}\right] \tag{5-22}$$

and its standard deviation is:

$$\xi_g = \sqrt{\ln\left[\left(1+COV_R^2\right)\left(1+COV_Q^2\right)\right]} \tag{5-23}$$

Substituting Equations 5-22 and 5-23 into Equation 5-21, the relationship for the reliability index, β, can be expressed as:

$$\beta = \frac{\ln\left[\left(\overline{R}/\overline{Q}\right)\sqrt{\left(1+COV_Q^2\right)/\left(1+COV_R^2\right)}\right]}{\sqrt{\ln\left[\left(1+COV_R^2\right)\left(1+COV_Q^2\right)\right]}} \tag{5-24}$$

Equation 5-24 is very convenient because it depends only on statistical data and not on the distribution of the combined function g(R, Q). A very precise definition of probability of failure, p_f, is in terms of reliability index, $F_u(\beta)$ (Withiam et al. 1997).

$$p_f = 1 - F_u(\beta) \tag{5-25}$$

A graphical representation of Equation 5-26 is presented in Figure 5-4. The shaded area in Figure 5-4 represents the probability of failure, p_f, to achieve a target reliability index, β_T.

In the latter equation, $F_u(x)$ is the standard normal cumulative distribution function.

$$F_u(\beta) = 1 - \int_{\beta}^{\infty} \frac{1}{\sqrt{2\pi}} \exp\left(-\frac{1}{2}x^2\right) dx \tag{5-26}$$

Another commonly accepted relationship between the reliability index, β, and the probability of failure, p_f, has been developed by Rosenblueth and Esteva (1972) for values between 2 and 6 as:

$$p_f = 460\exp(-4.3\beta) \tag{5-27}$$

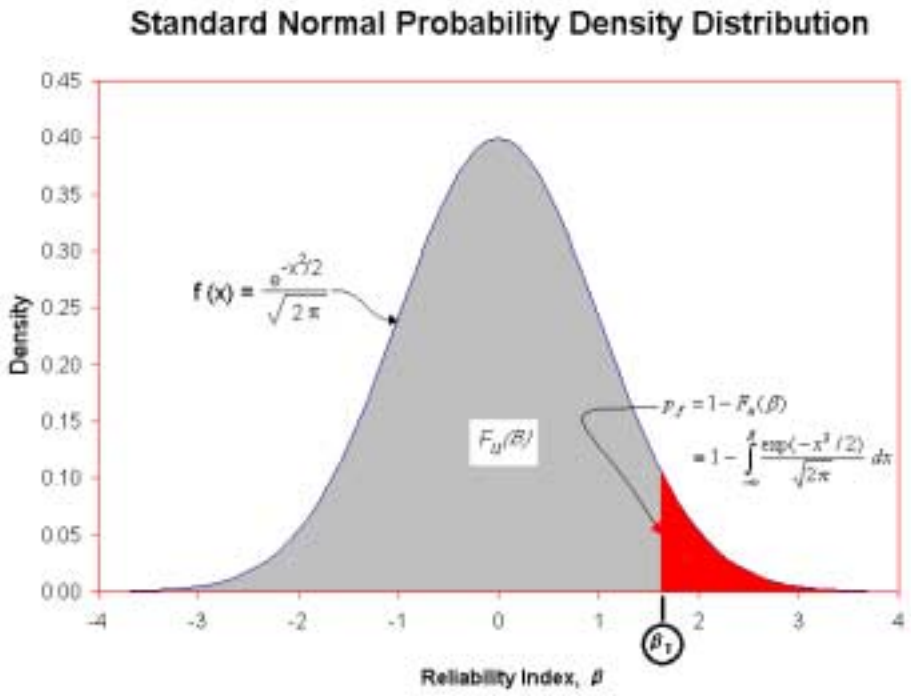

Figure 5-4. Reliability Definition Based on Standard Normal Probability Density Function

Figure 5-5 presents a comparison of the results for both, the Rosenblueth and Esteva method and the Withiam method, to determine the reliability index, β. It can be observed that Rosenblueth and Esteva approximation method will yield good values of probability of failure for values of reliability index between 2.0 and 6.0 as recommended by the authors of the method.

Resistance factor, ϕ.

Once the reliability index, β, is selected then a resistance factor, ϕ, may be calculated. Assuming lognormal distributions of load and resistance in Eq. 5-5 substituted into Eq. 5-24 gives the follow resistance, ϕ, equation:

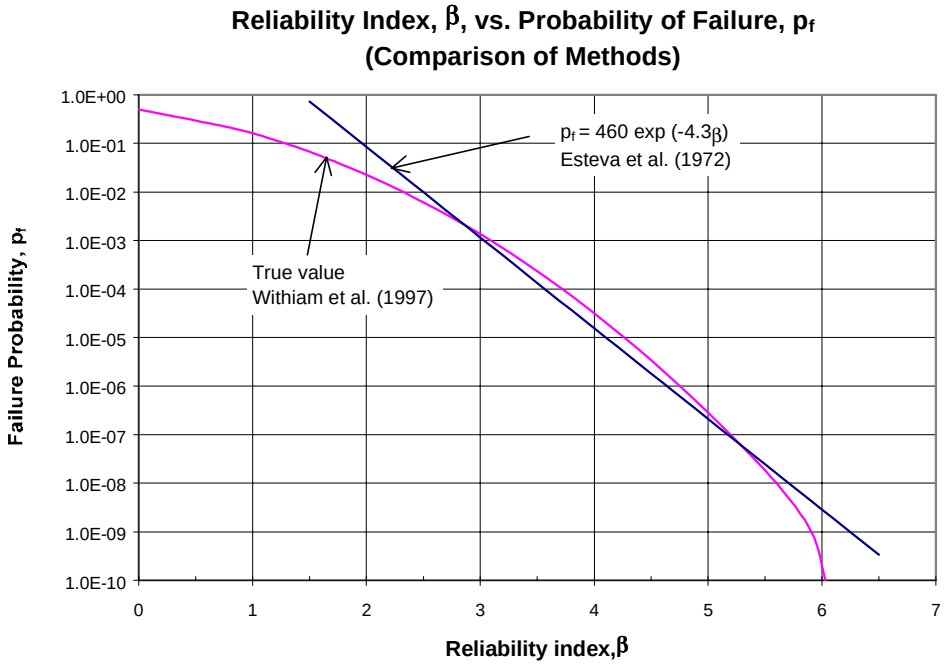

Figure 5-5. Comparison of Esteva and Withiam Methods to Obtain Reliability Index, β

$$\phi = \frac{\lambda_R(\gamma_D \frac{Q_D}{Q_L} + \gamma_L)\sqrt{\frac{1+COV_{QD}^2+COV_{QL}^2}{1+COV_R^2}}}{(\lambda_{QD}\frac{Q_D}{Q_L}+\lambda_{QL})\exp\left(\beta_T\sqrt{\ln[(1+COV_R^2)(1+COV_{QD}^2+COV_{QL}^2)]}\right)} \qquad (5\text{-}28)$$

where: ϕ Resistance Factor

λ_R Resistance Bias Factor

COV_R Resistance Coefficient of Variance

β_T Target Reliability Index

λQD, λ_{QL} Bias (Dead and Live Load)

Q_D/Q_L Dead to Live Load Ratio

The dead to live load ratio (Q_D/Q_L) in Eq. 5-28 varies with the bridge span. For any bridge the live load is obtain by a standard procedure, while the dead load is based upon the size of the structure. The dead to live load ratio has been correlated to the span of the bridges by the following representation (Hansell and Viest, 1971):

$$Q_D / Q_L = (1 + IM)(0.0132L) \tag{5-29}$$

where: Q_D/Q_L Dead to Live Load Ratio

IM Dynamic Load Allowance Factor (equal 0.33)

L Span Length (feet)

Table 5-1 presents typical values of bridges span and the corresponding dead to live load ratios.

Definition ϕ/λ_R and its importance.

The axial design capacity of a pile may be represented as

$$P_{\text{Design}} = \phi R_n \tag{5-30}$$

Table 5-1. Values of QD/QL Based on Bridge Span Length

Span Length, L (m)	Dynamic Load Allowance, IM	Q_D/Q_L
9	0.33	0.52
18	0.33	1.06
27	0.33	1.58
36	0.33	2.12
45	0.33	2.64
60	0.33	3.53

However, from Eq. 5-10, we know the nominal resistance may be expressed in terms of measured value as

$$R_n = \frac{R_m}{\lambda_{Ri}} \tag{5-31}$$

Substituting Equation 5-31 into Equation 5-30 the P_{Design} becomes

$$P_{Design} = \frac{\phi}{\lambda_{Ri}} R_m \tag{5-32}$$

Equation 5-32 gives the design capacity of a shaft for a specific site. If the bias λ_{Ri} is replaced by the bias factor λ_R, (which represents the average of the bias for the method), then the design capacity of the method is directly related to measured resistance (i.e., Davisson's capacity) through the LRFD fitting parameters ϕ, and λ_R. And the ϕ/λ_R ratio represents the percentage of Davisson capacity, which is allowed for design for a given probability of failure. Obviously, the higher the ratio, the fewer the number of piles which will be required and the better the method.

CHAPTER 6

LRFD ASSESSMENT

DATA REDUCTION

The number of cases for each method was determined based on the availability of parameters needed to obtain the estimated capacity for the corresponding method. For all dynamic methods, plots of measured (Davisson Capacity) vs. predicted capacity at End of Drive (EOD) and Beginning of Restrike (BOR) was constructed. Subsequently, the bias, λ, standard deviation, σ, and LRFD phi factors, ϕ were computed. The statistics, as well as some of the LRFD results (tables & graphs) for each method are contained within separate Appendices (i.e., Appendix A for all CAPWAP Procedure results, Appendix B for all PDA results, Appendix C for Paikowsky's Energy Method results, etc.). The specifics for some of the methods will be presented.

Figure 6-1 shows PDA's predicted BOR capacity versus the measured Davisson Capacity. A line with slope equal 45 degrees (prefect correlation) has been drawn to show the comparison between the predicted and measured pile capacity. Also shown in the plot is a regression line (fit between measured and predicted) with the corresponding slope and R^2 (data fit). This latter graph is ideal to visually determine how scattered the predictions are for each method. The second graph (Figure 6-2, PDA at BOR) presents the ratio of measured to predicted capacity on the vertical axis and the measured Davisson capacity on the horizontal axis. On each graph, the number of cases for each dynamic method, the mean (or bias factor, λ_R), and standard deviation, σ_R, and the ratio of measured to predicted capacity is also presented. Appendices A throughout H present the resulting plots for all the methods studied.

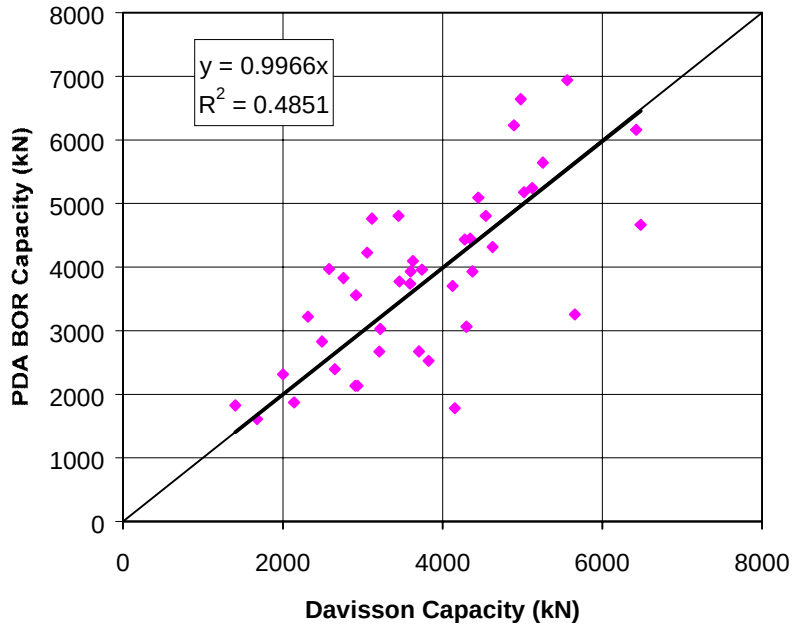

Figure 6-1. Davisson Capacity vs. PDA BOR Capacity

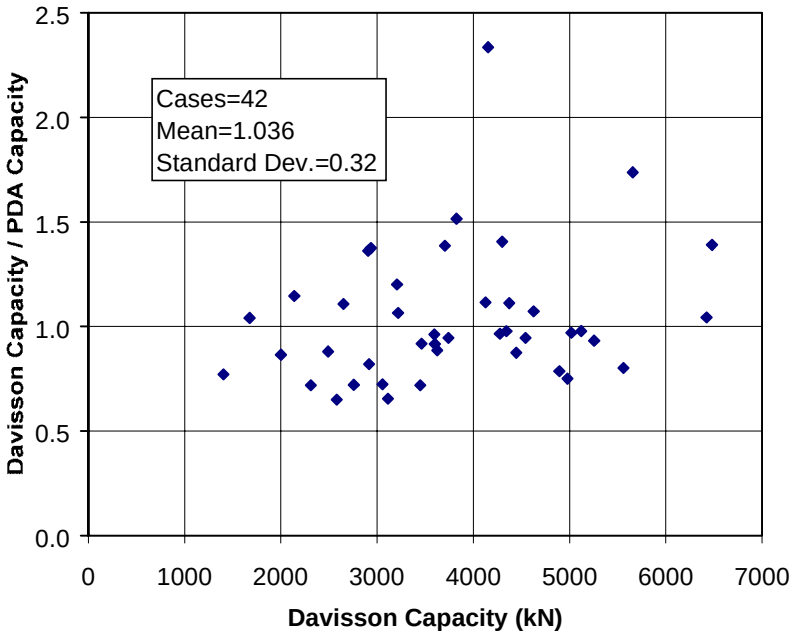

Figure 6-2. Measured Over Predicted Capacity for PDA at BOR

In addition to the mean and standard deviation, a lognormal probability density function was computed for each method. The latter may be used to represent the resistance distribution of a single pile. However, if the ratio of measured to predicted capacity is plotted, the subsequent distribution is a good indicator of a method's accuracy. Using Equations 5-14 to 5-16, the log normal probability density functions of measured to predicted capacities were determined for all of the methods. Figures 6-3 and 6-4 present a summary of the lognormal probability density functions for the eight dynamic methods at EOD and BOR studied, respectively. By inspection it can be observed that dynamic methods such as ENR and Modified ENR have a very small mean and standard deviation in comparison to the rest of the methods. On the other hand, the Energy (Paikowsky) method has an excellent mean (close to one) but a larger standard deviation. Figure 6-4 presents the lognormal probability density function of measured to predicted capacity for the BOR cases. Evident, the Energy (Paikowsky) has a mean close to one for EOD but a values less than one (over predicts) at BOR. Similarly CAPWAP underpredicts capacity at EOD, and does a better job at BOR.

At an early stage of this research, it was noted that the old methods (i.e., Gates, FDOT, ENR, and Modified ENR) gave good estimates of the Davisson capacity for piles with Davisson capacity less than 200 tons (1779 kN). This finding is clearly justified because the range of pile capacity in the past did not exceed 1779 kN for driven piles (limitation of construction equipment). Consequently, it was decided to consider the older methods under three load ranges: 1) piles with Davisson capacity less than 1779 kN; 2) piles with capacity larger than 1779 kN; and 3) no load limitations at all (i.e., combined).

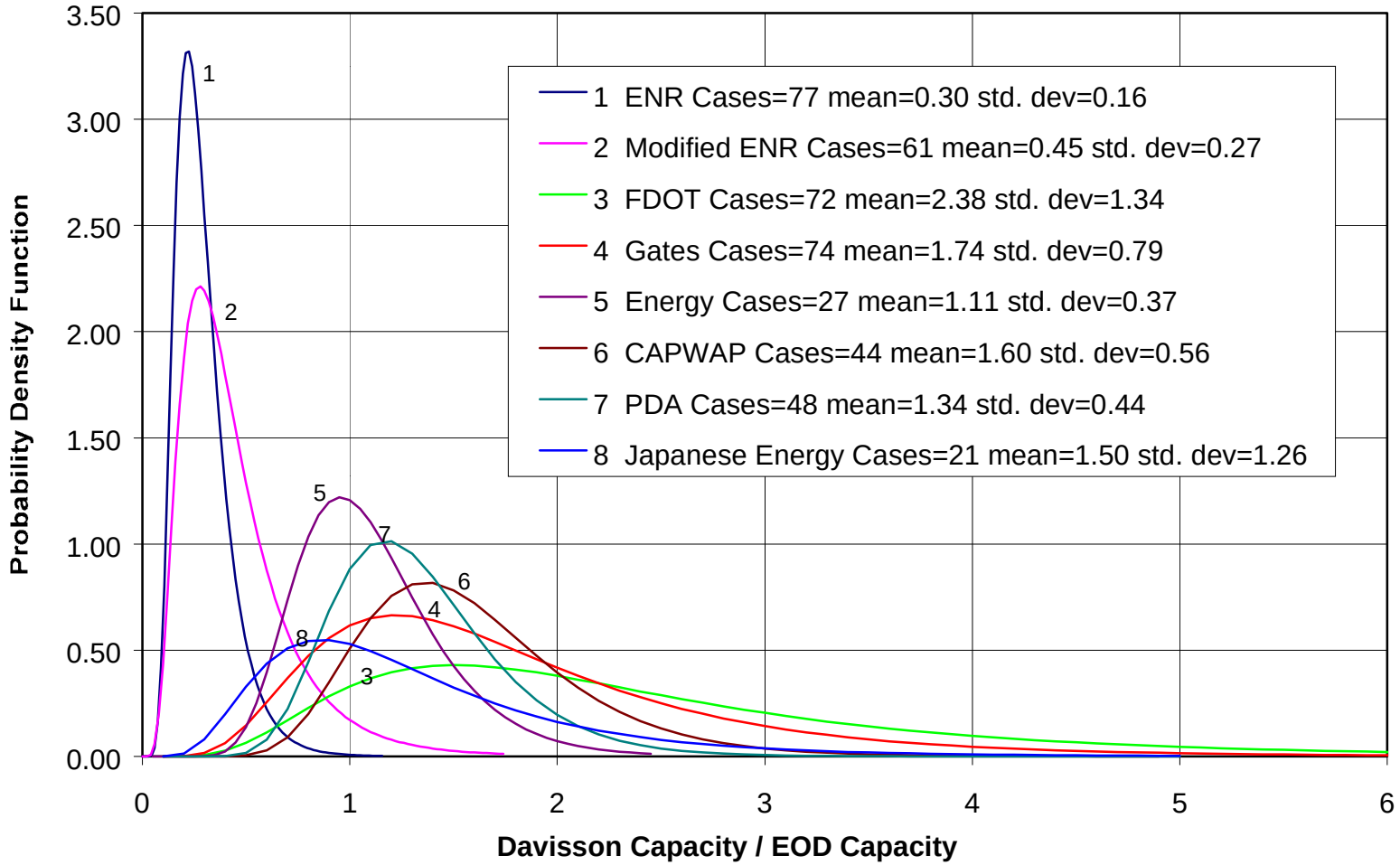

Figure 6-3. Log Normal Probability Distribution at EOD

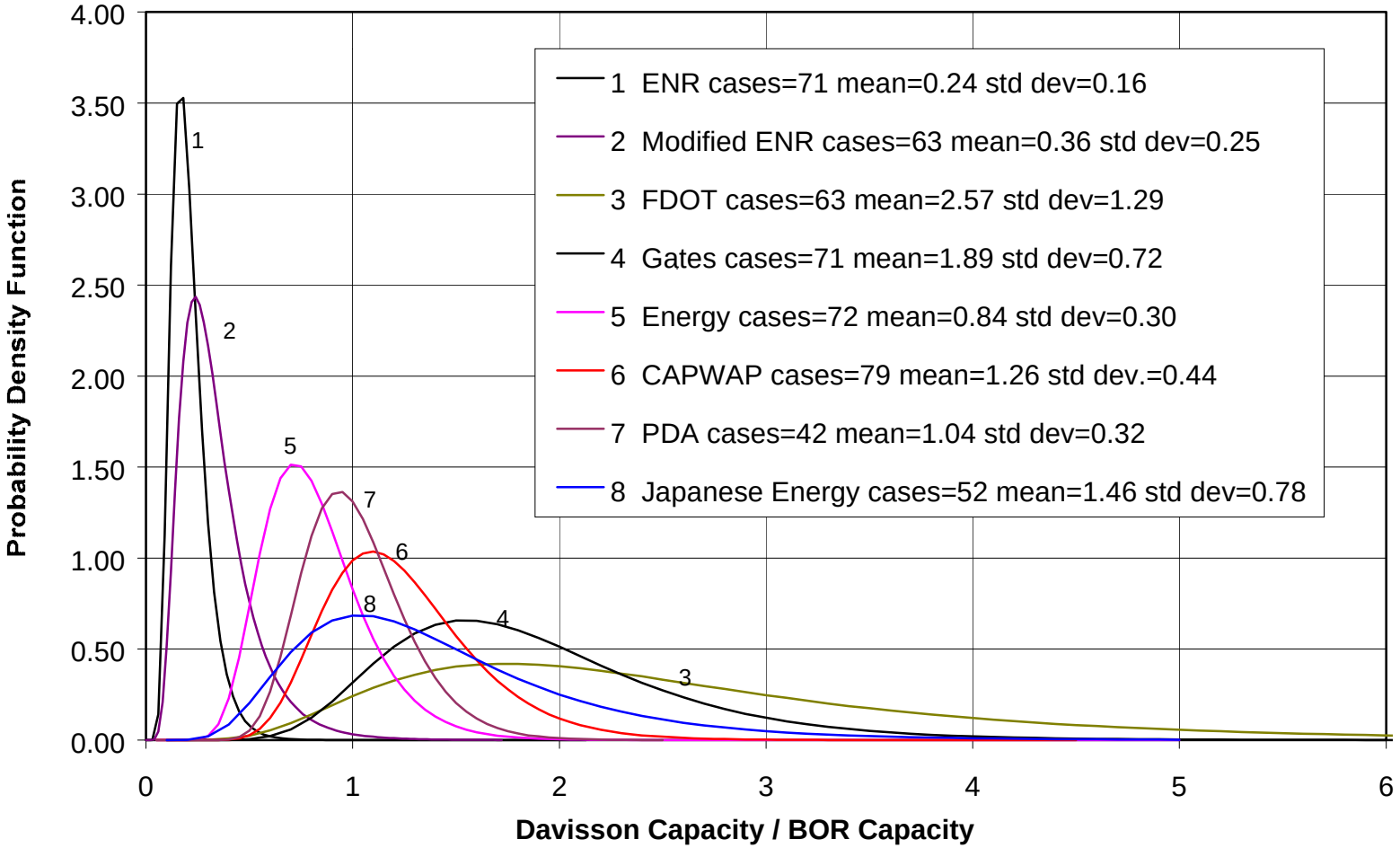

Figure 6-4. Log Normal Probability Distribution at BOR

Based solely on the statistical analysis and the lognormal probability distribution, a comparison of the eight dynamic methods is very difficult. For instance a number of the methods have means close to one, but large standard deviation (Figures 6-1 and 6-2) or vice versa. Consequently, it was decided to evaluate each approach by the percentage of measured Davisson capacity that was available for design given the same reliability (risk) for each method. The LRFD provides the framework to evaluate the latter.

LRFD ANALYSIS OF RESULTS

In order to obtain the LRFD resistance factor, ϕ, two approaches were considered. The first consists of fitting ASD to LRFD, by use of Equation 5-9. For this approach, the ϕ factor depends on the safety factor (ASD) and the ratio of dead load to live load for a given bridge. The second approach used was Reliability Calibration (See Chapter 5) in which the ϕ factor was determined based on the covariance of the measured to predicted (λ, bias), the reliability index, β, and the ratio of dead load to live load.

In order to perform the LRFD analysis, the $\sigma\tau\alpha\tau\iota\sigma\tau\iota\chi\alpha\lambda$ results calculated earlier were employed. For instance, the bias factor (λ_R) and standard deviation (σ_R) of the bias were used to calculate the covariance of the resistance (COV_R). These parameters were subsequently used with AASHTO's load statistics (See Chapter 5) and the failure probabilities also recommended by AASHTO to obtain the resistance factor, ϕ, from Eq. 5-28.

Additional attention was paid to the target reliability index, β_T. For this study, the reliability index was calculated using the Withiam method instead of the Rosenblueth and Esteva method, recommended by AASHTO (See Chapter 5). The values recommended with the Withiam method yield an exact reliability index, while the values obtained using the Rosenblueth

and Esteva result in an approximate quantity. Consequently, the probability of failure, p_f, suggested by AASHTO had to be back calculated from the reliability indexes.

Tables 6-1 through Table 6-6 show typical output results for each LRFD analysis performed. Tables 6-1 to 6-3 present the results for PDA at EOD, while Tables 6-4 to 6-6 present the commensurate for PDA at BOR.

Tables 6-1 and 6-4 summarize the resistance factors, ϕ, evaluated for four different failure probabilities (i.e., reliability indexes) and eight bridge span lengths based on LRFD calibration of the method. Tables 6-2 and 6-5 show the equivalent ASD safety factors based on the resistance factors calculated using the LRFD calibration method for the same bridge span lengths and failure probabilities. Finally, Tables 6-3 and 6-6 present the resistance factor, reliability index and probability of failure that correspond to the actual safety factor that have been used in current ASD procedures. Appendices A throughout H present in detail the LRFD analysis results for each dynamic method studied.

Effect of Bridge Span Length and Probability of Failure

The bridge span length evaluated in this study range from 9.0 to 60.0 meters, each length corresponding to a recommended (AASHTO) dead to live load ratio. After observing the results for the PDA, EOD and/or BOR it is evident that the bridge span length has negligible effect on the resistance factor, ϕ, or the corresponding safety factor. At a target reliability index of 2.5 for both EOD and BOR, the ϕ factor decreases only 6.8% and the safety factor decreases only 1.6% when the span length increased from 15.0 meters to 50.0 meters. The latter phenomenon was observed throughout all the methods evaluated. Thus, for practical purposes the rest of LRFD analysis results are summarized for a 27 meters bridge span length.

Table 6-1. ϕ Values Evaluated for PDA (EOD)

Span length (m)	Q_D/Q_L	Failure Probability p_f/Reliability Index β_T			
		2.50 E-02	6.22 E-03	1.22 E-03	1.79 E-04
		1.96	2.50	3.03	3.57
9	0.52	0.856	0.694	0.565	0.458
15	1.00	0.821	0.666	0.542	0.439
18	1.06	0.818	0.663	0.540	0.437
27	1.58	0.796	0.645	0.525	0.426
36	2.12	0.781	0.633	0.515	0.418
45	2.64	0.770	0.625	0.508	0.412
50	3.00	0.765	0.620	0.505	0.409
60	3.53	0.758	0.615	0.500	0.405

Table 6-2. ASD Design Safety Factor Values Evaluated for PDA (EOD)

Span length (m)	Q_D/Q_L	Failure Probability p_f/Reliability Index β_T			
		2.50 E-02	6.22 E-03	1.22 E-03	1.79 E-04
		1.96	2.50	3.03	3.57
9	0.52	1.845	2.276	2.796	3.449
15	1.00	1.827	2.253	2.769	3.415
18	1.06	1.825	2.251	2.766	3.412
27	1.58	1.814	2.237	2.749	3.391
36	2.12	1.806	2.228	2.738	3.377
45	2.64	1.801	2.221	2.730	3.367
50	3.00	1.798	2.218	2.725	3.362
60	3.53	1.795	2.214	2.720	3.356

Table 6-3. ϕ Factors for Safety Factor = 2.50 – PDA (EOD)

Span length (m)	Q_D/Q_L	ϕ	β_T	p_f
9	0.52	0.632	2.742	0.0035
15	1.00	0.600	2.767	0.0031
18	1.06	0.597	2.770	0.0031
27	1.58	0.578	2.786	0.0029
36	2.12	0.564	2.797	0.0028
45	2.64	0.555	2.804	0.0027
50	3.00	0.550	2.808	0.0026
60	3.53	0.544	2.813	0.0026

Table 6-4. ϕ Values Evaluated for PDA (BOR)

Span length (m)	Q_D/Q_L	Failure Probability p_f /Reliability Index β_T			
		2.50 E-02	6.22 E-03	1.22 E-03	1.79 E-04
		1.96	2.50	3.03	3.57
9	0.52	0.682	0.557	0.457	0.373
15	1.00	0.654	0.534	0.438	0.358
18	1.06	0.652	0.532	0.436	0.356
27	1.58	0.634	0.518	0.425	0.347
36	2.12	0.622	0.508	0.417	0.340
45	2.64	0.614	0.501	0.411	0.336
50	3.00	0.609	0.498	0.408	0.333
60	3.53	0.604	0.493	0.404	0.330

Table 6-5. ASD Design Safety Factor Values Evaluated for PDA (BOR)

Span length (m)	Q_D/Q_L	Failure Probability p_f /Reliability Index β_T			
		2.50 E-02	6.22 E-03	1.22 E-03	1.79 E-04
		1.96	2.50	3.03	3.57
9	0.52	2.316	2.835	3.458	4.234
15	1.00	2.293	2.807	3.424	4.192
18	1.06	2.291	2.805	3.421	4.188
27	1.58	2.277	2.787	3.400	4.163
36	2.12	2.267	2.776	3.386	4.145
45	2.64	2.260	2.768	3.376	4.133
50	3.00	2.257	2.763	3.370	4.127
60	3.53	2.253	2.758	3.364	4.119

Table 6-6. ϕ Factors for Safety Factor = 2.50 – PDA (BOR)

Span length (m)	Q_D/Q_L	ϕ	β_T	p_f
9	0.52	0.632	2.164	0.0418
15	1.00	0.600	2.191	0.0373
18	1.06	0.597	2.193	0.0369
27	1.58	0.578	2.210	0.0344
36	2.12	0.564	2.221	0.0328
45	2.64	0.555	2.229	0.0317
50	3.00	0.550	2.233	0.0311
60	3.53	0.544	2.238	0.0304

In terms of the probability of failure, p_f, a decrease in the probability of failure is directly related to an increase in reliability index, β, and a diminishment in the resistance factor, ϕ. This effect could be easily understood, because lowering the probability of failure for a given structure should be accompanied by a reduction of the resistance factor, which means, penalizing the structure resistance and producing a more conservative design. Different to the effect of the bridge span length, the reliability index has a big influence in the resistance factor ϕ, and the equivalent safety factor. The relation of ϕ factor and reliability index, β, is inversely proportional and linear. For piles AASHTO recommends a reliability index, β, of 2.0 to 2.5.

Level of Conservatism and Accuracy Indicators

A similar analyses as the PDA (Tables 6-1 to 6-6) was performed for each of the eight dynamic methods, as well as the older methods which were separated into capacities less than 1779 kN and greater than 1779 kN. A summary of these results is presented in Tables 6-7 and 6-8 for EOD and BOR respectively.

The results show that the higher the bias factor λ_R, for a given method the higher the resulting resistance factor. For example, for CAPWAP at BOR the mean is equal to 1.260 and ϕ is equal to 0.58 (for $\beta = 2.50$) while FDOT method shows a mean and resistance factor of 2.574 and 0.97 respectively for the same reliability index. This effect may be explained by the bias factors for each method. As defined previously, the bias factor is the ratio of measured to predicted capacity. The larger the bias factor, the more conservative the method. Consequently, LRFD will raise the resistance factor to generate the same probability of failure as another method with a much lower bias.

Although the resistance factor is a good qualitative measure of the degree of conservatism or unconservatism, it does not indicate the accuracy of the method. The combination of

Table 6-7. Load and Resistance Factor Design (LRFD) of Driven Piles Using Dynamic Methods at EOD

Prediction Method	Number Of cases	Mean, λ_R (Dav/Pred)	Standard Deviation	COV_R	P_f=0.62% (β_T=2.50)			P_f=2.50% (β_T=1.96)		
					ϕ	FS	ϕ/λ_R	ϕ	FS	ϕ/λ_R
CAPWAP	44	1.597	0.559	0.350	0.733	1.970	0.459	0.912	1.584	0.571
PDA	48	1.344	0.443	0.329	0.645	2.237	0.480	0.796	1.814	0.592
Paikowsky Energy	27	1.110	0.372	0.335	0.527	2.740	0.475	0.651	2.216	0.587
Sakai et al Energy	21	1.504	1.256	0.835	0.231	6.254	0.153	0.348	4.150	0.231
FDOT (overall)	72	2.381	1.341	0.563	0.669	2.160	0.281	0.909	1.588	0.382
FDOT (<1779 kN)	34	1.490	0.782	0.525	0.457	3.161	0.307	0.611	2.362	0.410
FDOT (>1779 kN)	38	3.158	1.248	0.395	1.307	1.104	0.414	1.658	0.871	0.525
ENR (overall)	77	0.299	0.159	0.532	0.090	16.024	0.301	0.121	11.935	0.405
ENR (<1779 kN)	34	0.250	0.129	0.515	0.078	18.395	0.314	0.105	13.801	0.419
ENR (>1779 kN)	43	0.338	0.171	0.507	0.108	13.388	0.319	0.143	10.074	0.424
Modified ENR (overall)	61	0.446	0.267	0.599	0.115	12.533	0.258	0.159	9.086	0.357
Modified ENR (<1779 kN)	25	0.325	0.222	0.683	0.069	20.818	0.214	0.099	14.604	0.305
Modified ENR (>1779 kN)	36	0.530	0.321	0.606	0.135	10.720	0.254	0.186	7.749	0.352
Gates (overall)	74	1.742	0.787	0.452	0.633	2.280	0.363	0.822	1.756	0.472
Gates (<1779 kN)	32	1.071	0.351	0.328	0.515	2.802	0.481	0.635	2.272	0.593
Gates (>1779 kN)	42	2.254	0.717	0.318	1.109	1.302	0.492	1.361	1.061	0.604

Table 6-8. Load Resistance Factor Design (LRFD) of Driven Piles Using Dynamic Methods at BOR

Prediction Method	Number Of cases	Mean, λ_R (Dav/Pred)	Standard Deviation	COV_R	P_f=0.62% (β_T=2.50)			P_f=2.50% (β_T=1.96)		
					ϕ	FS	ϕ/λ_R	ϕ	FS	ϕ/λ_R
CAPWAP	79	1.260	0.438	0.347	0.581	2.485	0.461	0.722	1.999	0.573
PDA	42	1.036	0.322	0.311	0.518	2.787	0.500	0.634	2.277	0.612
Paikowsky Energy	72	0.836	0.301	0.360	0.374	3.857	0.448	0.468	3.086	0.560
Sakai et al Energy	52	1.457	0.784	0.538	0.433	3.334	0.297	0.583	2.477	0.400
FDOT (overall)	63	2.574	1.293	0.502	0.832	1.735	0.323	1.103	1.309	0.429
FDOT (<1779 kN)	8	1.355	0.380	0.280	0.724	1.995	0.534	0.875	1.650	0.646
FDOT (>1779 kN)	55	2.751	1.284	0.467	0.966	1.495	0.351	1.262	1.144	0.459
ENR (overall)	71	0.235	0.160	0.681	0.050	28.597	0.215	0.072	20.080	0.306
ENR (<1779 kN)	9	0.186	0.057	0.306	0.094	15.348	0.505	0.115	12.562	0.617
ENR (>1779 kN)	62	0.242	0.169	0.698	0.050	28.841	0.207	0.072	20.120	0.296
Modified ENR (overall)	63	0.363	0.246	0.676	0.079	18.314	0.217	0.112	12.881	0.308
Modified ENR (<1779 kN)	8	0.277	0.062	0.224	0.166	8.704	0.598	0.196	7.356	0.708
Modified ENR (>1779 kN)	55	0.376	0.260	0.692	0.079	18.321	0.210	0.113	12.810	0.300
Gates (overall)	71	1.886	0.715	0.379	0.810	1.783	0.429	1.020	1.416	0.541
Gates (<1779 kN)	9	1.067	0.201	0.189	0.681	2.121	0.638	0.796	1.815	0.746
Gates (>1779 kN)	62	2.005	0.684	0.341	0.938	1.540	0.468	1.162	1.242	0.580

both, mean and standard deviation through the COV_R (i.e., ratio of standard deviation to the mean or bias) is a better indicator of the accuracy of a method. Under the latter criterion, PDA, Paikowsky, and CAPWAP are better, while ENR and modified ENR are not as accurate.

A simpler and more direct comparison of all the methods is through Eq. 5-32, i.e., ϕ/λ_R, which follows.

ϕ/λ_R Ratio

The efficiency or performance of every dynamic method can be evaluated by its ϕ/λ_R ratio (Eq. 5-22). The latter indicates the percentage of the measured Davisson capacity that can be utilized for design for pre-defined structure reliability. It should be noted that the average bias factor, $\lambda_{R,}$ is an average of all the pile biases, therefore, the ϕ/λ_R ratio is an "average" percentage of the measured Davisson capacity. The latter consideration makes the ϕ/λ_R ratio remarkably valuable from an economic point of view. The higher the ϕ/λ_R ratio, the more cost effective the method (shorter piles or fewer required).

Comparison of ϕ/λ_R for Each Method

Table 6-7 (LRFD Results for Dynamic Methods at EOD) presents the ϕ/λ_R ratio for all the methods at end of drive (EOD) at the reliability index, $\beta = 2.50$. Evident, is that all the newer methods: CAPWAP (ϕ/λ_R=0.459), PDA (ϕ/λ_R=0.480), and Paikowsky (ϕ/λ_R=0.475) give the highest ϕ/λ_R ratio, resulting in more economical design. The lower ϕ/λ_R values are given by the older driving formulas: FDOT (ϕ/λ_R=0.281), ENR (ϕ/λ_R=0.301), Modified ENR (ϕ/λ_R=0.258), and Sakai et al. (ϕ/λ_R=0.153) methods. The same trend was observed for a reliability index of 1.96.

In the case of Beginning of Restrike (BOR), the newer methods again resulted in higher ϕ/λ_R ratios (Table 6-8) as compared to the older methods. However, there was one exception,

the Gates method, which had an ϕ/λ_R ratio of 0.541 at a reliability index of 1.96. The latter compares favorably with the newer driving methods.

EOD versus BOR

From Tables 6-7 (EOD) and 6-8 (BOR), the bias (λ_R: ratio of measured to predicted), is clearly higher for EOD than BOR. The latter suggest that the predicted pile capacities are increasing from EOD to BOR on a whole for the database (i.e., independent of soil type). This effect may be attributed to pile freeze (increase in skin friction due to dissipation of pore water pressure, or increase in lateral total stress, or even soil strength). However, LRFD phi factors are influenced by both the bias, λ_R , and coefficient of variation, COV_R. In the case of the latter, the standard deviation, σ, is diminishing from EOD to BOR. However, the combined effect, COV_R (ratio of σ/λ) which controls accuracy is changed little. Consequently, since the COV_R is changing little, but the bias, λ_R, is diminishing (i.e., predicted capacity agree more closely to measured), the LRFD phi, ϕ, is diminishing. For instance, PDA, which has a bias, λ, of 1.344, standard deviation, σ, of 0.443, coefficient of variation, COV_R of .329, and a resulting LRFD ϕ of 0.645 at a reliability of 2.5. Whereas, at BOR, the PDA has a bias, λ, of 1.036, standard deviation, σ, of 0.322, coefficient of variation, COV_R of .311, and a resulting LRFD ϕ of 0.518 at a reliability of 2.5. However, the ϕ/λ_R ratio, indicating the percentage of the measured Davisson capacity that can be utilized for design, is 0.48 vs. 0.50 at EOD vs. BOR respectively. The latter suggests that if F.S. for ASD, and ϕ for LRFD at EOD vs. BOR were assigned different values (based on failure probabilities) then similar ϕ/λ_R ratios would be obtained. If so, similar pile lengths for design would occur and the resulting accuracy of EOD versus BOR would be comparable at least for the PDA, CAPWAP, and Paikowsky methods. The latter analysis is based on the present database (45 to 75 cases).

Evaluation of smaller piles (i.e., capacities less than 1779 kN).

In the case of the older methods (ENR, Gates, etc.) the cases were separated into capacities (i.e., bins) larger than 1779 kN and capacities smaller than 1779 kN. Subsequently, the statistics (mean, standard deviation, etc.) for each bin was performed and LRFD phi factors were determined for each method. The results are summarized in Tables 6-7 and 6-8. The following general conclusions were obtained.

For the Gates and FDOT methods, the bias for the capacities smaller than 1779 kN tended closer to unity in comparison to the overall (i.e., all cases) bias which tended to be a higher value. However, in the cases of the ENR and Modified ENR the biases are significantly less than one which makes them very unconservative. Moreover, the bias for cases with capacity smaller than 1779 kN tends to be even more unconservative (i.e., smaller).

In terms of ϕ/λ_R, as a general observation, the piles with capacity larger than 1779 kN have larger values than the overall cases, and the piles with capacity smaller than 1779 kN have smaller values than the overall cases. Therefore, the equivalent ASD factor of safety decreases for cases with capacity larger than 1779 kN. An example of this pattern is shown with the Modified ENR at EOD ($\beta = 1.96$), which safety factors decrease from 14.6 for pile with capacity smaller than 1779 kN to 7.75 for piles with capacity larger than 1779 kN. For a reliability index, β, equals 2.5 the decrease in safety factor is also by a half.

Recommended Safety Factors

The Factors of Safety shown in Tables 6-7 and 6-8 were calculated using Equation 5-9 with ϕ computed from Equation 5-28 (given in tables). All of the factors of safety that were calculated from Eq. 5-9 used a bridge span length of 27 meters to determine Q_D/Q_L. Table 6-9 summarizes the FS obtained for EOD and BOR in Tables 6-7 and 6-8 for the failure probabili-

Table 6-9. Recommended Safety Factors for Dynamic Methods

Prediction Method	FS at p_f =0.62%	FS at p_f =2.50%	FS at p_f =0.62%	FS at p_f =2.50%	Recommended FS	
	BOR	BOR	EOD	EOD	EOD	BOR
CAPWAP	2.48	2.00	1.97	1.58	1.80	2.25
PDA	2.79	2.28	2.24	1.81	2.00	2.50
Paikowsky Energy	3.86	3.09	2.74	2.22	2.50	3.50
FDOT (overall)	1.74	1.31	2.16	1.59	1.90	1.50
FDOT (<1779 kN)	2.00	1.65	3.16	2.36	2.75	1.80
FDOT (>1779 kN)	1.49	1.14	1.10	0.87	1.00	1.30
ENR (overall)	28.60	20.08	16.02	11.93	14.00	24.00
ENR (<1779 kN)	15.35	12.56	18.40	13.80	16.00	14.00
ENR (>1779 kN)	28.84	20.12	13.39	10.07	12.00	24.00
Modified ENR (overall)	18.31	12.88	12.53	9.09	11.00	16.50
Modified ENR (<1779 kN)	8.70	7.36	20.82	14.60	17.70	8.00
Modified ENR (>1779 kN)	18.32	12.81	10.72	7.75	9.20	16.50
Gates (overall)	1.78	1.42	2.28	1.76	2.00	1.60
Gates (<1779 kN)	2.12	1.81	2.80	2.27	2.50	2.00
Gates (>1779 kN)	1.54	1.24	1.30	1.06	1.20	1.40

ties, pf, of 0.62 % and 2.50 %, respectively. The latter represent AASHTO suggested range of failure probabilities. The recommended Factors of Safeties in the last two columns of Table 6-9 for each method at EOD and BOR is the average from the two failure probabilities.

It is evident, that the recommended FS in Table 6-9 are much higher than typically used for ENR and Modified ENR safety factors (FS=6.0). For such cases, Factor of Safety as high as 28.60 are recommended for a failure probability of 0.62 % at BOR. The latter suggests that ENR and Modified ENR are very unconservative (i.e., overestimate the pile capacity) methods.

The old FDOT method recommends a safety factor equal to 1, but according to the LRFD approach, a higher safety factor should be used for design. It is recommended that a FS of 1.50

for BOR and 1.90 for EOD be used for the old FDOT method. Other methods such as CAPWAP, PDA, and Gates should use different values for FS at EOD and BOR (freeze, etc.).

For the Paikowsky's Energy method, it is recommended to modify only the safety factor at BOR from 2.50 to 3.50, while at EOD the actual safety factor of 2.50 is appropriate.

Review of Typical ASD Safety Factors

Based on the database, the current ASD Factor of Safeties may be evaluated for the various dynamic methods. Shown in Table 6-10 is the typical ASD Safety Factors presented in the literature. Based on the ASD Safety Factors, and a typical 27 m bridge span length (i.e., fixed Q_D/Q_L), Equation 5-9 was used to compute the resistance factors, ϕ. Next based on the COV_R and bias, λ_R , from the database, the reliability index, β, for a given method was computed from Equation 5-28. Due to the range of the reliability index, β, the probability of failure was subsequently computed from Figure 5-4. Both the reliability index, β, and the probability of failure, pf, for each method based on the assumed ASD Safety Factors are given in Table 6-10. Based on the results of Table 6-10 and AASHTO's recommended probability of failure for single piles [i.e., should be between 0.62 % for (reliability index) $\beta = 2.50$ and 2.50% for $\beta = 1.96$] a number of conclusions are evident:

The older ENR and Modified ENR procedures show extremely high probability of failures, which reflect the level of unconservatism as discussed in preceding sections. On the other hand, Gates method show a probability of failure as between 0.010 % to 0.11% which is conservative. Of the newer methods, CAPWAP is generally conservative (pf of .1% at EOD and .596 % at BOR), and PDA is less conservative (pf of 0.267 % at EOD and 1.36% at BOR). Table 6-9 presents the recommended Safety Factors for these methods based on AASHTO's recommended probabilities of failure.

Table 6-10. Summary of Results for Fitting the ASD to the LRFD

Prediction Method	ASD FS	LRFD Equiv. ϕ	ASD Design (EOD)			ASD Design (BOR)		
			ϕ/λ_R	β	P_f (%)	ϕ/λ_R	β	P_f (%)
CAPWAP	2.5	0.578	0.362	3.089	0.100	0.458	2.515	0.596
PDA	2.5	0.578	0.430	2.786	0.267	0.557	2.210	1.357
Paikowsky Energy	2.5	0.578	0.520	2.267	1.171	0.691	1.449	7.374
Sakai et al Energy	2.5	0.578	0.384	1.293	9.810	0.396	1.976	2.411
FDOT (overall)	1.0	1.444	0.606	1.146	12.600	0.561	1.445	7.430
FDOT (<1779 kN)	1.0	1.444	0.969	0.369	35.630	1.065	0.536	29.620
FDOT (>1779 kN)	1.0	1.444	0.457	2.274	1.150	0.525	1.688	4.575
ENR (overall)	6.0	0.241	0.805	0.700	24.210	1.024	0.115	45.440
ENR (<1779 kN)	6.0	0.241	0.963	0.395	34.660	1.293	-0.032	51.300
ENR (>1779 kN)	6.0	0.241	0.713	0.976	16.470	0.994	0.146	44.220
Modified ENR (overall)	6.0	0.241	0.540	1.263	10.340	0.662	0.788	21.550
Modified ENR (<1779 kN)	6.0	0.241	0.741	0.605	27.280	0.868	1.306	9.586
Modified ENR (>1779 kN)	6.0	0.241	0.454	1.534	6.258	0.640	0.815	20.770
Gates (overall)	3.0	0.481	0.276	3.067	0.108	0.255	3.718	0.010
Gates (<1779 kN)	3.0	0.481	0.450	2.676	0.363	0.451	3.703	0.010
Gates (>1779 kN)	3.0	0.481	0.214	4.694	0.0001	0.240	4.177	0.0015

CHAPTER 7

DETERMINATION OF CASE DAMPING, J_C, AND SKIN AND TIP RESISTANCE FROM PDA TRACES

As discussed in the previous chapter, the PDA Case method was found to be as accurate as other dynamic methods, Paikowsky, CAPWAP, etc. to estimate static pile capacity. This trend was observed for driven piles at both, EOD and BOR. However, to determine the static pile capacity from the PDA Case method, the user is required to estimate the damping coefficient, J_c. The open literature suggests that the J_c values vary according to soil type, hammer size, pile size, etc. Typically from the Florida experience, engineers either employ GRL recommended J_c values based on soil type or use CAPWAP's estimate of J_c. CAPWAP selects the Coefficient of Damping, skin resistance, toe resistance and quake along the pile in such a way that the predicted and measured force traces match, from a given velocity trace. Unfortunately, due to CAPWAP's multivariable input, there is some question to its uniqueness, requiring significant expertise by the user. Consequently, it would be very beneficial if the PDA's Case damping, J_c could be determined in the field, along with both skin and tip resistance for the pile. The latter would combine the features of the PDA with CAPWAP, as well as provide real time results without delays.

In the next sections, two methods to determine the skin and the tip static capacity from the PDA traces are presented. The results will be compared to the Davisson's capacity determined by the static load test.

METHOD I FOR ESTIMATING SKIN AND TIP RESISTANCE

In this method, the GRL procedure to determine the total dynamic skin capacity is used as starting point. The GRL procedure (Likins et. al., 1988) makes use of the pile top measure-

ments of force and velocity histories during a hammer blow as recorded by the PDA. Figure 7-1 illustrates this procedure.

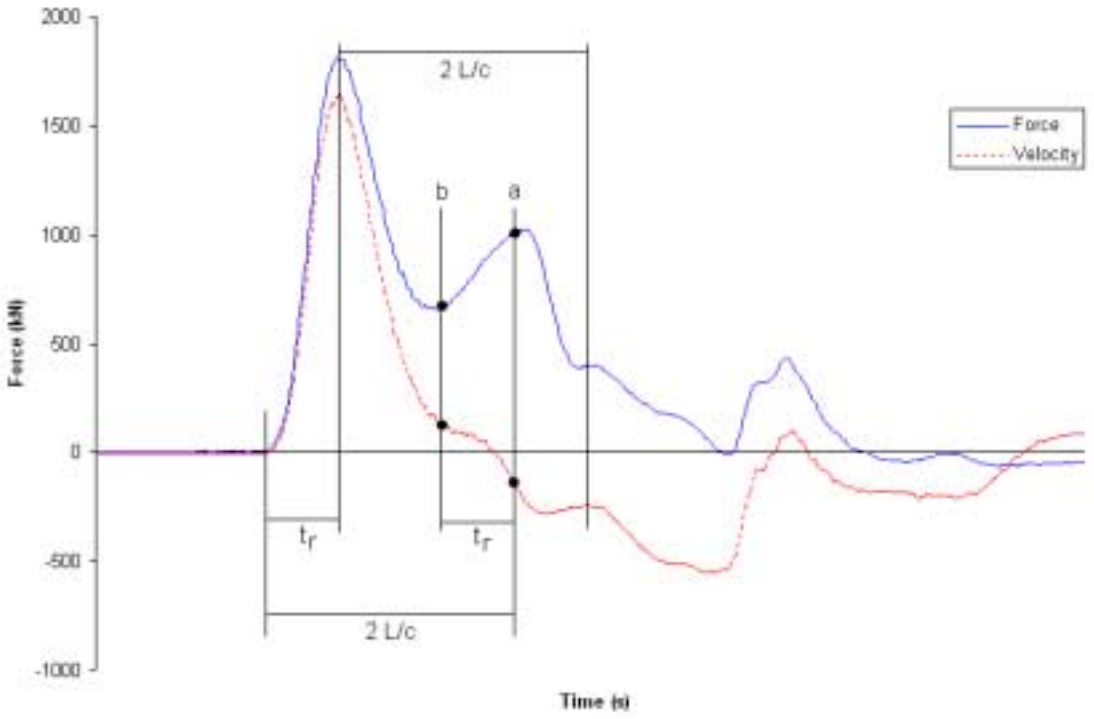

Figure 7-1. GRL Procedure to Determine the Total Skin Capacity of a Driven Pile

To obtain the total dynamic skin friction, the rise time, t_r , must be determined. The rise time is defined as the time between the beginning of blow (force pulse rise) and its peak. This rise time, t_r , is used to determine point "b" which is one rise time earlier than time "a."

At time "a," the separation between force and velocity (F_a –$Z*V_a$) represents the total pile skin friction above that point on the pile. The point "a" was moved back one rise time from 2 L/c to exclude any reflections from the pile tip of the initial input wave. The assumption of this method is that the skin friction at the bottom one rise length is the same as the one additional rise

time length above. Based on this assumption, the skin resistance is the separation of force and velocity at point "a" added to the increase in resistance from point "b" to point "a" as stated below.

$$SFT = (F_a - ZV_a) + [(F_a - ZV_a) - (F_b - ZV_b)] \quad (7\text{-}1)$$

Once the estimate of dynamic skin friction is determined using the GRL procedure, the static tip and skin capacity were calculated according to the following methodology (Method I). First, the total dynamic capacity, RTL, is determined using the Case solution for dynamic capacity (Equation 3-14 for J_c equals 0). Then, knowing the total dynamic capacity and the GRL estimate of skin dynamic capacity, the dynamic tip capacity, *TT*, is computed as:

$$TT = RTL - SFT \quad (7\text{-}2)$$

where: TT Dynamic Tip Capacity

RTL Total Dynamic Capacity

SFT GRL Estimate of Dynamic Skin Capacity

Next, the total tip to skin capacity ratio, T/S, is determined:

$$T/S = \frac{TT}{SFT} \quad (7\text{-}3)$$

The latter was developed to negate the damping in each (i.e., skin and tip), i.e., it is assumed that the tip to skin ratio for the dynamic capacity was similar to the tip to skin ratio for the static capacity. Finally, the total static capacity of the pile must be found. For this purpose, the PDA R_{max} obtained from the driving records is used.

METHOD II FOR ESTIMATING SKIN AND TIP RESISTANCE (PROPOSED)

Description and Main Assumptions

For this method, the tip/skin ratio is obtained directly from the force and velocity traces of the PDA. Figure 7-2 presents an example of a PDA force and velocity traces. This method

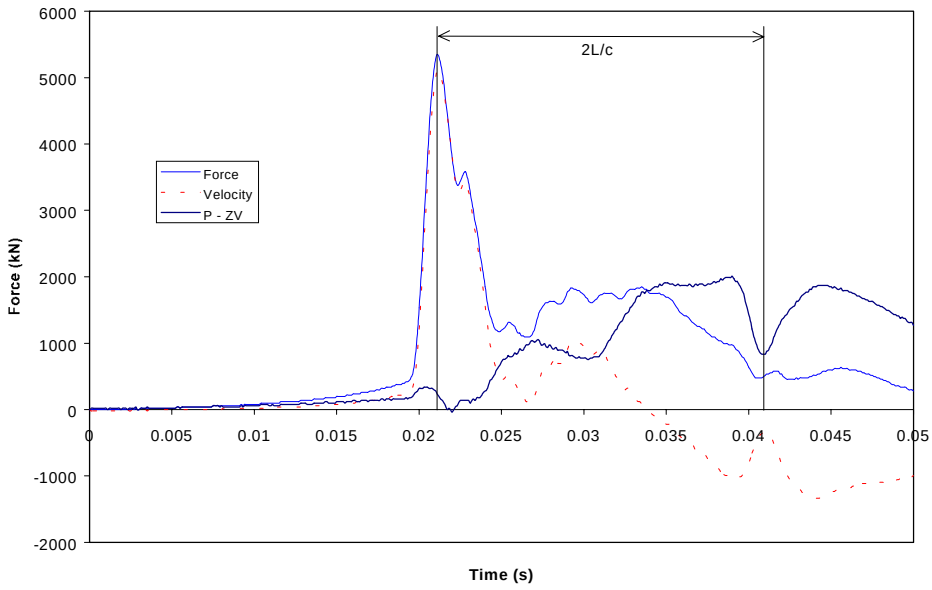

Figure 7-2. Typical Force, Velocity and Double Wave Up Traces from PDA

differs from Method I in the procedure to obtain the tip to skin ratio. Instead of determine the dynamic skin resistance (GRL procedure) by extrapolating the skin resistance from the rise time before the tip reflection, the method considers the skin capacity prior the tip reflection and the tip reflection itself.

For driven piles, when the hammer suddenly hits the pile, a compression wave is produced. The wave travels at a constant speed through the pile, eventually reaching the pile tip, and, depending on the soil tip resistance, reflects back as a tension or a compression wave. Before the compression wave reaches the pile tip, a series of compression waves are reflected back to the top due to the skin resistance of the pile. By measuring the Force and Velocity (and velocity multiplied by impedance) at the pile top, the skin resistance can be calculated as the force minus the velocity (twice the wave up). This principle only applies before any reflection from the tip arrives.

In order to determine the time at which the pile tip reflection arrives to the pile top, the rise time must be considered. The rise time accounts for how fast the tip reflection is developed and it will depend on how fast the hammer transmits the energy to the pile top. The larger the rise time, the more difficult to have an estimate of the skin capacity of the pile. Knowing the rise time allow us to determine the skin resistance at a distance "x" from the top of the pile as:

$$x = L - \frac{RT}{2c} \tag{7-4}$$

where: L Length of Pile Below Gages

c Wave Speed

RT Rise Time

Under this consideration all the skin capacity near the tip of the pile (length equals RT/2c) can not be calculated. Figure 7-3 shows the plot of force minus velocity for the same PDA signal presented in Figure 7-2 (i.e., double wave up). After that point in time (point "b") the reflection from the tip begins to arrive.

From point "b" to a time equals 2L/c from the force peak (point “c”), both skin and tip reflections interact creating an abrupt change in the force up trace. The decrease in the force up trace shown in Figure 7-3 corresponds to the increase in velocity and decrease in the force at time 2L/c (see Figure 7-2). This condition is attributed to piles with small tip capacity, and piles that, although they possess large tip capacity, the energy imparted by the hammer is too large to mobilize the tip capacity.

The proposed method makes use of the two concepts mentioned to determine the tip to skin ratio. The basic assumption of this method is that the tip/skin ratio is equal to the decrease in the wave up trace from point "b" (time 2L/c minus rise time) to point "c" (time 2L/c from

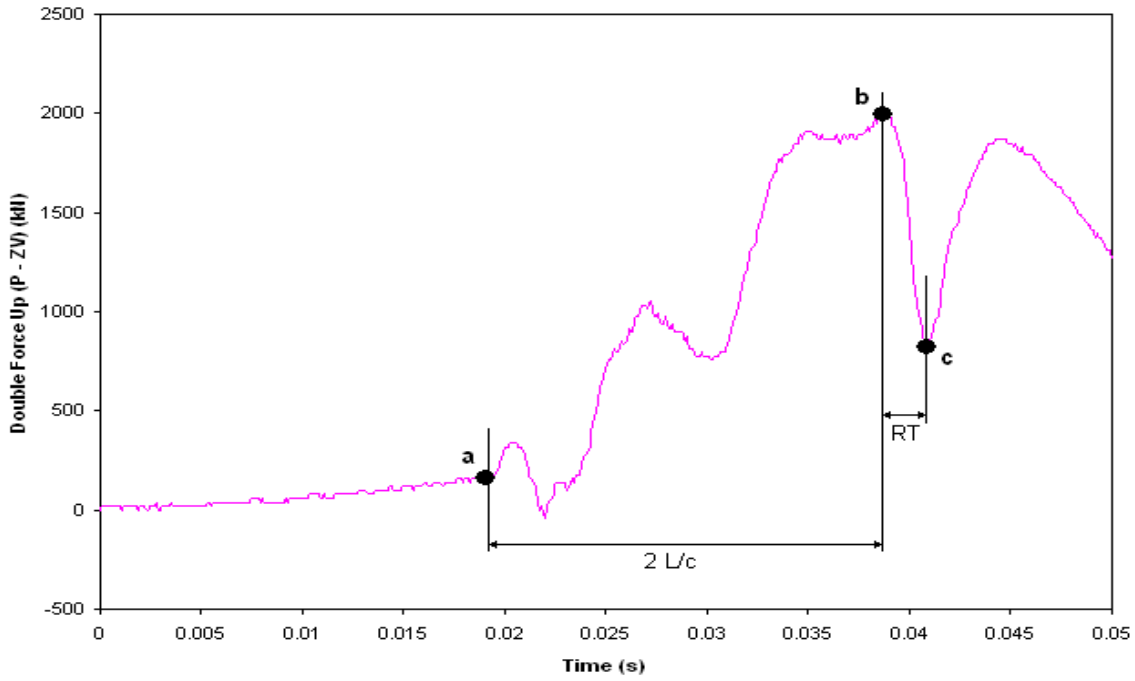

Figure 7-3. Procedure to Determine Tip to Skin Ratio for the Suggested Method

maximum force) divided by the net increase in the wave up trace from point "a" to point "b." The mathematical expression for the proposed method is

$$\frac{Tip}{Skin} = \frac{[(F_b - ZV_b) - (F_c - ZV_c)]}{[(F_b - ZV_b) - (F_a - ZV_a)]} \tag{7-5}$$

The use of wave up at point "a" is to account for any error in the instrumentation readings. Because a decrease in the wave up is needed to obtain a tip to skin ratio, the hammer must be able to mobilize the whole pile capacity.

Case Damping Coefficient, J_c, versus Tip to Skin Ratio

In the process of finding a method to obtain the Case damping coefficient, J_c, directly from the PDA signal, the relation between the tip to skin ratio and the J_c value was studied. For the latter, the measured Davisson's capacity was substituted as RSP in Equation 3-14, and the J_c

coefficient was back calculated. Subsequently, the computed damping value, J_c was plotted versus the suggested tip to skin ratio. The results are presented in Figure 7-4.

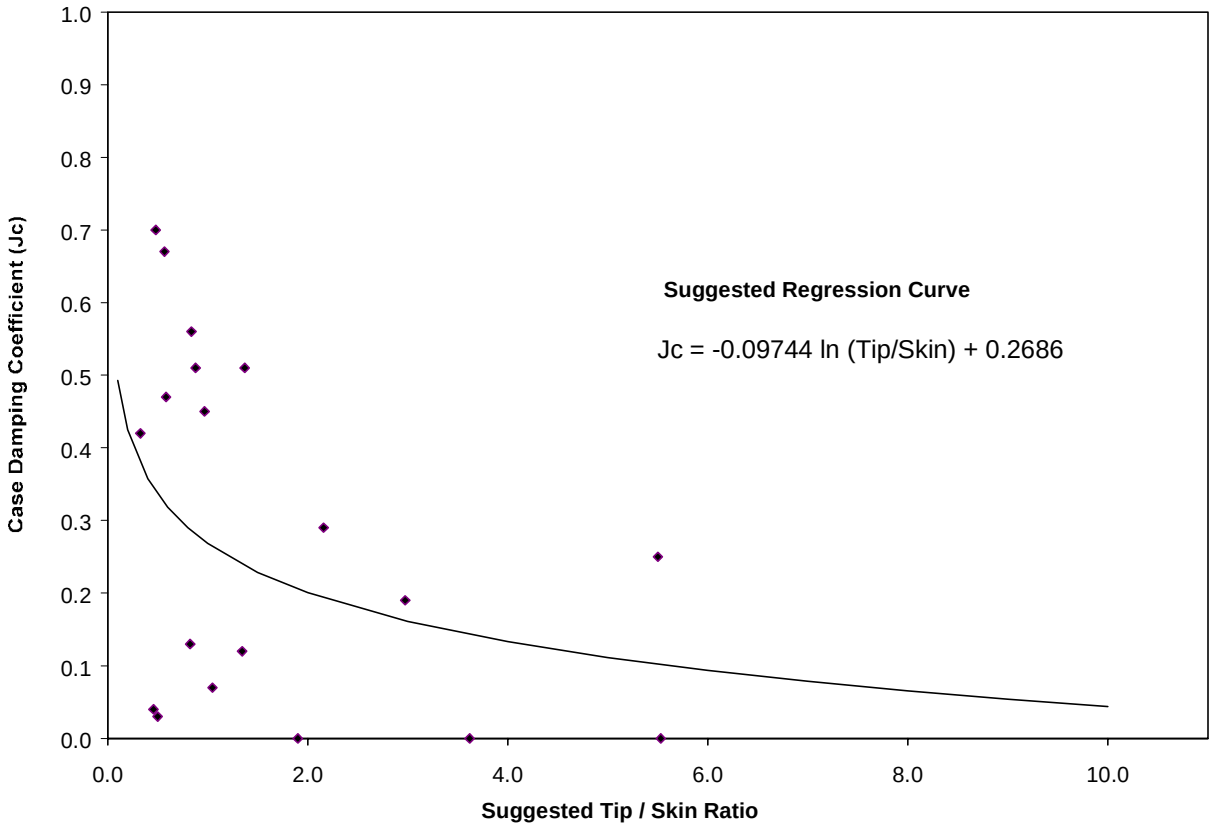

Figure 7-4. Suggested Tip to Skin Ratio versus Case Damping Coefficient

Two observations can be made from Figure 7-4. First, for tip to skin ratios smaller than 1.0, the J_c is on the order of 0.4 to 0.6, and there is a tendency for J_c to decrease as the tip to skin ratio is increased. Second, the values of Case damping are scattered. It is believed that there are two reasons for the latter: 1) the hammer may or may not impart enough energy to mobilize the static pile capacity (results in very low J_c values in Figure 7-4). And 2) PDA capacity predictions assume that all pile damping occurs at pile toe (may not always be true). However, as part of this study a sensitivity analysis was performed on the influence of J_c on the static pile capacity

(see next section). An important finding of this study is that a 30% variation in J_c results in only a 10 % variation in static pile capacity.

Figure 7-4 shows the proposed regression curve for the J_c versus Tip/Skin Ratio. This curve is significant, because it allows us to obtain a Case damping coefficient, J_c, directly from the PDA traces, without taking into consideration the soil type in which the pile is embedded. The suggested equation to correlate tip to skin ratio to J_c is:

$$J_c = -0.09744 \ln\left(\frac{Tip}{Skin}\right) + 0.2686 \qquad (7\text{-}6)$$

Automation of Proposed Method II

A Fortran program was developed in order to simplify the calculation process. This program is able to read directly the PDA recorded force and velocity signal and perform the data reduction. The input parameters for the program are the length of the pile below the gages, the wave speed, the material modulus, the cross-sectional area, and the data-sampling interval.

The output file begins with a general description of the pile itself and the driving information entered. Next, it presents in tabular form the time increment, velocity, force, velocity times impedance, displacement, and the double wave up (P – ZV) results (Figure 7-3). Finally, the program computes the Tip to skin ratio, and the case damping, J_c value.

Appendix I contains the PDA traces (force, velocity, double force up, and displacement) for the signals studied. At the end of the output file, the results from the Method I and II (suggested) are presented. In addition, the significant times such as maximum force, T1, time T2 (T1 + 2L/c), rise time, etc, are also presented. Appendix J presents an example of the Fortran output. Only the first five pages and the last page of the output are included.

SENSITIVITY ANALYSIS OF CASE DAMPING COEFFICIENT, J_C

In order to measure how sensitive the Case resistance (RSP) solution is to the variation of J_c, a sensitivity study was performed. The following steps were followed to obtain a relation between the coefficient of variance for the resistance and the coefficient of variance for J_c. Using the Case resistance approach for estimating pile capacity, R, the average (bars for average) resistance based on the average value of J_c is given as

$$\overline{R} = \frac{1}{2}\left[\left(1-\overline{J}_c\right)\left(F_1+ZV_1\right)+\left(1+\overline{J}_c\right)\left(F_2-ZV_2\right)\right] \tag{7-7}$$

If the standard deviation of the resistance is defined in terms of the standard deviation of the Case damping, we obtain:

$$\sigma_R = \frac{1}{2}\sigma_J\left[-\left(F_1+ZV_1\right)+\left(F_2-ZV_2\right)\right] \tag{7-8}$$

Then the covariance of the resistance can be written as:

$$COV_R = \frac{\sigma_R}{\overline{R}} = \frac{\sigma_J\left[-\left(F_1+ZV_1\right)+\left(F_2-ZV_2\right)\right]}{\left(1-\overline{J}_c\right)\left(F_1+ZV_1\right)+\left(1+\overline{J}_c\right)\left(F_2-ZV_2\right)} \tag{7-9}$$

If we define the constant η in terms of the force and velocity at time T1 and time T2 (T1 plus 2L/c), then

$$\eta = \frac{\left(F_2-ZV_2\right)}{\left(F_1+ZV_1\right)} \tag{7-10}$$

Next divide the numerator and denominator of Equation 7-10 by the average J_c and making the appropriate substitutions for η we obtain:

$$COV_J = COV_R\left[1+\frac{1}{J_c}\left(1+\frac{2}{\eta-1}\right)\right] \tag{7-11}$$

Equation 7-11 allows us to determine the variance in the J_c for a given percent of variance in the resistance, or vice-versa. The next section provides the results of a study of 18 piles.

SELECTION OF STATIC AND DYNAMIC LOAD TEST DATA

The criteria for selecting a load test for inclusion in this study involved: 1) a static load test was performed and Davisson's failure was obtained and 2)PDA force and velocity traces were available for the pile. For the dynamic load test, the selected blow (PDA) was chosen as close to the static load test date as possible (i.e., minimize freeze). For all the cases reported, the closest dynamic load test date occurred after the static load test was performed (i.e., the static capacity was compared to the Beginning of Restrike). Other useful information includes having a measured skin and tip resistance. The latter occurred through either pull out static load tests or Osterberg load cell test. For each pile, it was required to know both geometric and driving parameters, such as, wave speed, pile length below the gages, cross-sectional area, and material modulus. Based on the latter requirements, 18-test piles were considered. Table 7-1 summarizes general information of each load test pile. The pile population represents 9 sites and 3 diameters, while the range of depths of the piles below the gages varies from 9.15 to 34.45 meters. Only one test pile is from a location outside the State of Florida.

COMPARISON OF SKIN, TIP AND TOTAL PILE CAPACITIES

Results

In the following sections, the results from the proposed Method II will be presented in addition to the results of other methodologies: Method I, PDA (total capacity only), and CAPWAP (skin, tip and total). The reader is referred to Appendix I for the plots of force, velocity, double wave up, and displacement traces for each case studied. The first results presented are predicted versus measured total pile capacity. For Methods I and II, the J_c used in Equation 3-14 was obtained from Figure 7-4 with the Tip to skin ratio obtained from the force up traces and Equations 7-3 (Method I) and 7-5 (Method II). Next, the predicted and measured skin

Table 7-1. Geometric and Driving Information of Load Test Piles

File Name	Site Location	Pile Location	Shaft Length (m)	Shaft Diameter (m)	Wave Speed (m/s)	Material Modulus (kN/m^2)	Cross-Sec. Area (m^2)	Data Sampling Increment (s)
TS4I	Pascagoula, Mississippi	Test Site 4	34.45	0.61	4325.0	44905380	0.37	0.0001
TS1B102	Vilano Bridge	Test Site 1	29.88	0.61	3929.9	37684870	0.37	0.0001
B5RS2	Escambria Bridge	Bent 5 / Pile 27	26.83	0.61	4425.0	47005420	0.37	0.0001
TS13A1-A	Buckman Bridge	Test Site 13	33.84	0.76	3935.7	37184330	0.48	0.0001
TS19FRCB	Buckman Bridge	Test Site 19	32.74	0.76	3993.9	38292260	0.48	0.0001
TS24ALTA	Buckman Bridge	Test Site 24	30.98	0.76	3937.1	37211220	0.48	0.0001
TS29RC	Buckman Bridge	Test Site 29	29.27	0.76	3984.2	39470520	0.48	0.0001
F6-58A	Acosta Bridge	Pier F6 / Pile 44	19.21	0.61	3872.0	35989530	0.37	0.0001
G13-37	Acosta Bridge	Pier G13 / Pile 95	17.68	0.61	4325.0	39470519	0.37	0.0002
H2-27B	Acosta Bridge	Pier H2 / Pile 26	10.64	0.61	4116.2	40656360	0.37	0.0001
VLWA-61D	Vilano West Bridge	STA. 142+74	19.05	0.46	4186.6	42075920	0.21	0.0001
VLE-32C	Vilano East Bridge	STA. 183+47	10.98	0.46	3730.2	33402750	0.21	0.0001
BKM30J	Buckman Bridge	STA. 362+90	9.15	0.46	3900.6	36523850	0.21	0.0001
BZ83N	Seebreze Bridge	STA. 353+15	25.91	0.46	3926.6	37011970	0.21	0.0001
AUC63K	Aucilla Bridge	STA. 494+47	20.43	0.46	3993.8	38291580	0.21	0.0001
B1-76F	Choctawhatche Bridge	Pier FSB3 / Pile 2	24.36	0.61	4172.7	41796700	0.37	0.0001
PR5R2	Choctawhatche Bridge	Pier 5 / Pile x	18.63	0.76	4329.3	43612000	0.42	0.0001
B8-97R2	Choctawhatche Bridge	Pier 11 / Pile 38	29.76	0.76	4643.0	51750160	0.42	0.0001
B14-89R2	Choctawhatche Bridge	Pier 23 / Pile 13	29.27	0.76	4520.8	49062030	0.42	0.0001
B17-94R2	Choctawhatche Bridge	Pier 29 / Pile 7	29.00	0.76	4208.8	42524060	0.42	0.0001
PR35FIN	Choctawhatche Bridge	Pier 35 / Pile 7	27.16	0.76	4292.1	44224220	0.42	0.0001
B23-76F2	Choctawhatche Bridge	Pier 41 / Pile x	24.09	0.76	4412.0	46728270	0.42	0.0001
B27-63F	Choctawhatche Bridge	FSB 26 / Pile 3	19.82	0.61	4283.2	44041520	0.37	0.0001

and tip resistance for Methods I, II and CAPWAP are presented. For the predicted skin capacity of the piles, the latter was evaluated by either pullout tests or Osterberg tests in which skin friction failure occurred.

Table 7-2 summarizes the results for the suggested Method II and the load tests. The tip to skin ratio is presented together with the recommended Case damping coefficient, J_c. Based on the latter parameter, the PDA Case solution for total capacity was found. Also presented in Table 7-2 are the measured Davisson's capacity for all compression tests, and the skin capacity for piles with a performed tensile load test or an Osterberg test with skin failure.

Table 7-3 presents the estimated capacities using Method I and CAPWAP. For Method I, the total dynamic capacity was obtained using the Case solution for time T_1 located at the maximum force entering the pile. Then, the tip and the tip to skin ratio were calculated using Equations 7-2 and 7-3. With this tip to skin ratio and the PDA R_{max} the static skin and tip capacity for the Method I were calculated.

Total Capacity Predictions

A series of figures show the results from the three methods studied, i.e., CAPWAP, Method I (using PDA Rmax), and the suggested Method II in comparison with the measured capacity. Figure 7-5 shows the Davisson's capacity versus Method II (suggested) estimated static pile capacity. The CAPWAP estimated capacity versus the Davisson's capacity is presented in Figure 7-6, and Method I's estimated capacity vs. Davisson's capacity is presented in Figure 7-7.

For the total capacity analysis, only 18 cases out of 23 cases were used. The bias factor λ_R, the standard deviation, σ, and the coefficient of variance, COV_R, were calculated (see bias factor, standard deviation, and coefficient of variance definition on Chapter 5). Table 7-4 presents the findings for the three methods studied.

Table 7-2. Suggested Method II Results and Static Load Test Results

File Name	Location	Suggested Method Static Capacities						Load Test Results (kN)		
		Tip/Skin Ratio	J_c	Total (kN)	Skin (kN)	Tip (kN)	Type of Test	Davisson		
								Total	Skin	Tip
TS4I	Pascagoula, Mississippi	0.57	0.33	5069.7	3261.9	1807.8	Osterb.(T&T)	3282.6	1316.6	1966.0
TS1B102	Vilano Bridge	0.8	0.29	4140.9	2270.8	1870.1	Static (C&T)	4919.5	2775.6	2143.9
B5RS2	Escambria Bridge	1.34	0.24	3256.3	1389.9	1866.4	Static (C)	3780.8	n/a	n/a
TS13A1-A	Buckman Bridge	0.97	0.27	5456.4	2772.2	2684.2	Static (C&T)	4092.2	1601.3	2490.9
TS19FRCB	Buckman Bridge	2.16	0.19	5279.6	1671.2	3608.3	Static (C&T)	4376.8	1396.7	2980.2
TS24ALTA	Buckman Bridge	0.48	0.34	6599.9	4455.8	2144.1	Static (C&T)	4892.8	2490.9	2401.9
TS29RC	Buckman Bridge	2.98	0.16	4797.8	1207.0	3590.8	Static (C&T)	4519.2	1734.7	2784.4
F6-58A	Acosta Bridge	0.58	0.32	4096.2	2589.1	1507.1	Static (C)	3451.6	n/a	n/a
G13-37	Acosta Bridge	1.05	0.26	3990.6	1948.9	2041.7	Static (C)	4964.0	n/a	n/a
H2-27B	Acosta Bridge	5.50	0.10	3530.5	543.1	2987.3	Static (C)	2570.9	n/a	n/a
VLWA-61D	Vilano West Bridge	4.70	0.12	1403.8	246.5	1157.4	Osterberg	n/a	382.5	n/a
VLE-32C	Vilano East Bridge	1.06	0.26	2722.7	1325.2	1397.5	Osterberg	n/a	1150.3	n/a
BKM30J	Buckman Bridge	9.18	0.05	1561.5	153.4	1408.1	Osterberg	n/a	120.1	n/a
BZ83N	Seebreze Bridge	0.99	0.27	3244.8	1629.5	1615.3	Osterberg	n/a	1470.5	n/a
AUC63K	Aucilla Bridge	3.33	0.15	2419.9	558.4	1861.4	Osterberg	n/a	938.5	n/a
B1-76F	Choctawhatche Bridge	0.84	0.29	3349.8	1822.7	1527.1	Static (C)	2215.1	n/a	n/a
PR5R2	Choctawhatche Bridge	5.53	0.10	3722.9	570.2	3152.7	Static (C)	5444.4	n/a	n/a
B8-97R2	Choctawhatche Bridge	0.33	0.38	6618.2	4986.3	1631.9	Static (C)	6360.6	n/a	n/a
B14-89R2	Choctawhatche Bridge	1.37	0.24	4734.1	1997.2	2736.9	Static (C)	2846.7	n/a	n/a
B17-94R2	Choctawhatche Bridge	0.16	0.45	3196.9	2752.9	444.0	Static (C)	4074.4	n/a	n/a
PR35FIN	Choctawhatche Bridge	0.46	0.35	5013.0	3440.3	1572.7	Static (C)	6485.2	n/a	n/a
B23-76F2	Choctawhatche Bridge	3.62	0.14	4355.2	942.9	3412.3	Static (C)	6253.9	n/a	n/a
B27-63F	Choctawhatche Bridge	1.17	0.25	3547.6	1633.8	1913.8	Static (C)	4270.1	n/a	n/a

Table 7-3. CAPWAP and Method I Results

File Name	Location	Method I				CAPWAP Static Results			
		Tip/Skin Ratio	Total (PDA) (kN)	Skin (kN)	Tip (kN)	Tip/Skin Ratio	Total (kN)	Skin (kN)	Tip (kN)
TS4I	Pascagoula, Mississippi	1.6	4581.4	1785.4	2796.0	2.6	4518.3	1265.9	3252.4
TS1B102	Vilano Bridge	0.1	3433.9	3116.0	317.8	0.3	3915.1	2930.8	984.3
B5RS2	Escambria Bridge	1.1	2526.5	1217.6	1308.9	0.6	2610.1	1623.1	987.0
TS13A1-A	Buckman Bridge	0.9	4803.8	2468.6	2335.3	1.1	4007.6	1950.0	2057.6
TS19FRCB	Buckman Bridge	1.9	5640.1	1947.5	3692.5	2.1	6510.1	2087.9	4422.2
TS24ALTA	Buckman Bridge	9.0	6636.4	661.8	5974.6	0.5	6240.5	4123.7	2116.8
TS29RC	Buckman Bridge	3.1	5239.7	1276.1	3963.6	3.6	5115.2	1123.6	3991.6
F6-58A	Acosta Bridge	0.3	3771.9	2926.2	845.7	0.1	3474.8	3052.7	422.1
G13-37	Acosta Bridge	1.1	5177.5	2457.7	2719.8	1.2	4826.1	2224.0	2602.1
H2-27B	Acosta Bridge	3.2	3967.6	948.1	3019.6	5.2	4091.3	658.3	3433.0
VLWA-61D	Vilano West Bridge	1.5	1080.9	430.1	650.8	0.9	916.3	494.6	421.7
VLE-32C	Vilano East Bridge	0.8	2570.9	1395.0	1176.0	0.9	2691.0	1400.7	1290.4
BKM30J	Buckman Bridge	1.5	1961.6	772.6	1189.0	1.2	1939.3	881.6	1057.7
BZ83N	Seebreze Bridge	0.2	2628.8	2183.4	445.4	0.3	2361.9	1774.8	587.1
AUC63K	Aucilla Bridge	4.6	1757.0	313.4	1443.6	0.7	1823.7	1045.3	778.4
B1-76F	Choctawhatche Bridge	0.0	3220.4	3233.3	-12.9	0.2	2231.6	1907.3	324.3
PR5R2	Choctawhatche Bridge	8.7	3255.9	334.7	2921.2	6.0	2596.3	371.0	2225.3
B8-97R2	Choctawhatche Bridge	1.4	4554.8	1863.6	2691.1	0.2	3621.6	3033.1	588.5
B14-89R2	Choctawhatche Bridge	0.5	3131.4	2029.4	1102.0	0.1	1975.4	1802.3	173.0
B17-94R2	Choctawhatche Bridge	0.0	3700.7	3780.1	-79.4	0.0	3452.5	3288.9	163.7
PR35FIN	Choctawhatche Bridge	0.3	4661.5	3650.4	1011.1	0.3	4045.0	3231.9	813.1
B23-76F2	Choctawhatche Bridge	-7.9	4448.0	-645.7	5093.7	3.8	2155.9	453.7	1702.2
B27-63F	Choctawhatche Bridge	0.8	2673.2	1452.1	1221.2	3.6	2503.3	542.2	1961.1

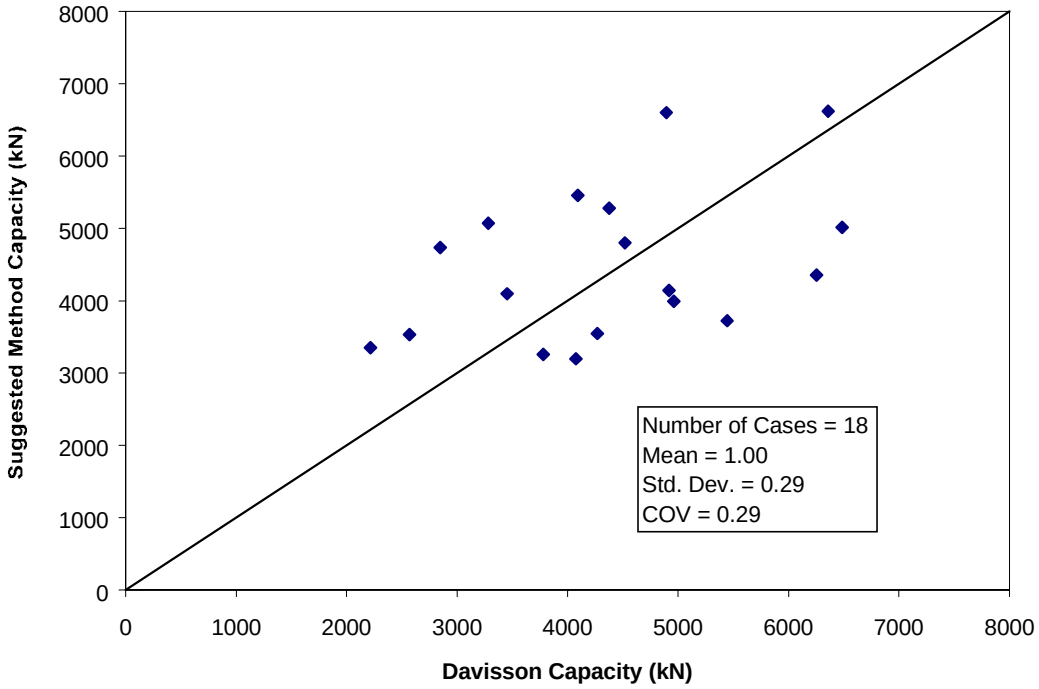

Figure 7-5. Davisson Capacity vs. Suggested Method II Capacity

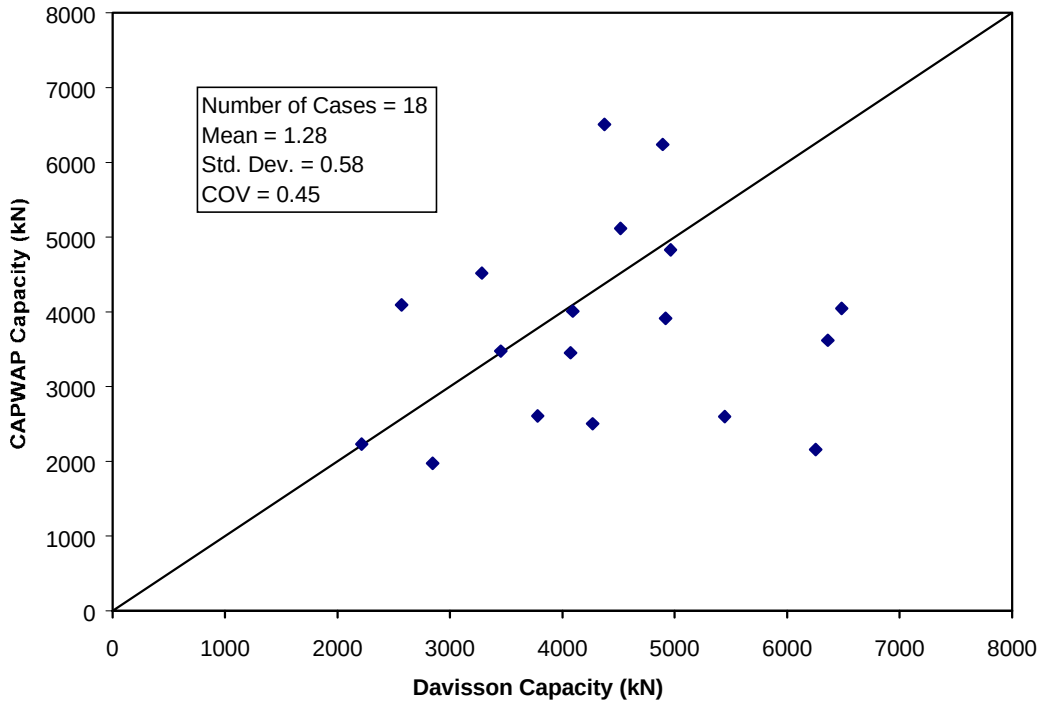

Figure 7-6. Davisson Capacity vs. CAPWAP Capacity

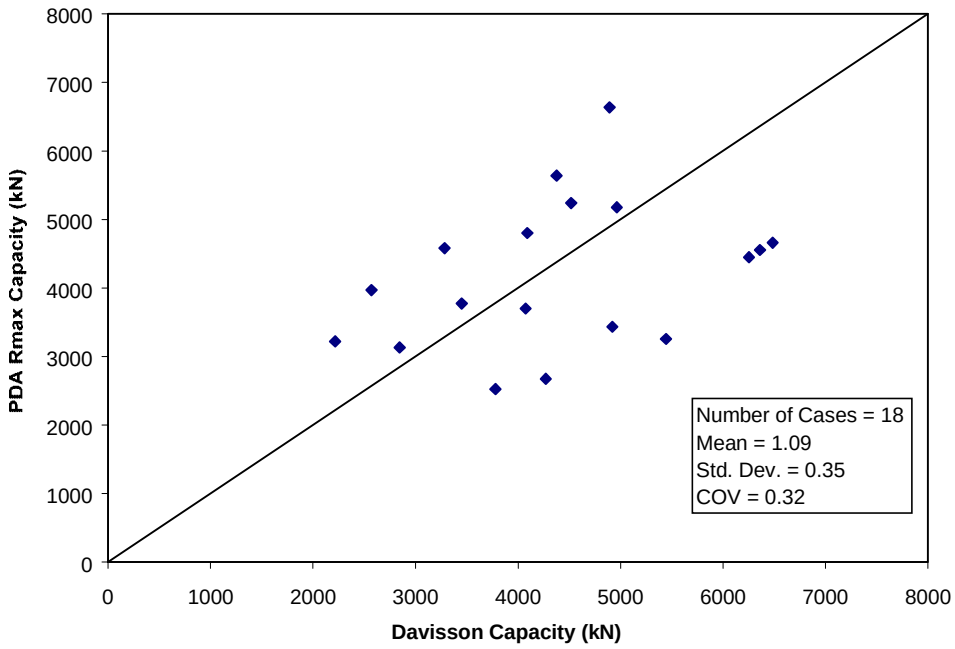

Figure 7-7. Davisson Capacity vs. PDA Rmax Capacity (used in Method I)

Table 7-4. Comparison of Mean, Standard Deviation, and COV_R.

Method	Mean, λ_R	Std. Dev. σ	COV_R
Suggested Method II	1.00	0.29	0.29
CAPWAP	1.28	0.58	0.45
Method I	1.09	0.35	0.32

It should be noted that although the number of cases studied were only 18, the mean, standard deviation, and coefficient of variance for CAPWAP and PDA show good agreement with the database. According to the database, for PDA capacity at BOR, the mean, standard deviation, and COV are 1.04, 0.32 and 0.31, respectively. For CAPWAP at BOR the mean is 1.26, the standard deviation is 0.44, and the COV_R is 0.35.

From Table 7-4, it can be observed that the best method to estimate the Davisson's capacity is the suggested Method II with a mean value of 1.0 (it is important to remember that the suggested method was calibrated to have a mean value of 1.00). The PDA underestimated the Davisson's capacity by 9 percent, while the CAPWAP procedure underestimated the Davisson's capacity by 26 percent at BOR.

In Chapter 6, it was explained how the coefficient of variance could be a useful tool to measure the accuracy of a dynamic method. Making use of this criterion, the suggested method (COV_R equals 0.29) can be considered the most accurate of the three methods followed by the PDA (COV_R equals 0.32). The CAPWAP procedure was the less accurate of the three methods (COV_R equals 0.45).

Skin and Tip Capacity Predictions

The number of cases to evaluate the skin and tip predictions is much smaller than the number of cases used for total capacity prediction. For the skin prediction, the total number of cases is 10, while for the tip prediction the number of cases drops to only six. The reason for this decrease in the number of cases is the limited number of tensile test and Osterberg tests. From the six Osterberg tests, one test failed at the tip and five failed at the skin). The tensile tests are very helpful to determine the skin capacity. With the skin capacity calculated, and knowing the total static capacity the tip capacity can be calculated.

Table 7-5 summarizes the statistical results for both, tip and skin predictions. Figures 7-8 to 7-10 present the predicted skin capacity versus the estimated skin capacity for the suggested Method II, CAPWAP, and Method I, respectively. For the same methods, the tip predictions versus the measured tip capacity are shown in Figures 7-11 to 7-13.

Table 7-5. Statistical Analysis for Skin and Tip Predictions

Method	Skin Capacity Prediction (10 Cases)			Tip Capacity Prediction (6 Cases)		
	Mean, λ_R	Std. Dev. σ	COV_R	Mean, λ_R	Std. Dev. σ	COV_R
Suggested Method	1.04	0.40	0.39	0.96	0.16	0.17
CAPWAP	0.80	0.35	0.43	1.08	0.59	0.55
Method I	1.29	1.15	0.89	1.94	2.47	1.27

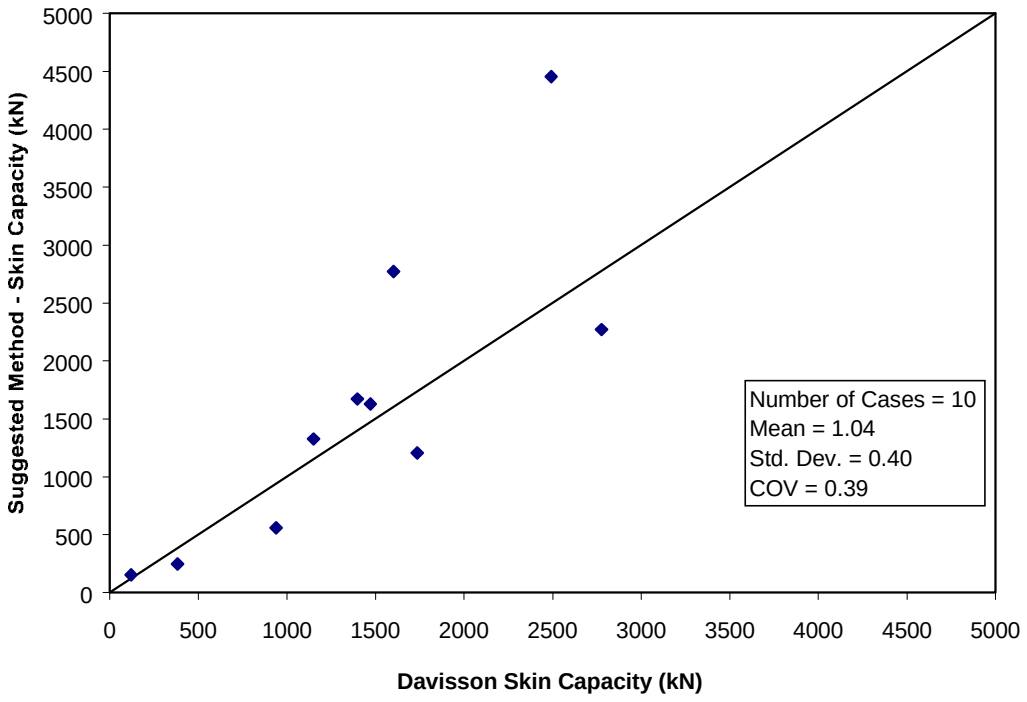

Figure 7-8. Davisson Capacity vs. Suggested Method Capacity (Skin Capacity)

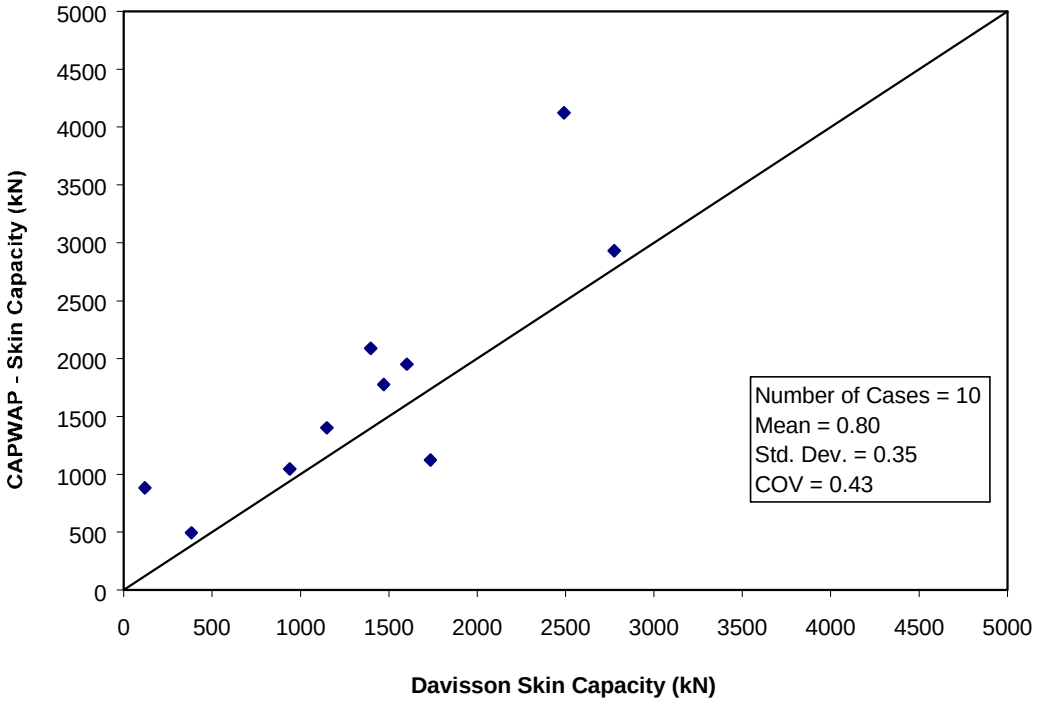

Figure 7-9. Davisson Capacity vs. CAPWAP Capacity (Skin Capacity)

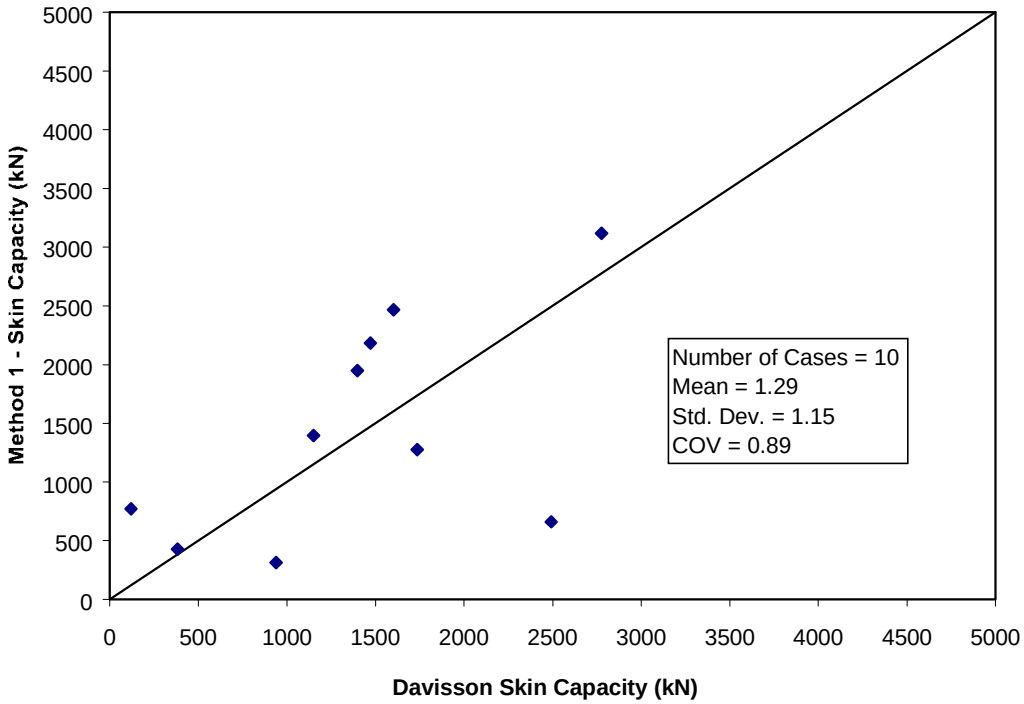

Figure 7-10. Davisson Capacity vs. Method I Skin Capacity

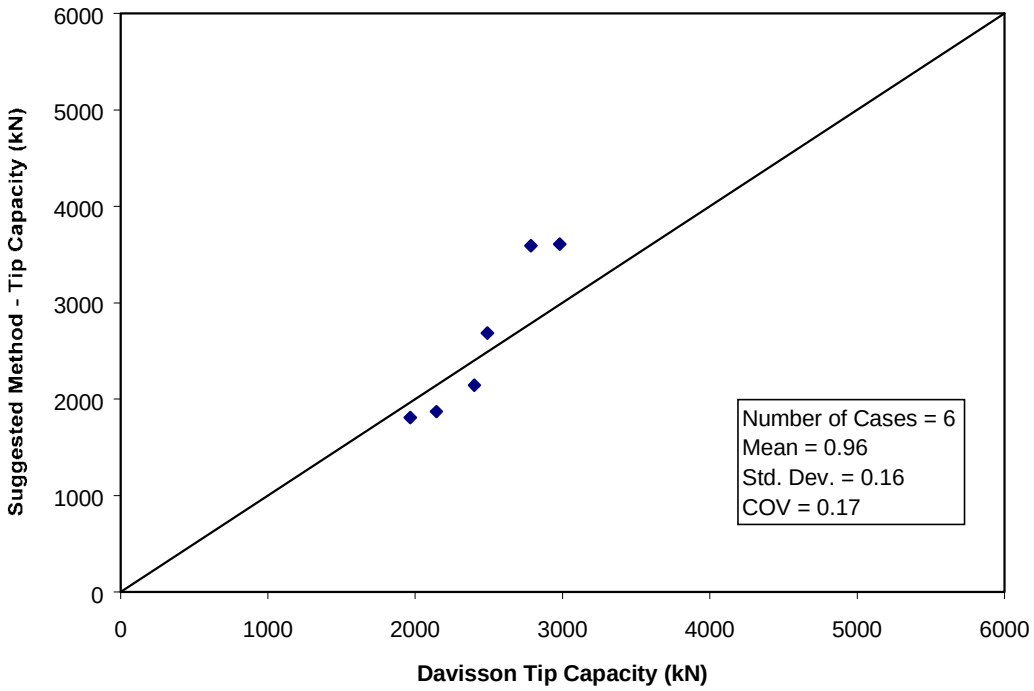

Figure 7-11. Davisson Capacity vs. Suggested Method II (Tip Capacity)

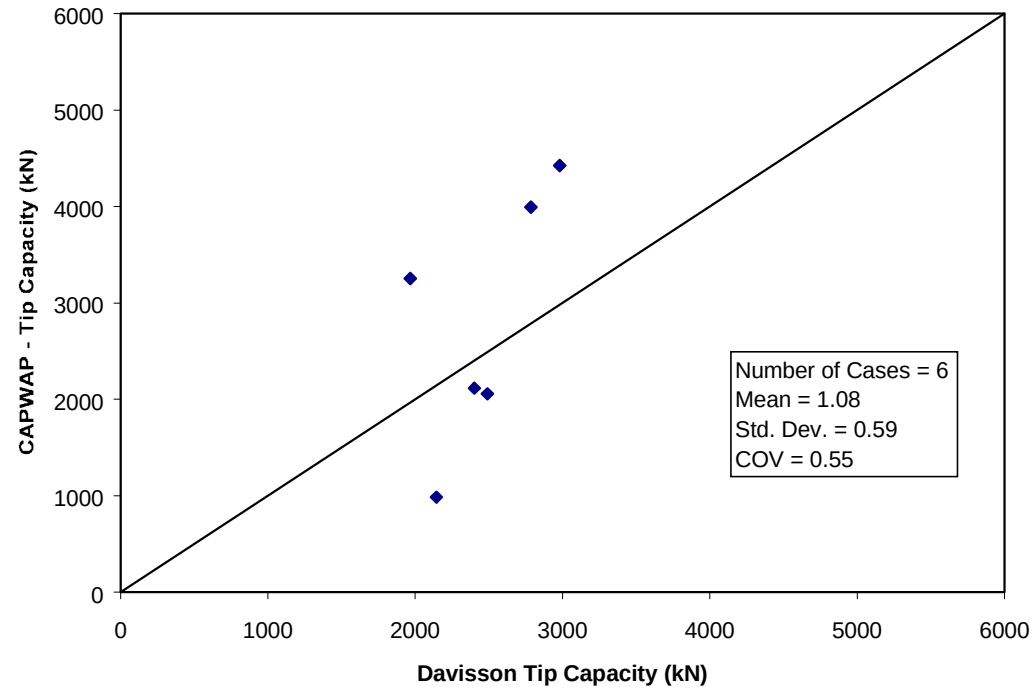

Figure 7-12. Davisson Capacity vs. CAPWAP Capacity (Tip Capacity)

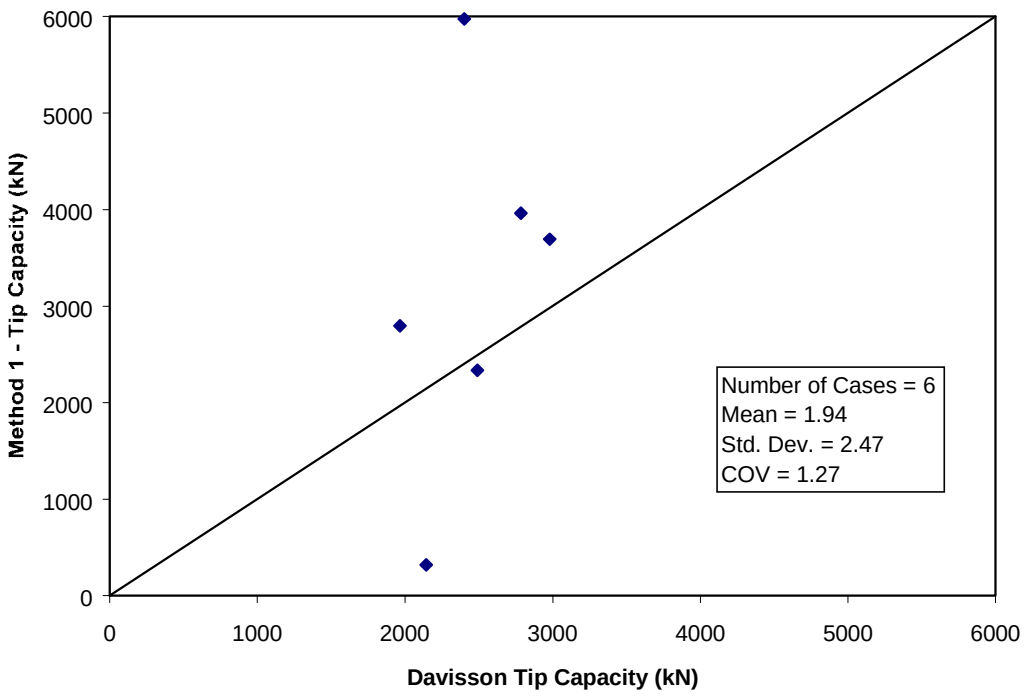

Figure 7-13. Davisson Capacity vs. Method I Capacity (Tip Capacity)

In terms of skin prediction, the suggested Method II, on average, slightly underestimate the measured skin capacity by 4 percent, while the CAPWAP procedure overestimate the measured skin capacity by 20 percent. On the other hand, Method I underestimates the skin capacity by 29 percent. The accuracy of the methods (govern by the coefficient of variance) is not as good as for determining the total capacity. Both, the suggested Method II and CAPWAP have very similar COV_R values (0.39 and 0.43, respectively), while Method I is the less accurate method with a COV_R of 0.89.

The tip predictions show excellent results for the suggested Method II with a mean of 0.96 and COV_R of 0.17. The CAPWAP procedure tends to underestimate the tip capacity by 8 percent and Method I by 94 percent. The accuracy is quite good for the suggested method

(COVR = 0.17), followed by CAPWAP (COVR = 0.55), and Method I with the worst accuracy of the three methods (COVR = 1.27).

Sensitivity of J_c and Pile Resistance

The 23 cases studied were analyzed using Equation 7-8 to determine the sensitivity of the J_c. Table 7-6 presents the results for a change in covariance of the resistance of +/- 10 %, and for a change in covariance of J_c for the same amount. An average value for each condition has been calculated at the bottom of the table. According to Table 7-6, if the coefficient of variance of J_c is modified by 10 %, the coefficient of variance of the resistance will be altered only 3.15 %. Another way to look at this finding is by changing the coefficient of variance of the resistance. If the coefficient of variance of the resistance is altered by 10 %, the resulting variation in J_c is on average 33.67 %. The latter proves that the pile's static resistance is not very sensitive to the Case-damping coefficient. The scattered pattern in the back calculated J_c on Figure 7-4 reflects the latter fact.

Figure 7-14 shows the sensitivity analysis results for variation on the pile resistance capacity by 10 and 20 %. The solid line represents the suggested curve (Equation 7-6) relating the tip to skin ratio to J_c. The dashed lines show how much the suggested line must be altered to obtain a change in the resistance of 10 or 20 percent.

Table 7-6. Sensitivity Analysis Results for Variation of Case Damping Coefficient and Pile Resistance

File Name	Site Location	P1 (kN)	ZV1 (kN)	P2 (kN)	ZV2 (kN)	J_c	η	Constant	Change COV (Rs)		Change COV (J_c)	
									(+10%) (J_c)	(-10%) (J_c)	(+10%) (Rs)	(-10%) (Rs)
TS4I	Pascagoula, Mississippi	6137.9	5713.3	772.1	-849.3	0.326	0.14	-3.040	-30.40	30.40	-3.29	3.29
TS1B102	Vilano Bridge	5662.7	5526.2	606.1	35.7	0.287	0.05	-2.859	-28.59	28.59	-3.50	3.50
B5RS2	Escambria Bridge	4936.9	3949.5	158	355.5	0.240	-0.02	-2.985	-29.85	29.85	-3.35	3.35
TS13A1-A	Buckman Bridge	7051.8	7688.8	-545.9	-682.4	0.271	0.01	-2.759	-27.59	27.59	-3.62	3.62
TS19FRCB	Buckman Bridge	7941	4895	-46.2	2216.1	0.193	-0.18	-2.629	-26.29	26.29	-3.80	3.80
TS24ALTA	Buckman Bridge	6690.3	6280.7	227.6	-3231.4	0.340	0.27	-4.080	-40.80	40.80	-2.45	2.45
TS29RC	Buckman Bridge	8014.4	8730	-238.5	3577.9	0.162	-0.23	-2.881	-28.81	28.81	-3.47	3.47
F6-58A	Acosta Bridge	5252.8	4527.1	276.5	-898.5	0.321	0.12	-2.966	-29.66	29.66	-3.37	3.37
G13-37	Acosta Bridge	5395	5157.5	576.8	407.2	0.264	0.02	-2.912	-29.12	29.12	-3.43	3.43
H2-27B	Acosta Bridge	5214.7	4994.4	807.9	2717.5	0.102	-0.19	-5.714	-57.14	57.14	-1.75	1.75
VLWA-61D	Vilano West Bridge	4074.9	3549.8	-231.1	3276.7	0.120	-0.46	-2.082	-20.82	20.82	-4.80	4.80
VLE-32C	Vilano East Bridge	4061.2	2975.7	1029.3	923.5	0.260	0.02	-2.964	-29.64	29.64	-3.37	3.37
BKM30J	Buckman Bridge	4383.7	3757.4	371.8	4735.9	0.050	-0.54	-5.041	-50.41	50.41	-1.98	1.98
BZ83N	Seebreze Bridge	4688.7	3506.6	965.3	571.3	0.270	0.05	-3.078	-30.78	30.78	-3.25	3.25
AUC63K	Aucilla Bridge	4328.3	3626.9	-160.3	1502.9	0.151	-0.21	-3.332	-33.32	33.32	-3.00	3.00
B1-76F	Choctawhatche Bridge	5251.1	3389	111.7	-297.9	0.286	0.05	-2.845	-28.45	28.45	-3.52	3.52
PR5R2	Choctawhatche Bridge	6337.9	5708.3	713.5	3777.6	0.102	-0.25	-4.828	-48.28	48.28	-2.07	2.07
B8-97R2	Choctawhatche Bridge	8312.8	7291.1	1625.4	-928.8	0.377	0.16	-2.691	-26.91	26.91	-3.72	3.72
B14-89R2	Choctawhatche Bridge	7144.5	6375.7	859.1	1537.4	0.238	-0.05	-2.800	-28.00	28.00	-3.57	3.57
B17-94R2	Choctawhatche Bridge	2904.7	2483.8	842	-1515.5	0.446	0.44	-4.730	-47.30	47.30	-2.11	2.11
PR35FIN	Choctawhatche Bridge	5709.8	5624	1159.1	-772.8	0.345	0.17	-3.090	-30.90	30.90	-3.24	3.24
B23-76F2	Choctawhatche Bridge	6795.9	6487	-485.4	1853.4	0.143	-0.18	-3.899	-38.99	38.99	-2.56	2.56
B27-63F	Choctawhatche Bridge	5008.1	3975.9	420.5	114.7	0.253	0.03	-3.231	-32.31	32.31	-3.09	3.09
								Averages	-33.67	33.67	-3.15	3.15

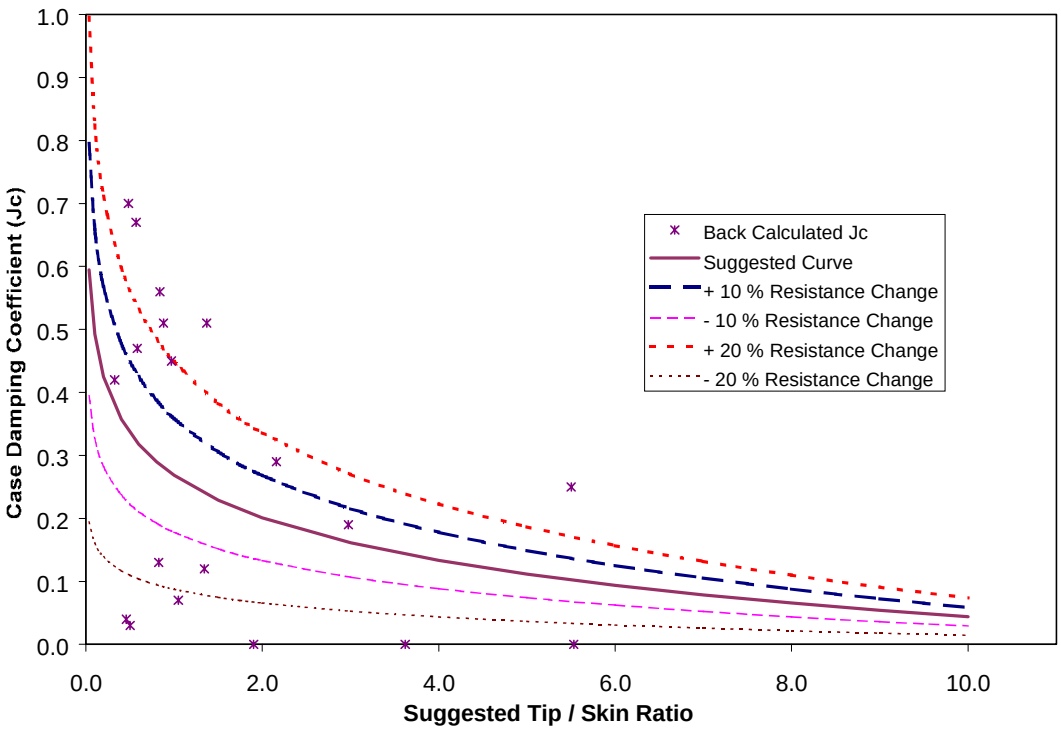

Figure 7-14. Case Damping Coefficient J_c Sensitivity Analysis Results

CHAPTER 8

DEVELOPMENT OF NEW FIELD INSTRUMENTATION

Currently, the Florida Department of Transportation (FDOT) recommends the use of the Pile Driving Analyzer (PDA instrumentation system) for dynamic testing of piles. Approximately 10% of the piles (Test Piles) in a foundation system are dynamically tested with the PDA (90% of the production piles in the foundation system are untested). The information from the Test Piles are used together with GRLWEAP and CAPWAP software to produce a driving criteria and production pile length for the rest of the production piles.

Without discrediting the immeasurable benefit of the PDA, several shortcomings in its application should be pointed out. The PDA is a very expensive (software, hardware, instrumentation) package to license and operate (> $70,000). Operation of PDA requires a well-trained engineer/technician. Moreover, the test is intrusive to the construction process, as it requires a technician to climb the leads to attach the sensors to the pile (close to the pile head). This is dangerous for the technician and delays the driving procedure, sometimes by about two hours. Finally, among several capacity assessment theories available, the PDA field unit only uses the CASE method for total capacity with no estimate of skin and tip resistances. This eliminates the possibility of using other dynamic methods for capacity assessment (Total, Skin, and Tip).

Recent new technology developed for LAN computer systems has made it possible to design and build new equipment for dynamic load testing and pile monitoring. Using state of the art in wireless communication technology, the equipment (Figure 8-1) transmits acceleration and strain information from the pile to a laptop computer in real time (10,000 readings/sec) for storage and signal processing (capacity assessment: total, skin and tip). Because of its small size,

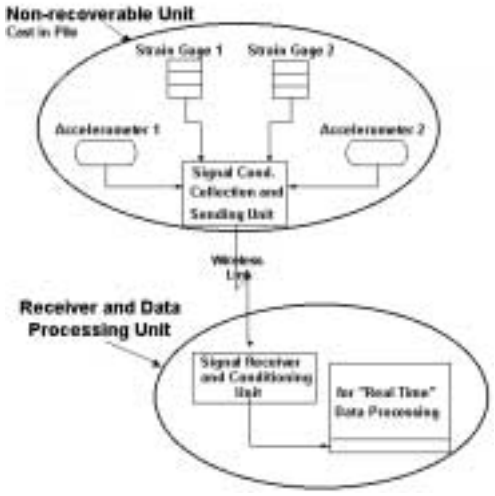

Figure 8-1. System Concept

low cost (instrumentation and transmitter), the equipment may be permanently cast in the pile. The latter does away with the consuming process of sensor installation, as well as climbing the pile leads to attach cables to the pile head which now occurs with standard PDA site work.

Due to the low cost of the new system, it would be possible to monitor every pile in the foundation, removing all uncertainty and eliminating the need for a driving criterion for production piles. Furthermore, the transducers could be installed in different locations along the pile axis. Example of the latter is at the pile tip (Figure 8-2), which would develop a clear differentiation between tip and skin resistances. Another use would be determining pile damping for improved static pile capacity assessment.

The equipment is separated into two major components (Figure 8-1): a **Non-Recoverable Unit** embedded in the concrete pile, and a **Receiver and Data Processing Unit** used to recover the information from the first unit and process it. Figure 8-1 depicts the system and Figure 8-2 schematically shows its operation.

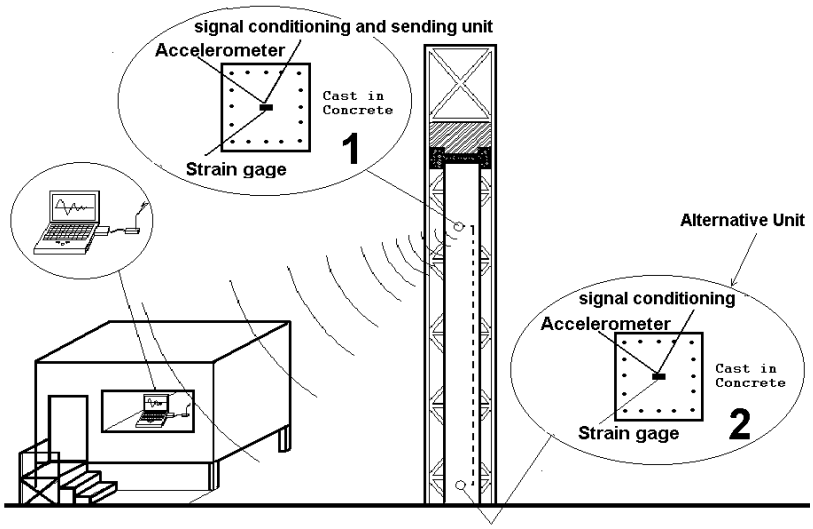

Figure 8-2. System Operation

The non-recoverable unit is composed of two accelerometers, two strain transducers, a signal conditioning unit and a sending unit with antenna (Figure 8-3 (a)). Every component is embedded in the pile including the antenna, which is mounted flush to the pile face.

The receiver and data processing module consists of three independent apparatus (Figure 8-3(b)), a receiver and conditioning unit, a data acquisition card, and a laptop computer with built in acquisition and data processing software. This entire unit is portable and can be placed up to 150 m (500 ft) away from the pile head (from transmitter antenna). A more in depth description of each component is presented in Chapter 10.

The acquisition and data processing software, called *Pile Monitoring*, controls the data acquisition card, retrieves the sensors signals, processes and presents the information, records it, and provides pertinent information about pile capacity and pile damage according to methods that will be described in Chapter 7. A detailed description of this software is given in Chapter 9.

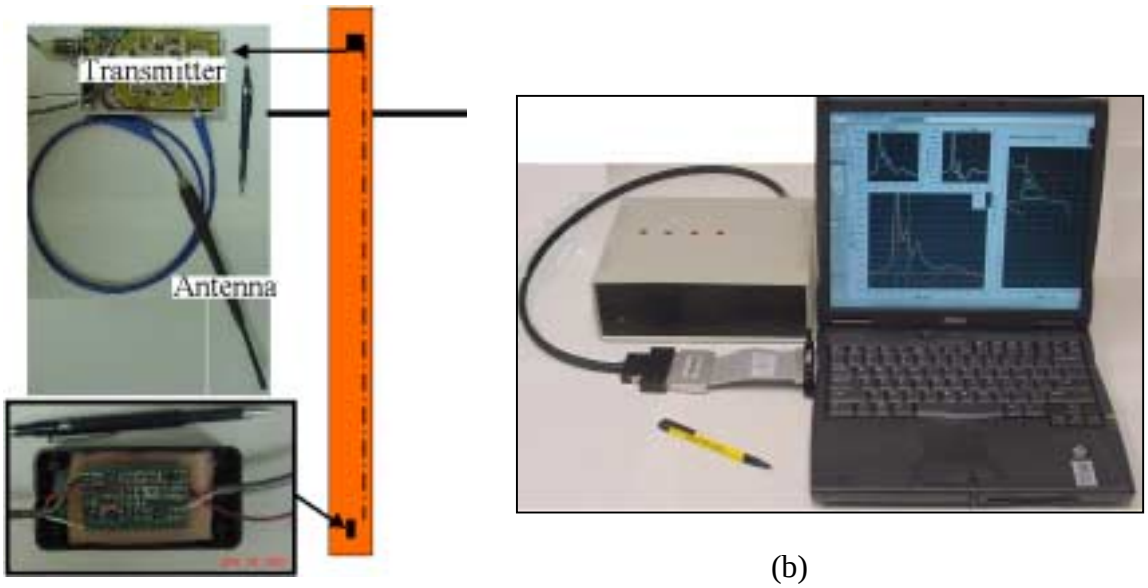

(a) (b)

Figure 8-3. Stress Wave Acquisition Device (a) Non-recoverable Unit (b) Receiver and Data Processing Unit

In addition to the CASE method for capacity determination, used by the PDA, other capacity methods are implemented in the software. These methods, encouraged by the Federal Highway Administration (FHWA) and the State Transportation Department, are the Paikowsky Energy method (FHWA) and the recently proposed University of Florida Method (UF Method). Next a brief discussion of the instrumentation (strain gauges and accelerometers) requirements will be presented.

CHAPTER 9

INSTRUMENTATION REQUIREMENTS FOR DYNAMIC TESTING EQUIPMENT

The new Instrumentation system should be composed of transducers, Signal Conditioning, and an apparatus for recording, reducing and displaying data. This chapter covers the ASTM D4945 requirements and the currently used apparatus, PDA, characteristics. A summary of all the requirements is presented later in this chapter.

TRANSDUCERS

According to ASTM specifications, the transducers should be capable of independently measuring strain and acceleration versus time at a specific location along the pile axis. For this purpose, at least two strain gages and two accelerometers should be used, as shown in Figure 9-1 (One accelerometer and one strain gage on one side and another accelerometer and strain gage on the opposite side). The latter is to eliminate bending. Also, the instrumentation should be securely attached so they do not slip.

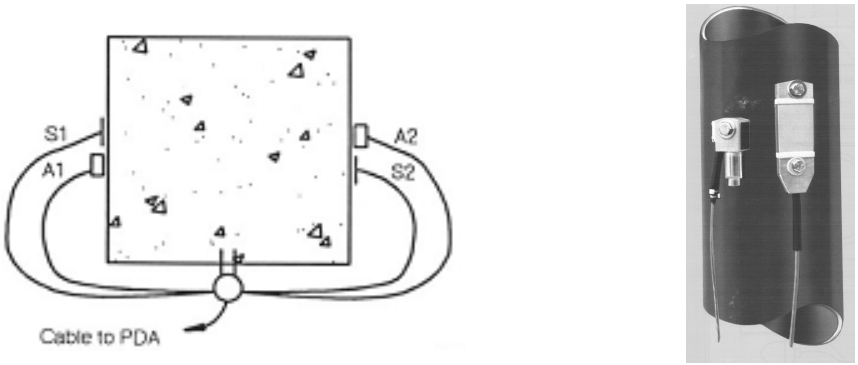

(a) (b)

Figure 9-1. PDA Strain Gages and Accelerometers (a) Installation Top View (b) Installation Side View

Force or strain transducers shall have a linear output over the entire range of possible strains, and their natural frequency higher than 2000 Hz. Acceleration, velocity or displacement transducers can be used to determine velocity, through the integration of acceleration records or derivation of displacements measurements with respect to time. These calculations should be automatically performed by an apparatus for reducing data.

Accelerometers should have a resonant frequency above 2500 Hz and their output shall be linear to at least 1000g ($g = 9.81\ m/sec^2 = 32.2\ ft/sec^2$) and 1000 Hz when used in concrete piles. If DC accelerometers are used, they should be damped with low pass filters having a minimum frequency of 1500 Hz.

The transducers should be calibrated to an accuracy of 3% through the applicable measurement range.

SIGNAL CONDITIONING

ASTM requires that the signal conditioning for force and velocity have equal frequency response curves to avoid relative phase shifts and relative amplitude differences. Signal conditionings are electrical circuits that provide power to the sensors, transforming the sensor's signals to an analog format, and increasing the amplitude of signal (gain) if required.

SIGNAL TRANSMISSION

ASTM specifies that the signals from transducers shall be transmitted to the apparatus for recording, reducing, and displaying data by means of cable or equivalent in such a way that electronic or other interferences are not limited.

APPARATUS FOR RECORDING, REDUCING AND DISPLAYING DATA

Signals from the transducers shall be recorded electronically in either analog or digital format with frequency components below 1500 Hz. The digitalization sample frequency shall be

at least 5000 Hz for each transducer channel. The apparatus for reducing data might be an analog or digital computer capable of providing signal conditioning, amplification, and calibration factors for the transducers. If strain gages are used the apparatus shall be capable of computing force from them. In the case of accelerometers, the apparatus shall integrate acceleration to obtain velocity. If required, the apparatus shall zero the Force and Velocity between impact events to account for the changing of zero offset (zero drift).

Signals from the transducers might be displayed on a LCD graphics screen in terms of Force (P) and Velocity (Z*Vel) for each hammer blow. The apparatus shall be capable of holding and displaying the signal from each selected blow for a minimum period of 30 seconds.

DATA QUALITY CHECK

The confirmation of data quality is a two step procedure. First, the force (P) and Velocity (Z*Vel) should be compared at the moment of impact for proportionality agreement. Ideally, these values should be identical but differences of 10% or less are usually acceptable. The second step is a consistency check, for this, Force and Velocity Traces of consecutive impact events are compared for repeatability (ASTM D 4945).

PILE DRIVING ANALYZER (PDA) EQUIPMENT

The Pile Driving Analyzer equipment, PDA, complies with ASTM D4945 (Standards for High-strain Dynamic Testing). It has been used worldwide for more than 30 years and it is recommended by the FDOT for Dynamic Load testing and Dynamic Pile Monitoring. The PDA is composed of accelerometer and strain transducers (Figure 9-1b), which are connected by cables to a PC based apparatus, Model PAK that processes the incoming signals.

The sensors, which are specially manufactured for this application, are attached to the pile by means of bolt connections, and are recovered after each test. The strain and acceleration

within the pile are transferred to the sensors by friction between the pile face and friction humps on the transducers. The force provided by the bolts guarantee enough frictional resistance for this purpose. Table 9-1 presents the properties of these transducers.

Table 9-1. PDA Sensors Specifications (PDA Manual)

Strain Gage	
Effective Length (mm)	50
Size (mm)	115 x 35 x 11
Material	Aluminum
Circuit	Full Bridge
Sensitivity (με/mV/V)	380
Strain Range (με)	2000
Shock Range (g)	5000
Operating Temperature Range ^{o}C	-50 to 120
Piezo Electric Accelerometer	
Circuit	Integral Impedance Converting Electronics.
Sensitivity (mV/g)	1
Acceleration Range (g)	5000
Frequency Range (Hz)	0.25 to 7000
Operating Temperature Range ^{o}C	-50 to 120
Piezoresistive Accelerometer	
Circuit	Full Bridge
Sensitivity (mV/g)	0.07
Acceleration Range (g)	10000
Frequency Range (Hz)	3
Operating Temperature Range ^{o}C	-50 to 90

The PAK is a PC based Pentium computer with special electrical components built into it. These elements include: signal conditioners for 4 accelerometers and 4 strain gages, analog

integrators to obtain velocity from accelerometers, amplifiers, low-pass filters, and eight 12-bit analog to digital converters that sample 8 channels simultaneously. A built in software is used to calculate and display Force and Velocity Traces, pile capacity, pile stress during driving, and damage detection. It also performs data quality checks and internal calibration. The amount of data recorded in the PAK is limited to 860 blows (14.09 Mbytes).

The PDA manual states that no accelerometer is perfect at all frequencies, therefore the velocity curve may not always return to zero at the end of the blow, in this instance, the PDA would perform a velocity adjustment. In this adjustment the entire Velocity Trace is rotated with reference to a pivot point (20 ms on the trace) until the last recorded Velocity (at 1024 ms on the trace) becomes zero.

The PAK is suited with various modes to record the Force and Velocity Traces; among them the most important is the CAPWAP format. This format is intended to reduce hard drive storage memory and is used for the final step of dynamic testing (matching the recorded traces with the modeling software CAPWAP).

A brief description of the CAPWAP format is shown in Figure 9-2. On this Figure, Force (P) and Velocity (V*Vel) are transformed to FOR and VEL using Equations 9-1 and 9-2 respectively. Then FOR and VEL are transformed to integers and stored in that form. Column 1, in Figure 9-2, contains the values of FOR and VEL obtained from such equations, while columns 2 to 11, contain the relative increase (FOR or VEL) with respect to the previous column.

$$VEL := (Z \times Vel) \times 100 / Z = Vel \times 100 \tag{9-1}$$

$$FOR := (P) \times 100 / Z \tag{9-2}$$

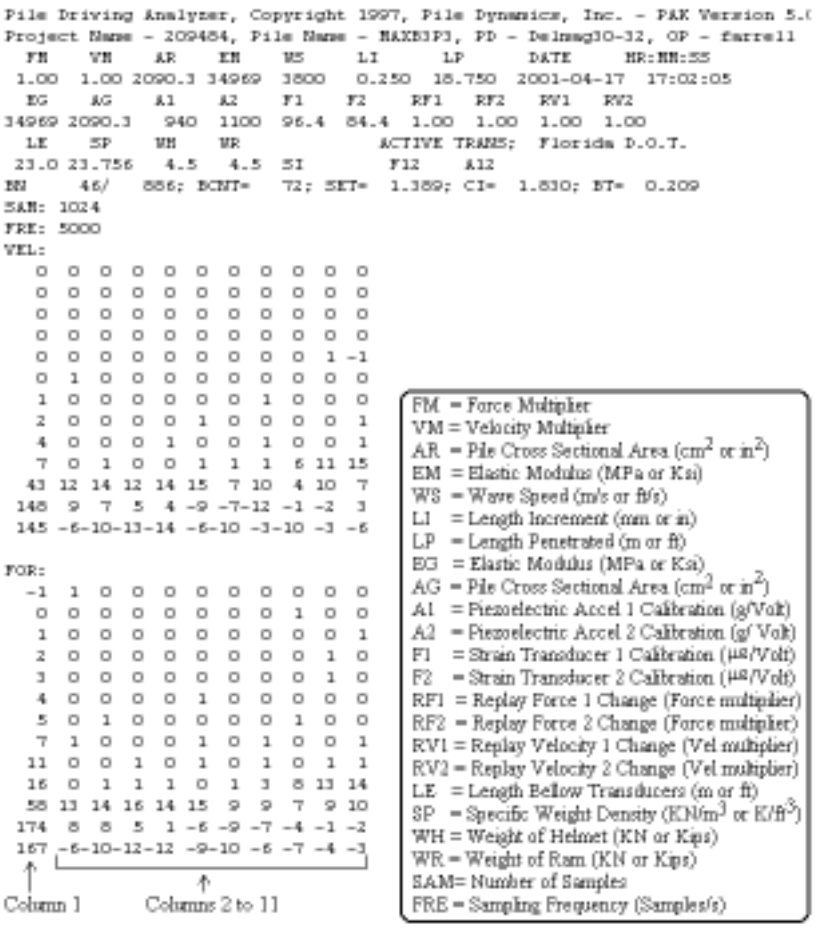

Figure 9-2. CAPWAP Format (incomplete file)

SUMMARY OF REQUIREMENTS AND SUGGESTIONS

Table 9-2 presents a summary of the identified requirements plus some suggestions. The requirements are the provision by ASTM, and the suggestions include some of the PDA characteristics. It should be noted that the PDA is not only used for concrete piles, but also for steel piles, which are out of the scope of this report. Some assumptions have also been taken in this table: the maximum pile length is 33 m (100 ft), the maximum driving time is 4 hours, and the prestress level might be zero if the sensors are located close to the pile ends (transfer length).

This is important because the proposed strain gages will be embedded in the concrete (they will measure the prestress in the concrete and wave stresses, summed together).

Table 9-2. Summary of Requirements and Suggestions

	Requirements and Suggestions	Source
Improvements	Non-Intrusive: no leads, no setup, etc.	
	Monitor Force and Velocity at the tip of the pile	
	Assess pile Stresses (for damage) at top and bottom of pile	
	Determine both Skin and Tip Resistance (Scour)	
	Use PDA Case method, Paikowsky and UF methods	
	Minimum expertise required (automatic)	
	Cheap: Monitor every pile – Elimination of Driving Criteria	
Mounting	Non-recoverable should be securely mounted before concrete is poured	Concrete pouring procedure
	Non-recoverable unit temperature resistance up to 160^{o}F (Concrete curing)	
	Non-Recoverable unit should withstand stresses due to the concrete pouring	
	Instruments should be properly aligned and in the proper direction	

Table 9-2. Summary of Requirements and Suggestions (Cont.)

	Requirements and Suggestions	Source
General	Real time capacity assessment and pile monitoring	ASTM D4945
	Non-Recoverable unit should withstand stresses up to 30.9 MPa and -11.5 MPa	FDOT Current Practice
	Sensor's operating temperature form -50 to 120 ^{o}C	PDA System
	Strain gage range at least 1014 με το -377.9 με	FDOT Current Practice
	Strain gage should have a linear output	ASTM D4945
	Strain gage natural frequency above 2000 Hz	ASTM D4945
	Strain accuracy of 2.14 με	Signal Characteristics
	Minimum strain gage effective length of 50 mm	PDA System
	Accelerometer resonant frequency above 2500 Hz	ASTM D4945
	Accelerometer should have a linear output up to at least 1000g and 1000 Hz	ASTM D4945
	Acceleration accuracy of 5.1 g	Signal Characteristics
	Accelerometer sensitivity of 1 mV/g or smaller value	PDA System
	Low Pass filter minimum frequency of 1500 Hz	ASTM D4945
	Sensor calibration to 3% accuracy	ASTM D4946
	Signal conditioning of both sensors should have same frequency response	ASTM D4947
	Minimum sampling frequency of 5000 Hz for each channel	ASTM D4948
	Testing duration of 4 hours and reuse at 72 hours after driving	FDOT Current Practice
	Minimum data transmission distance of 34 m (110 ft)	FDOT Current Practice
	Sensors have to be attached 2 to 3 diameters below the pile top	FDOT Current Practice
	Use at least two accelerometer and two strain gages	ASTM D4948
	Signal displayed in an LCD screen at least for 30 seconds	ASTM D4949
	Perform real time data quality tests	ASTM D4950
	Use simultaneous 12 bit A/D converters for signal digitalization	PDA System
	Record traces in digital format	ASTM D4950
	Minimum storage capacity of 860 blows	PDA System
	Store Data in CAPWAP Format	PDA System
	Present recovered data over a period of 0.1024 seconds and the acceleration signal sent after 0.02 sec.	Signal Characteristics

Non-recoverable unit is the instrumentation package to be permanently embedded in the pile.

CHAPTER 10

SIGNAL CHARACTERISTICS

The final product with any new instruments, conditioners, and data transfer is a signal. Knowing the ranges of signal for both the strain and acceleration are required to capture the whole signal. Consequently, this chapter focuses on past signals recovered from earlier FDOT projects. The twenty-two PDA traces studied were the signals used in Chapter 7 (Table 7-1 and 7-2) for the development of skin and tip resistance capacities. The latter signals were used to find signal characteristics such as frequency response, amplitude, and signal accuracy.

FORCE AND VELOCITY TRACES

The Force and Velocity Traces are not exactly the same with each other, as shown in Figure 10-1 and 10-2. However, the trends in Force Trace from one pile to another are similar, as well as the trends in Velocity Trace for the different piles. This similarity as well as amplitudes is studied for the twenty-two piles.

From all the Force Traces, Figure 10-1, their average (thick line) was found. Similarly, the average Velocity Trace (thick line) is shown in Figure 10-2. Maximum values:

Maximum Force = 8312.968 KN (1868.83 Kips)
Maximum Velocity (Z*Vel) = 8730.061 KN (1962.60 Kips)
Minimum Force = -1240.337 KN (-278.84 Kips)
Minimum Velocity (Z*Vel) = -4278.126 KN (961.76 Kips)

General observations were that the maximum Force and maximum Velocity values are very similar and are located at the beginning of the trace. Also, the Velocity shows a high negative value after the peak, indicative of a tension wave coming back up the pile.

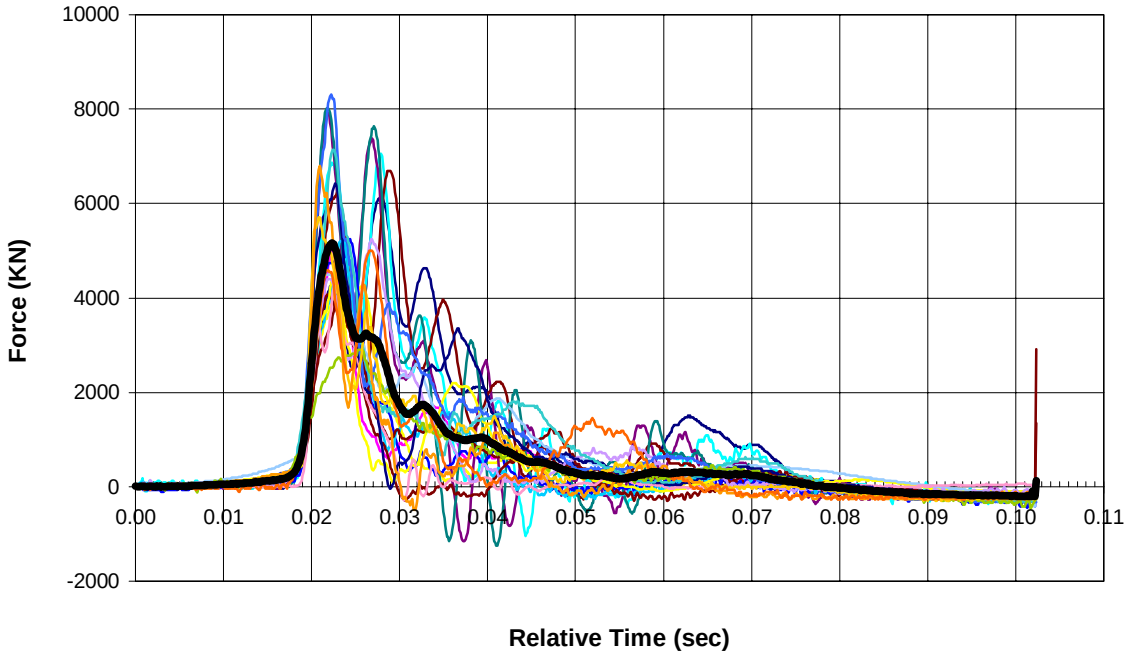

Figure 10-1. PDA Force Traces of 22 Piles in PILEUF

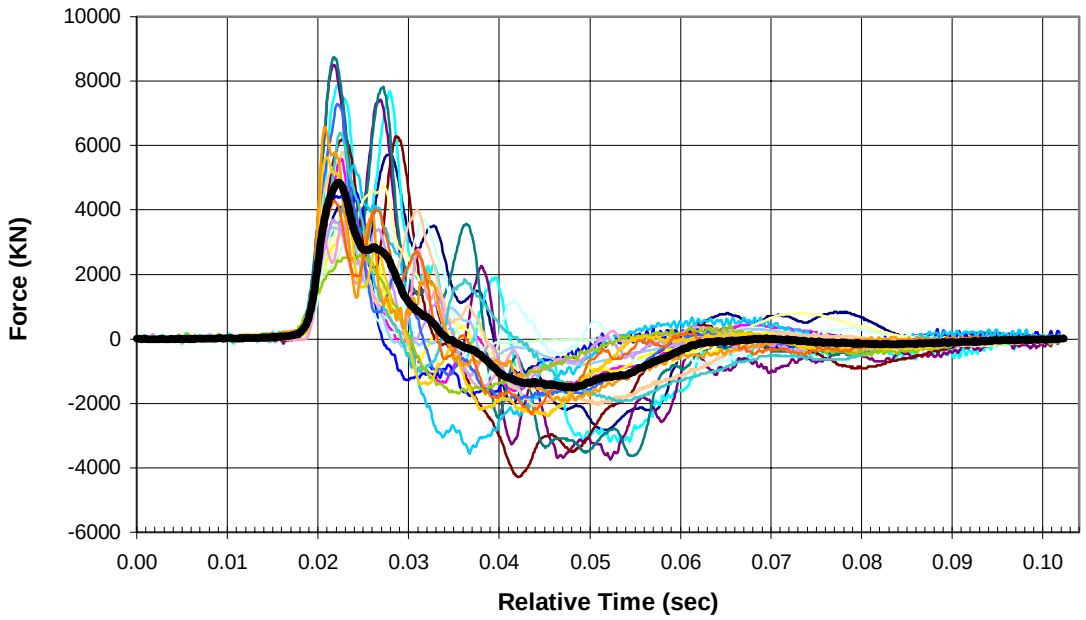

Figure 10-2. PDA Velocity (Z*Vel) Traces for 22 Piles of PILEUF

Other observations were both of the Force and Velocity Traces start at a zero value and increase to a maximum value, after which their magnitude decreases almost to a null value. From this behavior it can be inferred that the stress wave is still traveling through the pile but with very small amplitude. The difference between Force and Velocity Traces is that the Velocity Trace decreases to a value smaller than zero before the stress wave vanishes.

Every trace was composed of 1024 discrete data points distributed uniformly in a time period of 0.1024 seconds. It is interesting to note that $2^{10} = 1024$, making the data very suitable for performing a Fast Fourier analysis (FFT) (discussed later). Also, this short time period contains all the necessary information for obtaining pile capacities (from a single blow), hammer efficiency, and pile damage.

Figure 10-2 shows a more consistent initiation of the stress wave than Figure 10-2. The Velocity Traces start at 0.016 seconds, while the Force Traces start somewhere between 0.01 and 0.018 seconds.

The information presented was originally obtained from strain gage and accelerometer output signals. The raw signal may be obtained using the reverse procedure. The raw signals (voltage) will serve as a guide for instrumentation adequacy, data acquisition, and electrical circuitry requirements.

STRAIN AND ACCELERATION TRACES

Strain and acceleration traces can be back calculated from Force and Velocity Traces by using simple structural and dynamic equations as described in Chapters 5-7. PDA traces are discrete points; therefore, the following equations (discrete format) are used:

$$\varepsilon_i = \frac{P_i}{E \times A} \qquad \text{(10-1a)}$$

$$a_i = \frac{1}{2 \times Z} \times \left[\left(Z \times Vel_{i+1} - Z \times Vel_i \right) + \left(Z \times Vel_i - Z \times Vel_{i-1} \right) \right] \times SamplingRate \qquad (10\text{-}1b)$$

where: P_i Force (from Force Trace)

E Modulus of Elasticity of Pile

A Cross Sectional Area of Pile

Z Pile Impedance E*A/c

c Wave Speed

Vel_i Velocity (from Z*Vel/Z)

Sampling rate = usually 10,000 samples/second

Figure 10-3 shows the strain and acceleration traces obtained by this procedure using the PDA traces that were shown in Figures 10-1 and 10-2. Values of E, A, Z and c, have been obtained from Table 7-1.

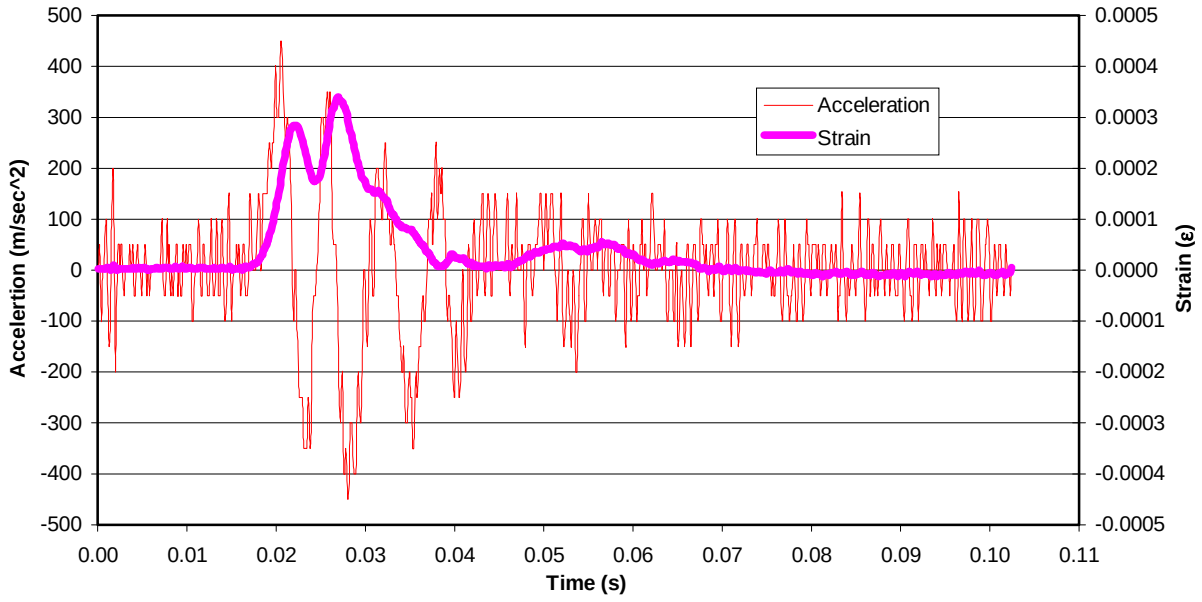

Figure 10-3. General Form of Strain and Acceleration Traces

The thick line in Figures 10-4 and 10-5 again represents the average among the 22 traces in each Figure. It will subsequently be referred to as average-strain and average-acceleration.

The average-strain curve has a similar shape to the 22 individual strain traces. The average-accelerometer curve does not closely follow the same trend as the individual ones, nevertheless, its shape is very similar over the fist 0.025 seconds. Over this period, the wave return is observed even for the longest pile under study (Table 7.1: 2L/c = 2*34.45/4325 = 0.016sec). Consequently, both average traces will be used as the representative curves for future reference.

From these figures some additional and valuable information can be recovered as:

Maximum Strain = 0.0006036 = 0.60364 mε

Minimum Strain = -0.0000654 = -0.06547 mε

Maximum Acceleration = 1400 m/s^2 = 142.71g

Minimum Acceleration = -1200 m/s^2 = -122.32g

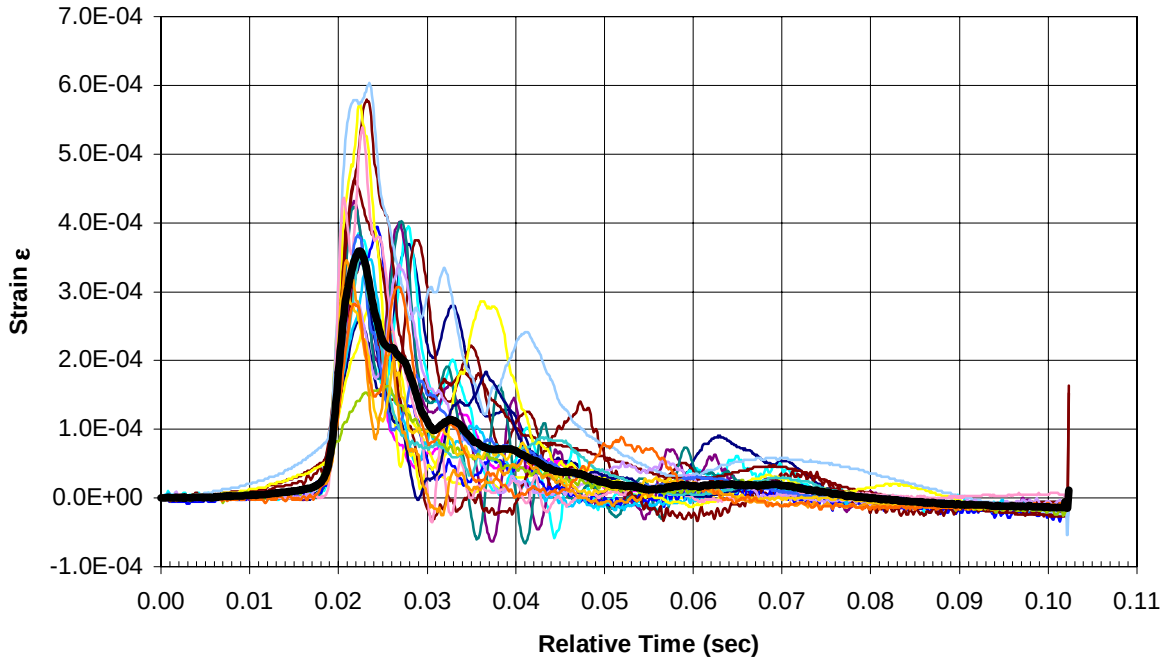

Figure 10-4. PDA Strain Traces for 22 Piles of PILEUF

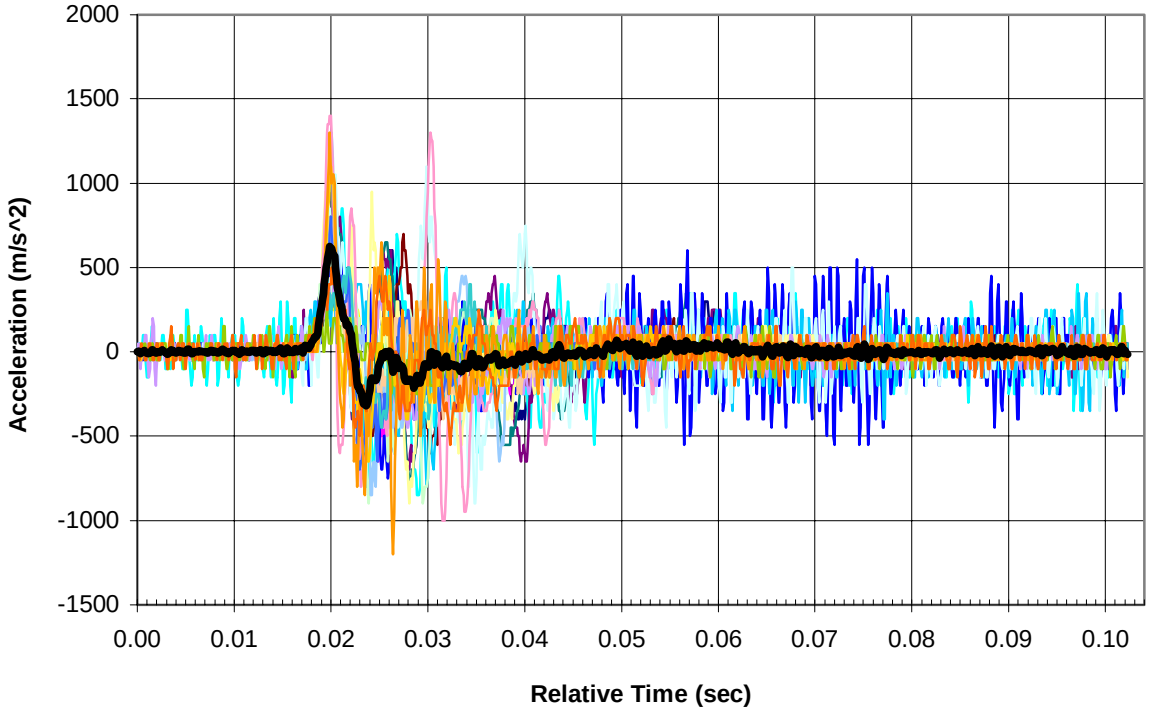

Figure 10-5. PDA Acceleration Traces for 22 Piles of PILEUF

ACCURACY OF STRAIN AND ACCELERATION MEASUREMENTS

The accuracy of the acceleration and strain measurements is the main factors that control the accuracy of Force and Velocity Traces and further calculations (including pile capacities). These values are calculated from the traces obtained in the last section.

The strain and acceleration plots shown in Figures 10-4 and 10-5 are discrete series of points with their accuracy defined as the minimum increase/decrease between two consecutive data points (zero increase not considered). The following equation is used for this intention:

$$\Delta\varepsilon_i = \varepsilon_i - \varepsilon_{i-1} \qquad \text{and} \qquad \Delta a_i = a_i - a_{i-1} \tag{10-2}$$

where: ε_i Strain (from Figure 10-4)

a_i Acceleration (from Figure 10-5)

Using this equation with the information shown in Figures 10-4 and 10-5, the relative change is obtained for strain and acceleration. The results are presented as a cloud of points in Figures 10-6 and 10-7 for strain and acceleration respectively. These clouds of points are organized in horizontal groups. The same distance separates the groups in the vertical direction. This distance is the minimum relative increase and may be considered as the accuracy (very repetitive), and was found to be:

Strain accuracy = 2.137με

Acceleration accuracy = 5.097g

It is important to point out that the above analyzed accuracy is applicable only to the 22 piles in the database and not to the PDA equipment. As described in the PDA section, the PAK (PDA) is available with various modes to record the Force and Velocity Traces; among them the CAPWAP format (Figure 9-2) that was used for the 22 piles in the database. This type of format alters the accuracy of the measured signal (Equations 9-1 and 9-2).

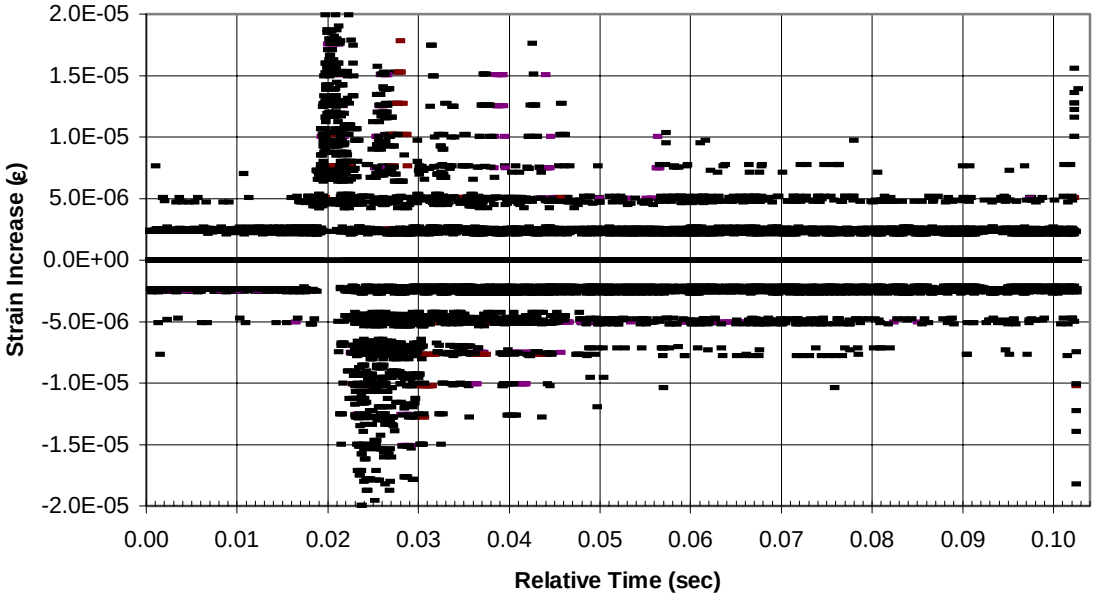

Figure 10-6. Strain Increase for 22 Piles in Database

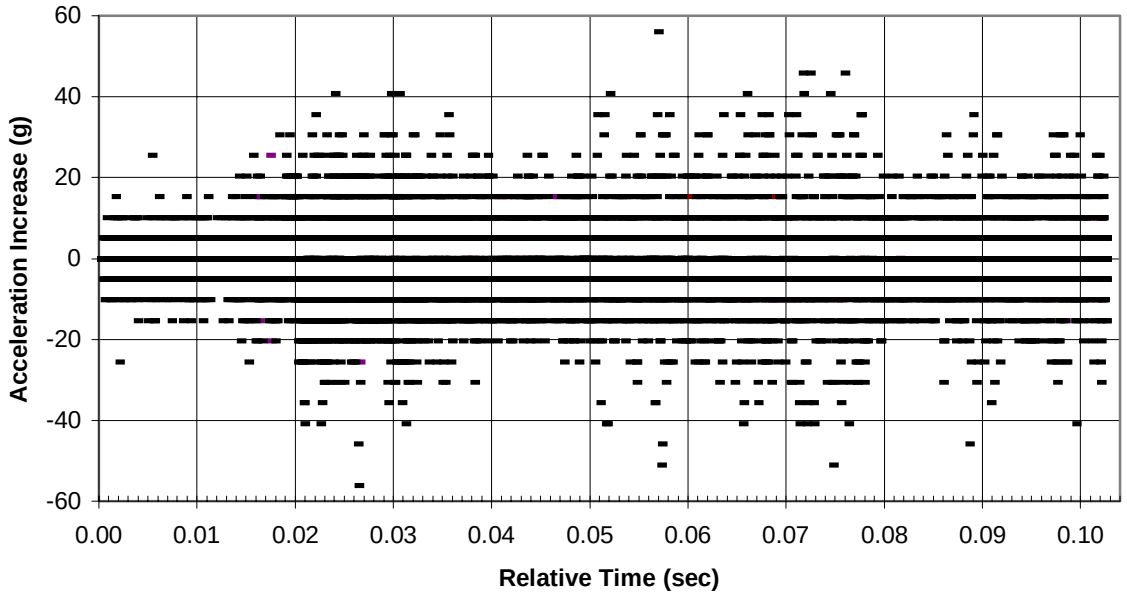

Figure 10-7. Acceleration Increase for 22 Piles in Database

It should be noted that the PDA PAK does not measure acceleration. The PAK is supplied with analog integrators to transform the accelerometer output into velocity, which is subsequently digitized for further analysis. Therefore, the above mentioned acceleration-accuracy is questionable, and should be used carefully. Nevertheless, that accuracy will be used as a reference point for the proposed instrumentation.

The same can be said about the strain accuracy. Even though the PDA strain-measurements are altered by storing this information in the CAPWAP format, this distorted accuracy is further used to assess the pile capacities in CAPWAP software. Since the output of this software is accepted in practice, the calculated strain-accuracy will also be used as a reference point. A more in depth analysis of the strain-accuracy reveals that this value equals the inverse of the wave speed times 100 (Equation 9-2).

FREQUENCY OF STRAIN AND ACCELERATION TRACES

The frequency of the acceleration and strain traces, Figures 10-4 and 10-5, was calculated using Fast Fourier analysis (FFT). This analysis was performed in LabVIEW for the 22 traces, and is presented in Figures 10-8 and 10-9 for strain and acceleration respectively. Disregarding small amplitudes, the useful frequency content was found to be:

Strain: 0 to 300 Hz

Acceleration: 10 to 3,000 Hz

Within these ranges, the significant values are those with the highest amplitude, and are referred as the predominant periods. They are the major contributor to the signal, which make up the strain and acceleration traces (Figures 10-4 and 10-5). It is found, from Figures 5-8 and 5-9, that these frequencies are concentrated within narrow ranges:

Major Strain frequency content: 5 Hz and 30 Hz (highest at 10 Hz)

Major Acceleration frequency content: 10Hz -500 Hz, 1,100Hz - 1,700Hz.

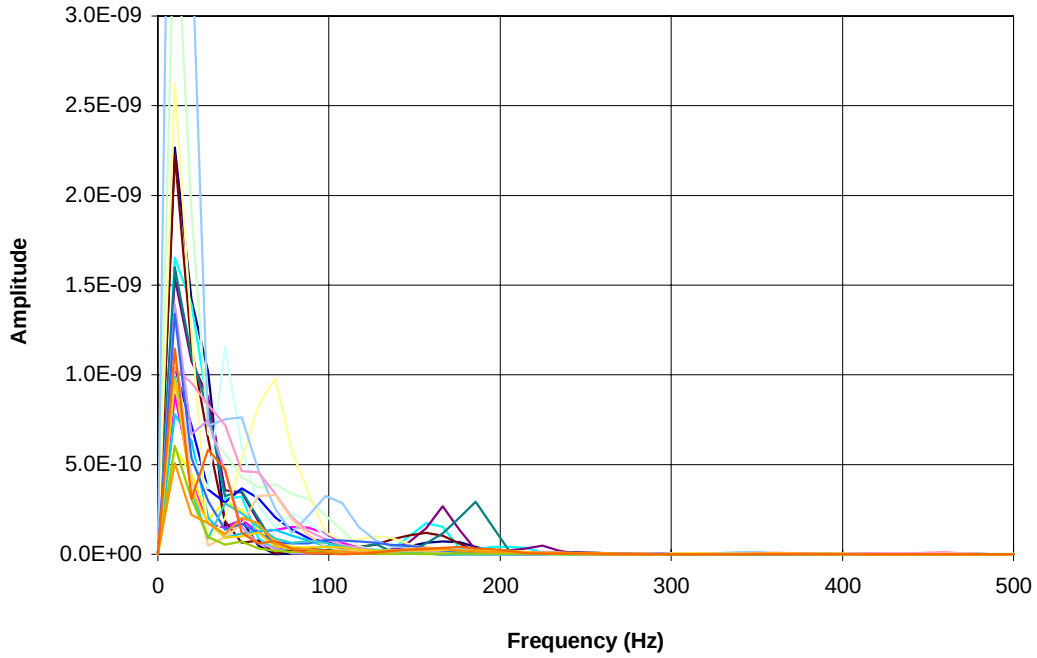

Figure 10-8. FFT Strain for 22 Piles in Database

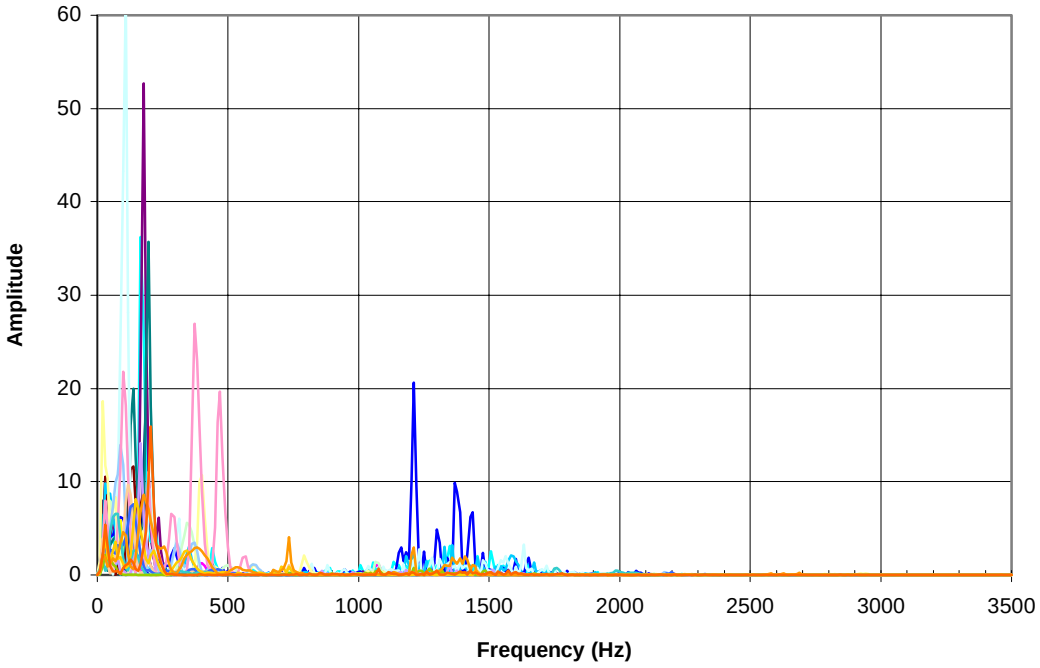

Figure 10-9. FFT Acceleration for 22 Piles in the Database

ACCELEROMETER AND STRAIN GAGE OUTPUT TRACES IN TERMS OF VOLTAGE

The raw product from most types of instruments is voltage, which is directly correlated to the intended measurement. When it's linearly proportional to the physical action being measured, the constant factor is called sensitivity.

The sensitivity of the sensors used in each one of the 22 piles in the database was required in order to obtain strain and acceleration traces in terms of voltage. Unfortunately, the sensitivity values were not recorded in the database. Nevertheless, the sensors used by PDA are of a standard type, with sensitivity values close to a nominal value provided by the PDA brochure, shown in Table 9-1. From the table, the nominal strain gage sensitivity is 380 με/mV/V,

and the accelerometer nominal sensitivity is 1.0 mV/g or 0.07 mV/g, (for a piezoelectric accelerometer and piezoresistive accelerometer, respectively).

It will be assumed that the excitation voltage for the strain gage is 10 Volts. This is a common value and provides a stable signal in terms of noise immunity (i.e., signal to noise ratio). Furthermore, a perfectly linear transducer response will be assumed for the analysis; but it be should remembered that the latter is particularly not true for piezoelectric accelerometers.

The analog traces for the 22 files were calculated, and are plotted in Figures 10-10, 10-11, and 10-12. They correspond to the standard PDA strain gage, piezoelectric accelerometer, and piezoresistive accelerometer. Using the sensitivity values given above, the traces were calculated as follows:

$$\varepsilon_i = \frac{P_i}{E \times A} \tag{10.3a}$$

$$a_i = \frac{1}{2 \times Z} \times \left[\left(Z \times Vel_{i+1} - Z \times Vel_i \right) + \left(Z \times Vel_i - Z \times Vel_{i-1} \right) \right] \times Samplin\ Rate \tag{10.3b}$$

It is clear, that the traces in Figures 10-10, 10-11, and 10-12 have the same shape as the strain and acceleration traces in Figures 10-4 and 10-5 (but the magnitudes are different). Therefore, the shape and frequency characteristics, pointed out earlier, are applicable to the analog traces. Additional information from Figures 5-10, 5-11, and 5-12 were:

Maximum Strain gage Output = 0.01588 Volts
Minimum Strain gage Output = -0.001723 Volts
Maximum Acceleration Output = 0.1427 Volts
Minimum Acceleration Output = -0.1223 Volts

The general trend of the traces shown in Figures 10-4 and 10-10 shows that up to 0.0045 seconds the strain in the pile is almost zero. The peak strain value is recorded between 0.02 seconds and 0.025 seconds. Finally, after 0.09 seconds the strain goes back to zero, or close to it.

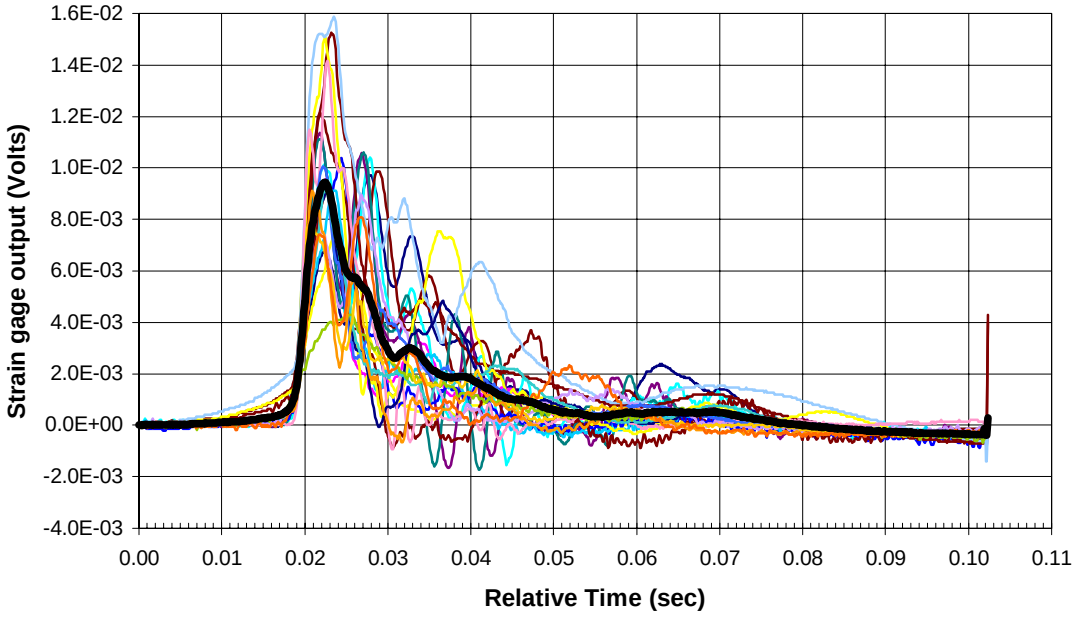

Figure 10-10. PDA Strain Gage Output for 22 Piles in Database

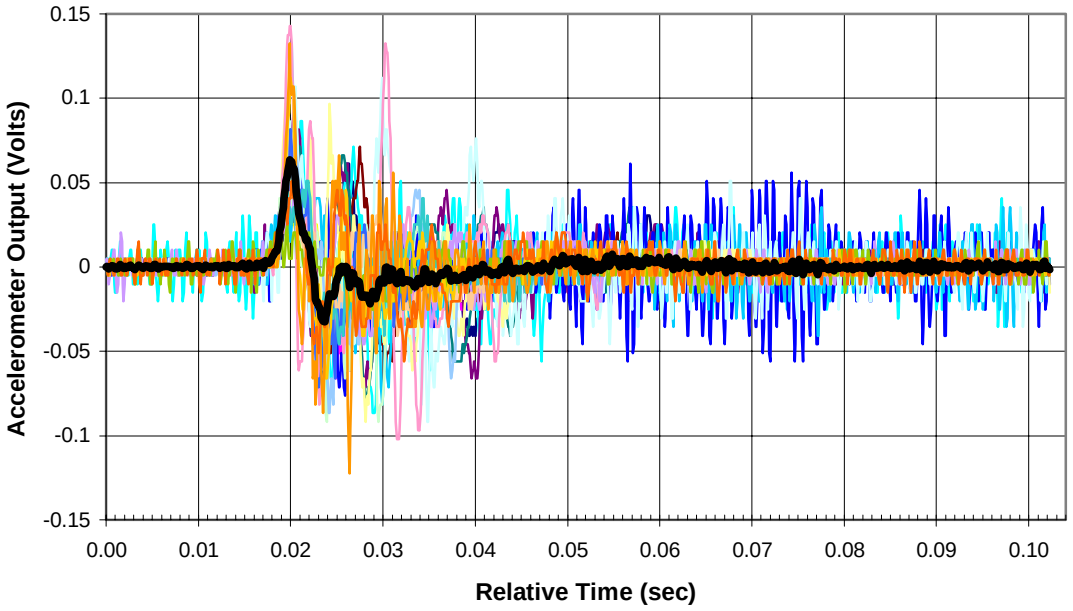

Figure 10-11. PDA Piezoelectric Accelerometer Output for 22 Piles in Database

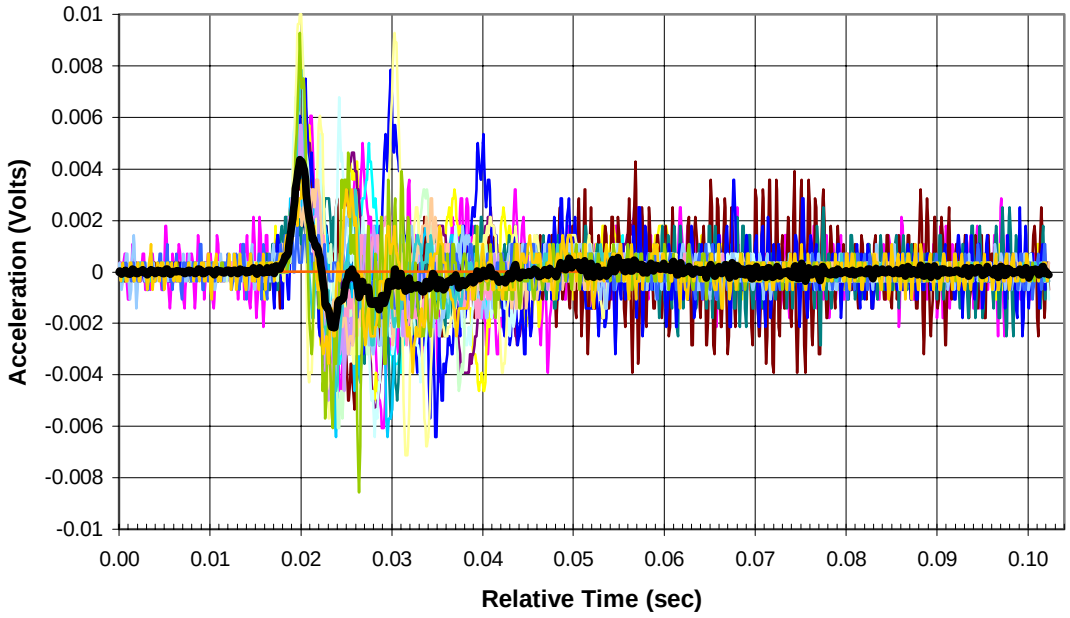

Figure 10-12. PDA Piezoresistive Accelerometer Output for 22 Piles in Database

In Figures 10-5, 10-11, and 10-12 the traces show that the peak acceleration is located between 0.19 seconds to 0.21 seconds. Most of the acceleration traces present two peak values within this time frame.

CHAPTER 11

THE NEW WIRELESS ANALYSIS PACKAGE (WAP)

A new wireless analysis package for driven pile has been developed and is shown in Figure 11-1. The package has been designed to satisfy the requirements stated in Chapter 4, with applicability to the current practice (Chapter 9).

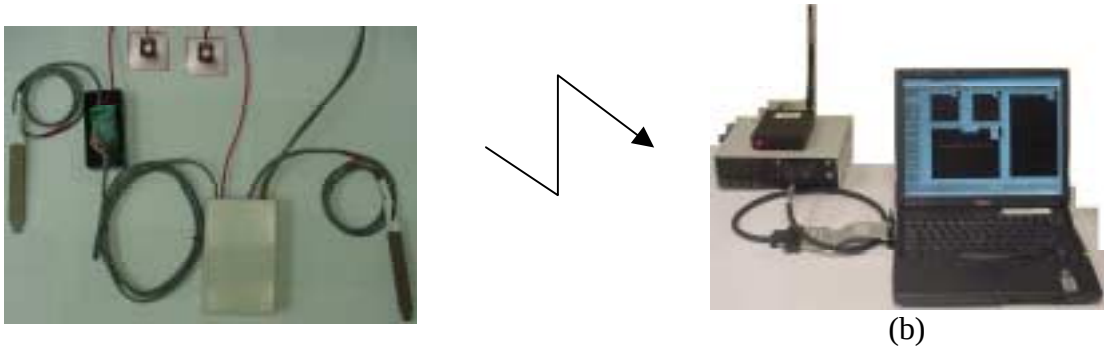

(a) (b)

Figure 11-1. New Instrumentation System (a) Non- Recoverable Unit; (b) Signal Receiver and Data Processing Unit

To achieve the improvements stated in Table 9.2 the system is physically divided into two modules, which communicate, by a wireless link. One of the modules is called **Non-Recoverable Unit** (Figure 11-1a). This unit is capable of being embedded in concrete piles and broadcasting stress wave information to the second module (for data processing) during installation. Since the Non-Recoverable Unit is pre-installed in the pile, no installation setup is required at the time of driving. The second module receives the information from the Non-Recoverable Unit to calculate Force Traces, Velocity Traces, and pile capacities. This module is called **Receiver and Data Processing Unit** (Figure 11-1b). The cost of the Non-Recoverable unit is

below $300. The cost of the Receiver and Data Processing Unit is $6,400 and it may be used in other tests.

In this chapter, the two units are presented in more detail. Some aspects, such as the electrical design, will be avoided since the system is protected by patent law and disclosure agreements. Nevertheless, a detailed explanation of their operation is given as well as a description of their installation.

NON-RECOVERABLE UNIT

The Non-Recoverable Unit is shown in Figure 11-1a. This unit gathers six components that will be described independently:

- Two strain gages
- Two accelerometers
- A Signal Conditioning and Sending Unit
- Antenna

Since the unit is designed for installation in concrete piles, it must withstand harsh environments. Examples of the latter are hydration temperatures of 70^{o}C (160^{o}F); damage in the casting process by portable concrete vibrators; and possibility of high shock and vibration (200g and 3,000Hz) during the driving process. A brief discussion on system preparation (signal conditioning and sending unit) is presented later.

Strain Gages

Micro-Measurements Group Inc manufactures the selected strain gages, Model EGP-5-120. These transducers (Figure 11-2) are specifically designed for measuring mechanical strains inside concrete structures. They have a foil-sensing grid that is protected by a rugged outer concrete resin. This body is used to resist mechanical damage during concrete pouring and provides protection from moisture as well as corrosive attack. The strain gages are provided with a three-

Figure 11-2. Special Purpose Embedment Strain Gage EGP-5-120

conductor cable, intended to eliminate thermal effects on the cable. See specifications in Table 11-1.

Table 11-1. Strain Gage Specifications, Requirements, and Recommendations

Strain Gage	EGP-5-120	Requirements	Recommendations
Resistance (Ohms)	120 + /- 0.8	-------	-------
Gage Factor	2.05 + /- 1	-------	-------
Effective Length (mm)	100	-------	> 50
Size (mm)	17 x 130 x 10	-------	115 x 35 x 11
Material	Concrete Resin	no aluminum	-------
Natural Frequency (Hz)	not available	> 2000	-------
Shock Limit (g)	> 200	-------	5000
Circuit	Quarter Bridge	-------	Full Bridge
Excitation Voltage	2.5	------	10
System Sensitivity (με/V)	313.5	-------	380
Strain Range (με)	1561	-------	2000
Strain Accuracy (με)	3.13	------	< 2.14
Calibration Accuracy (%)	4.74	< 3	-------
Linear Output (με)	1,100 to –461	1,014 to –377.9	-------
Operating Temperature Range ^{o}C	-45 to 55	------	-50 to 120
Maximum Temperature Range ^{o}C	> 70	> 70	------

The outer protective concrete resin has a modulus of elasticity of 11,031 Mpa ($1.9*10^6$ psi) which is approximately one third of the minimum specified for the FDOT piles. The latter ensures that the protective body will deform properly while providing protection to the measuring grid. Furthermore, this protective body is dimpled to provide a good bonding/mechanical interlocking with the surrounding concrete.

The measuring grid, 100 mm (4 in) length, offers a good span to measure strain in aggregate materials such as concrete. The grid is made of nickel-chromium alloy, similar to Karma. A good fatigue life and excellent stability characterize this material, which is required for our dynamic measurements. It is also self-temperature compensated to minimize thermal effects on the output signal.

A quarter bridge configuration, with 5.0 volt DC excitation, is used with the strain gage. Further details on the electrical conditioner for this transducer and placement in the pile, are presented later.

Accelerometers

A piezoelectric accelerometer, manufactured by Endevco was selected for this application (Figure 11-3). This is a rugged, low-cost, high-performance, transducer that requires no electrical power for operation. It meets the ASTM requirements for dynamic testing (Chapter9) and its specifications are presented in Table 11-2.

The accelerometer is composed of piezo electric crystals inside an alumina case with two thick film gold connectors. Its output is characterized by a linear charge that is transformed to DC voltage by a charge converter circuit in the **Signal Conditioning and Sending Unit**.

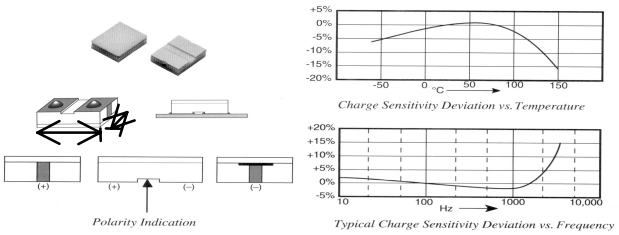

(a) (b)

Figure 11-3. Endevco Accelerometer (a) Characteristics (b) Size Compared with a Mechanical Pencil

Table 11-2. Accelerometer Specifications, Requirements, and Recommendations

Accelerometer	Endevco	Requirements	Recommendations
Material	Alumina	-------	-------
Charge Sensitivity (pC/g)	2	-------	-------
Transverse Sensitivity (%)	5	------	-------
Resonant Frequency (Hz)	10000	> 2500	40000
Frequency Range (Hz)	10 to 2000	-------	0.25 to 7000
Acceleration Range (g)	1000	1000	5000
Circuit	Charge Converter	-------	Integral Impedance Converting Electronics
System Sensitivity (g/V)	93.22	-------	1000
Acceleration Accuracy (g)	2.7	>5.1	------
Calibration Accuracy (%)	4.43	< 3	-------
Linear Output (g), (Hz)	+/-1000, 1000	1000, 1000	-------
Operating Temperature Range ^{o}C	-65 to 150	-------	-50 to 120
Maximum Temperature Range ^{o}C	> 150	> 70	-------

The accelerometer is connected to the Signal Conditioning and Sending Unit with a thin, but high-resistant, coaxial low-noise cable (manufactured by Endevco). Its major task is to eliminate electrical noise and spurious signals generated by stressing the cable (as the stress wave

passes through). Unacceptable signal generation was observed on regular coaxial cables during slight bending.

The size of the Endevco accelerometer makes it ideal for pile driving application because it displaces a very small volume of concrete. However, its size also makes it difficult to properly mount and align it inside the pile. Therefore, an enclosure (3.81*3.81cm*1 cm) was fabricated with the transducer installed in it (Figure 11-4b). Besides providing the means for alignment, this enclosure protects the transducer (harsh and humid environment), as well as waterproofing it. Moreover, the enclosure acts as a mechanical filter to eliminate frequencies above 3,000 Hz. The latter guarantees that the accelerometer will not be subjected to frequencies close to and above 10,000 Hz (natural frequency of accelerometer) and associated zero shifts.

(a) (b)

Figure 11-4. (a) Accelerometer Mounting Technique; (b) Protective Enclosure

Signal Conditioning and Sending Unit

The **Signal Conditioning and Sending Unit** is shown in Figure 11-5. This unit is used to provide power source to the sensors, condition the sensors, filter background noise, digitize the signal, and send the information to the **Receiver and Data Processing Unit**. The characteristics of the Signal Conditioning and Sending Unit are presented Table 11-3.

(a) (b)

Figure 11-5. Signal Conditioning and Sending Unit (a) To be used at the pile top; (b) Alternative tip sensor's conditioners.

The unit encloses a number of electrical systems, which are contained in a single plastic box:

- Three 9-Volt batteries
- Power control board
- Two Strain Gage Conditioners
- 2 Accelerometer Conditioners
- Digitalization and Data Encoding circuit
- Transmitter

These elements can be gathered, according to their task, into four components that will be described next. The plastic box is filled with a liquid epoxy, which hardens after 24 hours. This compound protects, as well as supports all the electrical elements during the shock and vibration of pile driving. Also, the compound is temperature retardant which eliminates dynamic thermal effects on the electronic part from rapid changes in temperature during the driving process.

Table 11-3. Signal Conditioning and Sending Unit Specifications, Requirements, and Recommendations

Signal Recovery and Transmission	Specifications	Requirements	Source
Transmission	Real time	Real time	ASTM D4945
Type of transmission	Digital		
Carrier Frequency (MHz)	908/922 Unlicensed	Unlicensed	FFCC
Selectable Carrier Frequencies	8 Channels		
Antenna Type	Whip Style		
Antenna Size (cm)	23		
Transmission distance (m)	152	$\geq$ 34	FDOT Current Practice
Stress Limits inside the pile (MPa)	Eliminated with Foam	-11.5 to 30.9	FDOT Current Practice
Low Pass filter for both conditioners (Hz)	5,000	$\geq$1,500	ASTM D4945
Sampling frequency per channel (Hz)	10,000	5,000	ASTM D4948
Operation time (Hours)	6	$\geq$6	FDOT Current Practice
Power Supply	Three 9-Volt Batteries		
Power Saving	Automatic turn on-turn off		
Accelerometer Channels	2	$\geq$ 2	ASTM D4947
Strain Gage Channels	2	$\geq$ 2	ASTM D4948
Digitalization Accuracy (bits)	15	$\geq$ 12	PDA System
Signal digitalization	Simultaneously	Simultaneously	PDA System
Max. Temperature (Concrete Curing)	> 70 ^{o} C (160 ^{o} F)	$\geq$ 70 ^{o} C (160 ^{o} F)	FDOT Current Practice
Concrete resistant (%)	100	100	FDOT Current Practice
Size (mm)	146*89*25.4		
Cost ($)	<200		

Batteries.

Three 9 Volt batteries are used to provide DC power for a minimum period of 12 hours. The selected batteries were Lithium for two reasons. First, the electrical circuits had to have a

minimum voltage, as well as a significant active and dormant life. Second, the batteries had to survive the casting process and the associated thermal rises due to hydration and possible steam curing. To help with the active life cycle, three 9-Volt batteries, connected in parallel were selected which provided at least 7.1 Volts for 12 hours. For the second issue, temperature, of the 15 companies approached only one would guarantee battery survival for temperatures of 70°C (160°F) expected during the concrete hydration.

Power control board.

Since the concrete aging process may take 28 days, and the dynamic testing may last for 72 hours (EOD vs. BOR), the recording process (strain and acceleration) could not be continuous. Since the pile driving process as well as restrike will be less than a few hours, it was decided to shut down the system in order to preserve the batteries when in inactivity (i.e. not driving). Consequently, a Power Control Board (electrical circuit) was built into the unit, which activated the system with the first strike and turned the system off if another strike was not received within 3.5 minutes. A waiting period of 3.5 minute was selected due to the possibility of set checks and/or forms of pile inspection at End of Driving. It should be noted that the first blow, which turns the system on, has incomplete strain and acceleration data.

Strain gage conditioners.

The strain gage conditioners use a quarter bridge configuration, analog amplifier, and low pass filter. Its size is 76.2*28.6*3.2 mm^3 (3*1.125*0.125 in^3), and shown in Figure 11-6. The entire conditioner works with a 5-Volt DC input, and outputs the signal in analog format from 0 to 5 Volt.

The conditioner was developed with economy and accuracy in mind. In particular, the excitation (5-volts DC) was selected to reduce power consumption. However the 0-5 volts

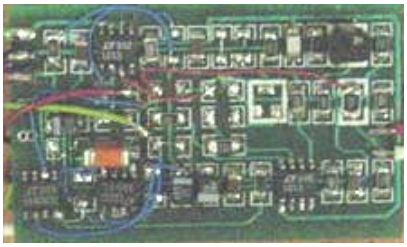

(a)

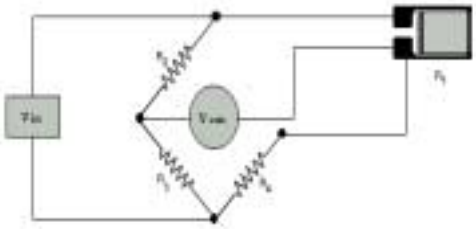

(b)

Figure 11-6. Strain Gage Conditioner (a) Entire Circuit Board; (b) Quarter Bridge

output signal was significant enough to eliminate or minimize background noise, and improve the signal quality.

The bridge is composed of four resistors: two 5 KΩ, one 120Ω and the 120Ω strain gage. The thermal coefficients of these resistors match each other so that the bridge maintains balance.

The common practice of using potentiometers on the bridge was found unacceptable due to their instability under thermal variation and vibration conditions. In addition, they may generate a dynamic signal on the strain gage channel, as well as result in drift of the signal beyond the sampling limits (0 to 5 volts).

Since the output signal from the bridge by itself is very low, an analog amplifier was used to introduce a gain factor of 1,000. This value is intended to accommodate the expected strain in the 0 to 5 Volts range. The signal is subsequently filtered with a 5,000 Hz low pass filter.

Accelerometer conditioners.

The accelerometer conditioning uses a charge converter, an analog signal amplifier, and low pass filters of the same type as the strain gage conditioner. Its size is $73 \times 28.6 \times 3.2$ mm^3

($2.88 \times 1.125 \times 0.125$ in.^{3}) and is shown in Figure 11-7. The entire conditioner works with a 5 Volts DC input voltage, and outputs the signal in analog format from 0 to 5 Volts.

Figure 11-7. Accelerometer Conditioner

The charge converter is a standard circuit recommended by Endevco to convert the accelerometer output from Pico-Coulombs to DC voltage. Background noise on this signal is minimized using a 5,000 Hz low pass analog filter. The signal is amplified by a factor of 100, using an analog amplifier, to bring the expected acceleration signals within 0 to 5 Volts.

Digitalization and data encoding.

The analog signal provided by the two-accelerometer conditioners and two strain gage conditioners, is transformed to a digital format. The four analog signals are sampled simultaneously using four sample-and-hold analog circuits. They deliver the information sequentially (Channel 1, 2, 3, 0) to a single Analog to Digital converter (A/D converter) of 16 bit resolution. The A/D converter works with a 40,000 Hz clock in order to provide a sampling rate of 10,000 Hz in each one of the four channels. The input and output range is from 0 to 5 Volts.

The digital data complies with TTL format and uses Manchester encoding technology. TTL is a digital format that defines voltages from 0 to 1.5 Volts with 0 logic level, and 3.5 to 5 Volts as 1 logic level. Manchester guarantees logic levels change for every bit time, and has a

self-clock generation (Figure 11-8) at the receiver end, that will be used to properly decode the data.

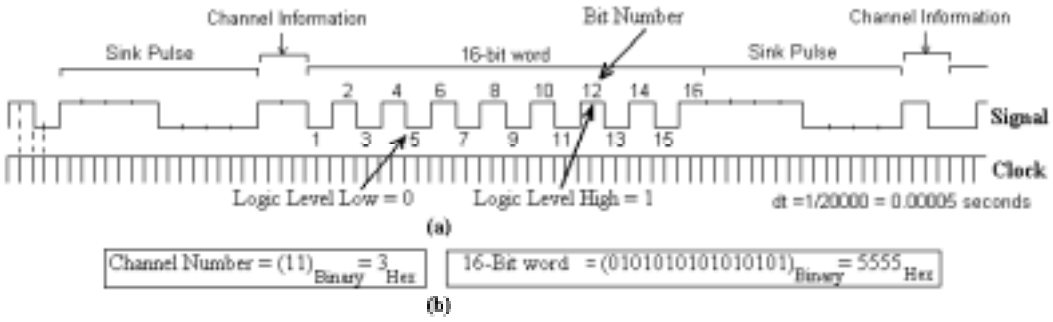

Figure 11-8. Digital Data String (a) TTL Format; (b) Numeric Format

The digital signal is further improved by introducing a Sink Pulse and two additional digital levels. The Sink Pulse introduced on the signal, as shown in Figure 11-8, defines the start of the 16–bit word (one sample in one channel). Two digital levels are then added right after the sink pulse to carry channel information. This is necessary in order to separate the four signals at the receiver.

Transmitter.

A digital transmitter, T900V (Figure 11-9), manufactured by Applied Wireless is used for this application. This transmitter was selected on the basis of affordability and its high band width (5 MHz). Transmitting in the 908/922 MHz unlicensed band, this transmitter is capable of broadcasting up to 5 Mbps of information. The actual speed used is 1.04 Mbps (described in the previous section) for which the signal is both stable and immune to noise interference. The transmission distance can reach up to 150 m (500 ft) but it was tested only up to 45 m (150 ft).

The transmission frequency can be pre-selected among 8 different values, ranging from 908 to 922 MHz. With the latter, multiple piles and systems may be working in close proximity with another without interfering with each other's signal.

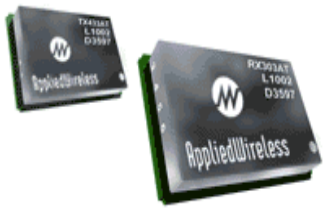

Figure 11-9. Digital Transmitter T900V, from Applied Wireless

In the development stages, the manufacturer was concerned that the crystal component might be damaged under high shock vibrations. Nevertheless, they were confident that a foam enclosure would provide sufficient energy absorption to ensure the continuous function of their device. As will be discussed in the next chapter, the latter will be proven true.

Transmitter Antenna

The transmitter antenna is a flexible 23 cm (9 in) quarter whip style antenna, shown in Figure 11-5a. A rubber membrane protects it, which is resistant to the concrete environment, corrosion, UV rays, water, and pile handling. It is also detachable so that it can be replaced. This antenna is connected to the transmitter with a thick coaxial cable.

RECEIVER AND DATA PROCESSING UNIT

The Receiver and Data Processing Unit is shown in Figure 11-1b. This unit can be located up to 150 m (500 ft) from the transmitter antenna (Non-Recoverable Unit in pile) and still receive and decode a signal.

The Receiver and Data Processing Unit is made of several components and will be described separately:

- Receiver Antenna
- Receiver and Conditioning Unit
- Data Acquisition Card
- Laptop Computer
- Data Acquisition and Processing Software

Receiver Antenna

Different types of antennas can be used for the receiver. In terms of this application which has a directional signal (pile antenna), a directional 1-meter antenna as shown in Figure 11-10a (similar to a TV antenna) was employed. The receiver antenna is mounted separately from the data-conditioning unit and is connected to it through a rugged coaxial 50-Ohm cable. The antenna provides the longest transmission distance, 150 m (500 ft). A smaller antenna may be used (Figure 11-10b) for closer transmission distances, up to 45 m (150 ft). However, it is important to place this antenna in a vertical position in order for it to work properly.

(a)

(b)

Figure 11-10. Receiver Antennas (a) Directional 1 m Antenna; (b) 23 cm Whip Style Antenna

It should be noted that the antenna might also receive unwanted information from other nearby transmitters, etc. However, if the antenna size is reduced, the undesirable noise will also be diminished or eliminated because the broadcast distance is also reduced.

Signal Receiver and Conditioning Unit

The Signal Receiver and Conditioning Unit (Figure 11-11) receives the information from the antenna, decodes the signal, and parses the signal for the Data Acquisition Card. As explained in Figure 11-8, the transmitted signal is arranged in a serial string, with Manchester coding, which involves sink pulses, and channel ID information. Also, the signal needs to be separated into four independent (separate) channels (strain, and acceleration) along with time for the Data Acquisition Card.

All the components of the Signal Receiver and Conditioning Unit are contained in a portable enclosure (Figure 11-11). The components can be grouped into two categories: the digital receiver and the signal conditioning.

Figure 11-11. Signal Receiver and Conditioning Unit

Six LED indicators specify the proper function of the unit. The first (bottom box –Figure 11-11), located at the top middle of box, indicates the unit is powered up. The second (top box – Figure 11-11), shown on the left of the top box indicates the digital receiver is powered up. The remaining four LEDs (upper right box Figure 11-11) indicate the strength of the transmis-

sion signal. If all four LEDs are lit the wireless link is working at optimum antenna location, orientation, etc. However, if none of them are lit then there is a poor signal or no signal at all.

The carrier frequency for signal transmission can be selected with a knob control at the back of the digital receiver. Any of eight available frequencies (from 908 to 922 MHz) may be used. The selection of a different carrier frequency will allow multiple transmitters to be in proximity to one another without interference.

The unit is provided with a 12-Volt commercial Battery and AC plug-in socket. The batteries will work for up to 10 hours, and they can be replaced any time the unit is not operating, or recharged using the AC adapter.

Some precautions when using the receiver with antennae are: 1) The antenna needs to be attached firmly with proper orientation; 2) The antenna should not be touched during the dynamic testing; and 3) The receiver needs to be placed in a stable position. Testing experience with this unit has noted that excessive vibration induces undesired interference (noise) in the dynamic signal.

Digital receiver.

A R900V commercial receiver (Figure 11-11) is used to capture the broadcasted signal. This receiver is manufactured by Applied Wireless to work with the T900V transmitter described in the previous section. This receiver has the same transmission characteristics as the transmitter.

As described before, the information coming out of this receiver includes Manchester encoding technology, sink pulse, and channel ID information in a serial string (Figure 11-8). A clock is also generated to indicate the location of proper data bits. This clock is generated using Manchester technology.

Signal conditioning at the receiver.

Using the digital information, and clock from the receiver, the Signal Conditioning identifies the sink pulses, determines the 16 bit word, and finally separates the bit words in the proper format required for the Data Acquisition Card (Analog and Digital).

For Digital Data Acquisition Cards the signal is arranged in 18-bit parallel strings. The first 2 bits carry the channel information, and the remaining 16 bits carry the digital value of one measurement in one channel. TTL (Figure 11-8) is also used for this information. Two extra lines (request and acknowledgement) are also provided to work with the handshaking mode. Handshaking mode involves an interaction between the Data Acquisition Card and Receiver Conditioning Unit. A low-bit on the request line, generated by the receiver conditioner, informs the Data Acquisition Card that the data is ready to be read. When the Data Acquisition Card has properly read the information, it sends a low-bit to the Signal Condition Unit (using the acknowledge line) reporting that it is ready for the next reading. At this time, the request line is reset to a high-bit, waiting for the next transmitted measurement.

For the Analog card, the digital signal is transformed back into a voltage reference signal and divided into four channels, each one containing the information for one sensor. The output range is from 0 to 5 volts, and it may be changed to cover the sampling range for any specific Data Acquisition Card. To change the signal from digital to analog format, four independent digital to analog converters are used with a 5,000 Hz low pass filter.

Data Acquisition Card

Any analog or digital Data Acquisition Card may be used for this application, provided they have the required speed and resolution. PCMCIA cards are preferred since they are portable

and easily inserted into a Type II slot of a standard laptop computer. Two models are currently used, DAQCard 6533 (digital, Figure 11-12) and DAQP-12 (analog, Figure 11-13).

Figure 11-12. DAQCard 6533 Data Acquisition Card (Digital)

Figure 11-13. DAQP-12 Data Acquisition Card (Analog)

The DAQCard 6533 is a high-speed 32-bit digital I/O Card. The maximum sampling rate is 740 Kbytes/second for 32 parallel lines (digital TLL) of incoming information at 100 Hz (exceeds the required speed and resolution of dynamic pile testing). It is also provided with a 68-pin connector cable, Figure 11-12, which is connected to the Signal Receiver and Conditioning Unit.

The Analog DAQP-12 card, from Quatech, is shown in Figure 11-13. This card allows up to 16 single-ended (8 differential) input channels. The maximum sample rate is 100 KHz, and the resolution is 12 bits. This is more than adequate for this application since the current require-

ment is 20,000 Hz (5,000 Hz in each cannel) with less than 12 bit resolution. The input range is selectable, from 0 to 5 Volts.

Laptop Computer

The laptop computer may be any commercial system, which is fast enough (CPU) to process the incoming data and have sufficient memory (RAM) to hold the data (buffers) for real time analysis and display of all the signals. Also, the machine must have a PCMCIA Type II socket or USB connector for the data acquisition card. Currently a DELL model Latitude C600 computer is used (Figure 11-1b). Its specifications are as follows:

- P-III 800 MHz processor
- 14 inch screen
- 256 MB RAM
- 10 GB HD
- 100 MHz buss speed
- 32 bit resolution
- 24x CD-ROM
- 1.44 MB floppy
- 2 type II PCMCIA slots
- 2^{nd} Lithium ion battery (backup)
- AC adapter

The laptop's batteries will work for 6 hours, slightly less than the Non-Recoverable Unit operation. If further piles were to be tested, extra batteries would have to be used. Another option would be to recharge the batteries. The latter would take 30 minutes to recharge the batteries to their full capacity.

CALIBRATION

The sensitivity of the accelerometers and strain gages is provided by the manufactures. However, as identified from the previous discussion, the signal from the instrumentation is transformed (analog to digital and back) many times before reaching the Data Acquisition Card. Therefore the entire system needs to be calibrated. For this purpose two calibration devices are used (Figure 11-14). These devices simulate strain and acceleration signals of the same characteristics as the proposed transducers. These signals are pre-selected (known) and sent to the Non-Recoverable Unit, to be broadcasted to the Signal Receiver and Data Processing Unit. By knowing the input signal characteristics, the output signal can be calibrated.

(a)

(b)

Figure 11-14. Calibration Equipment (a) Portable Simulator 4830A (b) Precision Calibrator 1550

A Portable Simulator (Figure 11-14a) manufactured by ENDEVCO, the same brand as the accelerometers, was used to calibrate the accelerometer channels. A sinusoidal signal of the same characteristics and sensitivity as the accelerometer chip is generated at any selectable acceleration and frequency. Generating and transmitting a known signal allows its comparison on the laptop computer.

For the strain gage calibration a Precision Calibrator (Figure 11-14b), model 1550 form Measurements Group, was used. It embodies a true whetstone bridge, which provides a known repeatable resistance. For instance, the latter allows a known strain to be sent from the transmitter unit and be compared at the receiver end; this can be done for at least 20 selectable strain values.

The calibration is performed for each strain gauge channel independently from one another. The results are presented in numerical and graphical format in the following pages. This calibration also provides the means to verify the proper function of the proposed system, like output linearity, output range, and accuracy.

The strain gage indicator has selectable strains, but they represent half the strain if a quarter bridge is used (as in our application). The gage factor for this indicator is 2 and the gage factor for the EGP-5-120 is 2.05; therefore, the selected strain on the indicator has to be modified according to the following equation:

$$\varepsilon_{EGP\text{-}5\text{-}120} = (\varepsilon_{Indicator}/2)*2/2.05 \qquad (11\text{-}1)$$

To test the system, the following steps were performed. First, the indicator was substituted in the place of one of the strain gages in the Non-Recoverable Unit. Next, its signal was sent wireless to the Receiver and Data Processing Unit, where the output was stored in the laptop computer as **output** (Volts). The recorded signal had a duration of one second, for which the maximum, minimum, and average values were found. The average value was then plotted versus the calculated strain for the EGP-5-120 and the slope of the trend line is the calibration factor. The following plot (Figure 11-15) shows the process.

STRAIN GAGE #1 CALIBRATION USING STRAIN INDICATOR

Strain of Indicator	Strain of EGP-5-120	Output			Relative Output (respect to 0 με)			Max Output Error	
		Average	Maximum	Minimum	Average	Maximum	Minimum		
με	με	Volts	Volts	Volts	Volts	Volts	Volts	Volts	με
0	0.000	0.30086	0.32119	0.28174	0	0.020328	-0.019119	0.0203	6.37
200	97.561	0.60454	0.6281	0.58027	0.303682	0.327239	0.279407	0.0243	7.61
400	195.122	0.88267	0.92794	0.79403	0.581811	0.627074	0.493171	0.0886	27.79
600	292.683	1.10059	1.20239	0.91712	0.79973	0.901527	0.616258	0.1835	57.52
800	390.244	1.36881	1.50336	1.20289	1.067944	1.202499	0.902031	0.1659	52.01
1000	487.805	1.74217	1.82878	1.54037	1.441311	1.527914	1.239506	0.2018	63.26
1200	585.366	2.12769	2.15877	1.96982	1.82683	1.857912	1.668954	0.1579	49.49
1400	682.927	2.4506	2.47567	2.42514	2.149738	2.174813	2.124276	0.0255	7.98
1600	780.488	2.76449	2.78972	2.73855	2.463623	2.488861	2.437693	0.0259	8.13
1800	878.049	3.10065	3.12443	3.07785	2.799789	2.823567	2.776992	0.0238	7.45
2000	975.610	3.42376	3.44839	3.39815	3.122901	3.147532	3.097292	0.0256	8.03
2200	1073.171	3.74242	3.76858	3.71903	3.441559	3.467717	3.418164	0.0262	8.20
2400	1170.732	4.05886	4.08612	4.03414	3.757997	3.785258	3.733276	0.0273	8.55
2600	1268.293	4.37535	4.39814	4.35237	4.074493	4.097276	4.051504	0.0230	7.21
2800	1365.854	4.69008	4.71438	4.6659	4.389217	4.413519	4.365037	0.0243	7.62
3000	1463.415	4.99766	5.02369	4.97475	4.696795	4.722828	4.673884	0.0260	8.16
3200	1560.976	5.30235	5.32637	5.28184	5.001491	5.02551	4.980974	0.0240	7.53
3400	1658.537	5.42516	5.42642	5.42415	5.124297	5.125559	5.12329	0.0013	0.40
3600	1756.098	5.41818	5.42049	5.41749	5.117316	5.119632	5.116626	0.0023	0.73
3800	1853.659	5.41596	5.41711	5.41559	5.1151	5.116247	5.114732	0.0011	0.36
4000	1951.220	5.41497	5.41662	5.41293	5.114103	5.115759	5.112067	0.0020	0.64
4200	2048.780	5.41193	5.4131	5.41152	5.111073	5.112243	5.110654	0.0012	0.37
4400	2146.341	5.41182	5.41311	5.41166	5.110958	5.112249	5.110796	0.0013	0.40
4600	2243.902	5.41191	5.41305	5.41139	5.111049	5.11219	5.110528	0.0011	0.36

Figure 11-15a. Calibrating the Strain Gauge Equipment

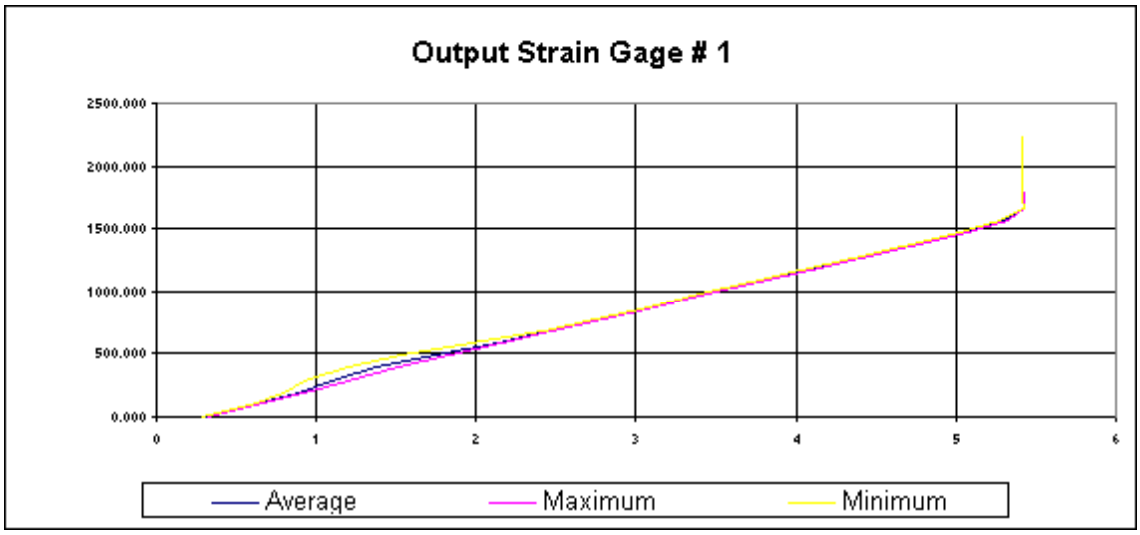

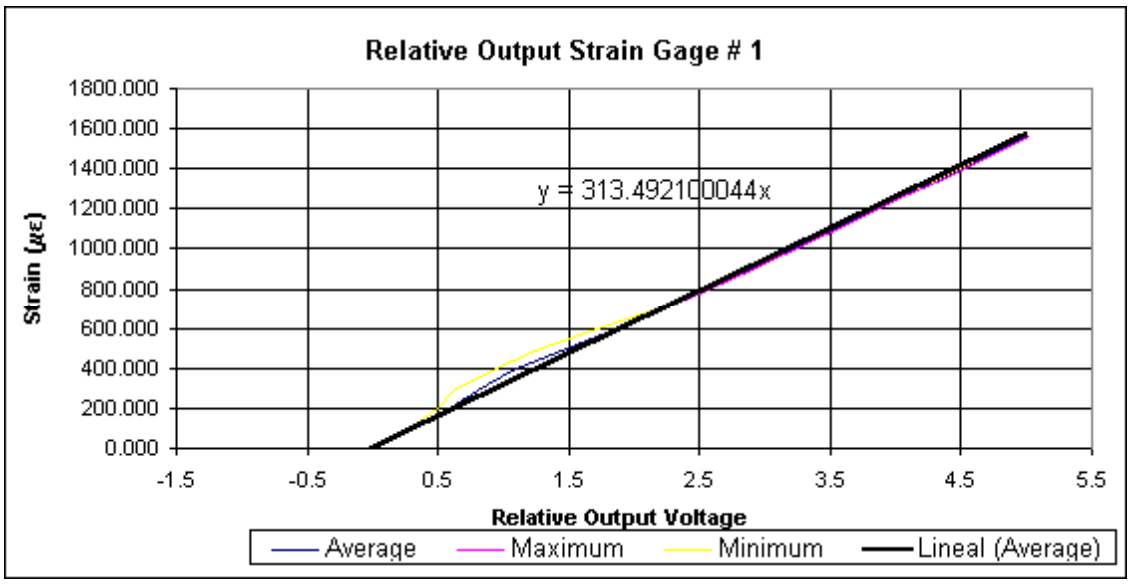

NOTE: The offset is different for the strain gage EGP-5-120

Sensitivity =	**313.49**	**με/Volt**

STRAIN LIMITS BASED ON TANDARD FDOT PILES AND GIDELINES

Maximum expected ε due to driving =	603.64με	=	ΔV =	1.93	Volts
Maximum ε due to prestress =	251.23με	=	ΔV =	0.80	Volts
Maximumε due to prestress and drivability =	1014.07με	=	ΔV =	3.23	Volts
Minimum ε due to prestress and drivability =	-320.84με	=	ΔV =	-1.02	Volts

Overall Output Range =	**4.26**	**Volts**	
Max Error (+/-)=	**63.26**	**με =**	**4.7392 %**

Strain Indicator Used: 1550-A STRAIN INDICATOR CALIBRATOR (From Micro-Measurements)

Fig. 11-15b. Calibrating the Strain Gauge Equipment (continued)

To calibrate the accelerometer equipment, the portable simulator (Figure 11-16) was employed. The frequency and amplitude are selectable, and they are increased from 0 to 1,500 Hz and 0 to +/-250g. The calibration process and data process is the same as the strain indicator.

ACCELEREMOTER #1 CALIBRATION USING ACCELEROMETER SIMULATOR

Induced Acceleration (+/-) g	Induced Frequency Hz	Average Output Offset Volts	Average Among Peak Values ΔV	Maximum Acceleration (Absolute Value V) ΔV	Error Volts
0	0	-0.001258907	0.001258907	0.045127811	0.043869
50	30	-0.001555631	1.003324447	1.062897494	0.059573
50	60	-0.001386824	1.025655778	1.063371477	0.037716
50	100	-0.00116358	1.043060605	1.079769037	0.036708
50	200	-0.001467657	1.048808691	1.08739953	0.038591
50	500	-0.001425273	1.050460419	1.091104024	0.040644
50	1000	-0.00143403	1.041308545	1.093231497	0.051923
100	30	-0.001147773	1.997966151	2.08991668	0.091951
100	60	-0.001169683	2.048700051	2.104543208	0.055843
100	100	-0.001680954	2.081011782	2.1385168	0.057505
100	200	-0.001101422	2.095838708	2.139096332	0.043258
100	500	-0.001070968	2.100534039	2.150723465	0.050189
100	1000	-0.000975458	2.081674582	2.153260382	0.071586
150	30	-0.000960448	3.038234501	3.107254884	0.06902
150	60	-0.000812205	3.05425425	3.129375783	0.075122
150	100	-0.001413189	3.09677124	3.163034283	0.066263
150	200	-0.002037587	3.128117588	3.177588878	0.049471
150	500	-0.001343433	3.127686278	3.183471021	0.055785
150	1000	-0.001424479	3.099656386	3.191732096	0.092076
200	30	-0.001054307	3.937560051	4.098954698	0.161395
200	60	-0.001128641	4.077471123	4.17703298	0.099562
200	100	-0.001704511	4.10906499	4.19019002	0.081125
200	200	-0.002160764	4.138022655	4.200463987	0.062441
200	500	-0.002088994	4.153284008	4.220228642	0.066945
200	1000	-0.001664201	4.115014624	4.236006697	0.120992
250	30	-0.00242682	4.906060003	5.10008307	0.194023
250	60	0.001994552	5.070773265	5.199116288	0.128343
250	100	-0.000384666	5.114732497	5.213848732	0.099116
250	200	-0.000754616	5.165591347	5.237587669	0.071996
250	500	-0.000763443	5.164991672	5.26229808	0.097306
250	1000	-0.001797519	5.11715747	5.270419278	0.153262

Figure 11-16a. Calibrating the Accelerometer Channel

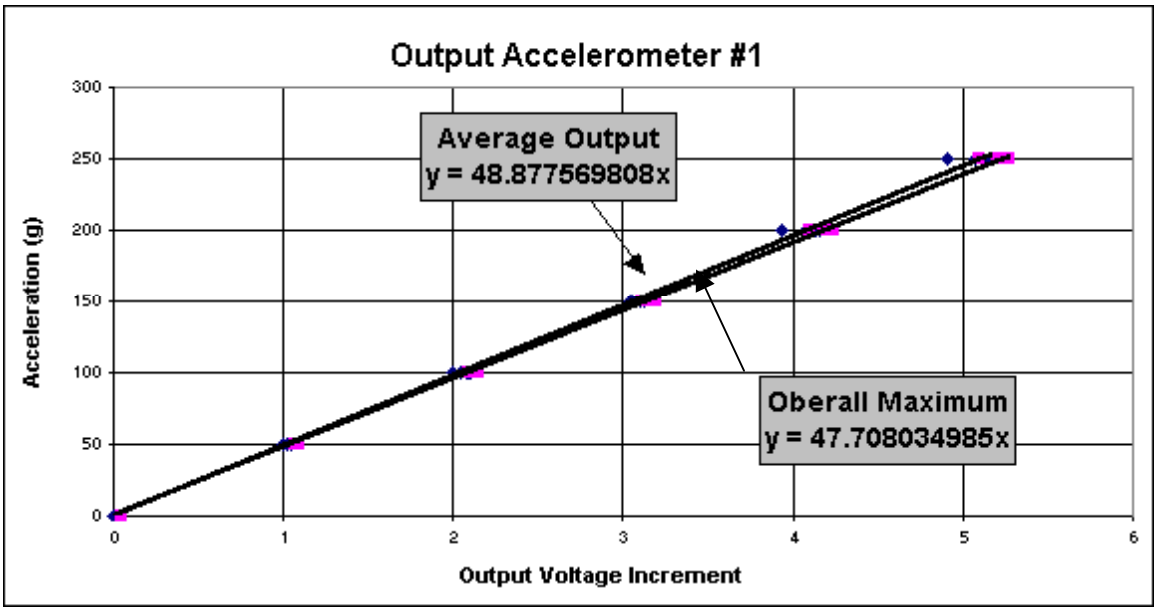

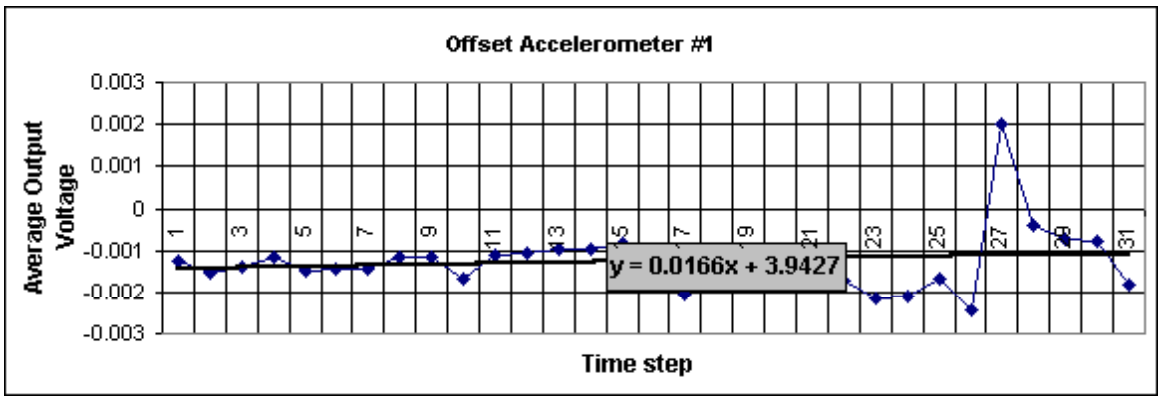

Sensitivity =	**48.878**	**g/Volt**

ACCELEROMETER LIMITS BASED ON PILE-UF

Maximum expected acceleration (+/-) = 250g

Overall Output Range (+/-) =	**5.11**	**Volts**	
Max Error due to noise (+/-) =	**0.19**	**Volts =**	**9.4834 g**
Calibration Accuracy % =	**6.87**		

Signal Generator used: Portable Generator Model 4830A (from ENDEVCO)

No filter used in the in the VI, Therefore the error is big.

Accelerometer Sensitivity = 1.74 Pc/g # 3 P.Order 10039584; Box No. 17

Figure 11-16b. Calibrating the Accelerometer Channel (continued)

MOUNTING OF THE NON-RECOVERABLE UNIT

It is very important that the strain gages and accelerometers be positioned in the pile correctly. The latter ensure that the signals include only the intended measurements. To accomplish the latter the transducers must be aligned with the axial direction of the pile. The proper alignment can be achieved using the strands as reference lines as well as support for the transducers.

The strain gages and accelerometers can be firmly supported using plastic ties as shown in Figure 11-17. If only one strain gage is used, it should be placed at the center of gravity of the of the pile cross section, as show in Figure 11-17 (a). This will guaranteed that the measurement is the average strain in the pile area (bending effects eliminated). If two strain gages are used they should be equally spaced from the pile center of gravity, as shown in Figure 11-17 (b). The latter assures that bending effects are eliminated if the average of the two gages is used. This arrangement will also provide information about bending in the pile. The accelerometers should be placed close to the strain gages, and as far as possible from the strands to avoid measuring the wave in the strands (Figure 11-17 a).

(a)

(b)

Figure 11-17. Instrumentation Placement (a) When One Strain Gage is Used; (b) When Two Strain Gages Are Used

The Signal Conditioner and Sending Unit should be placed between the sensors and the pile top. The unit should be separated from the transducers by at least 2 times the diameter of the pile. The latter will minimize the interference with the stress wave propagation in the pile. Also, any wave reflection from the unit will not unduly influence the instrumentation signal. Finally, the Unit should be placed at the pile's center of gravity to avoid induced bending stresses (Figure 11-18).

Figure 11-18. Signal Conditioning and Sending Unit Placement in the Concrete Forms

CHAPTER 12

ACQUISITION AND DATA PROCESSING SOFTWARE (Pile-Monitoring.vi)

As mentioned in Chapter 8, an *acquisition and data processing software* was written for pile capacity determination, as well as pile stress monitoring during driving. This program is called ***Pile-Monitoring.vi.*** Its principal task is to obtain pile capacity from the accelerometer and strain gage signals. For this purpose, the program uses three theoretical methods of capacity assessment: PDA Case Method, Paikowsky Method (FHWA Method), and UF Method (Chapter 7). The software also performs pile integrity and stress analysis.

In order to apply the methods, the software calculates three types of traces for each blow event: the Force (P) Trace, the Velocity (Z*Vel) Trace, and displacement (z) trace. The traces are obtained using the pile properties, and signals acquired by the Data Acquisition Card (raw signal). The raw signal is a discrete series of digital strain and acceleration voltages during driving. These values are transformed to real strain and acceleration, and then to Force, and Velocity. The displacement is obtained from the double integral of acceleration.

This chapter is divided into three sections which 1) provides a brief explanation of the programming language used, LabVIEW, 2) describes the User Interface (Front Panel of the software), and 3) describes the written code (Block diagram of the software).

LabVIEW OVERVIEW

LabVIEW was the programming language used to create Pile-Monitoring.vi. Developed by National Instruments Corporation, its main purpose is data acquisition and instrumentation control. Its tight integration with hardware allows for rapid development of data acquisition, analysis, and visual presentation of results.

LabVIEW is a high-end language written to simplify data acquisition. With the latter in mind, LabVIEW uses a graphical programming language, G, to create programs (Virtual Instruments, VIs) in block diagram form similar to a electrical circuit. LabVIEW provides libraries of functions and tools for specific application, which are available in other and programs. Each VI has three basic components:

1. The user interface, or front panel, controls the operation of the VI. It resembles the front of an actual instrument with buttons and displays. The user can input parameters using the keyboard or mouse.
2. The block diagram, is the source code for the data acquisition evolution. It uses the input parameters from the user interface to direct the process.
3. Icon connections that allow lower level VI's to be called for operation by a higher-level VI. These are basically subroutines called SubVI.

The input and output information is transferred between the front panel and the block diagram using special connections. There is a great variety of connectors available in LabVIEW. They are divided into two major groups: controls and indicators. Controls are used to input data into the program at any time. Indicators are use to present the output of the program.

FRONT PANEL DESCRIPTION AND OPERATION

The Front Panel, shown in Figure 12-1, is the user interface of the software. It is used to start and stop the program and also to input and display data in numerical and graphical format.

The upper left buttons (arrow and stop sign) are used to start and stop the program at any time. As soon as the arrow button is pressed (left mouse click), the program starts operating and brings up a dialog-box asking for a directory to save data.

Once the directory has been selected, a new window shows up (Figure 12-2) asking for input parameters (to be introduced by the user). These parameters are shown in Figure 12-2 and

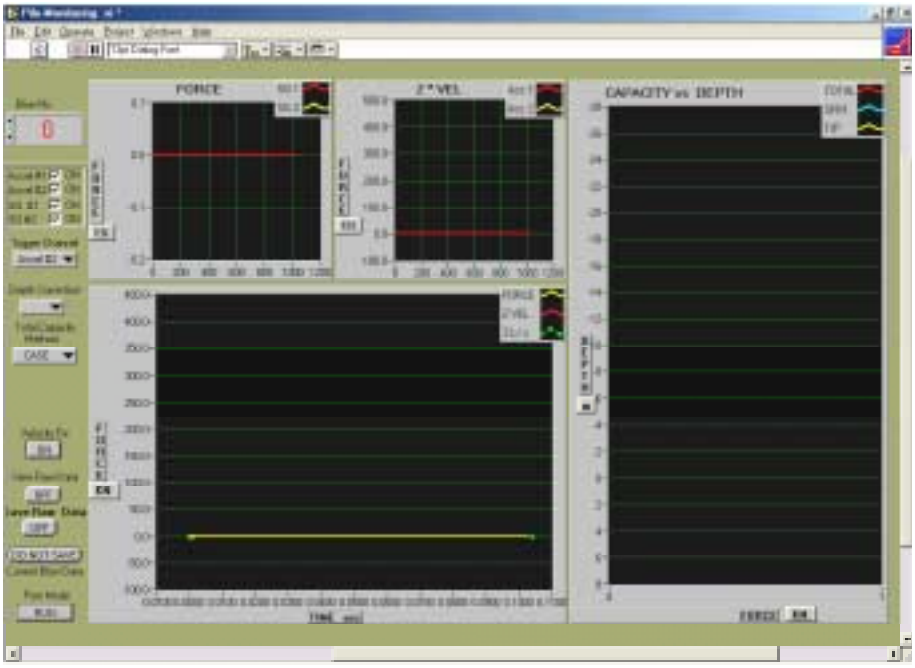

Figure 12-1. Pile-Monitoring.vi Front Panel

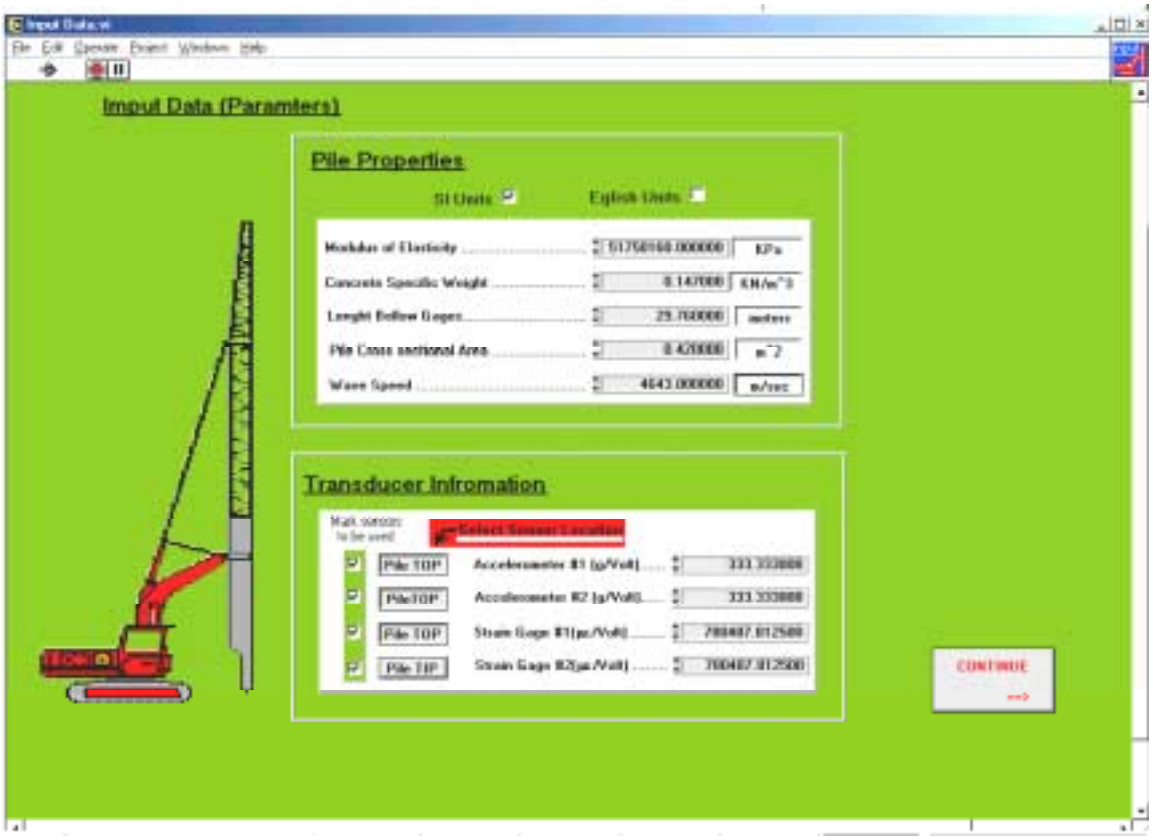

Figure 12-2. Input-Data Front Panel

they have been gathered into two groups: Pile Properties and Transducer Information. They are required for capacity determination and incoming data reduction, respectively.

Figure 12-2 shows two square options (check or no check) named **SI Units** and **English Units**. They are used to select the type of Units to input the pile properties. The pile properties are introduced in the third column and their specific units, either in SI or English, is shown in the right column.

On the bottom half of the screen, four columns show the transducer input information (Figure 12-2). The first column is used to select the transducers to be used. The second column is used to specify the transducer location (pile tip or pile top). The third column specifies the transducer name. Finally, the fourth column is used to input the sensor sensitivity. The sensitivity is obtained from the calibration of the entire wireless system, as described in Chapter 11.

Once the required data is inputted, the **Continue** button (Figure 12-2) should be pressed, and the Front Panel (Figure 12-1) reappears. At this time the data acquisition process starts. After each pile strike, the Front Panel will output new or updated information, as shown in Figure 12-3.

Four graphs show the program output (numbered from 1 to 4 in Figure 12-3). Graphs 1 and 2 show two Force Traces and two Velocity Traces respectively, in terms of force versus time. These graphs are internally obtained from the output signal of two strain gages and two accelerometers respectively. Graph 3 shows two plots, one is the average of the two Force Traces (Graph 1) and the other is the average of the two Velocity Traces (Graph 2). In the event that one set of transducers is placed at the pile tip, Graph 3 disregards it and will display only the Force and Velocity from the transducers at the pile top. The last graph, Graph #4, shows the pile

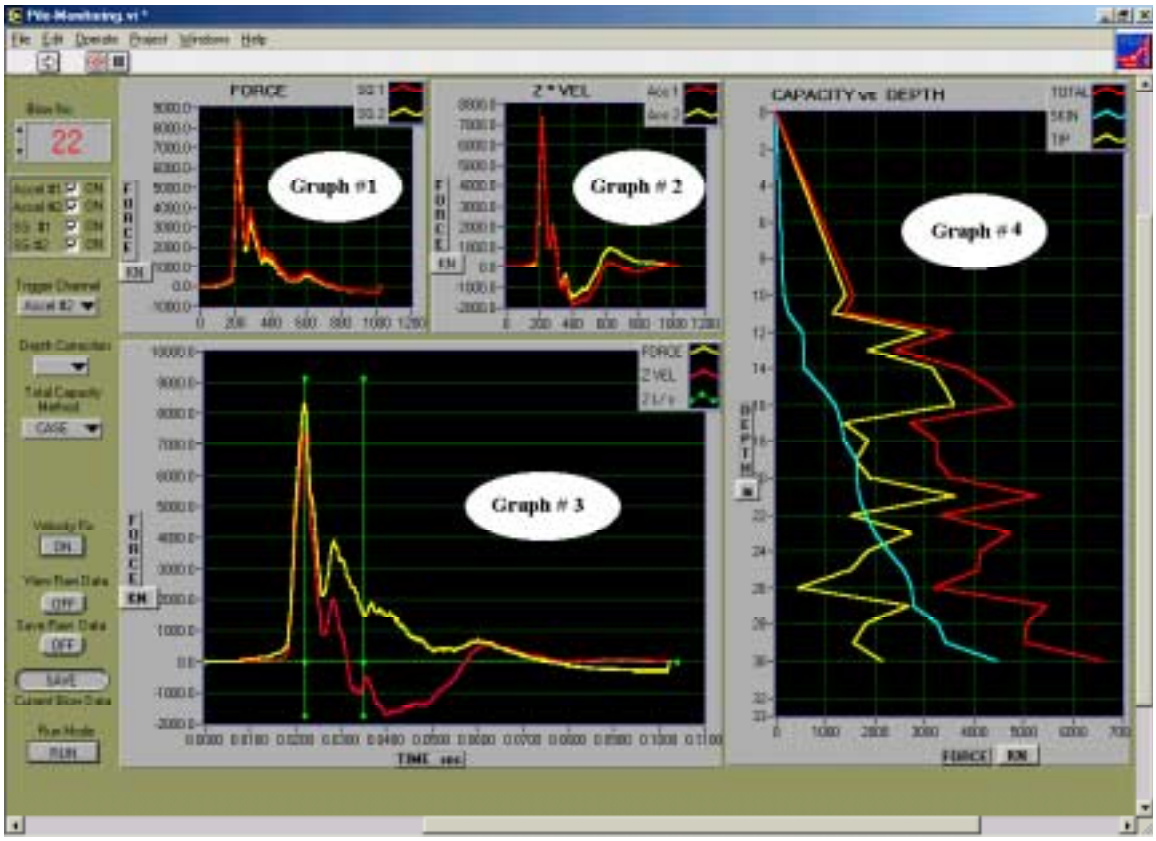

Figure 12-3. Pile-Monitoring.vi Front Panel (after 22 pile strikes)

capacities (Skin, Tip and Total) versus the pile penetration depth. Graphs 1 to 3 are specific for a single blow while Graph 4 represents the entire driving history.

Every time the hammer strikes the pile head, a new set of accelerations and strains are delivered to the software. Traces on Graphs 1 to 3 are replaced by the new incoming information while Graph 4 is updated with the new capacity and penetration (from the new blow). The new capacity and pile displacements are calculated from the new traces on Graph 3.

Graphs 1 and 2 are used to provide information about the transducers performance. Force Traces and Velocity Traces should look similar to the ones presented in Chapter 5, otherwise there might be a problem with the instrumentation package. If one of the Force Traces or

one of the Velocity Traces looks incorrect, they can be turned off with the **ON/OFF** controls on the Front Panel (upper left in Figure 12-1). The signal will not be used, but it will be stored for further reference.

If all transducers are at the same location along the pile axis, both Force Traces and both Velocity Traces should look very similar. If there is a great difference between Velocity Traces, one accelerometer might not be working properly and should be turned off. The same could happen with the Force Traces, one strain gage might be damaged, or more likely indicate bending stresses in the pile. Bending stresses should be kept within safe limits (FDOT specs.). For the purpose of capacity determination, taking the average of the two Force Traces (Graph 3) eliminates the bending effect.

Graph 3 is used for data quality checks (Chapter 10), pile stress monitoring, and pile damage detection.

The total pile capacity, in Graph 4, is calculated using the CASE method or the Paikowsky Method (Chapter 7). The method is selected in the **Total Capacity Method** selector on the left side of the front panel. The Skin and Tip Capacities are obtained using the UF Method described in Chapter 7.

The pile penetration, in Graph 4, is calculated from the cumulative penetration obtained after each blow. However, since penetration during each blow is calculated with the double integration of the acceleration signal, errors in the cumulative penetration can arise. To account for this error, a **Depth Correction** selector has been incorporated in the Front Panel. Consequently, operator has the option of periodically updating the total penetration depth.

The **Velocity Fix** control knob, shown on the Front Panel, is used to correct the Velocity Trace in Graph 4. The Velocity Trace may be forced to come back to 0 at the end of the trace

using the method described in Chapter 6. Using the start of the trace as a pivot point, the entire trace is rotated until the velocity at time 0.1024 seconds becomes 0 (similar to PDA).

The **Trigger Channel** selector, shown on the Front Panel, is used to pick up one of the four incoming signals for triggering purposes. During the acquisition process a few of the incoming signals carrying the dynamic activity of the pile are selected for further analysis. Some typical incoming signals were presented in Figures 10-10 and 10-11 for the strain gage and the accelerometer respectively. The program will use the selected channel to look for these types of specific signals for further analysis.

The **View Raw Data** control knob is used to display a new window where the incoming data from the sensors can be continually observed (Figure 12-4). This graph is used to analyze the operation of the instrumentation system, including excessive offset, background noise, and

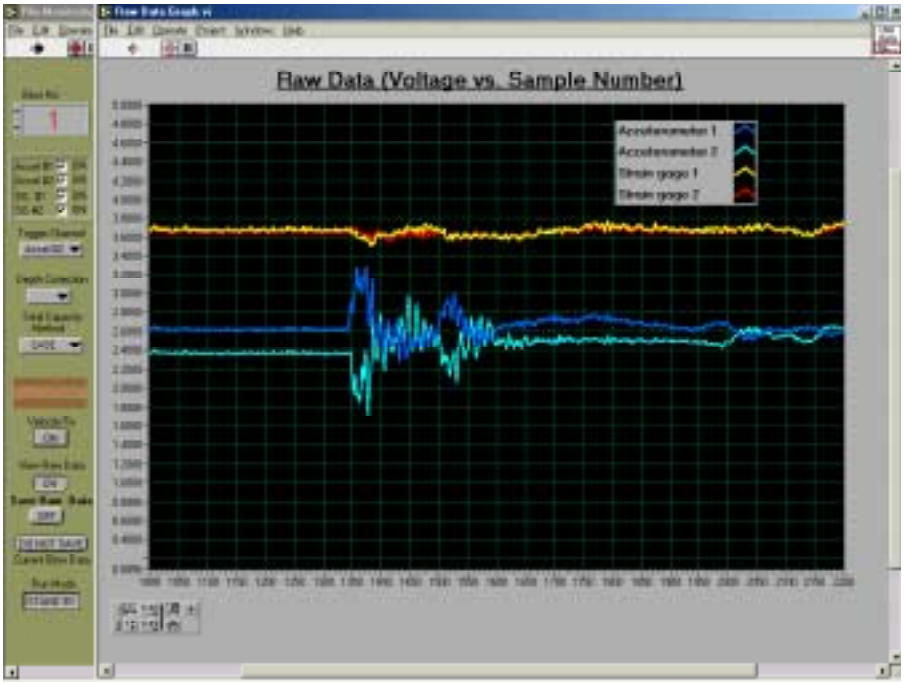

Figure 12-4. View Raw Data Window

signal stability. The input signal shown in this graph should be between 0 and 5 volts, with the offset close to 3.75 Volts for the strain gage channels and close to 2.5 Volts for the accelerometer channels. The noise level should be below 10 mV for each channel. If the signal shows unexpected sharp spikes (digitalization error), then the receiver antenna is not well oriented, or it is too far from the pile.

The **Run Mode** control knob, shown on the Front Panel, is used to select the operation mode of the software. The program has two modes of operation: Run and Standby. The Run Mode is used during the driving procedure to pick up the transferred signals from the pile and perform the activities described above. The Standby Mode is used to replay past blow traces that have been stored in the hard drive of the computer. In Standby Mode the software performs the same activities as in Run Mode, except data acquisition. The same controls and graphs described above are available.

Additional features of the Front Panel include the **Blow No. Indicator** and the **Current Blow Data** save control. The **Blow No.** indicates for which blow the traces are plotted in Graphs 1 to 3. It is also used to replay previous blows when the program is in Standby Mode. The **Current Blow Data** save control is used to store the blow information as raw data, in the previously selected directory. They are individually stored in text format under the name of BLOW #, where # indicates the actual blow number. In Standby Mode, this knob will resave the stored information in CAPWAP format (Figure 9-2).

The pile capacity and depth are saved after each pile strike by using the excel format (in the previously selected directory). The input data (Figure 12-1) is also stored in this directory under the parameter name.

BLOCK DIAGRAMS

As explained in the introduction, the Block Diagram, shown in Figures 12-5 to 12-15, is the actual program code. The details of the language are not discussed herein, but a brief layout of the VI is given below.

The Block Diagram of the software is divided into two main sequences. The first group (sequence # 0) is in charge of the data input, and the second group (sequence # 1) is in charge of the data acquisition, storage and display. These sequences will be referred as **Input Sequence** (sequence #0) and **Data-Processing Sequence** (sequence # 1).

The Input Sequence is composed of two sections shown in Figures 12-5 and 12-6. The first section is in charge of asking the user for the input directory. Using this directory, file paths are created to store further information (parameters, raw data, capacity, and a temporary directory to keep input parameters). The second section asks the user for input parameters (Figure 12-2), stores the latter information and transfers it to the Data-Processing Sequence.

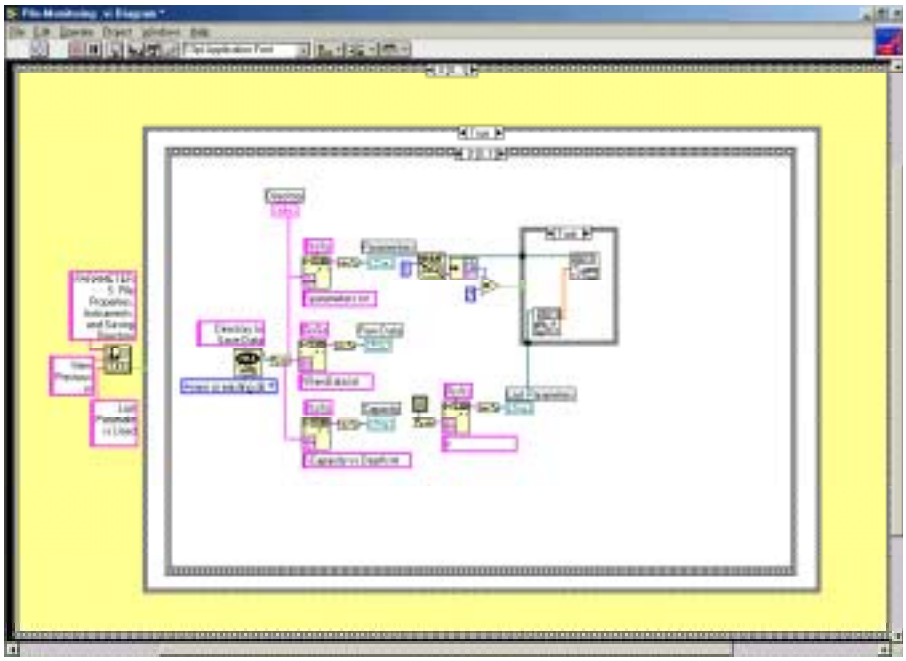

Figure 12-5. Code Used to Select Directory and File Paths

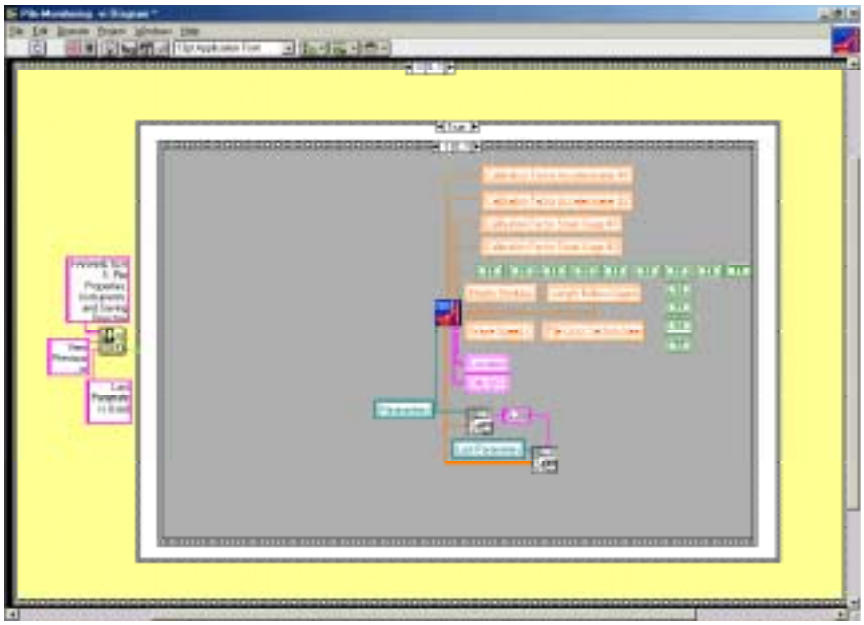

Figure 12-6. Code Used to Input Data

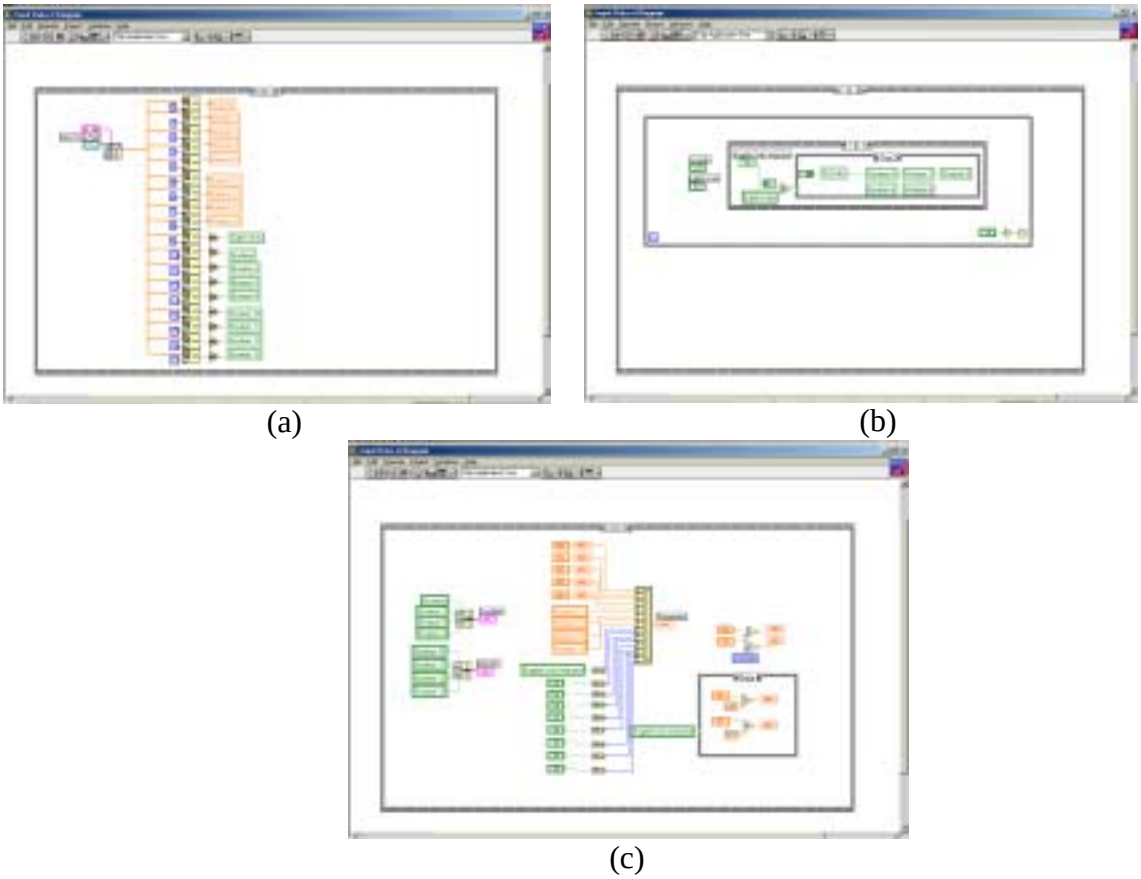

Figure 12-7. Input Data Sub VI Code (a) Read Parameters from Previous File; (b) Check Units Selected by the User; (c) Transfer Parameters to the Input Sequence

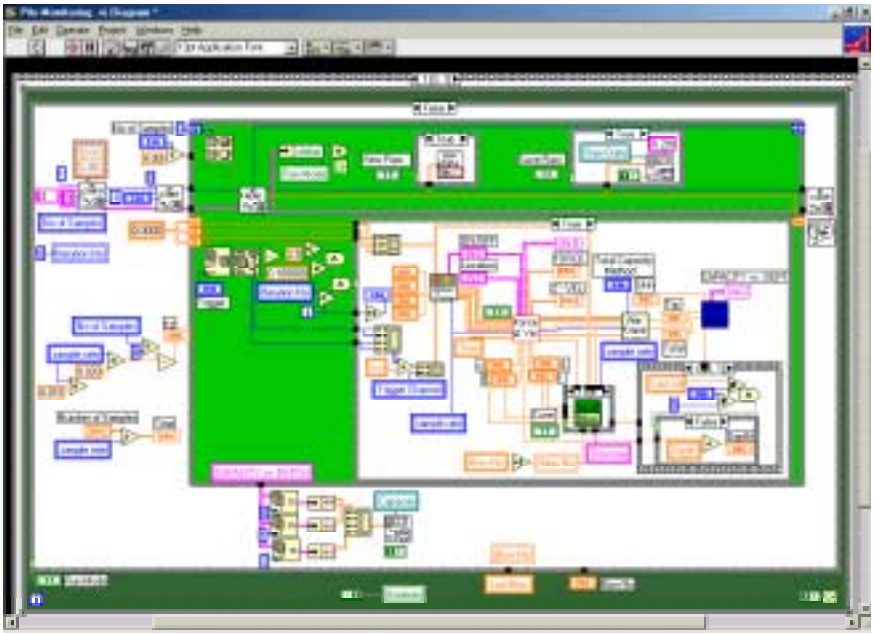

Figure 12-8. Code Used for Run Mode

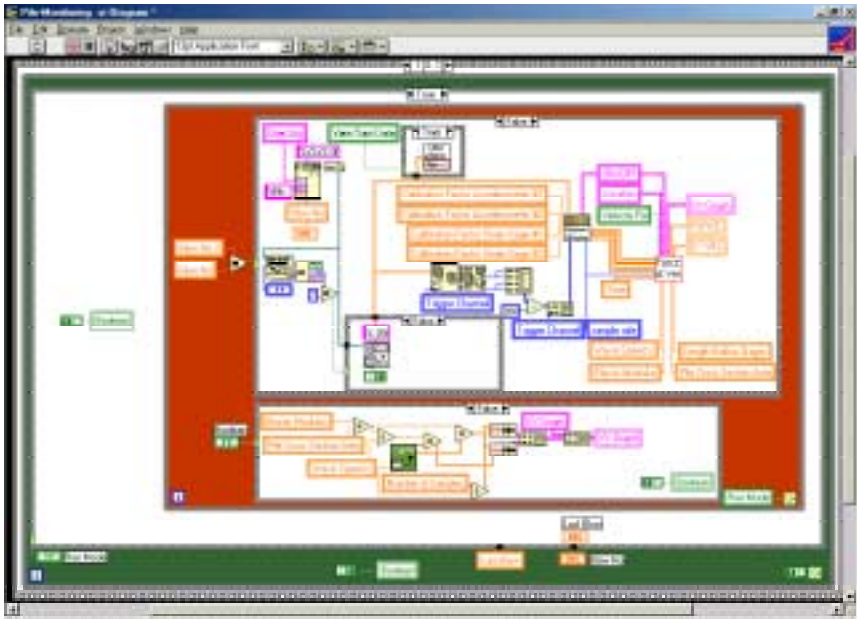

Figure 12-9. Code Used for Standby Mode

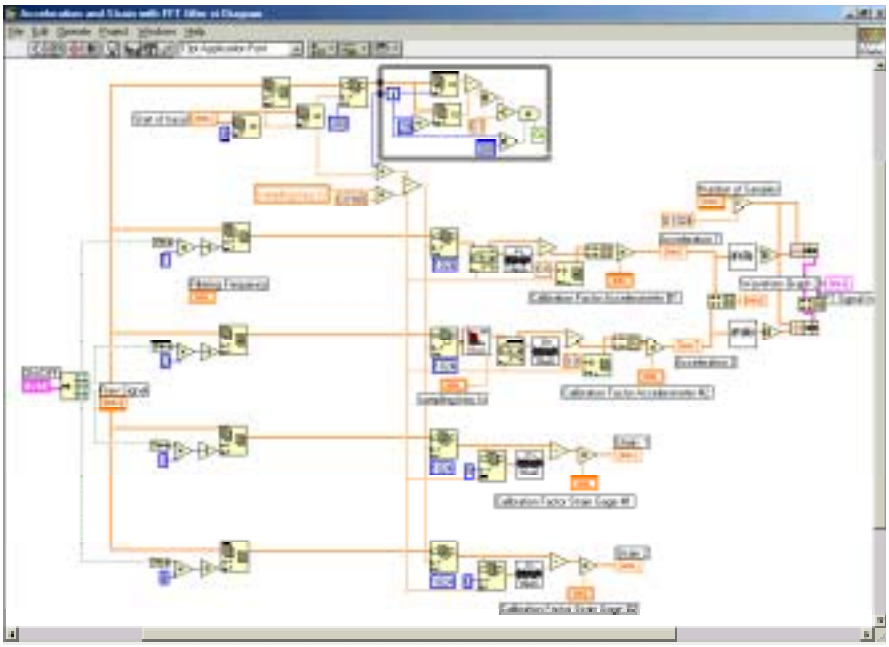

Figure 12-10. Strain and Acceleration Sub VI Code

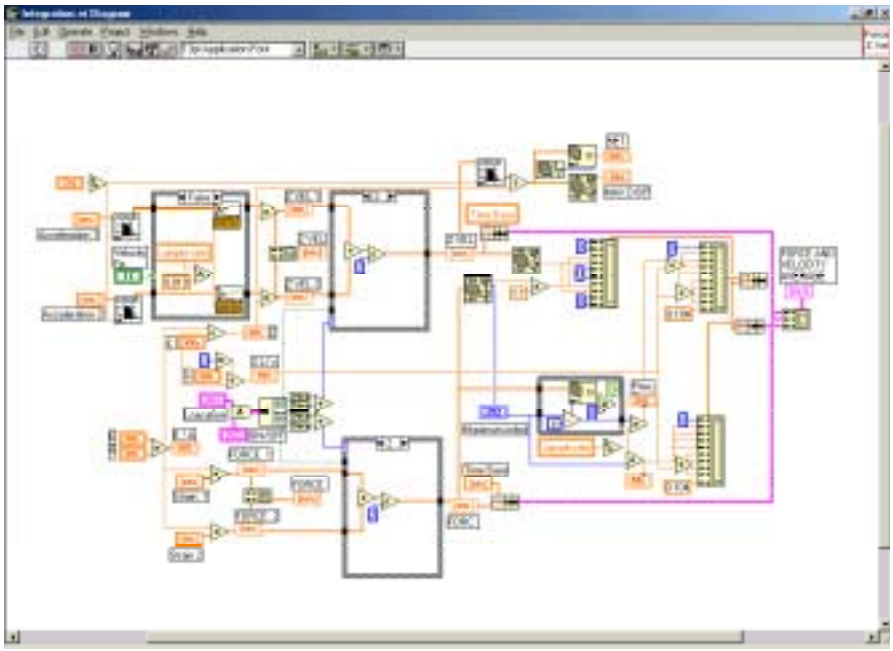

Figure 12-11. Integration Sub VI Code

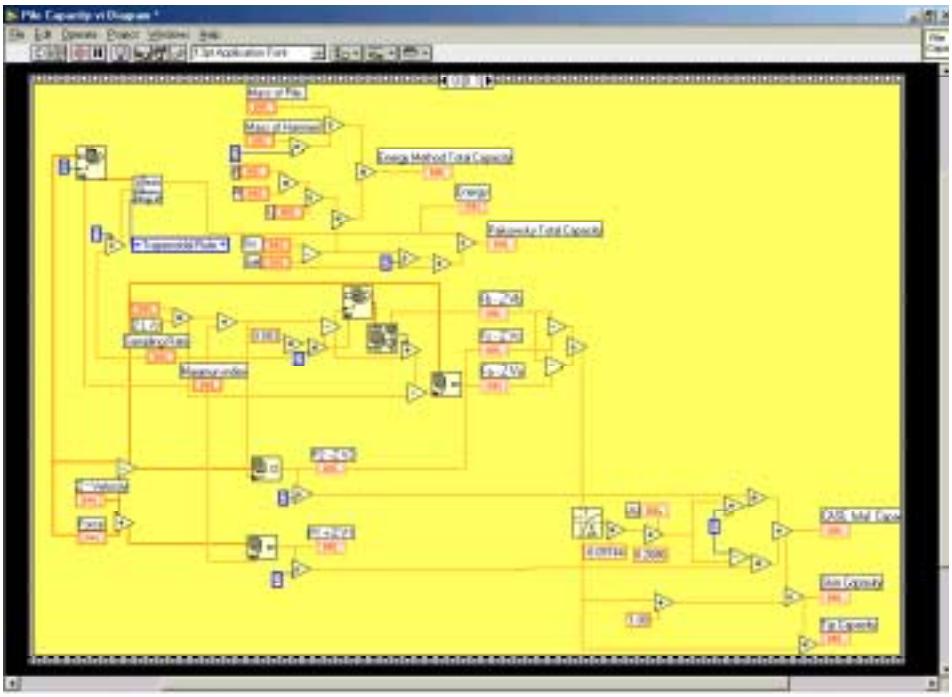

(a)

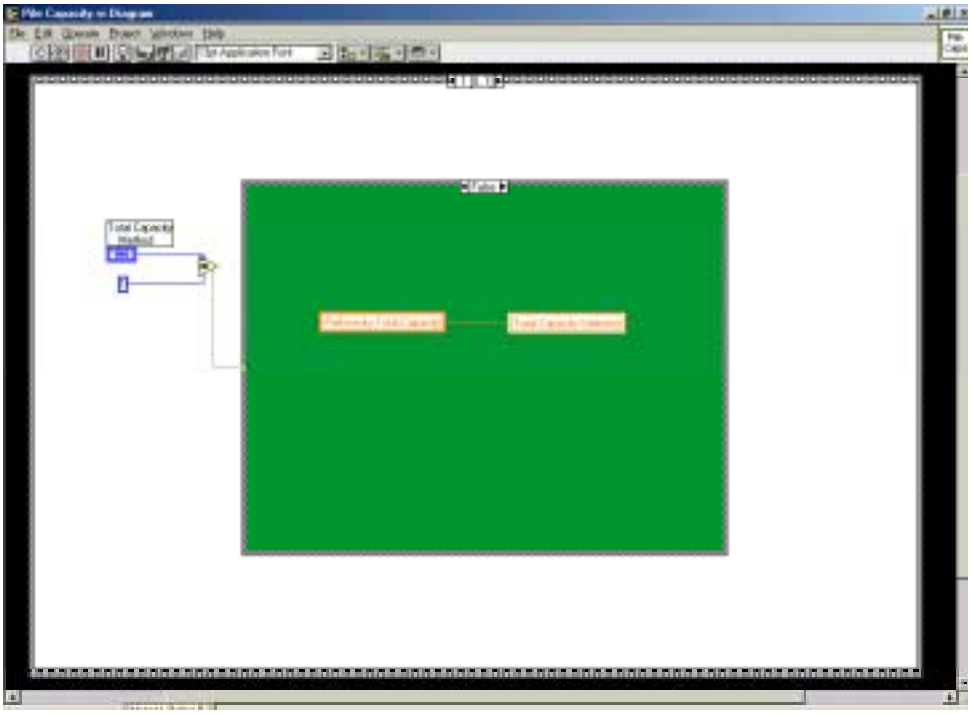

(b)

Figure 12-12. Capacity Sub VI Code

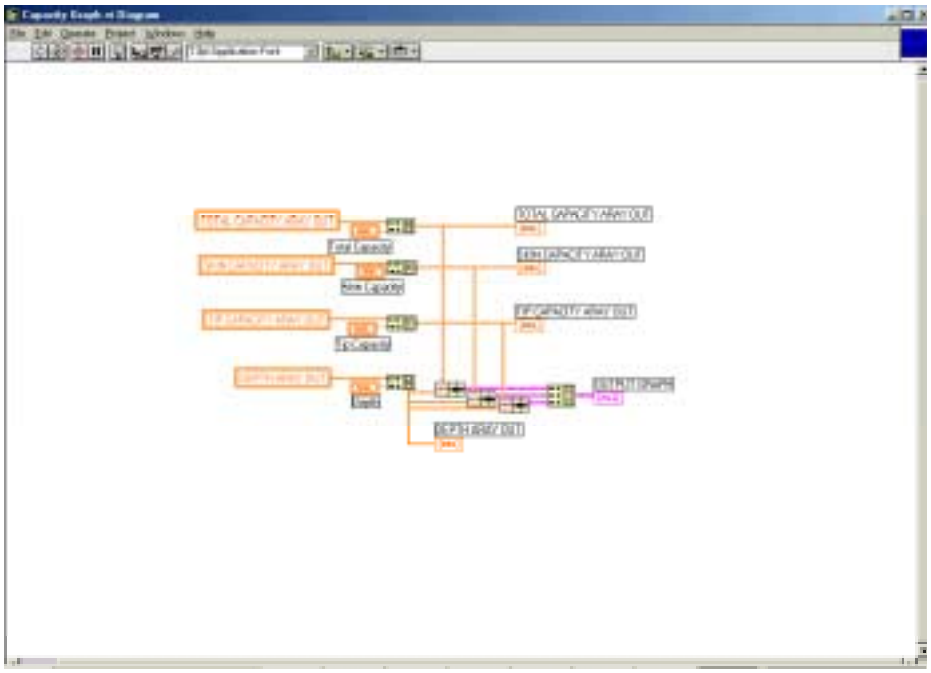

Figure 12-13. Capacity Graph Sub VI Code

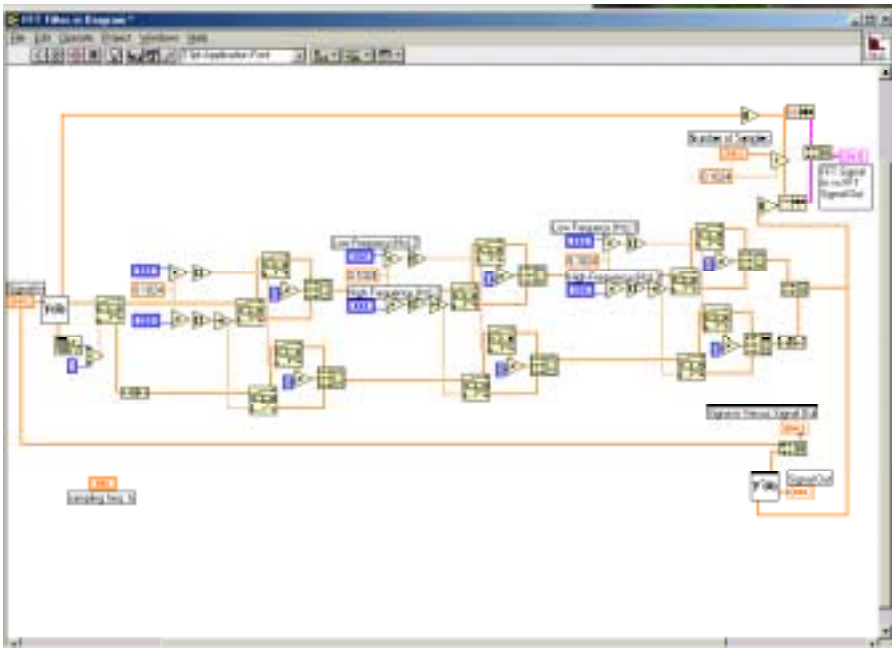

Figure 12-14. FFT Filter Sub VI Code

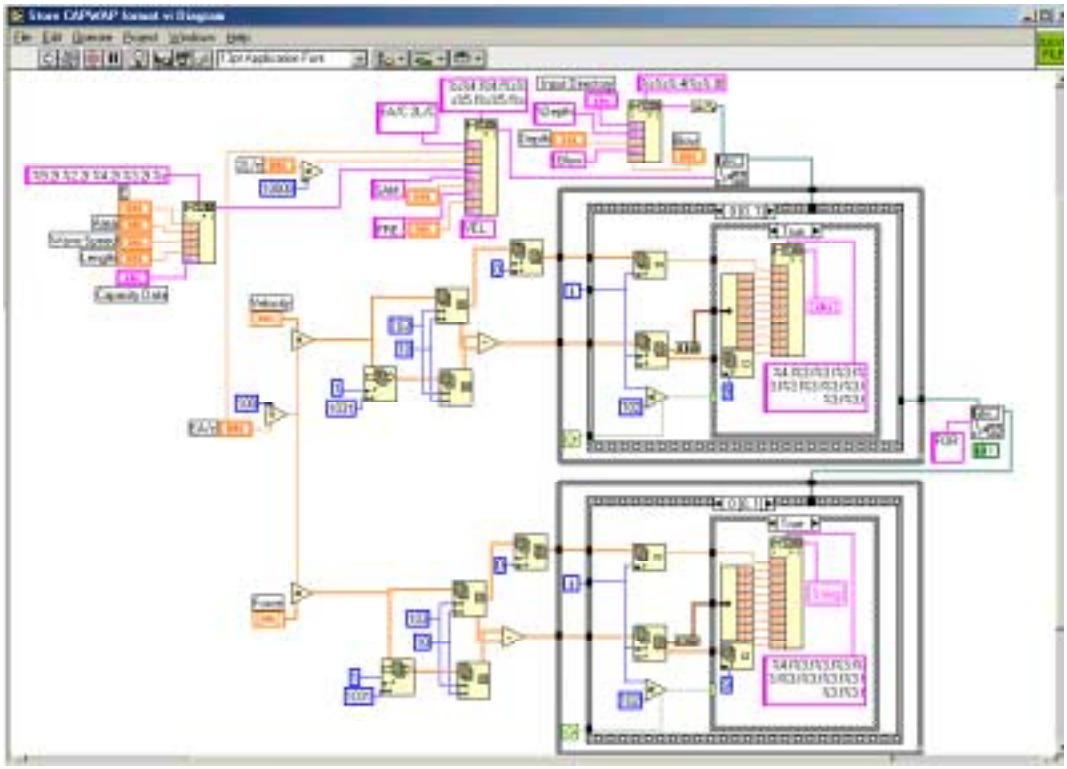

Figure 12-15. Save in CAPWAP Format Sub VI Code

Right in the middle of Figure 12-6 is a small square called Input. This SubVI (subroutine) is in charge of displaying the input window shown in Figure 12-2. The code for this SubVI is shown in Figure 12-7. It is composed of three groups that operate in sequence. Figure 12-7a is in charge of recovering previously stored parameters in the event that the user requires a replay of previous driving records. Figure 12.7b analyzes the units selected by the user. And Figure 12.7c gathers the input parameters and sends them to the higher level code.

Figures 12-8 and 12-9 shows the **Data–Processing Sequence** (mentioned at the beginning of this section). Figure 12-8 presents the code used when the program is in Run Mode and Figure 12-9 presents the code used when the program is in Standby Mode. Both areas of the program are similar, with the major difference that one recovers the strain and acceleration signals

from the transducers and the other recovers that information from a file. Since both codes are similar, only the Run Mode will be described.

The first step (Figure 12-8) involves querying the Data Acquisition Card as to its readiness. The Data Acquisition Card is configured to recover four signals (two accelerometers and two strain gages) at 10,000 samples per second each. A buffer size capable of holding 4,000 samples is set up to transfer the signals from the Data Acquisition Card to the computer. This buffer size has proven (hundreds of hours of testing) to be stable during the transfer process. The incoming signals have the following channel allocations:

Channel 0: accelerometer #1
Channel 1: accelerometer #2
Channel 2: strain gage #1
Channel 3: strain gage #2

Note, the specified sampling rate (10,000 Hz) is higher than the minimum specified by ASTM D4945 (Chapter 9) but results in good signal resolution.

The second step of the code in Run Mode is to recover the information in the while loop shown in Figure 12-8. A number of other activities also take place within this while loop.

A trigger determines if there is dynamic activity in one of the four channels (selected with the **Trigger Channel** knob on the front panel). If the amplitude between maximum and minimum spikes overpass a predefined value (0.1 Volts = 27g), the data processing will be triggered. The incoming data will then be processed and plotted in the front panel. For this purpose four SubVIs (Figure 12-8) are used. Special icons as shown identify them. Next to each icon is the name of each SubVIs followed by a brief description of its activity in the software.

 Strain and Acceleration.vi. This sub VI transforms the raw data into strain and acceleration, as well as select which channels are in use (ON/OFF control in the front

panel). The process starts by filtering the signal from 0 to 5 Hz and 3,000 to 10,000 Hz using an FFT filter (Figure 12-14). Next it changes the signal offset to 0, and rounds out to 0 any values that are smaller than the noise level (<10 mV). Finally, it multiplies each signal by its calibration factor to obtain strain and acceleration records. The code is shown in Figure 12-10.

 Integration.vi. Uses the strain and acceleration from the last SubVI to obtain Force, Velocity (Z*Vel), and displacement traces. Integrates the acceleration to obtain velocity, performs the PDA velocity fix (if selected on the front panel), obtains Force and Velocity Traces to be plotted in the Front Panel (Graph 1 and 2). Calculates the average Force Trace and average Velocity Trace (from sensors at the pile top) to be plotted on the Front Panel (Graph # 3), and to be used in further analysis. Obtains displacement trace from the average velocity and finds the start of that trace, the rise time, 2L/c, set, and displacement. The code is presented in Figure 12-11.

 Capacity.vi. Uses the Force average, Velocity average, set, and displacement from the last SubVI to estimate pile capacity (Tip, Skin, Total). The methods described in Chapter 7 are used for this purpose. This code is presented in Figures 12-12.

 Capacity Graph.vi. Uses the capacity assessments from the last SubVI to update the previous assessments (prior blow) for plotting on the Front Panel. The code is presented in Figure 12-13.

 Store CAPWAP.vi. Stores the average Force and Average Velocity (from the Integration.vi) in CAPWAP Format. The code is presented in Figure 12-15.

Evident from the prior discussion, the processing of the information involves many activities. Also, the trigger plays a key role in this program. The amount of information recovered at 10,000 Hz is enormous, and much of it is not used. As described in Chapter 9, only 0.1024 seconds of sampled data is required to analyze a single blow. To show the magnitude of the data, consider a hammer with blow rate of 60 blows per minute. In one minute (60 blows), 6.14 seconds of data is of interest, and the data recorded over the remaining 53.86 seconds (60 sec – 6.14 sec) is redundant. The latter represents 2.15 million values of useless data (53.86 sec * 4 channel * 10,000 samples/sec/channel).

Consequently, minimizing operations (removal of unwanted data) was a major concern in this software. As can be seen, in Run Mode, more than 4,000 values need to be managed to obtain the pile capacities at a given blow, another 12,300 values are analyzed for redundancy, and 4,000 new incoming data points are sampled and saved. Therefore, the redundant information must be detected and eliminated as soon as possible with minimum amount of operations.

CHAPTER 13

LABORATORY AND SMALL SCALE FIELD TESTS

In developing the wireless instrumentation equipment, a significant amount of laboratory and small scale field-testing was performed. In the case of laboratory work, each component was tested for calibration purposes, as well as minimizing signal noise. The small-scale field-testing was to ensure that the instrumentation package held up to the rigors of pile driving, as well as the identification of any other problems (transmission distance, noise, etc.). The field tests involved embedding the non-recoverable units in a miniature prestressed concrete pile and driving it into to the ground (more than 60 blows) with a small air/steam hammer. The small pile was also used in laboratory for calibrating and validating equipment response. The laboratory testing and field testing are described as follows.

MINIATURE PILE

A miniature prestressed concrete pile, shown in Figure 13-1, was built in the University of Florida's Structures Lab. The purpose of this pile was to create a proper environment, similar to FDOT concrete piles to test the instrumentation package in the laboratory and in the field. The dimensions and properties of the pile are presented in Figure 13-1.

(a)

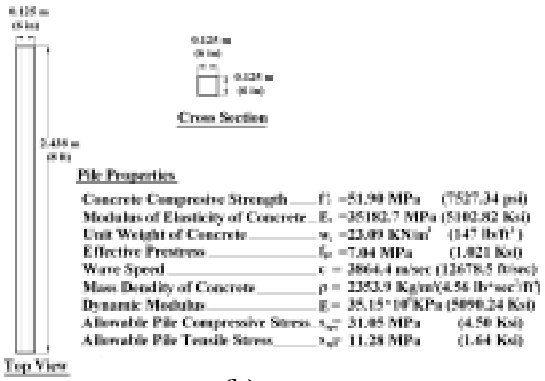

(b)

Figure 13-1. Miniature Pile (a) In the structures laboratory; (b) Properties

The pile was instrumented in such way that it could be monitored by two independent systems: I) the proposed **wireless system** and II) a separate **wired system**. The wired system was a simplified version of the wireless system with the same instrumentation package but hard wired directly to the data acquisition system. Consequently, there were eight sensors (Figure 13-2) embedded in the pile, four of which form part of the wireless system (Non-Recoverable Unit), and the remaining (four) which were connected to external conditioners outside the pile using cables. The difference between the two systems was intended to localize problems in the wireless link, as well as identify shock and vibration issues with the conditioners and transmitter. Furthermore, the additional sensors served as backup instrumentation for the Non-Recoverable Unit (in the event that they were damaged during casting of the pile).

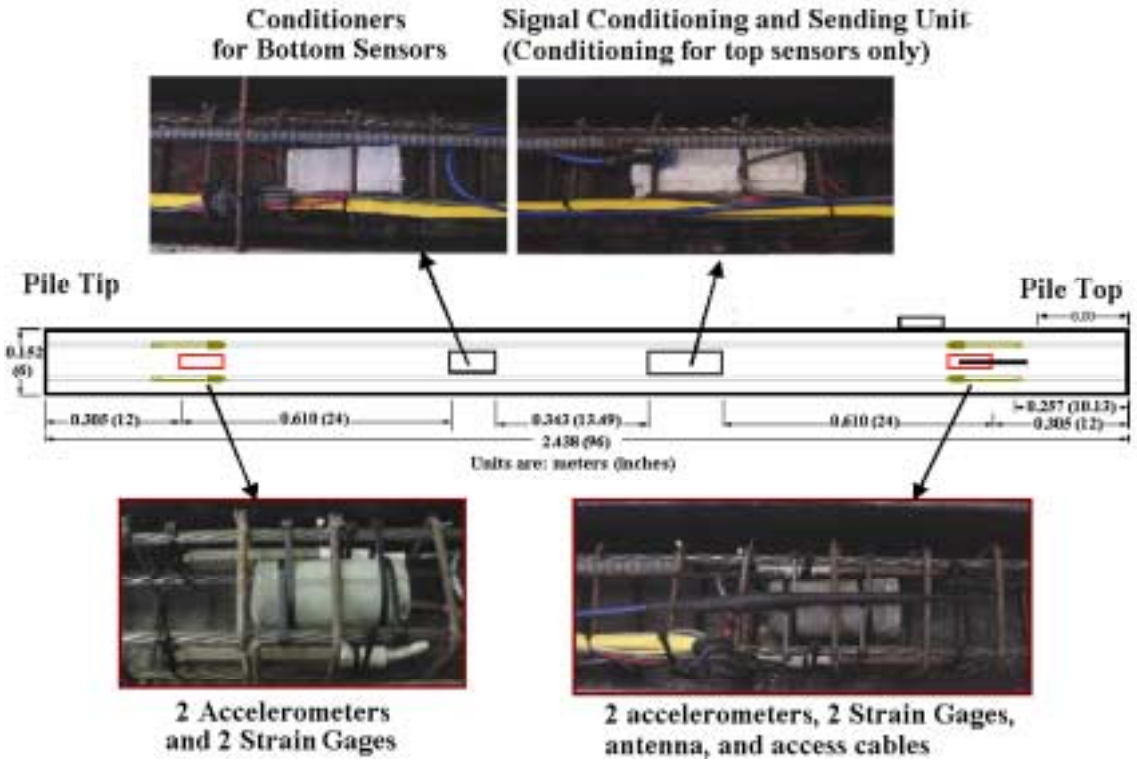

Figure 13-2. Installation of Non-Recoverable Unit and Wired Sensors

Figure 13-2 shows the instrumentation arrangement prior to pouring the concrete. The four transducers of the Non-Recoverable Unit were installed two pile diameters below the pile top and two diameters above the pile tip; one set of transducers (1 accelerometer and 1 strain gage) at each location. The four wired sensors were installed in the same way and in the same cross section as the other four transducers.

The strain gages were aligned using four plastic ties each; one pair to support the strain gages from the top strand, and the other pair to keep the strain gage alignment during the concrete pouring (attached to bottom strands). The strands and plastic ties provided the proper alignment, in one direction, and uniform separation between strain gages and strands achieved the alignment in the other direction.

It is important to note that the accelerometers (Endevco) were mounted in this pile using an older technique than the one presented in Chapter 11. The accelerometers were first mounted in a 10-cm by 5-cm (4 in. by 2 in.) concrete cylinder using adhesive mounting. A low noise cable was soldered directly to the top of the accelerometer. Then, the top and lateral sides of the accelerometers were covered with a layer of silicone to avoid compression stresses and to protect the accelerometer from moisture. Finally, the side of the concrete cylinder was covered with more concrete to protect the accelerometer during the casting procedure. This cylinder was aligned in the pile using four plastic ties attached to two strands.

STRAIN GAGE AND CONDITIONERS

Two different types of tests were performed to verify the suitability of the proposed strain gages and conditioners. The first test was to verify the output linearity of the gages and conditioners, and the second was to ensure proper dynamic response time.

For the output linearity, one strain gage was embedded in a concrete cylinder and loaded as shown in Figure 13-3. The strain gage was connected to conditioners outside the cylinder (Black Box) and then to a voltmeter. A special dial gage connected to the cylinder provided information about the induced strain and the voltmeter indicated the output voltage from the strain gage and conditioners. The plot of induced strain versus output voltage, Figure 13-3, reveals the linearity with a maximum error of 2.16 % (30 με *100/1391.9 με) over the intended measuring range (Table 9.2). This test was repeated many times to verify repeatability and the calibration procedure presented in Chapter 11.

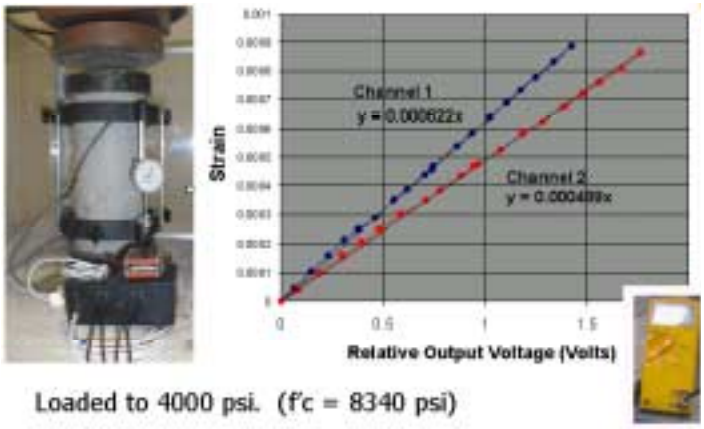

Figure 13-3. Output Linearity Test of Strain Gage and Conditioner

It is important to note that the voltmeter output conceals the channel noise because it averages the voltage over a time interval. Nevertheless, during the strain gage calibration process (Chapter 11), it was observed that the noise influence was low. The measured amplitude of noise was 10 mV (2.78 με), which represents an additional 0.2% error. The total maximum error is 2.36% (below the required maximum 3% in Table 9.2).

Next, the dynamic response of the strain gages and conditioners was checked against the PDA strain gages with a Fast Fourier analysis (FFT). The PDA strain gages were attached to the

miniature pile (Figure 13-4a) at the same location of the embedded strain gages. The wired strain gage present at this location was connected to external conditioners and then to a laptop computer (with the same software as the wireless system). The pile was struck with a hand held hammer to create a force wave to be recorded by both apparatus independently (Figure 13-4b).

(a) (b)

Figure 13-4. Comparison Between PDA and Transducers Embedded in the Miniature Pile (a) PDA sensors on miniature pile; (b) Simultaneous monitoring using PDA and the proposed new system

Shown in Figure 13-5 is the Force Trace recorded in the laptop computer versus the one recorded by PDA. The bottom graph in Figure 13-5 shows the frequency content of both traces (FTT). Both graphs show good frequency and fair amplitude agreement, considering that the transducers were not in the same exact position (PDA vs. Proposed). Moreover, the frequency response shows frequencies above the minimum expected (300 Hz). This test also served to verify that the strain gage calibration procedure was correct.

In Figure 13-5 the maximum error in terms of amplitude is 13% with respect to the maximum recorded force, and 0.22 % with reference to the maximum expected force (E*A*1391.9). Note this error is in the same range as the noise (10 mV).

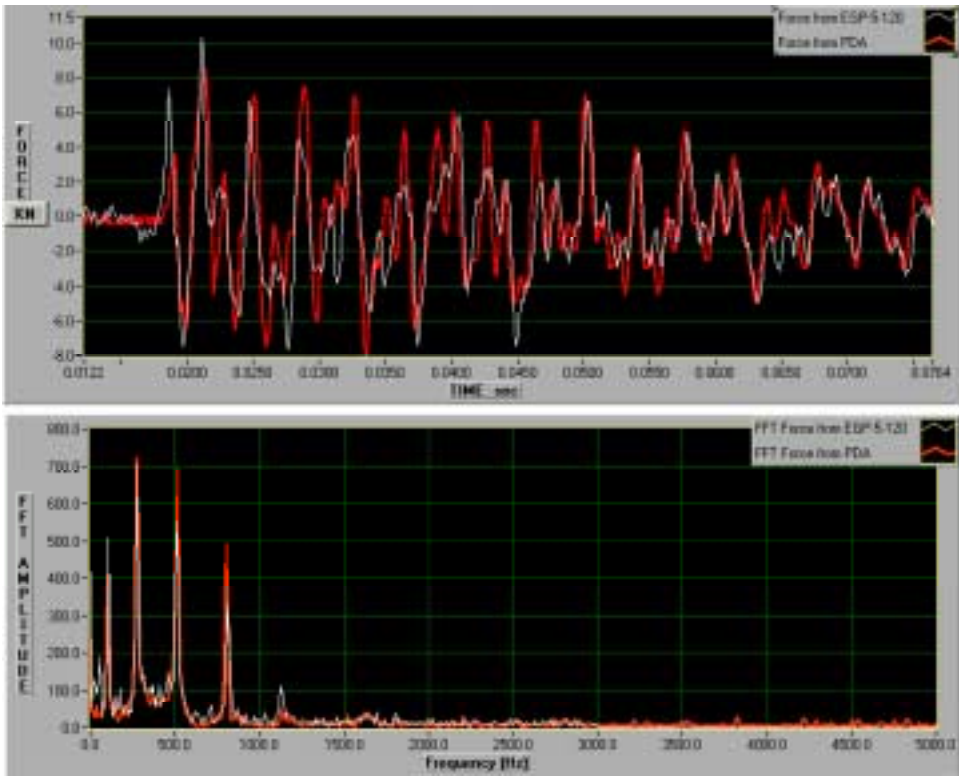

Figure 13-5. Force Traces Obtained with the Proposed Equipment and PDA, and FFT

ACCELEROMETER, CONDITIONERS AND FILTERS

Many tests were conducted to verify the suitability of the proposed accelerometers, conditioners and filters. Many of the early lab tests revealed problems, that were fixed and tested again. Other problems were discovered in driving the miniature pile, which were later fixed. A brief discussion of both the laboratory testing and miniature pile testing of accelerometers, conditioners, and filters are described herein.

From early in the work, a major concern was the development of a viable, cheap accelerometer, which was accurate for the pile dynamic testing. After identifying the Endevco accelerometer, as a likely candidate, an appropriate housing and conditioner circuit had to be designed and subsequently tested. In the case of the latter, the accelerometer, conditioners, and

filters had to be able sustain high shock and vibration for concrete piles (+/-200g and 10 to 3000 Hz). To test the latter, the accelerometer and conditioner were cast in a miniature pile and struck with a hand held hammer to induce accelerations, which were monitored. In addition, a high quality accelerometer (DC), as well as the PDA accelerometers were attached to the outside of the miniature pile for comparison purposes. Both amplitude and frequency content were of interest.

For the first tests, the Endevco accelerometer was mounted on the back of the PDA accelerometer, and the PDA accelerometer was mounted on the miniature pile. In this test the Endevco accelerometer was installed on a flat plate, and the plate was glued to the PDA accelerometer. Figure 13-6 shows the signal comparison for one blow event in three forms: acceleration, frequency content and Velocity Trace. Figure 13-7 shows the same graphs as in Figure 13-6 but in a smaller time frame. In these graphs a 5 Hz low pass filter was used on the acceleration signal to eliminate any zero shift effect (Charter 9). These figures show a good match between both accelerometers, in terms of acceleration and frequency response. The Velocity Traces also show agreement up to 0.05 seconds, which is more than the time of interest (0.03 seconds to capture the wave return). It should be noted that the Velocity Traces in Figures 13-6 and 13-7 were forced to return back to zero at the end of the trace (0.1024 seconds), as explained in Chapter 12.

From the latter tests it can be seen that the accelerometer and its installation on the flat plate are adequate for the intended application (similar to PDA). Also, it is shown that the calibration, in accordance with Chapter 11, is reliable. The maximum acceleration achieved during these tests was 81g. The maximum-recorded error was 20% with respect to the maximum acceleration measured, but only 4% with respect to the expected range of accelerations (+/-500g).

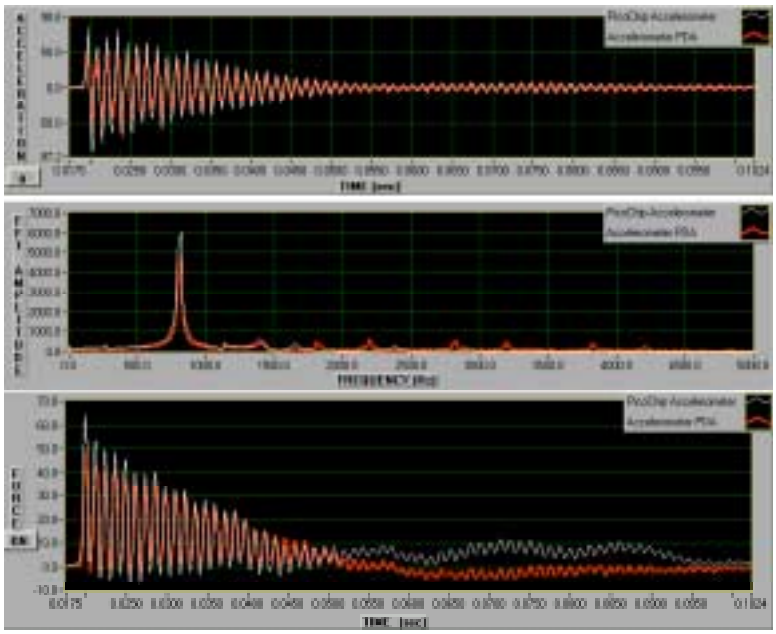

Figure 13-6. Accelerometer Output Comparison Between Proposed Equipment and PDA in Terms of Acceleration, Frequency Spectrum and Velocity Trace (0-0.1 sec.)

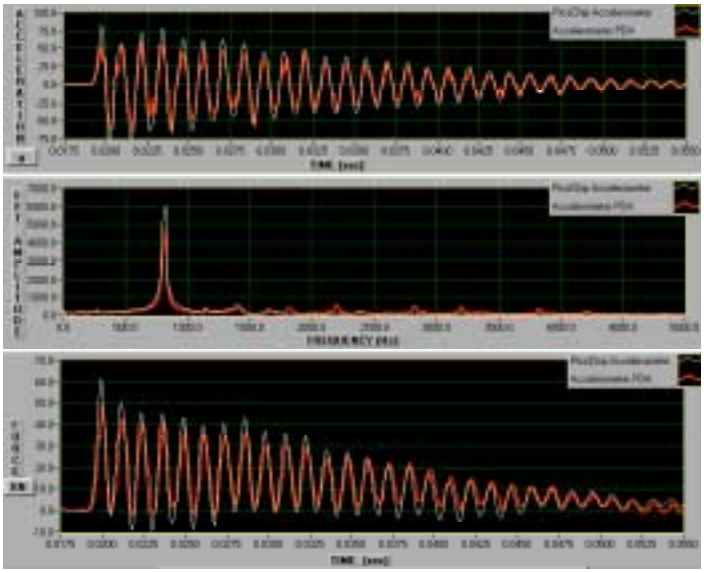

Figure 13-7. Accelerometer Output Comparison Between Proposed Equipment and PDA in Terms of Acceleration, Frequency Spectrum and Velocity Trace (0-0.055 sec.)

The maximum error found in the Velocity Trace was 18% with respect to the maximum Velocity recorded, but only 1.1% with respect to the expected range of Force (Z*Vel).

A second series of tests were performed on the Endevco accelerometer after placed in its new sealed enclosure. The accelerometer was subsequently glued to the end of the miniature pile along with a DC (piezoresistive) accelerometer. The DC accelerometer, model 7270A (from Endevco), is considered a top quality (price: $5000) accelerometer used for calibration and comparison purposes. Figure 13-8 shows how the accelerometers attached to the miniature pile. Figure 13-9 shows the signal comparison for one blow in terms of acceleration, frequency response and Velocity Trace. The velocity adjustment and the 5 Hz low pass filter were used, as in the last tests, to obtain the Velocity Trace. Evident from the figure is the good agreement between the two accelerometers.

It should be noted that the DC accelerometer is a piezoresistive accelerometer, which is not likely to present zero shifts. Also, the signal from DC accelerometer showed good similarity with the PDA accelerometer. This was observed during a test where the DC accelerometer was

Figure 13-8. Accelerometer Installation at the Pile Tip

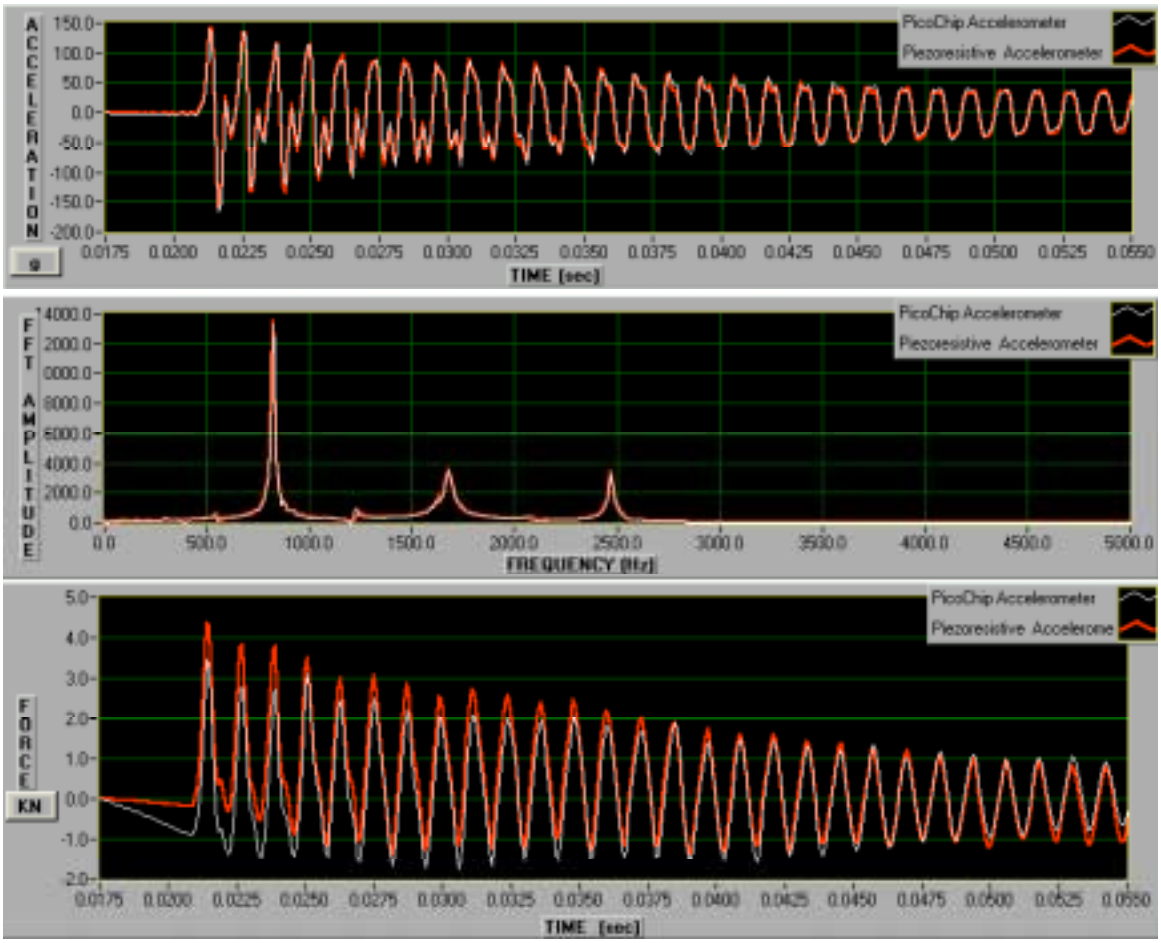

Figure 13-9. Accelerometer Output Comparison Between Proposed Equipment and DC Accelerometer in Terms of Acceleration, Frequency Spectrum and Velocity Trace

mounted on top of the PDA accelerometer, and the PDA accelerometer on the pile. In these tests the maximum acceleration recorded was close to 150g, and the frequency was below 3000 Hz. These are typical values as described in Chapter 5. The maximum error recorded was 3% with respect to the maximum measurement, but only 1% with respect to the expected range of accelerations (+/-500g). The maximum error found in the Velocity Trace was 22.7% with respect to the maximum velocity recorded, but only 0.1% with respect to the expected range of forces (Z*Vel).

SMALL SCALE DRIVING TEST

The miniature pile described earlier was driven in Green Cove Springs, Florida. An 8.9 KN (2 kips) air/steam hammer, with 0.30 m (1 ft) stroke, was used to drive the pile 0.91 m (3ft) into a compacted layer of limestone overlaying a layer of silty sand to sandy silt (Figure 13-10). Three independent apparatus were used to monitor the driving: the wireless system, an additional wired system, and the PDA. It is important to remember that the accelerometers, embedded in this pile, were mounted using an older technique than the technique explained previously. Also, the wireless system used for this pile is an older version, which tend to show more noise than the latest version (65 mV versus 10 mV).

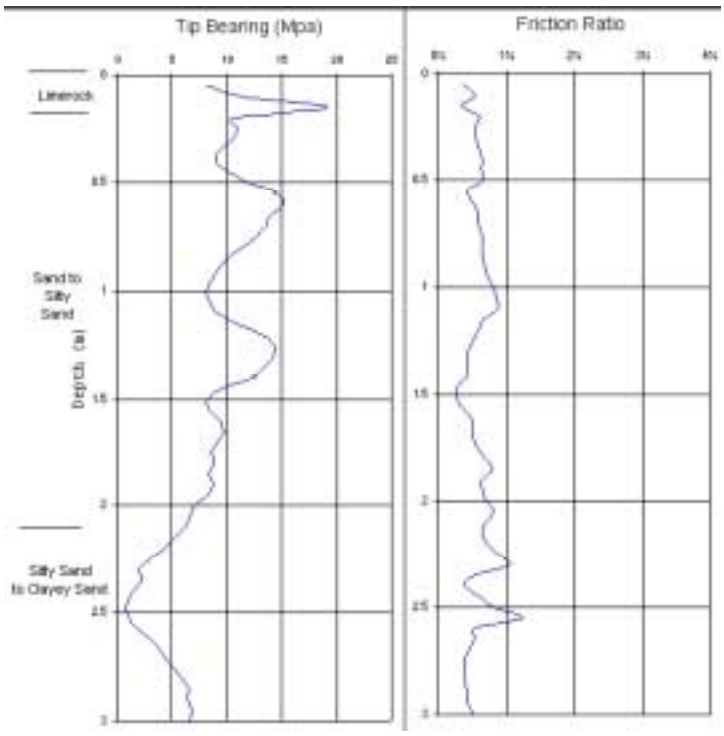

Figure 13-10. Cone Penetration Test in Green Cove Springs. 30 m (100 ft) Away from the Driving Location

The pile properties were obtained in the laboratory (one-day prior driving). These properties are shown in Figure 13-1. The wave speed was checked in the field and showed no significant variation with respect to the laboratory measurements.

The pile was positioned on the leads and the verticality checked with a hand level. The Receiver and Data Processing Unit was located 10 m (30 ft) away from the pile with the 1-meter directional antenna in direct alignment with the transmitter antenna (inside the pile). Figure 13-11 (a) also shows the cables running out of the pile from the wired transducers. These cables are connected to a laptop computer shown in Figure 13-11 (b) (upper laptop). The lower laptop computer in this figure belongs to the wireless system.

(a) (b)

Figure 13-11. Shows the Pile in the Leads and the Receiver and Data Processing Unit Ready to Start Driving

Figure 13-12 shows the PDA sensors being attached to the pile. The PDA transducers were installed 21.3 cm (0.7 ft) below the embedded sensors. They were not installed exactly in the same section as the embedded sensors because the pile cracked at the anchor bolt locations were the PDA sensors were to be attached initially. Consequently, only one accelerometer and one strain gage were used because of the cracking, and space constrains (small pile).

Figure 13-12. PDA Transducers Attached to the Pile

The driving consisted of 62 blows (Table 13-1). During the first 22 blows only the wireless system was used. Over the remaining 40 blows, the PDA package and the wired package were also used for comparison with the proposed instrumentation package.

Table 13-1. Driving Records

Penetration	Number of Blows
0.1 m (1 ft)	26
0.2 m (2 ft)	29
0.3 m (3 ft)	7

For the fist 22 blows, the driving was stopped several times to evaluate the operation of the instrumentation package components. Figure 13-13 shows the software output for one of these blows. The system seemed to work properly at this point in time. The following issues were checked:

- The Non-Recoverable Unit woke (sent signals) after the first strike
- The wireless link showed a full strength signal (4 LEDs were lighted)

- The software displayed Force and Velocity Traces for each blow.
- The capacity graph in the software was updated for each blow

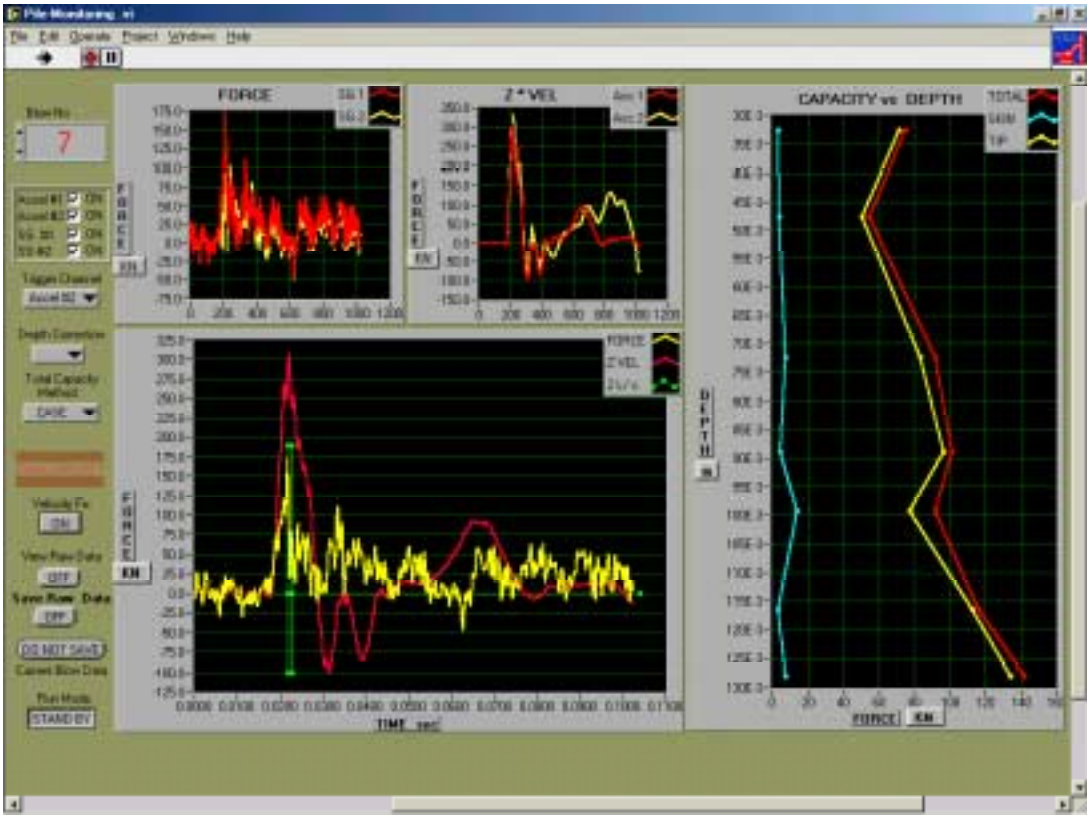

Figure 13-13. Pile-Monitoring.vi Front Panel for Blow # 7 During the Driving Test in Green Cove Springs

Over the last 40 blows the wireless system, the PDA, and wired System were used. Typical Force and Velocity Traces are shown in Figures 13-14 for the PDA System. Some problems were identified as follows:

- The PDA Force Traces showed high negative values not recorded by the wireless and wired packages
- The Velocity Traces from the PDA and the wireless system equipment did not match after the first peak value

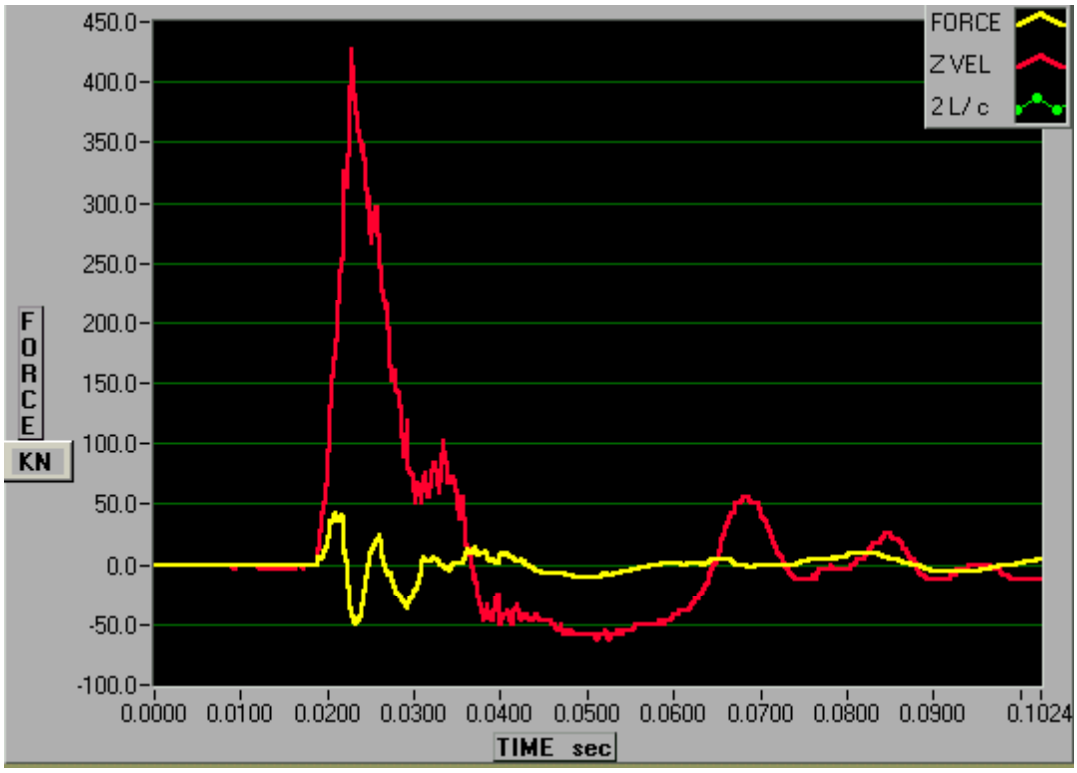

Figure 13-14. Typical Force and Velocity Traces from the PDA During the Driving Test in Green Cove Springs. Blow # 35

- The data quality check failed for both the PDA and the wireless equipment.
- The wave return was not observed at 2L/c but at a later time
- The top accelerometer for the wireless system did not work

The recorded difference in the Force Traces between the equipment is attributed to two known and one possible problem. The fist known was that only one strain gage was used in each instrumentation system; therefore, bending stresses strongly influence the Force Traces, especially for the PDA strain gage (far from the pile's center of gravity). The second known was that the measuring point for the PDA transducers was below the measuring point of the embedded strain gages. Finally, a possible problem is that the PDA strain gage might have been wrongly

attached. This last issue is addressed by the fact that laboratory tests conducted in the laboratory showed fairly good agreement among embedded gages and the PDA strain gages using the same pile.

The difference between Velocity Traces is attributed to two possible problems. Fist the measuring point as mentioned in the last paragraph. Secondly, zero shift effect on the acceleration signal. The observed zero shift effect was the reason to improve the mounting technique as explained in Chapter 11.

The data quality failure and the late wave return are attributed to the small size of the pile and the placement of the instrumentation in the top of the pile (Non-Recoverable components). For further testing, i.e. full-scale piles, the components would be placed between the top sensors and the pile top, or between the tip sensors and the pile tip. This would result in no interruption of the stress wave propagation.

Even though this pile did not performed 100% as expected, some valuable information was obtained:

- The instrumentation Package survived the shock and vibration during driving
- The instrumentation Package survived the stresses under driving
- The Non-recoverable Unit transmits the signal without being influenced by the pile movement, shock, vibration, and compression.
- The transmitter antenna works properly when it is partially embedded in the pile, and show no interference due to vibration
- The software performed properly, triggering for every blow, and displaying Force and Velocity Traces, plus pile capacities

Other addition problems identified and fixed after the field tests were:

- The noise was reduced from 66 mV to 10 mV.
- The accelerometer mounting technology was changed and tested to avoid zero shift effect.
- The Signal Receiver and Conditioning Unit output range (0 to 2.5 Volts) was increased to 0 to 5 Volts.
- The gain factor on the strain gage channels has increased by a factor of 2.
- Finally, a protective circuit was added to the conditioners to avoid damage to the transmitter in the event of a shorted or open strain gage.

CHAPTER 14

FULL SCALE TESTS AT CYPRESS CREEK

Two full-scale piles were driven in Tampa, Florida (February 2002) with the proposed wireless equipment. The piles were 24 inch prestressed concrete, sixteen meters (52.5 ft) long, and part of a bridge pier bent. The bridge is located on State Road 54 (SR 54) over Cypress Creek, North of Tampa.

Each pile was monitored during driving using 2 accelerometers and 2 strain gages. The first pile had all of instrumentation at the pile top, whereas the second pile had one pair of sensors near the pile top and the other pair close to the pile tip. Additionally, both piles were monitored with the PDA for comparison purposes.

The difference in layout of the instrumentation for the two piles was to check repeatability, consistency (pile 1), as well as measure stresses at the pile tip (pile 2, proposed future studies). For pile #1, the output from the two accelerometers should be identical, but depending on bending behavior, the two top strain gages may show slight differences. For pile #2, the transducers at the pile tip were intended to measure the stresses, rather than estimate them based on the top measurements. It is also proposed that the force and velocity measurements at the pile tip be used for future studies to better assess damping, tip resistance, residual stresses, and skin friction on piles.

SR-54 SITE DESCRIPTION

A forty-two meter long multiple span concrete bridge is under construction in Pasco County, North of Tampa. Located on SR 54, the bridge spans Cypress Creek (Figure 14-1), and it replaces a smaller single span bridge.

(a) (b)

Figure 14-1. Job Site (a) Location; (b) Picture of the Creek and Piles on the East Side

The new bridge foundation was designed with two abutments and a center pier. Both abutments (ends) and center pier are supported on standard 24-inch FDOT prestressed concrete piles. The abutments had 8 piles each and the center pier had 6 piles. The bridge elevation is shown in Figure 14-2 and the pile distribution in Figure 14-3.

Two of the eight piles on the west side of the creek were instrumented with the wireless instrumentation packages. The piles are labeled as pile number 1 and 3, and are located in the left bent shown in Figure 14-3. There were three SPT bring logs for the whole site, with only

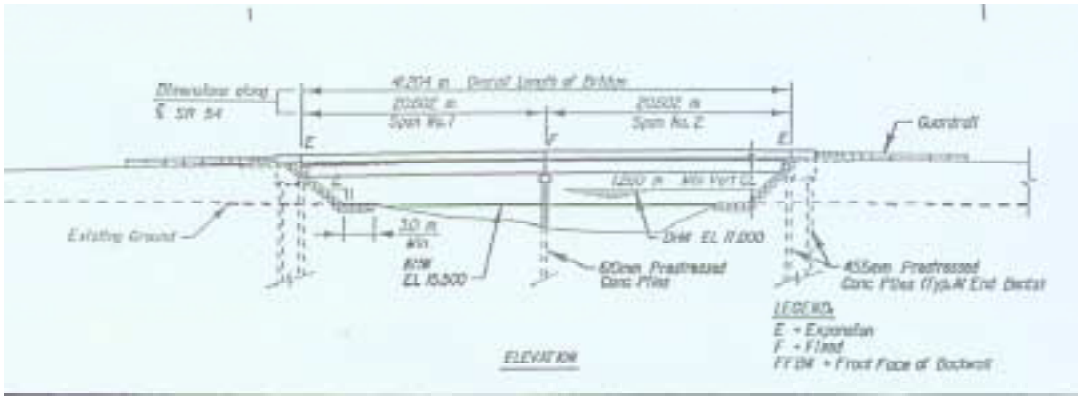

Figure 14-2. Bridge Elevation

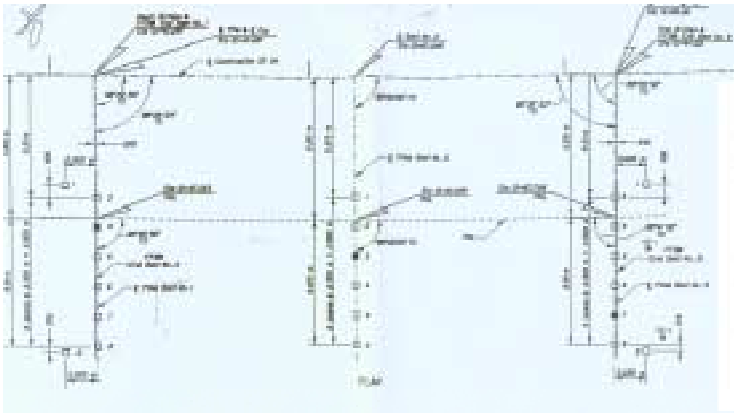

Figure 14-3. Pile Distribution in Two Abutments and One Center Pier

one of them, BB-2, located on the west side of the creek. The latter boring, BB-2 was west of pile # 7, and is to a depth of 17 meters. Boring log BB-2 is presented in Figure 14-4 b.

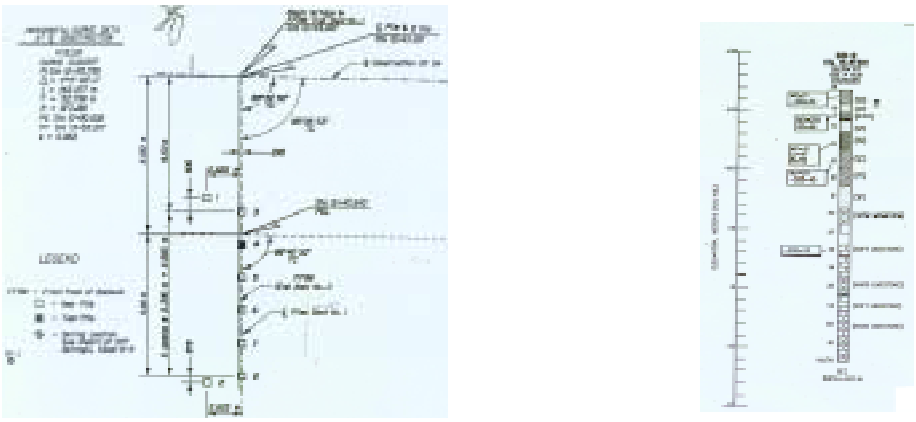

(a) (b)

Figure 14-4. SPT Boring on the West Side of the Creek (a) Location; (b) Boring Log

There was approximately 10 ft of mixed soils overlying limestone. Since, a portion of the upper soil was compacted fill; it was predrilled in accordance with FDOT specifications for pile driving.

It is important to note again that piles #1 and #3 in end bent #1 were part of the production piles. Their length was set at 16 meters based on earlier test pile monitoring in later December 2001 with the PDA. Three test piles were performed at that time, pile #4 in end bent #1, pile #3 in bent #2, and pile #7 in end bent #3.

PILE INSTRUMENTATION

Each pile was instrumented with four sensors: two accelerometers and two strain gages, plus backup sensors and conditioners to be used in case of transducer breakage, cable damage, misalignment or unexpected problems.

Each transducer was pre-installed on a 31-mm (1/8-inch) Plexiglas plate, as shown in Figure 14-5, to allow ease of installation and alignment during pile construction in the casting yard. Each plate held one accelerometer and one strain gage as shown in Figure 14-5 (a). The plate was installed in the pile's steel form using two steel rebars attached to the pile's longitudinal pretension strands. The latter both aligned the instrumentation packages as well as anchored them during the concrete placement.

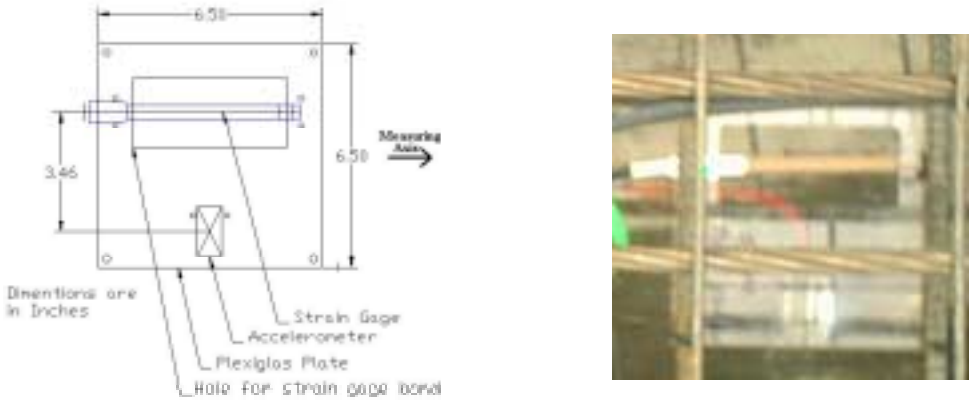

(a) (b)

Figure 14-5. Instrumentation Mounting Technique (a) Schematics; (b) Picture

The Plexiglas plates were connected to the steel bars using plastic ties and the bars were connected to the strands using wire ties. The transducers were connected to the plate using 10 cm (4 inch) plastic ties. The accelerometer was glued to the Plexiglas plate due to provide resistance to concrete flow during casting. In order to ensure good bonding between the strain gage and the concrete, the Plexiglas plate was cut out underneath the strain gage's active length (i.e., sensing area).

Pile #3 was instrumented with two accelerometers and two strain gages at the same cross sectional area (6 ft from the pile top). Both strain gages were equally spaced from the pile centerline line to ensure average stresses (account for bending moments), consistency, and similarity. Additionally, a backup accelerometer and strain gage was installed between the active transducers. Figure 14-6 shows the instrumentation set up. The alignment of the transducers attached to the Plexiglas plate was with a steel square placed against the pile's formwork. The distance

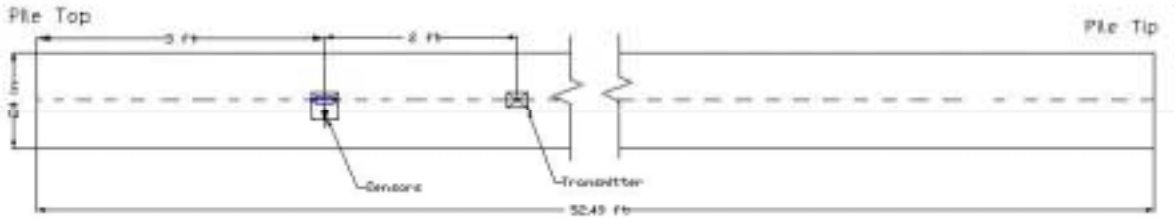

(a)

(b)

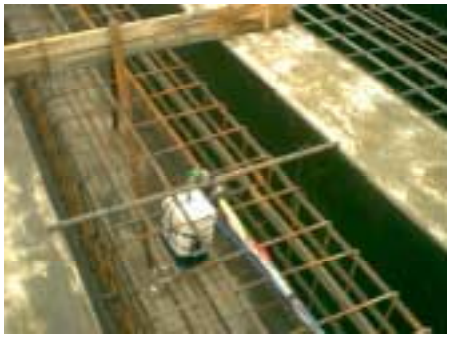

(c)

Figure 14-6. Instrumentation of Pile #3 (Transmitter Unit #4) (a) Instrumentation Placement in Plan View; (b) Picture of Sensors; (c) Picture of Transmitter Plus Electronics

of the sensors to the Transmitter (Signal conditioning and Sending Unit) was 2B (48") in order to avoid unwanted wave return or end effects. The transmitter used for this pile was defined as Unit #4. The antenna was located between the sensors and the transmitter to avoid signal interference by the pile cap.

Pile #2 was instrumented with one accelerometer and one strain gage near the pile's top (6 ft from the top) and with one strain gage and one accelerometer close to the pile's bottom (6 ft from the pile tip). Additionally a backup accelerometer and strain gage was used near the pile top, as well as the pile tip (5 ft from the pile top and 5 ft from the pile tip). Figure 14-7 shows

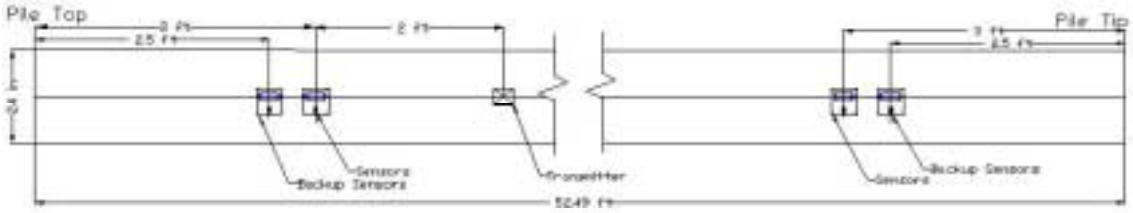

(a)

(b)

(c)

Figure 14-7. Instrumentation of Pile #1 (Transmitter Unit #5) (a) Instrumentation Placement in Plan View; (b) Picture of Sensors at the Top; (c) Picture of Transmitter Plus Electronics

the instrumentation set up. For pile #2, the strain gages were aligned at the pile's central axis using a square and a ruler. As in pile #3, the distance from the sensors to the Transmitter (Signal conditioning and Sending Unit) was 2 B to avoid unwanted wave returns. The antenna was located between the top sensors and the transmitter. The transmitter for this pile was identified as Unit #5.

Since this was the first full-scale test, all of the sensors had a section of their cables coming to the pile surface (flush with the concrete) for access, testing and possible switching in case of problems. Pile #3 had one access point close to the pile top, and pile #1 had two access points, one at the pile tip and the other at the pile top. A typical access point is shown in Figure 14-8. The backup transducers and conditioners were not needed for pile #3 but they were used for the top sensors of pile #1.

(a) (b)

Figure 14-8. Access Points: (a) Covered; (b) Open to Test Transducers and Conditioners

For pile #1 the strain gage conditioners at the pile top failed, so the backup conditioner and transducer replaced it. Also, the accelerometer at this location was replaced (backup used), not because it was defective but to recover both strain and velocity measurements at the same pile cross section.

It should be noted that UF researchers placed the instrumentation in both piles and subsequently left the casting yard. The personnel at Standard Concrete poured the concrete for the two test piles along with the rest of the piles in the bed later that night. Consequently, it is believed that the instrumentation package placement, and concrete pouring may be handled in the casting yard by casting personnel.

Next, striking the pile with a hand held hammer tested the activity on each sensor. First striking the pile on its side, close to the transmitter turned on the system. It was noted that striking the pile with a hand held hammer close to its end was very difficult to wake system up (Figure 14-9). After waking the pile, the accelerometer response was verified with and external accelerometer. The wave speed measured with the external accelerometer showed good agreement with the embedded accelerometer, giving indication of proper alignment (accelerometer not moved by the abrasive activity during the casing).

Figure 14-9. Testing the Instrumentation Package on the Casting Yard by Striking the Piles with a Hand Held Hammer

DRIVING TEST

Both piles were driven with an ICE 80-S single acing diesel Hammer. The hammer, Figure 14-10, has a total weight of 15.4 tons, a ram weight of 8 ton, maximum stroke of 10 ft (Energy 80,000 - 32,000 lb-ft), and a maximum blow rate of 55 blows per minute.

(a) (b)

Figure 14-10. Driving Equipment and Setup (a) Diesel Hammer ICE 80-S and Leads; (b) 150 Ton Crane, Leads and Hammer, Template, Pile #3 Driven, Pile #1 to be Driven

Each pile was driven with a new pile cushion made of plywood. Several sheets of plywood were used to make each cushion 190 mm thick.

Before driving, pile on the ground, the WAP instrumentation was turned on, the wave speed measured, and the PDA transducer holes were installed (Figure 14-11b). The WAP equipment was turned on with a strike of a hand held hammer. Using the wireless link and the embedded accelerometer the wave speed was measured several times following the procedure described in Chapter 8. For Pile # 1, the wave speed was also checked using the time of wave travel from the top to the tip transducer and the distance separating them. Later the PDA trans-

(a) (b)

Figure 14-11. Pile Setup Preparation (a) Pre Drilling; (b) PDA Transducer Holes

ducer holes and anchor bolts were installed in the same location as the WAP transducers (6 ft below the pile top for pile #3 and 5 ft below the pile top for pile #1). The PDA transducers were installed on the lateral sides of the pile to avoid interference from our antenna (front face the pile - Figure 14-11b).

Before driving each pile, a template was placed on top of the ground to locate and support the pile. The template was made of steel I-beams and kept in place with concrete weights (Figure 14-11a). Prior to placement of the pile, a hole was predrilled through the template. The hole, predrilled to a depth of six meters with a continuous auger (Figure 14-11a) passed through the existing compacted fill to natural soil. Next, the pile was inserted and then the leads plus hammer was installed around and on top of the pile. The orientation of the pile was checked with a hand level on the leads.

Prior to driving, the directional 1-m antenna was mounted on a pole and installed as shown in Figure 14-12c. The laptop computer was installed at the back of a Van and connected to the antenna using a long coaxial cable (Figure 14-12a).

(a)

(b)

(c)

Figure 14-12. Set Up (a) WAP Laptop; (b) PDA PAK; (c) Receiver Antenna and Pile #1 on the Leads

The pile was placed such the embedded antenna was facing the directional antenna, as shown in Figure 14-12c. It was discovered due to lead construction that some of its frame elements were periodically in front of the embedded antenna. However no problems were recorded other than a minimum decrease in signal strength whenever those elements (Figure 14-12c) were in front of the embedded antenna.

During the actual driving the transmission distance was keep within 50 ft (horizontal distance) from the pile. For the fist driven pile, pile #3, the distance was 20 ft and for the second pile, pile #1, the distance was 50 ft.

During the early stages of driving, the WAP system was not able to wake up from the hammer strike accelerations. The latter was attributed to low g levels recorded with the PDA (acceleration less than 60g). To partially solve the problem and have some records for early stages of driving, the pile was struck with a hand held hammer close to the embedded Signal Conditioning and Sending Unit. This turned the system on and allowed the recording of 2.5 minutes approximately, after which the pile had to be struck by hand again to turn the system on again.

It was not until in later stages of driving (after 12m) that the wakeup system worked as expected. This is attributed to higher accelerations (a > 70 g) recorded by the PDA as well as the WAP equipment. Consequently, only the last WAP records (last 175 blows for pile #3 and last 235 blows for pile #1) were correlated with the PDA values. They will be shown in the following two sections.

Once the pile was driven (met the driving criteria), the transmission distance was further tested by moving the receiver antenna away from the pile in multiple directions and striking the pile with a hand held hammer. The maximum distance achieved was 200 ft with the maximum possible signal strength. It is important to note that the directional 1 m antenna was used for the latter tests.

Regardless of the small problems mentioned, the WAP output signals were strong with little noise (less than 10 milivolts) and compare very satisfactorily with the PDA outputs. The results as well as other special during details are described in the following sections.

Pile # 3 at End Bent #1

Pile # 3 was driven on February 14 of 2002. The actual driving occurred over a one-hour time frame with 7.25 m of penetration. The PDA recorded 1345 blows and the WAP recorded

827 blows. The latter was due to the previously described problem with the wake up system. The contractor personnel recorded 1297 blows.

Figure 14-13 shows the WAP output at the very last blow. It is important to note that the capacity graph shows the driving history for the last 500 blows. The total pile capacity shown is based on the CASE method. The UF method (Chapters 7 & 8) was used to assess the case damping constant, J_c, as well as the tip and skin capacities.

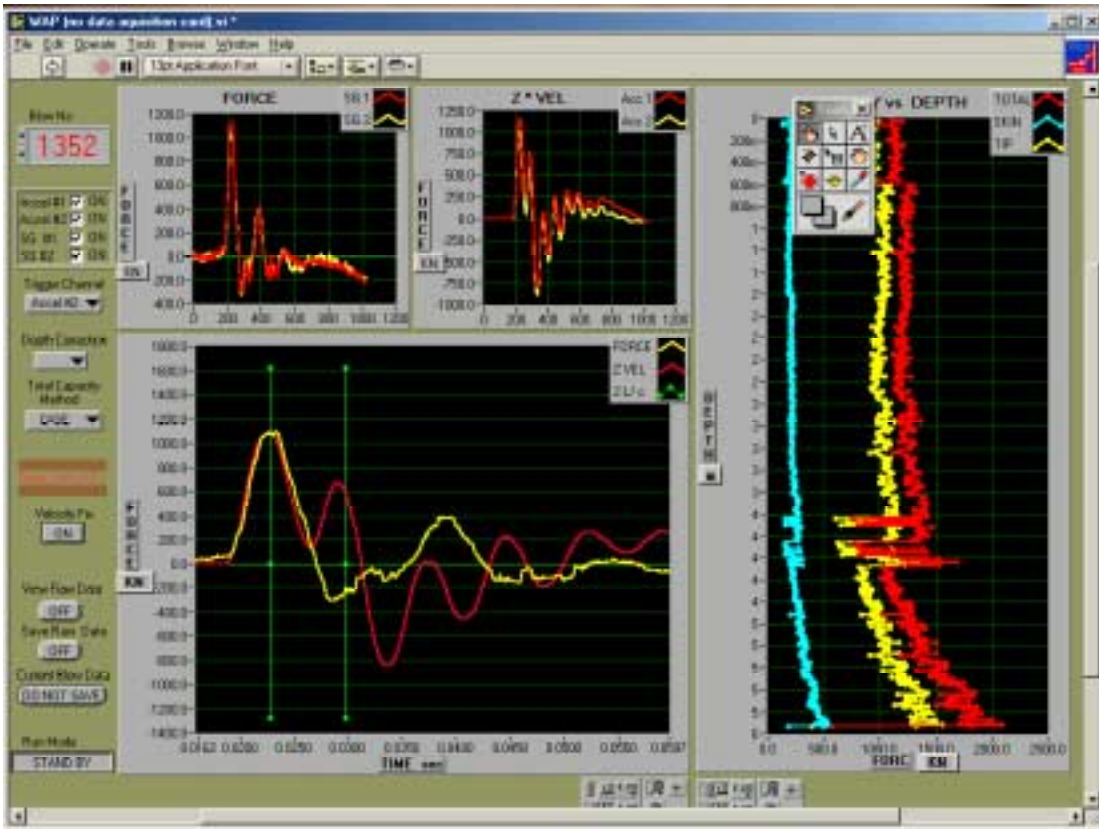

Figure 14-13. WAP Records for the Last 500 Blows on Pile #3

Force and velocity traces recorded in this pile were very consistent as shown in Figure 14-14 through 4-16. The top two graphs in each figure are the forces based on the strains and accelerometers. In each window there are two graphs, which report the response from two

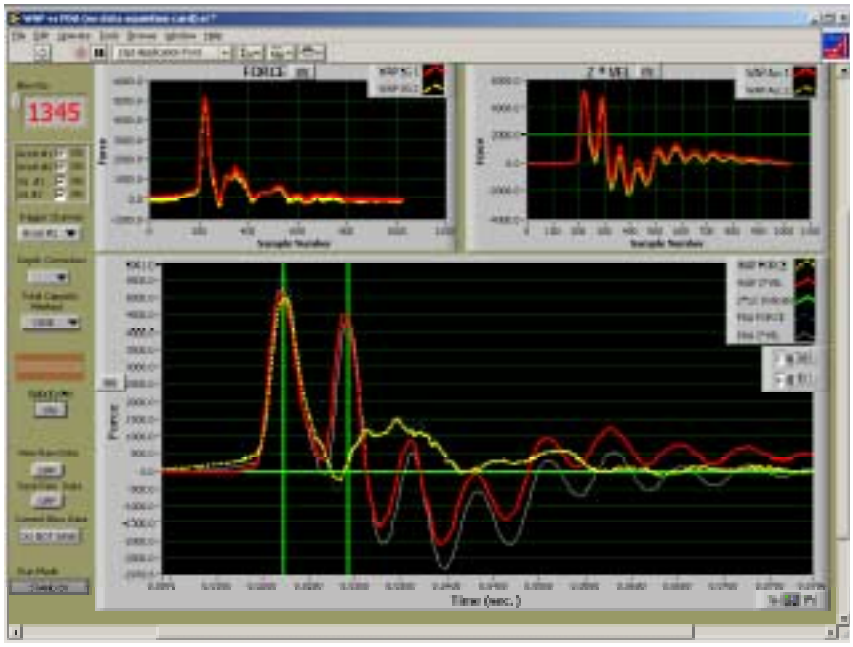

Figure 14-14. Traces versus PDA Traces for Blow 1345 (last Blow Pile #3)

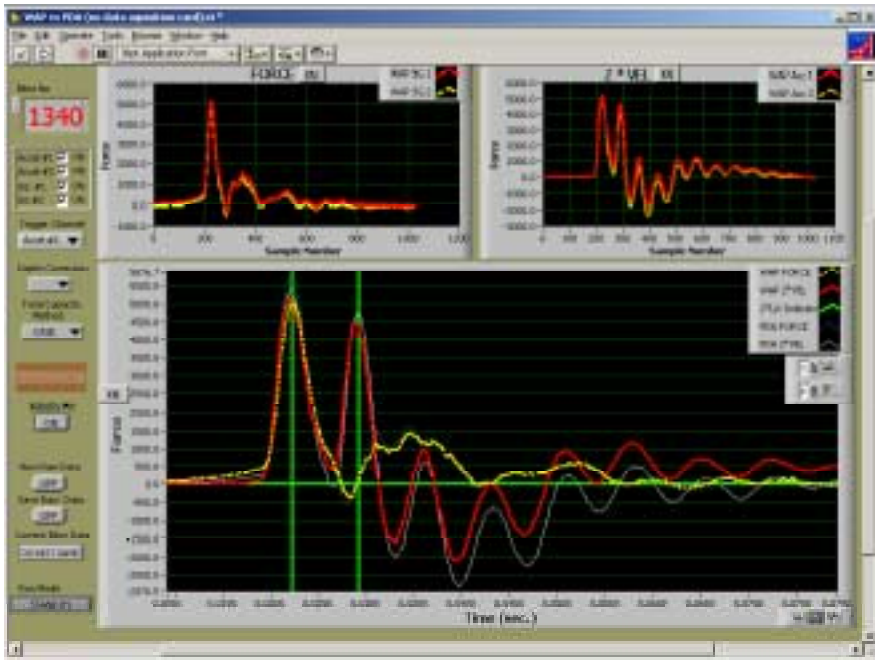

Figure 14-15. Traces versus PDA Traces for Blow 1340 (Pile #3)

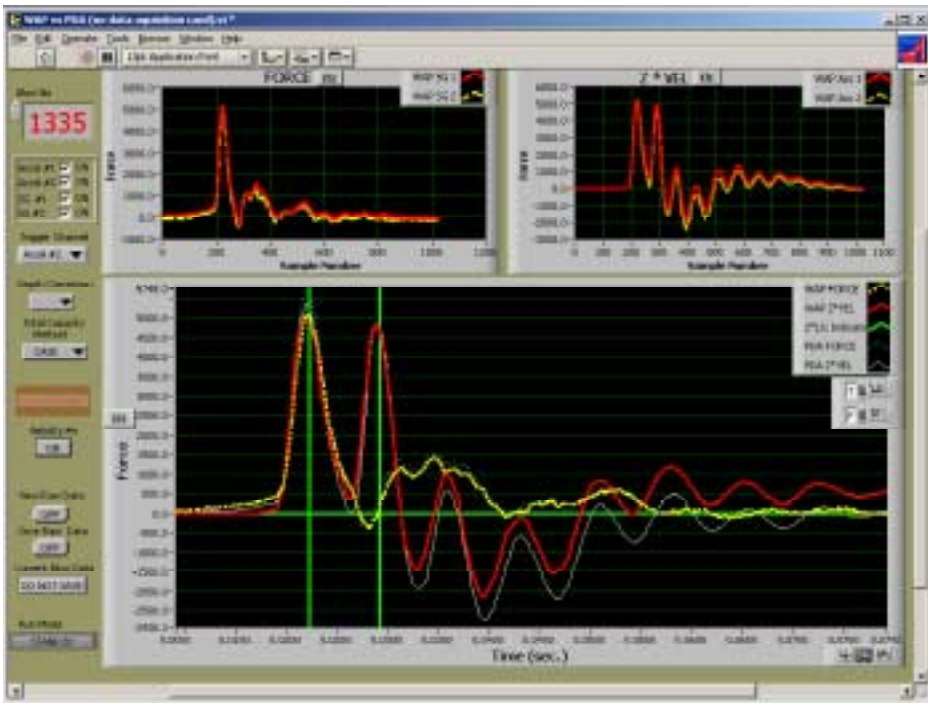

Figure 14-16. Traces versus PDA Traces for Blow 1335 (Pile #3)

gauges (strains or accelerometers), at similar elevation but at different offsets. Note the very similar response of each. Also shown in the larger plot below the smaller graphs is the combined force plots from both strain and accelerometer. Included in this plot are the response recorded with the PDA equipment. The comparison is very good up to 2L/c (green vertical lines), after which the computed force from the PDA accelerometer deviates slightly from the WAP value. It is not known if the latter is due to the zeroing process that the PDA software employs (rotates acceleration trace from maximum peak to zero at 0.1 sec).

A further and more in depth comparison between the WAP output and PDA is presented in terms of compression and tension stresses in the pile. Shown in Figure 14-17 are maximum compression stresses predicted both by PDA and WAP. Agreement is very good, especially for the last 175 blows were both instruments were recording simultaneously.

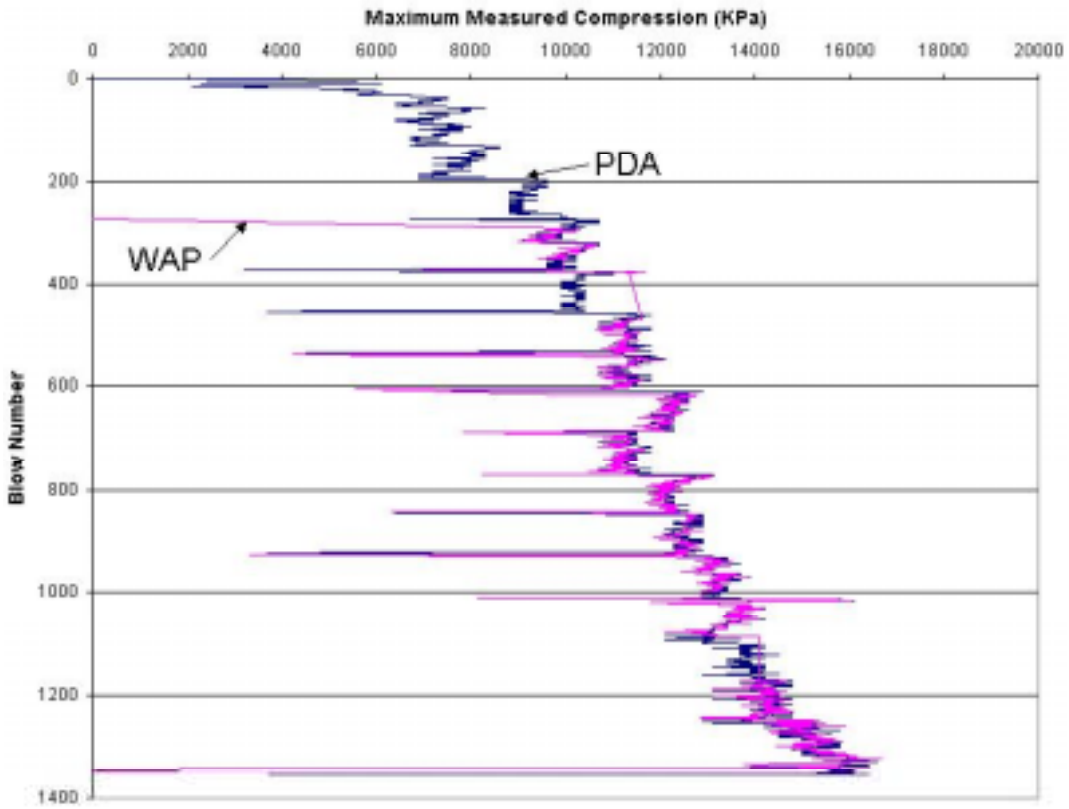

Figure 14-17. Comparison of Maximum Compression Stress Between WAP and PDA Records at the Pile Top

Tension stresses are very important in concrete piles. Using the Wave Up one can easily investigate whether tension stresses are present. Generally, if the soil resistance is small, the Wave Up will show tensile stresses, which will arrive at time 2L/c. The maximum tension stress occurs at the minimum point of the downward compression stress (Wave Down at time t_3 in Figure 14-18). The maximum tension is found using Equation 14-1a and 14-1b for easy and hard driving, respectively.

$$T_{MAX} = F_{(UP,t2)} + F_{(DOWN,t3)} = \frac{[P_2 - Z \times Vel_2]}{2} + \frac{[P_3 + Z \times Vel_3]}{2} \qquad (14\text{-}1a)$$

$$T_{MAX} = F_{(UP,t3)} + F_{(DOWN,t2)} = \frac{[P_3 - Z \times Vel_3]}{2} + \frac{[P_2 + Z \times Vel_2]}{2} \qquad (14\text{-}1b)$$

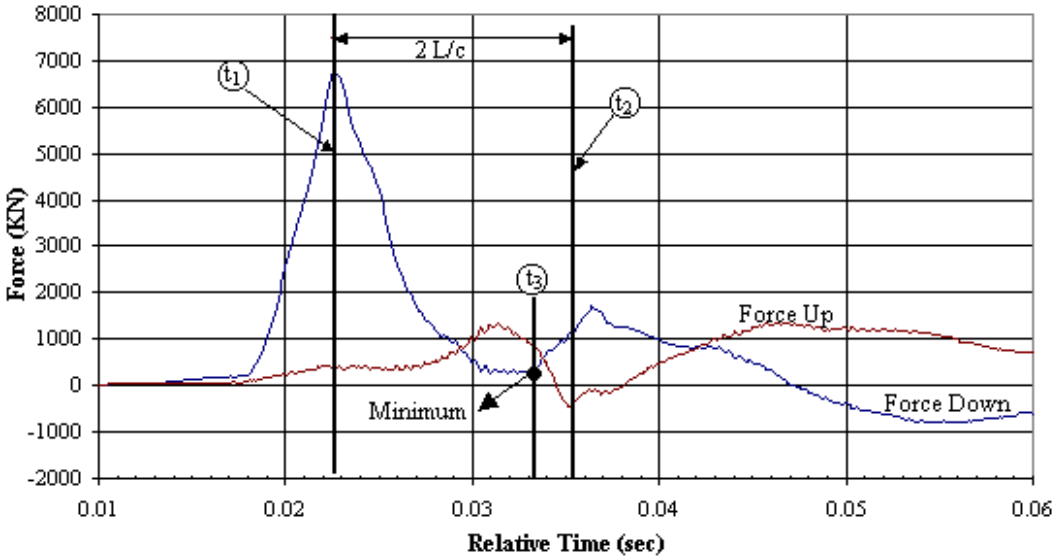

Figure 14-18. Determination of Tension Stresses in the Pile

Using Eqs. 14, the maximum tension stresses in the pile were computed for all the blows using WAP and PDA data (Figure 14-19). Agreement is very good, especially for the last 175 blows were both instruments were recording simultaneously.

Pile # 1 at End Bent #1

Pile # 1 was driven on February 15 of 2002. The driving was from 11:15 am to 11:50 am with a driving penetration of 6.0 meters. The PDA recorded 909 blows and the WAP recorded 770 blows. The difference was that the early driving did not exceed 50 to 60 gs which is the threshold to wake up the WAP system. The contractor personnel recorded only 891 blows.

Figure 14-20 shows the WAP output recorded for the very last blow. The capacity graph (right picture) in the figure shows the driving history for the last 500 blows (latter figure is up-dated for each blow). The total capacity prediction was based on the CASE method and the UF method was used to assess the case-damping constant, as well as the tip and skin capacities.

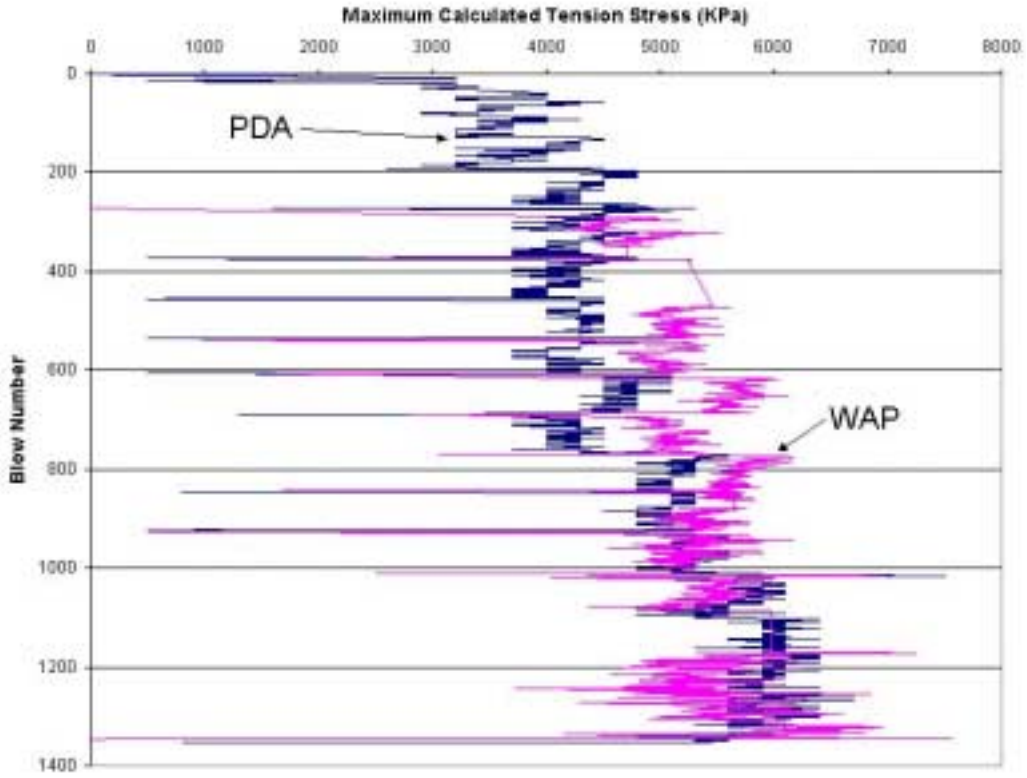

Figure 14-19. Comparison of Maximum Tension Stress Between WAP and PDA

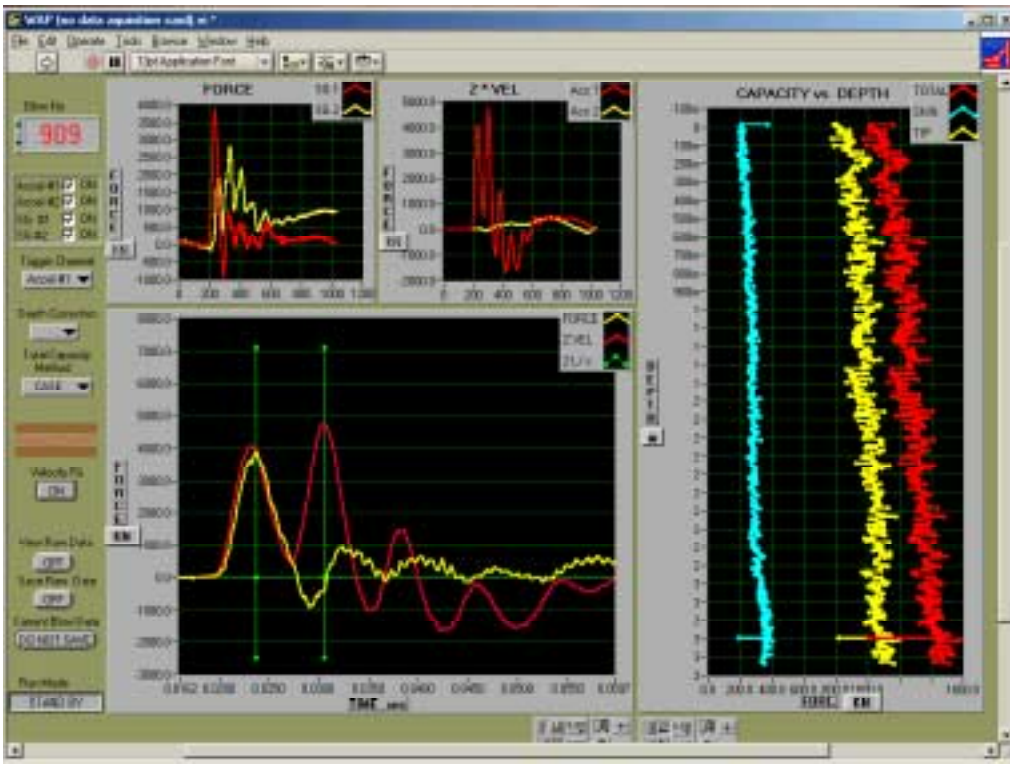

Figure 14-20. WAP Records for the Last 500 Blows on Pile #1

Evident from the capacity graph is that the total pile capacity is gradually increasing with depth and that the pile's resistance is approximately 30% skin and 70% end bearing.

A comparison of WAP and PDA response at the top of the pile is given in Figures 14-21 to 14-23. The comparison is very good up to 2L/c (green vertical lines), after which the computed force from the PDA accelerometer deviates slightly from the WAP value. It is not known if the latter is due to the zeroing process that the PDA software employs (rotates acceleration trace from maximum peak to zero at 0.1 sec).

Also shown in upper to graphs of Figures 14-21 to 14-23 are the forces at the pile tip (yellow lines). This data is not available with the PDA equipment, but only through the WAP system. The data in the left graph is based on strain and the values in the right are based on the velocities (integration of acceleration). The latter shows that for most blows that the velocity is very small, which is typical for piles with considerable tip capacity (see capacity graph, Fig 14-20). From the soil borings (Fig 14-4b), it was noted that the piles were tipped in limestone.

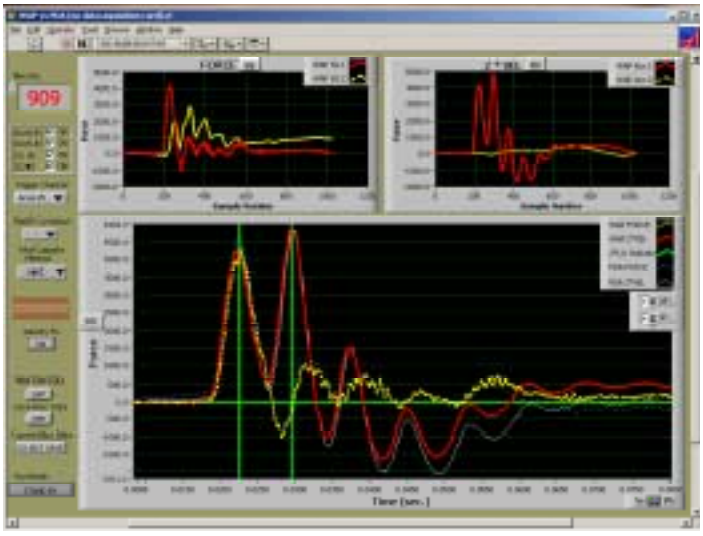

Figure 14-21. WAP Traces versus PDA Traces for Blow 909 (last Blow Pile #1)

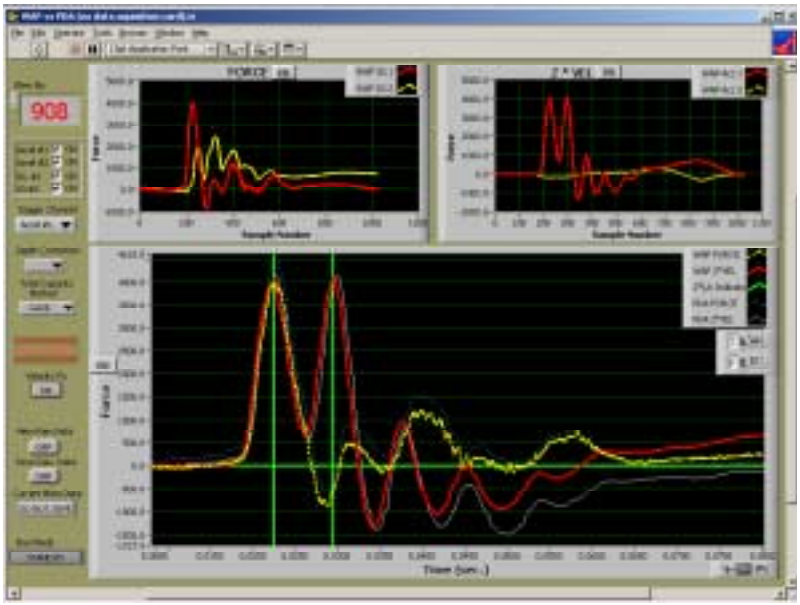

Figure 14-22. WAP Traces versus PDA Traces for Blow 908 (Pile #1)

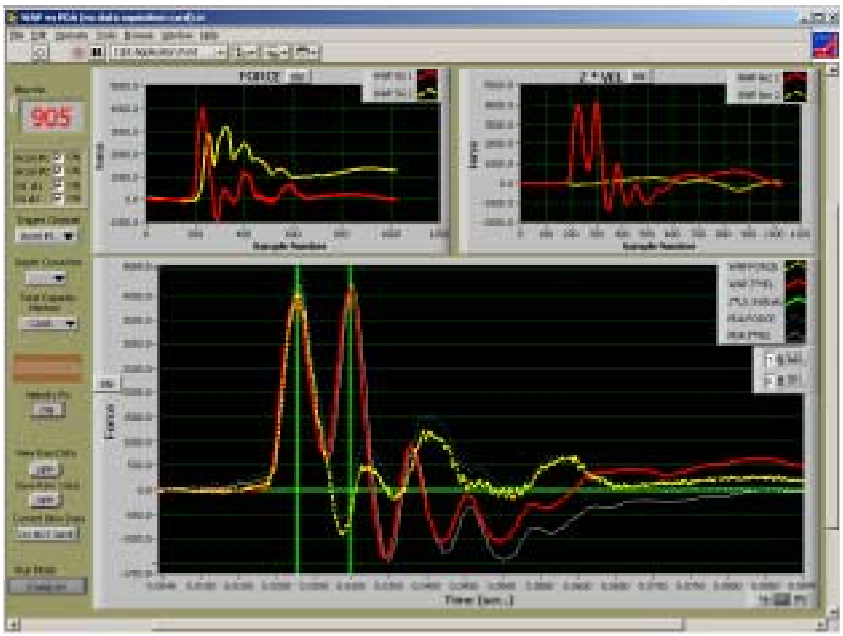

Figure 14-23. WAP Traces versus PDA Traces for Blow 905 (Pile #1)

Also, the force plot (from the strain gauge) shows considerable offset at the end of trace. However, the latter offset generally returns back to the vicinity of zero after 1.5 to 2 seconds. The latter is not shown in the figures, but it is recorded with the WAP equipment (continuously monitoring the pile between blows). Consequently, it is believed that the early offset is tip stresses, which diminish due to creep, and/or are redistributed through the pile as residual stresses.

Similar to pile #3, a more in depth comparison between the WAP and PDA outputs was performed and is presented in Figures 14-24 to 14-26. Figure 14-24 shows the maximum compression stress recorded with the strain gages at both the top and bottom of the pile. The PDA recorded values at the top of the pile are also shown for comparison. Agreement between PDA and WAP at the top of the pile are very good.

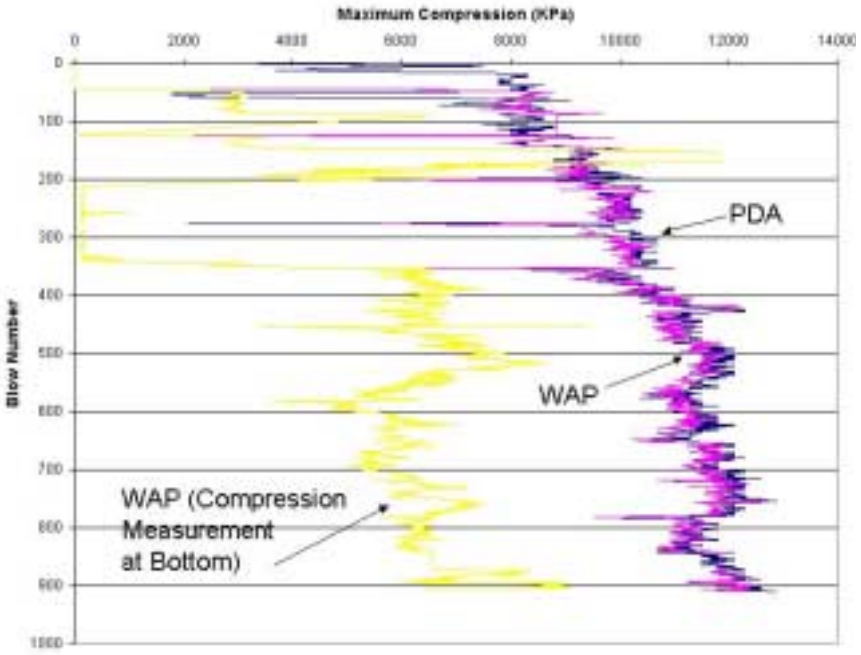

Figure 14-24. Comparison of Maximum Compression Stress Between WAP and PDA at the Pile Top and WAP at Pile Bottom

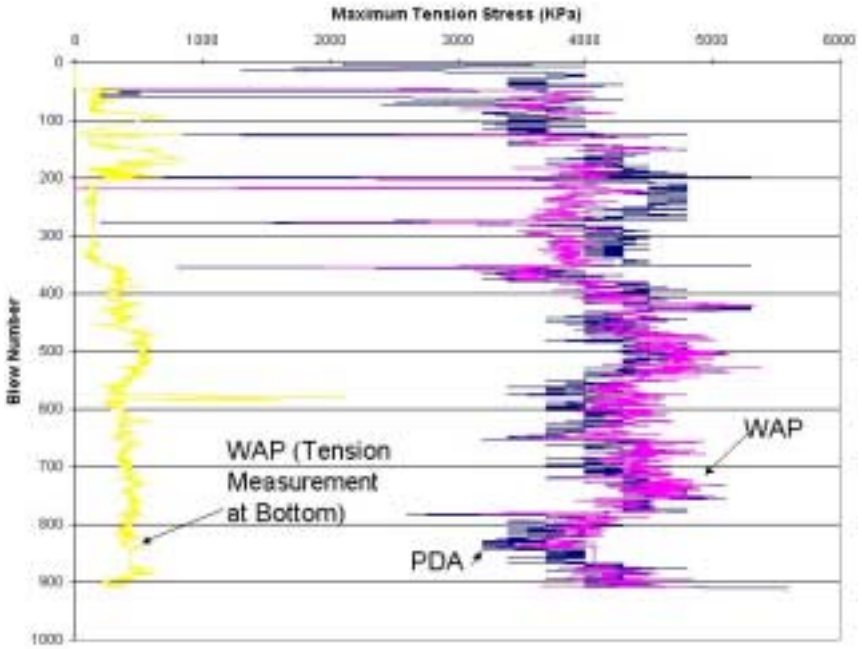

Figure 14-25. Comparison of Maximum Tension Stress Between WAP and PDA at the Pile Top and WAP at Pile Bottom

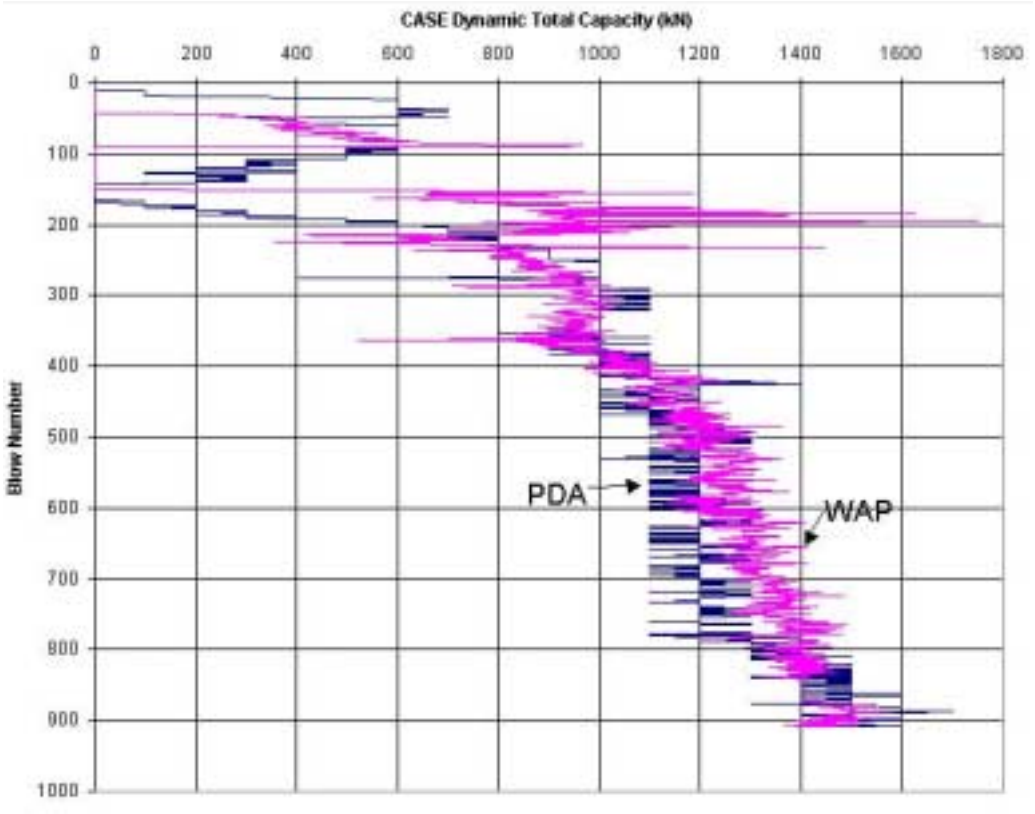

Figure 14-26. Comparison of Dynamic Capacity Assessment WAP and PDA

Shown in Figure 14-25 is the tension stresses in pile #3 computed from Equations 14-1 for both the PDA and WAP records. WAP data was available for both the top and bottom of the pile, whereas the PDA was available for top of pile only. Again similarity between PDA and WAP at the top of the pile is excellent. As expected for predominately tip resistance pile (founded in limestone), WAP shows very little if any tension stresses at the pile's tip.

Figure 14-26 plots the total pile capacity with the $J_c = 0$ as calculated with equation 3-14 for both PDA and WAP. It should be noted that some values for the WAP are copied from the previous ones due to the loss of data from wake up problems described earlier. Consequently, the blow number recorded by WAP might not be exactly the same as the PDA for earlier values but are the same for the last 235 blows. Again, the figure shows very good agreement between PDA and WAP especially for the last blows.

Finally, URS which performed the PDA and CAPWAP analysis on pile # 1 independently of this research, reported the following CAPWAP results: Total capacity - 1600 kN, skin resistance - 700 kN, and tip resistance - 900 kN at the end of drive. Comparing the latter with the WAP values given in Figure 14-20 (Total resistance, 1550-1600 kN, skin resistance, 500-600 kN, and tip resistance, 1000-1100 kN), agreement is very good for total capacity assessment. The slight difference in end bearing may be attributed to the difficulty CAPWAP has in differentiating skin and tip resistance near the end of the pile.

CHAPTER 15

CONCLUSIONS AND RECOMMENDATIONS

The conclusions and recommendations presented herein are subdivided into three sections. The first deals with the assessment of dynamic methods to estimate static pile capacity from Load and Resistance Factored Design (LRFD). The second concerns the determination of PDA Case damping coefficient, J_c, as well as predicting the skin and tip resistance from measured stress wave propagation in a pile. Finally, a new cast insitu instrumentation package and wireless transmission system is presented. In the case of the latter, comparisons with current practice (PDA), as well as future applications are discussed.

LRFD CALIBRATION FOR EIGHT DYNAMIC METHODS

Eight dynamic methods were evaluated based on a Florida database and LRFD design procedures. The following conclusions can be drawn from this study:

1. The bridge span length has negligible effect on the resistance factor, ϕ, or the corresponding safety factor.
2. The COV_R or ϕ/λ_R-values, rather than the absolute values of the ϕ factor, should be used to evaluate the accuracy and efficiency of a dynamic method.
3. The accuracy (COV_R & ϕ/λ_R) of dynamic methods from testing at BOR show negligible increase over the same testing at EOD.
4. The evaluation of ϕ/λ_R shows that the newer dynamic methods (PDA, Paikowsky, CAPWAP) are generally more cost effective to meet a reliability index in comparison with the older methods.

5. The CAPWAP procedure tends to underestimate the Davisson capacity by 28 percent, while the PDA underestimate the Davisson capacity by only 9 percent at EOD.
6. The older methods (i.e., Gates, FDOT, ENR, and Modified ENR) result in better estimates of Davisson capacity for pile capacity less than 200 tons (1779 kN).
7. The Gates formula, when used separately for Davisson capacity larger than 1779 kN and less than 1779 kN, may have comparable accuracy with the modern methods.
8. For Allowable Stress Design (ASD) design with dynamic methods, the following safety factors are recommended to meet a probability of failure of 0.62 ~ 2.50 %: 1.8, 2.0 and 2.5 for CAPWAP, PDA, and Paikowsky's energy method at EOD, and 2.25, 2.5 and 3.5 at BOR, respectively. Currently, a safety factor of 2.5 is used for CAPWAP, PDA, and Paikowsky's method, for both, BOR, and EOD. The driving formulas are usually applied at EOD only, and safety factors of 1.9, 14.0, 11.0, and 2.0 are recommended for FDOT, ENR, modified ENR, and Gates formulas, respectively.

Recommendations

The results presented in this study reflect the pile driving history of Florida. The number of piles considered is based on the availability of dynamic and static load test data. In addition, sometimes the available information is not sufficient to evaluate a given dynamic method. Based on the latter facts, the following recommendations are presented.

1. In order to have a more representative LRFD calibration for the Florida practice, any pile driving and static load test information not included in this study should be added to the existing Florida database.

2. The LRFD resistance factors should be monitored on a semi annual event as more information (cases or pile types: cylinder, etc.) is obtained from the field or other sources (National).

Determination of Case damping coefficient, J_C , and skin & tip resistance from measured stress wave propagation in a pile.

An important finding of this research was that the coefficient of variance of the static capacity changed by only 10 percent when the Case damping, J_c , was modified by 30 percent. The latter makes the PDA static pile estimate Equation very attractive. However, two shortcomings of the PDA equipment are 1) determining J_c ; and 2) estimating the skin and tip resistance of the pile in the field real time. Based on the PDA traces of force and velocity, two methods were developed to determine the ratio of static Tip/skin resistance for a pile. In addition, the Tip/skin ratio was correlated to the Case Damping, J_c value. Subsequently, the developed methods, as well as CAPWAP were compared to a database of 23 piles, which had static results. The following was concluded:

1. For the total static capacity prediction, proposed Method II ($COV_R = 0.29$) was the most accurate of the three methods evaluated, followed by the original PDA with user supplied J_c ($COV_R = 0.32$) and then the CAPWAP procedure ($COV_R = 0.45$).
2. In terms of the static skin resistance, the suggested Method II ($\lambda_R = 1.04$, $COV_R = 0.39$) proved to be the best method followed by CAPWAP ($\lambda_R = 0.80$, $COV_R = 0.43$) and then Method I ($\lambda_R = 1.29$, $COV_R = 0.89$).
3. The tip static prediction from the suggested Method II ($\lambda_R = 0.96$, $COV_R = 0.17$) was superior to the predictions of CAPWAP ($\lambda_R = 1.08$, $COV_R = 0.55$) and Method 1 ($\lambda_R = 1.94$, $COV_R = 1.27$).

4. The suggested method II is simple to perform, and its calculations *may be performed **automatically***.
5. A programming code has been developed to obtain the total, skin, and tip static capacities from Method II. The latter permits the rapid (computer) assessment of skin, tip and total capacities for every blow in the field real time.

Recommendations

The proposed Method II has been proven to be an accurate tool in determining the driven pile static capacity. However, there have been some limitations in this study. The following suggestions take into consideration those limitations and the feasibility for further research in the evaluation of this new method.

1. The number of cases used to evaluate the total, skin, and tip static resistances were 18, 10 and 6, respectively. It is recommended that more driving information for a pile, which includes static load testing, which monitors skin and tip resistance be undertaken.
2. Method II does not take into consideration the soil properties. It is recommended to investigate the distribution of soil for the piles studied and for any other new pile to be evaluated.

WIRELESS ACQUISITION OF A PILE'S (WAP) DYNAMIC RESPONSE

Chapters nine through fourteen describe the design, construction and testing of a new wireless instrumentation package for high strain dynamic testing of piles. The package has proven to perform properly under both laboratory and field conditions. The latter involved installing the WAP system at SR-54 at Cypress Springs, Florida. In the latter case top of one pile and the top and bottom of another pile was monitored. More than one thousand blows were

analyzed for two the 24-inch prestressed concrete piles. The signals, stresses, etc. compared very favorably with externally mounted PDA instrumentation. In the case of the internally cast WAP system, information at the pile tip (stresses, displacements, etc.) was also available.

Many problems arose in the development of the equipment, which had to be overcome. Three of the biggest problems had to do with the wireless transmission, the accelerometer (price, mounting, etc.) and overall cost of the system.

Two transmitter modules were developed initially before the final one presented herein. The first was an analog transmitter, which failed because it was incapable of transmitting static strain signals. The second, a radio transmitter (FM), failed because it was incapable of transmitting four signals at once (signal overlap was recorded) and noise.

The major problem with the accelerometer was its cost and mounting technique (to avoid the zero shift effect). The former was overcome by using an accelerometer developed for the automotive industry. The mounting was overcome through a significant amount of testing of materials, adhesives and dimensions, with the accelerometer in the laboratory. All options were benchmarked against both high quality accelerometers and existing PDA accelerometers.

In this research, the cost was a major limitation. The system was required to comply with a maximum cost of $300 in parts, for the non-recoverable equipment (transmitters, conditioners, and instruments: accelerometers, strain gauges, etc.). The latter could not of been feasible ten years ago due to unavailability of cheap transmitters, accelerometers, etc. However, with rapid technology growth in wireless LAN systems, automotive industry, cell phone etc., a digital 5 Mbs system (cast insitu) was developed for $250 per pile. The latter included four 10,000 words per second signals (two strain and two acceleration), which are transmitted digitally. A receiver, PCMCA card, laptop computer, and LABVIEW software (costs less than $3000) is required to

process the signals. Developed in the LABVIEW software (VIs) are routines to display forces, stresses, total capacities, as well as skin and tip resistance based on earlier work. Comparison of the results (Chapter 14) for SR-54 from PDA, and CAPWAP are very favorable.

Recommendations

Given the cost of the new WAP system, it is now viable to cast the system into every pre-cast concrete pile. The latter would allow the elimination of the current driving criterion based on blow count, which does not handle changing driving conditions (soil, rock hammer, etc.). For instance, consider the two SR-54 test piles (chapter 14) which had estimated capacities of 1600 kN, and 2200 kN (WAP and CAPWAP), but had similar blow counts at the end of drive. Also, if every pile was monitored, current FDOT Factors of Safety could possibly be lowered from over two to less than two, resulting in less pile lengths and total costs.

It is expected with WAP's successful installation of instrumentation at the pile tip (Chapter 14), improved analysis of total capacity, as well as skin and tip resistance will continue to occur.

Finally, it is recommended that the FDOT convene a panel of construction, geotechnical and structural engineers to identify how the WAP system may be implemented into FDOT's "Standard Specifications for Road and Bridge Construction Manual."

REFERENCES

AASHTO (1994). LRFD Highway Bridges Design Specifications, SI Units, First Edition. American Association of State Highway and Transportation Officials, Washington, D.C.

ACI (1999), "Building Code Requirements for reinforced Concrete (ACI 318-99)", American Concrete Institute, Detroit, MI.

American Society of Civil Engineers (2000), "Annual Book of ASTM Standards" Volume 04.08- ASTM D4945-96 Standard Test Method for High-Strain Dynamic Testing of Piles, West Conshohocken, PA.

Chu, Anthony (1987), Technical Paper, "Zero Shift of Piezoelectric Accelerometers in Phyro-shock Measurements", The Shock and Vibration Information Center, Naval Research Laboratory, Washington, DC.

Coduto, Donald P. (1994). Foundation Design Principles and Practices. Prentice Hall Inc., Englewood Cliffs, N.J., 403-416.

Davisson, M.T. (1972). "High Capacity Piles, Proceedings, Soil Mechanics Lecture Series on Innovations in Foundation Construction." American Society of Civil Engineers, ASCE, Illinois Section, Chicago, 81-112.

Florida Department of Transportation (1991). "Standard Specifications for Road and Bridge Construction." Tallahassee, Florida, 419-443.

Florida Department of Transportation (1994). "Supplemental Specifications to the 1991 Standard Specifications for Road and Bridge Construction." Tallahassee, Florida, 109-161.

Florida Department of Transportation (1999). "Standard Specifications for Road and Bridge Construction." Tallahassee, Florida, 398-451.

Gates, M. (1957). "Empirical Formula for Predicting Pile Bearing Capacity." Engineering New Record, 26-28, 33-34.

Goble Rausche Likins and Associates Inc. (2000), "Dynamic Load Testing", Cleveland, Ohio.

GRL (1996). Case Pile Wave Analysis Program – CAPWAP Manual. Cleveland, Ohio.

GRL (1993). GRLWEAP – Wave Equation Analysis of Pile Driving Manual. Cleveland, Ohio.

Hansel, W.C. and I.M. Viest (1971). "Load Factor Design for Steel Highway Bridges." AISC Engineering Journal, Vol. 8, No. 4, 113-123.

Housel, William S. (1966). “Pile Load Capacity: Estimates and Test Results.” ASCE Journal of the Soil Mechanics and Foundations Division, Vol. 92, No. SM4, 1-30.

Likins, Garland E. and Hussein, Mohamad (1988). “A Summary of the Pile Driving Analyzer Capacity Methods – Past and Present.” Cleveland, Ohio.

Measurements Group Inc. (1999), EGP-5-120 Embedment Strain Gage Data Sheet, Raleigh, North Carolina.

Measurements Group, (1993), “Catalog 5000 Precision Gages”, Measurements Group Inc., Raleigh, North Carolina.

National Instruments (1998), “LabVIEW User Manual”, Austin, Texas

National Instruments (1997), “DIO 6533 User Manual”, National Instruments Corporation, Austin, Texas.

Paikowsky, S.G., Regan, J.E., and McDonnell, J.J. (1994). “A simplified field Method for Capacity Evaluation of Driven Piles.” Publication No. FHWA-RD-94-042.

Pile Buck (1992), “Foundations”, Pile Buck Production, Jupiter, Florida

Pile Dynamics, Inc. (1990), “Model GCX Pile Driving Analyzer Manual”, Cleveland, Ohio.

Pile Dynamics, Inc. (1992). Pile Driving Analyzer (PDA) Manual. Cleveland, Ohio.

Pile Dynamics, Inc. (1995), “Pile Driving Analyzer Manual PAK”, Cleveland, Ohio.

Pile Dynamics, Inc. (1996), “Strain and Motion Sensors from Pile Dynamics” Data Sheet, Cleveland, Ohio.

Rosenblueth, E. and Esteva, L. (1972). “Reliability Basis for Some Mexican Codes.” ACI Publication SP-31, American Concrete Institute, Detroit, Mi.

Sakai, T., Sawai, H., and Shioi, Y. (1996). “Theoretical Analysis of the Pile Driving Formula.” Proceeding, 5th International Conference on the Application of Stress Wave Theory to Piles. September 11-13, 1996. Orlando, Florida, 81-88.

Shearman, Sam (2001), Signal Processing Easies Vibration Transducer Selection, National Instruments, Austin Texas.

Shear Robert (1999), “Piezoelectric Sensors for OEM Applications”, The journal of Applied Sensing Technology, Endevco, San Juan Capistrano, California.

Willington, A.M. (1893). Piles and Pile-Driving. Engineering News Publishing Co., New York.

Withiam, J.L., Voytko, E.P., Barker, R.M., Duncan, J.M., Kelly, B.C., Musser, S.C., and Elias, V. (1997). Load and Resistance Factor Design (LRFD) for Highway Bridge Structures. FHWA Report DTFH61-94-C-00098. Federal Highway Administration, Washington, D.C.

APPENDIX A

LRFD ANALYSIS RESULTS - CAPWAP PROCEDURE

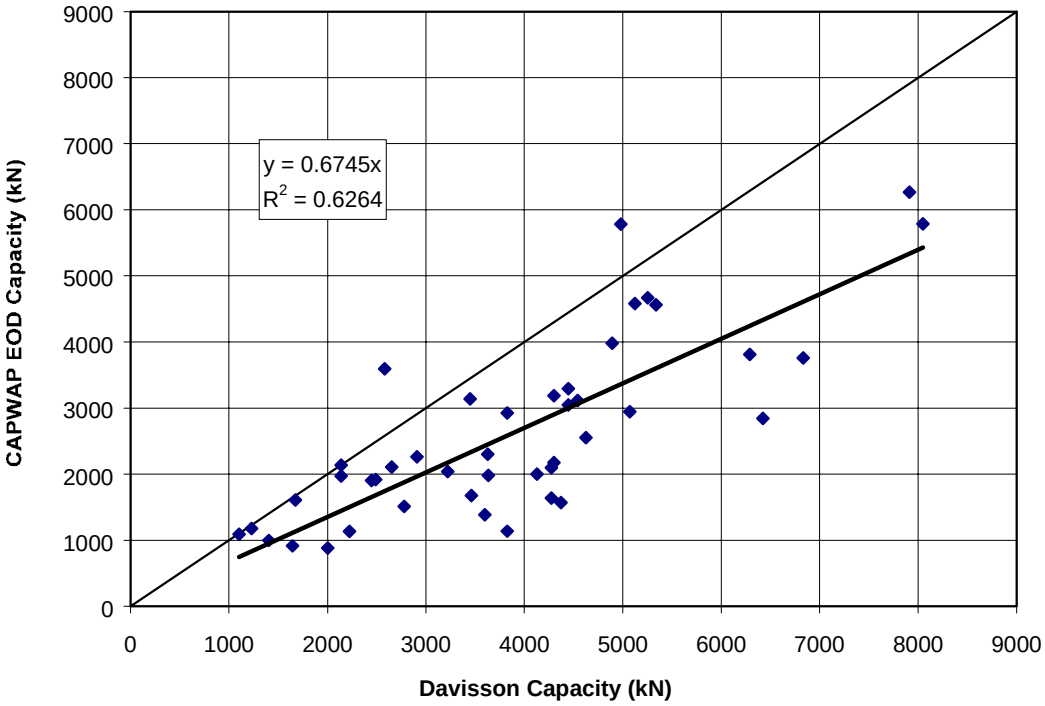

Figure A-1. Davisson Capacity vs. CAPWAP EOD Capacity

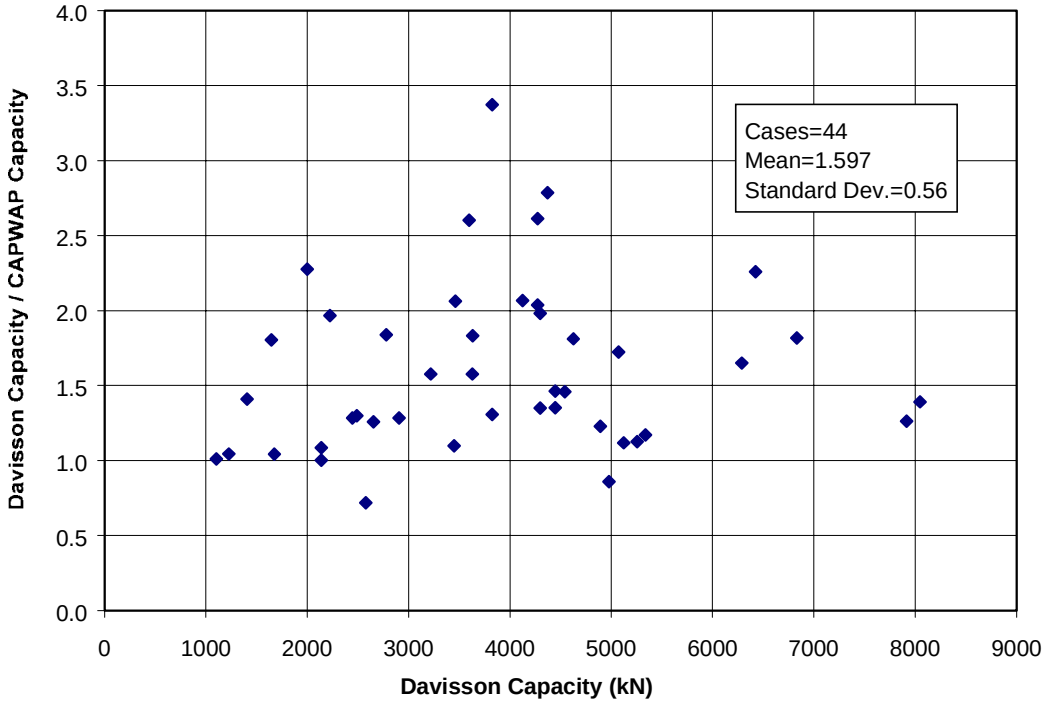

Figure A-2. Measured Over Predicted Capacity for CAPWAP at EOD

Table A-1. ϕ Values Evaluated for CAPWAP (EOD)

Span length (m)	Q_D/Q_L	Failure Probability p_f / Reliability Index β_T			
		2.50E-02	6.22E-03	1.22E-03	1.79E-04
		1.96	2.5	3.03	3.57
9	0.52	0.980	0.788	0.636	0.511
15	1.00	0.940	0.756	0.610	0.490
18	1.06	0.937	0.753	0.608	0.489
27	1.58	0.912	0.733	0.591	0.475
36	2.12	0.894	0.719	0.580	0.466
45	2.64	0.882	0.709	0.572	0.460
50	3.00	0.876	0.704	0.568	0.457
60	3.53	0.868	0.698	0.563	0.453

Table A-2. ASD Design Safety Factor Values Evaluated for CAPWAP (EOD)

Span length (m)	Q_D/Q_L	Failure Probability p_f / Reliability Index β_T			
		2.50E-02	6.22E-03	1.22E-03	1.79E-04
		1.96	2.5	3.03	3.57
9	0.52	1.611	2.004	2.483	3.089
15	1.00	1.595	1.984	2.459	3.059
18	1.06	1.594	1.982	2.456	3.056
27	1.58	1.584	1.970	2.441	3.037
36	2.12	1.577	1.962	2.431	3.024
45	2.64	1.572	1.956	2.424	3.015
50	3.00	1.570	1.953	2.420	3.011
60	3.53	1.567	1.949	2.415	3.005

Table A-3. ϕ Factors for Safety Factor = 2.50 – CAPWAP (EOD)

Span length (m)	Q_D/Q_L	ϕ	β_T	p_f
9	0.52	0.632	3.047	0.00116
15	1.00	0.600	3.071	0.00107
18	1.06	0.597	3.074	0.00106
27	1.58	0.578	3.089	0.00101
36	2.12	0.564	3.099	0.00097
45	2.64	0.555	3.107	0.00095
50	3.00	0.550	3.111	0.00093
60	3.53	0.544	3.115	0.00092

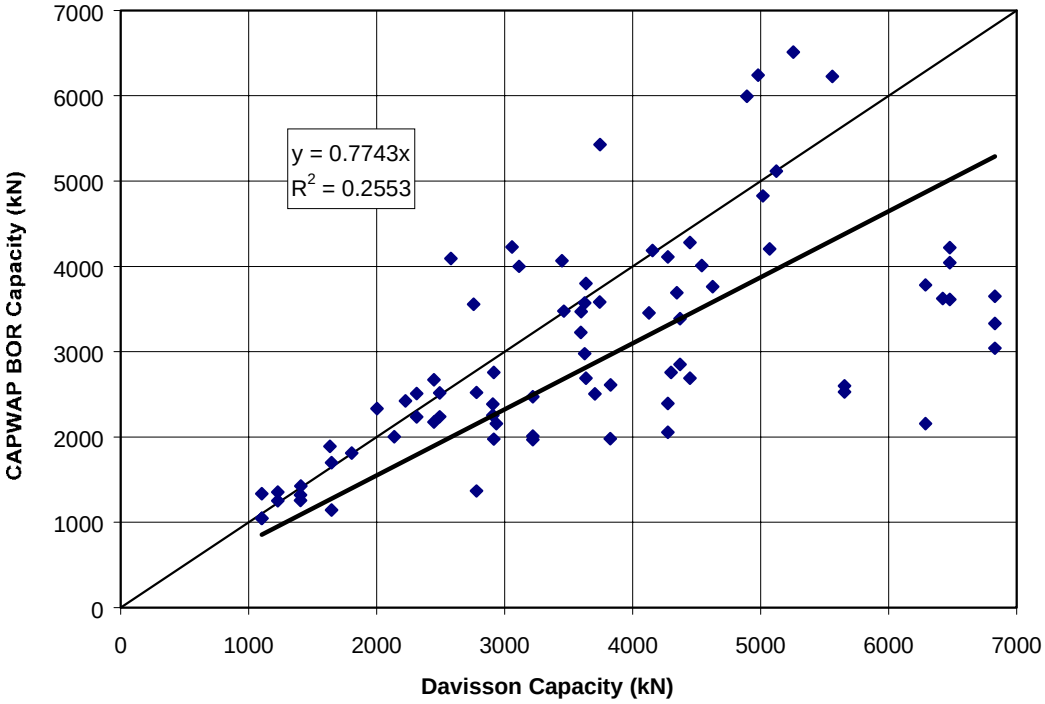

Figure A-3. Davisson Capacity vs. CAPWAP BOR

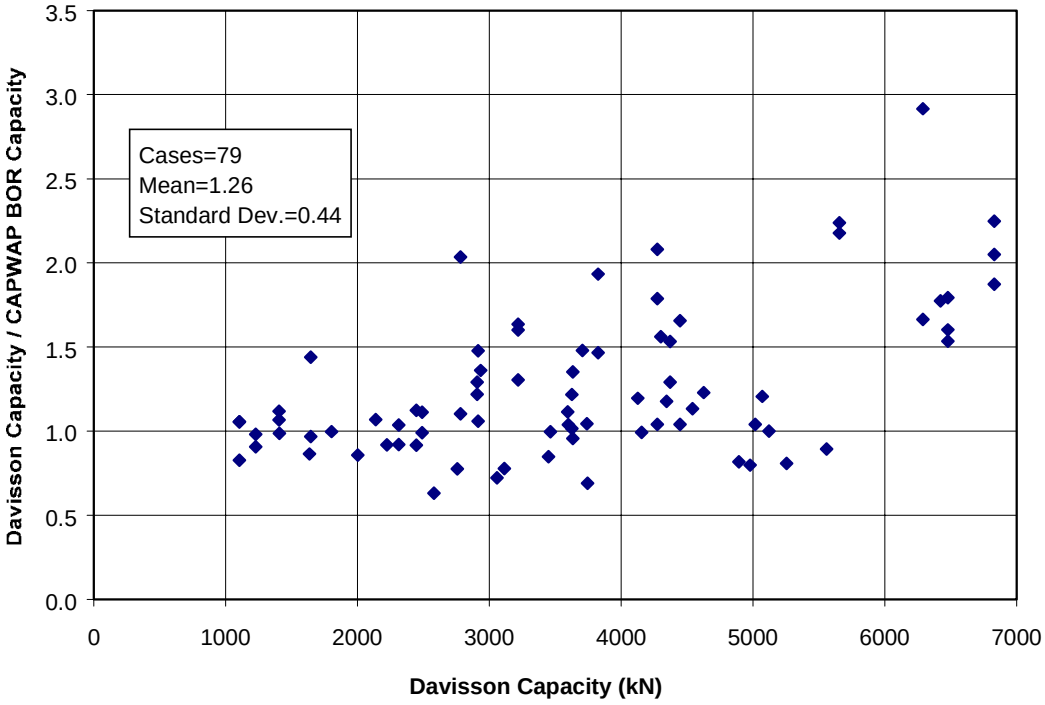

Figure A-4. Measured Over Predicted Capacity for CAPWAP at BOR

Table A-4. ϕ Values Evaluated for CAPWAP (BOR)

Span length (m)	Q_D/Q_L	Failure Probability p_f / Reliability Index β_T			
		2.50E-02	6.22E-03	1.22E-03	1.79E-04
		1.96	2.50	3.03	3.57
9	0.52	0.776	0.625	0.505	0.406
15	1.00	0.745	0.599	0.484	0.390
18	1.06	0.742	0.597	0.482	0.388
27	1.58	0.722	0.581	0.469	0.378
36	2.12	0.708	0.570	0.460	0.371
45	2.64	0.699	0.562	0.454	0.366
50	3.00	0.694	0.558	0.451	0.363
60	3.53	0.688	0.553	0.447	0.360

Table A-5. ASD Design Safety Factor Values Evaluated for CAPWAP (BOR)

Span length (m)	Q_D/Q_L	Failure Probability p_f / Reliability Index β_T			
		2.50E-02	6.22E-03	1.22E-03	1.79E-04
		1.96	2.50	3.03	3.57
9	0.52	2.033	2.527	3.128	3.888
15	1.00	2.013	2.502	3.098	3.850
18	1.06	2.012	2.500	3.095	3.846
27	1.58	1.999	2.485	3.076	3.823
36	2.12	1.991	2.474	3.063	3.806
45	2.64	1.985	2.467	3.054	3.795
50	3.00	1.982	2.463	3.049	3.789
60	3.53	1.978	2.459	3.043	3.782

Table A-6. ϕ Factors for Safety Factor = 2.50 – CAPWAP (BOR)

Span length (m)	Q_D/Q_L	ϕ	β	p_f
9	0.52	0.632	2.473	0.00671
15	1.00	0.600	2.498	0.00625
18	1.06	0.597	2.500	0.00622
27	1.58	0.578	2.515	0.00596
36	2.12	0.564	2.526	0.00578
45	2.64	0.555	2.533	0.00566
50	3.00	0.550	2.537	0.00560
60	3.53	0.544	2.542	0.00552

APPENDIX B

LRFD ANALYSIS RESULTS – PDA METHOD

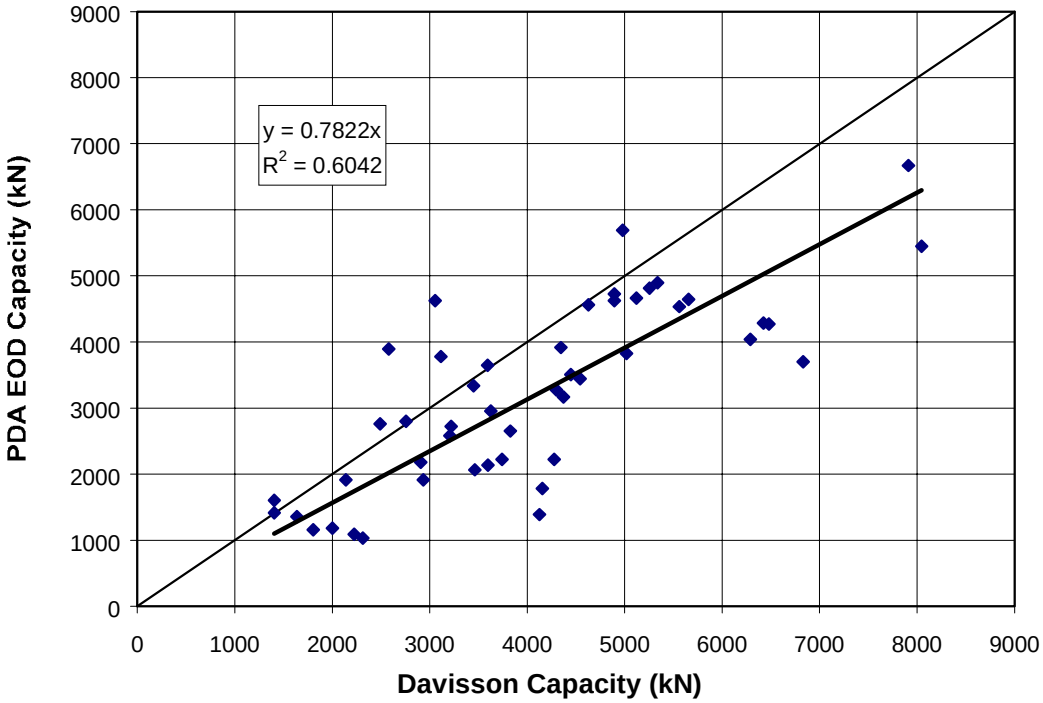

Figure B-1. Davisson Capacity vs. PDA EOD Capacity

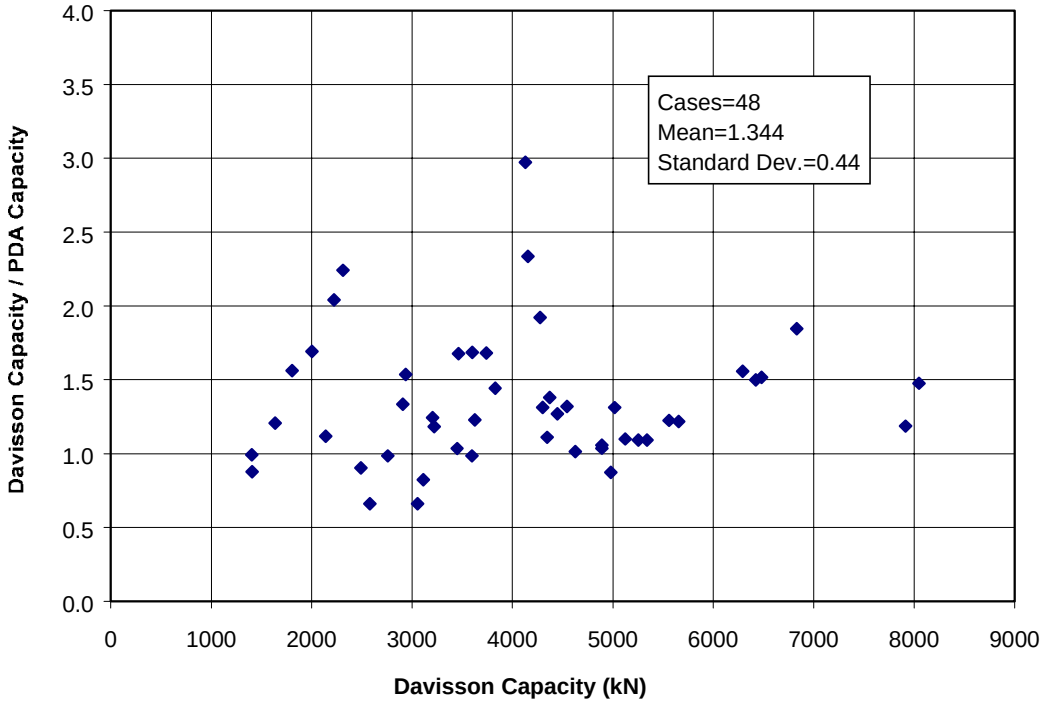

Figure B-2. Measured Over Predicted Capacity for PDA at EOD

Table B-1. ϕ Values Evaluated for PDA (EOD)

Span length (m)	Q_D/Q_L	Failure Probability p_f / Reliability Index β_T			
		2.50E-02	6.22E-03	1.22E-03	1.79E-04
		1.96	2.5	3.03	3.57
9	0.52	0.856	0.694	0.565	0.458
15	1.00	0.821	0.666	0.542	0.439
18	1.06	0.818	0.663	0.540	0.437
27	1.58	0.796	0.645	0.525	0.426
36	2.12	0.781	0.633	0.515	0.418
45	2.64	0.770	0.625	0.508	0.412
50	3.00	0.765	0.620	0.505	0.409
60	3.53	0.758	0.615	0.500	0.405

Table B-2. ASD Design Safety Factor Values Evaluated for PDA (EOD)

Span length (m)	Q_D/Q_L	Failure Probability p_f / Reliability Index β_T			
		2.50E-02	6.22E-03	1.22E-03	1.79E-04
		1.96	2.5	3.03	3.57
9	0.52	1.845	2.276	2.796	3.449
15	1.00	1.827	2.253	2.769	3.415
18	1.06	1.825	2.251	2.766	3.412
27	1.58	1.814	2.237	2.749	3.391
36	2.12	1.806	2.228	2.738	3.377
45	2.64	1.801	2.221	2.730	3.367
50	3.00	1.798	2.218	2.725	3.362
60	3.53	1.795	2.214	2.720	3.356

Table B-3. ϕ Factors for Safety Factor = 2.50 – PDA (EOD)

Span length (m)	Q_D/Q_L	ϕ	β_T	p_f
9	0.52	0.632	2.742	0.003058
15	1.00	0.600	2.767	0.002833
18	1.06	0.597	2.770	0.002807
27	1.58	0.578	2.786	0.002672
36	2.12	0.564	2.797	0.002583
45	2.64	0.555	2.804	0.002528
50	3.00	0.550	2.808	0.002496
60	3.53	0.544	2.813	0.002458

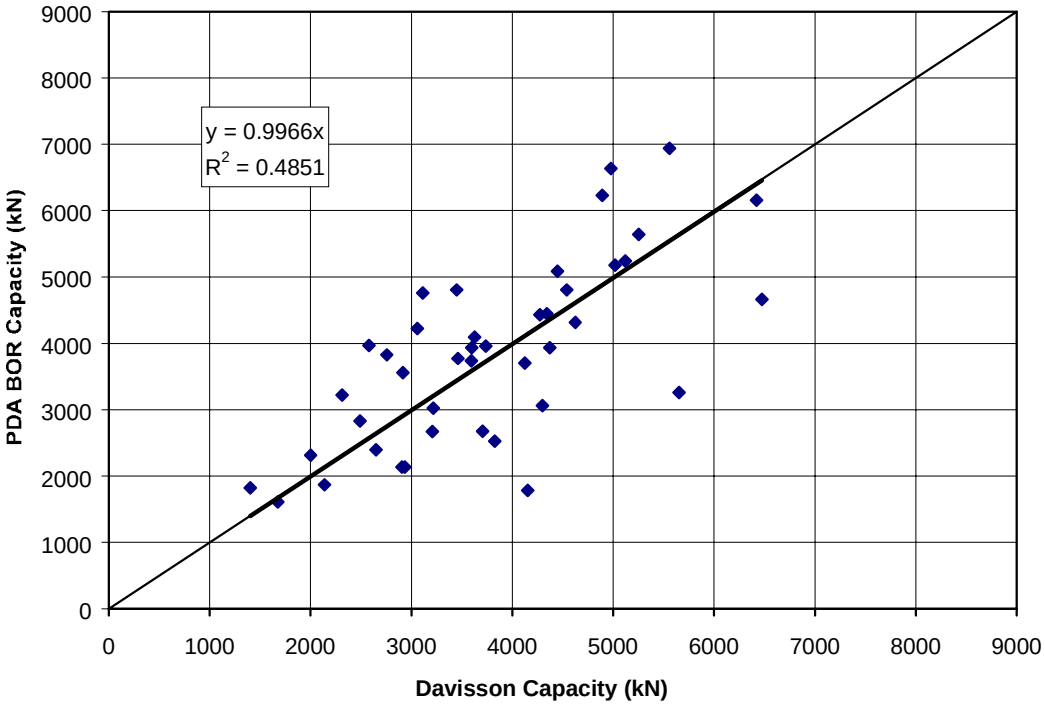

Figure B-3. Davisson Capacity vs. PDA BOR

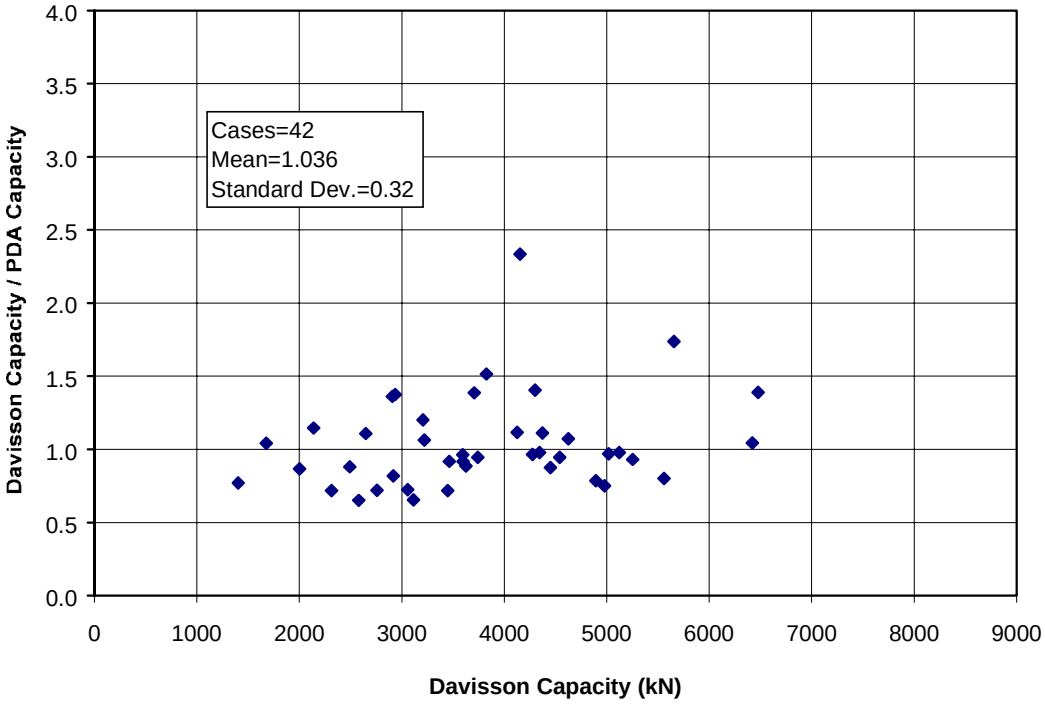

Figure B-4. Measured Over Predicted Capacity for PDA at BOR

Table B-4. ϕ Values Evaluated for PDA (BOR)

Span length (m)	Q_D/Q_L	Failure Probability p_f / Reliability Index β_T			
		2.50E-02	6.22E-03	1.22E-03	1.79E-04
		1.96	2.50	3.03	3.57
9	0.52	0.682	0.557	0.457	0.373
15	1.00	0.654	0.534	0.438	0.358
18	1.06	0.652	0.532	0.436	0.356
27	1.58	0.634	0.518	0.425	0.347
36	2.12	0.622	0.508	0.417	0.340
45	2.64	0.614	0.501	0.411	0.336
50	3.00	0.609	0.498	0.408	0.333
60	3.53	0.604	0.493	0.404	0.330

Table B-5. ASD Design Safety Factor Values Evaluated for PDA (BOR)

Span length (m)	Q_D/Q_L	Failure Probability p_f / Reliability Index β_T			
		2.50E-02	6.22E-03	1.22E-03	1.79E-04
		1.96	2.50	3.03	3.57
9	0.52	2.316	2.835	3.458	4.234
15	1.00	2.293	2.807	3.424	4.192
18	1.06	2.291	2.805	3.421	4.188
27	1.58	2.277	2.787	3.400	4.163
36	2.12	2.267	2.776	3.386	4.145
45	2.64	2.260	2.768	3.376	4.133
50	3.00	2.257	2.763	3.370	4.127
60	3.53	2.253	2.758	3.364	4.119

Table B-6. ϕ Factors for Safety Factor = 2.50 – PDA (BOR)

Span length (m)	Q_D/Q_L	ϕ	β	p_f
9	0.52	0.632	2.164	0.01525
15	1.00	0.600	2.191	0.01424
18	1.06	0.597	2.193	0.01417
27	1.58	0.578	2.210	0.01357
36	2.12	0.564	2.221	0.01319
45	2.64	0.555	2.229	0.01292
50	3.00	0.550	2.233	0.01279
60	3.53	0.544	2.238	0.01263

APPENDIX C

LRFD ANALYSIS RESULTS – PAIKOWSKY'S ENERGY METHOD

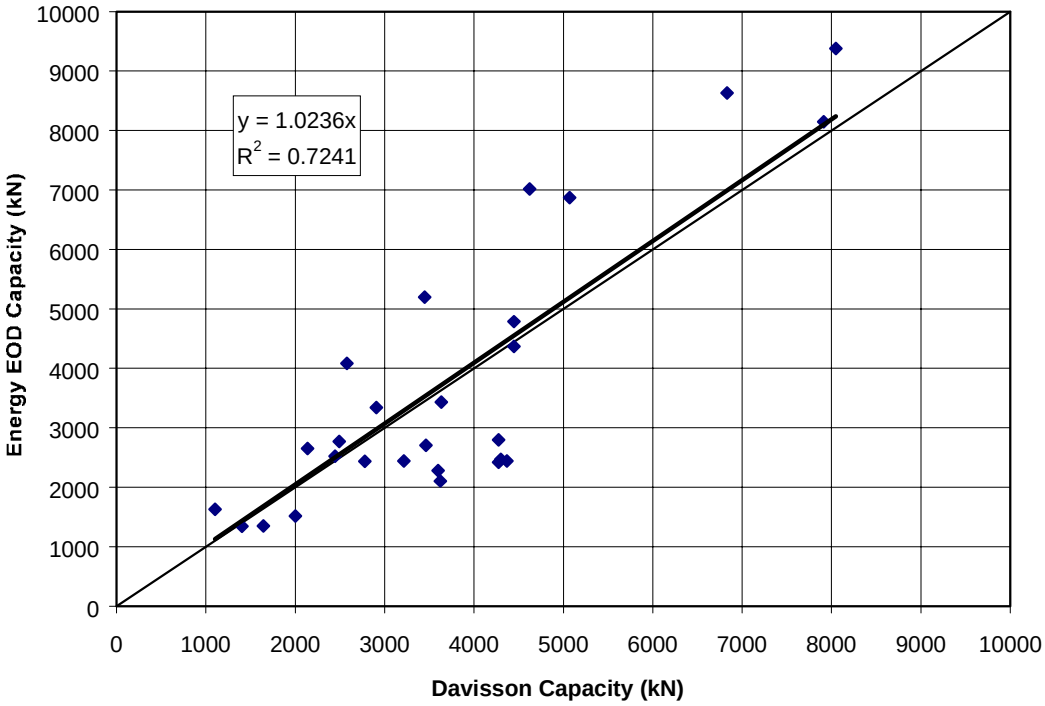

Figure C-1. Davisson Capacity vs. Paikowsky's Method EOD Capacity

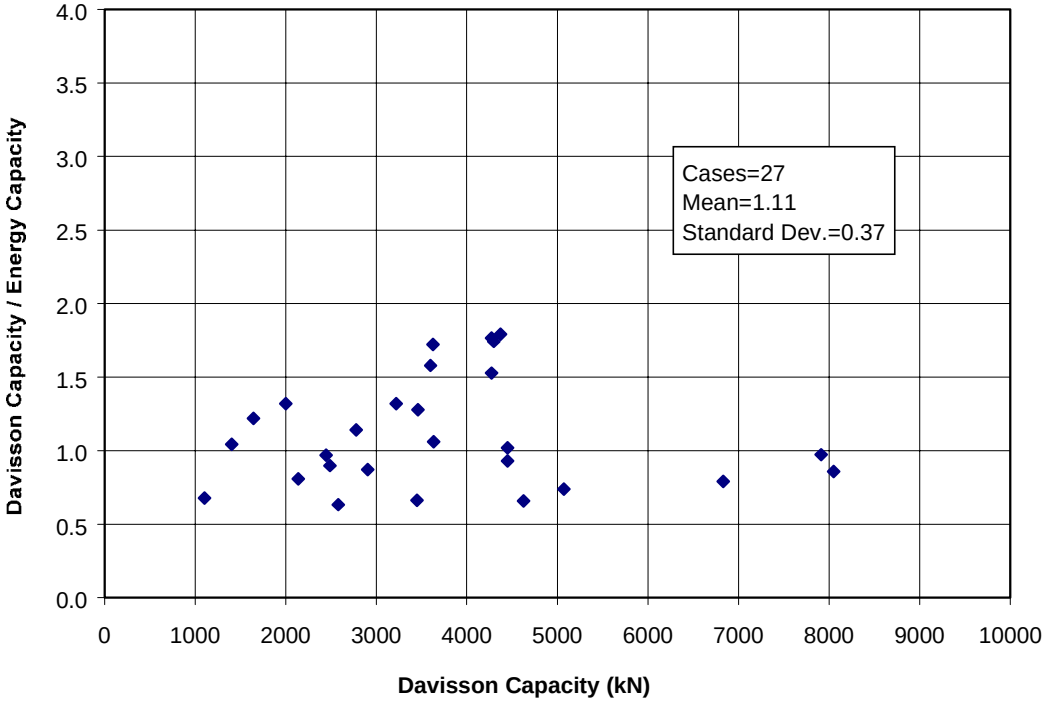

Figure C-2. Measured Over Predicted Capacity for Paikowsky's Method at EOD

Table C-1. ϕ Values Evaluated for Paikowsky's Method (EOD)

Span length (m)	Q_D/Q_L	Failure Probability p_f / Reliability Index β_T			
		2.50E-02	6.22E-03	1.22E-03	1.79E-04
		1.96	2.5	3.03	3.57
9	0.52	0.700	0.567	0.460	0.372
15	1.00	0.672	0.544	0.441	0.357
18	1.06	0.669	0.541	0.440	0.356
27	1.58	0.651	0.527	0.428	0.346
36	2.12	0.639	0.517	0.420	0.340
45	2.64	0.630	0.510	0.414	0.335
50	3.00	0.626	0.506	0.411	0.333
60	3.53	0.620	0.502	0.408	0.330

Table C-2. ASD Design Safety Factor Values Evaluated for Paikowsky's Method (EOD)

Span length (m)	Q_D/Q_L	Failure Probability p_f / Reliability Index β_T			
		2.50E-02	6.22E-03	1.22E-03	1.79E-04
		1.96	2.5	3.03	3.57
9	0.52	2.254	2.787	3.432	4.242
15	1.00	2.232	2.759	3.398	4.201
18	1.06	2.230	2.757	3.395	4.197
27	1.58	2.216	2.740	3.374	4.171
36	2.12	2.207	2.728	3.360	4.153
45	2.64	2.200	2.720	3.350	4.141
50	3.00	2.197	2.716	3.345	4.135
60	3.53	2.193	2.711	3.338	4.127

Table C-3. ϕ Factors for Safety Factor = 2.50 – Paikowsky's Method (EOD)

Span length (m)	Q_D/Q_L	ϕ	β_T	p_f
9	0.52	0.632	2.224	0.01309
15	1.00	0.600	2.249	0.01227
18	1.06	0.597	2.251	0.01221
27	1.58	0.578	2.267	0.01171
36	2.12	0.564	2.278	0.01138
45	2.64	0.555	2.285	0.01117
50	3.00	0.550	2.289	0.01105
60	3.53	0.544	2.294	0.01091

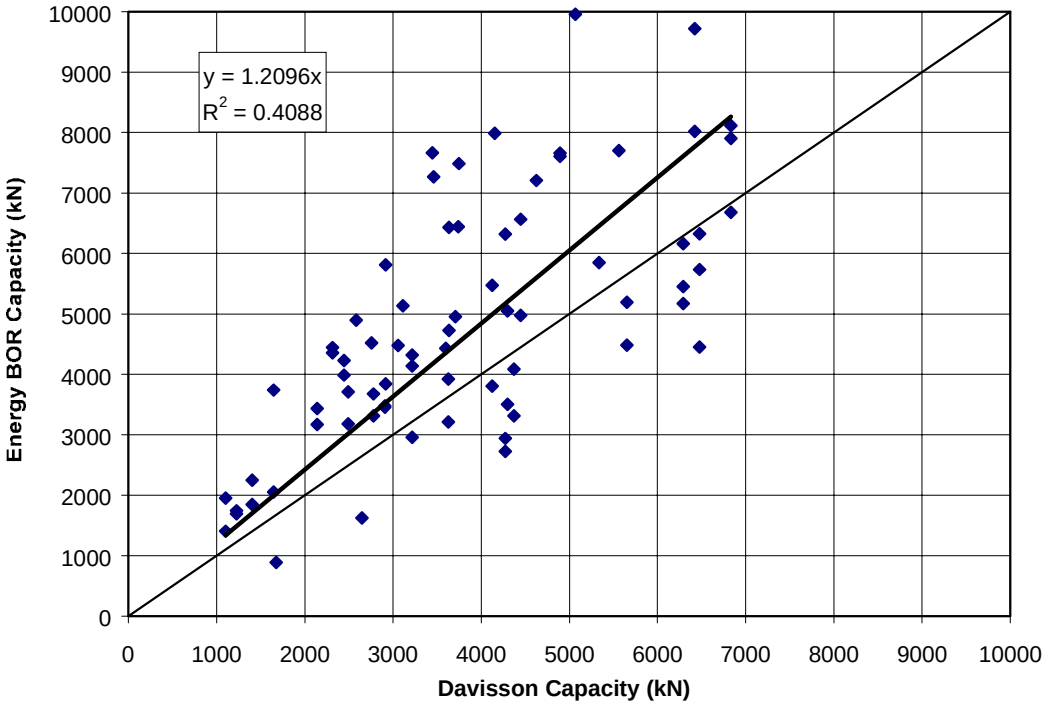

Figure C-3. Davisson Capacity vs. Paikowsky's Method BOR

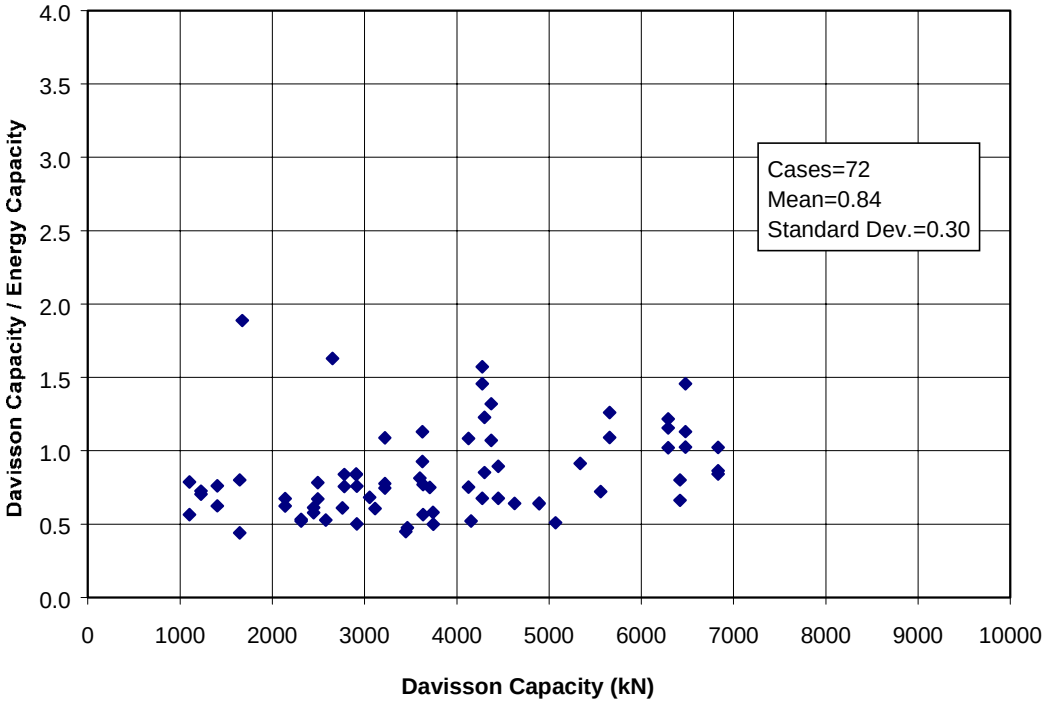

Figure C-4. Measured Over Predicted Capacity for Paikowsky's Method at BOR

Table C-4. ϕ Values Evaluated for Paikowsky's Method (BOR)

Span length (m)	Q_D/Q_L	Failure Probability p_f / Reliability Index β_T			
		2.50E-02	6.22E-03	1.22E-03	1.79E-04
		1.96	2.50	3.03	3.57
9	0.52	0.503	0.403	0.323	0.259
15	1.00	0.483	0.386	0.310	0.248
18	1.06	0.481	0.385	0.309	0.247
27	1.58	0.468	0.374	0.301	0.241
36	2.12	0.459	0.367	0.295	0.236
45	2.64	0.453	0.362	0.291	0.233
50	3.00	0.449	0.360	0.289	0.231
60	3.53	0.445	0.356	0.286	0.229

Table C-5. ASD Design Safety Factor Values Evaluated for Paikowsky's Method (BOR)

Span length (m)	Q_D/Q_L	Failure Probability p_f / Reliability Index β_T			
		2.50E-02	6.22E-03	1.22E-03	1.79E-04
		1.96	2.50	3.03	3.57
9	0.52	3.139	3.923	4.881	6.100
15	1.00	3.108	3.884	4.834	6.040
18	1.06	3.105	3.881	4.829	6.034
27	1.58	3.086	3.857	4.799	5.997
36	2.12	3.073	3.840	4.779	5.972
45	2.64	3.064	3.829	4.765	5.955
50	3.00	3.059	3.823	4.758	5.945
60	3.53	3.054	3.816	4.749	5.934

Table C-6. ϕ Factors for Safety Factor = 2.50 – Paikowsky's Method (BOR)

Span length (m)	Q_D/Q_L	ϕ	β	p_f
9	0.52	0.632	1.408	0.07964
15	1.00	0.600	1.432	0.07614
18	1.06	0.597	1.434	0.07586
27	1.58	0.578	1.449	0.07374
36	2.12	0.564	1.460	0.07221
45	2.64	0.555	1.467	0.07126
50	3.00	0.550	1.471	0.07071
60	3.53	0.544	1.475	0.07017

APPENDIX D

LRFD ANALYSIS RESULTS – SAKAI ET AL (JAPANESE) METHOD

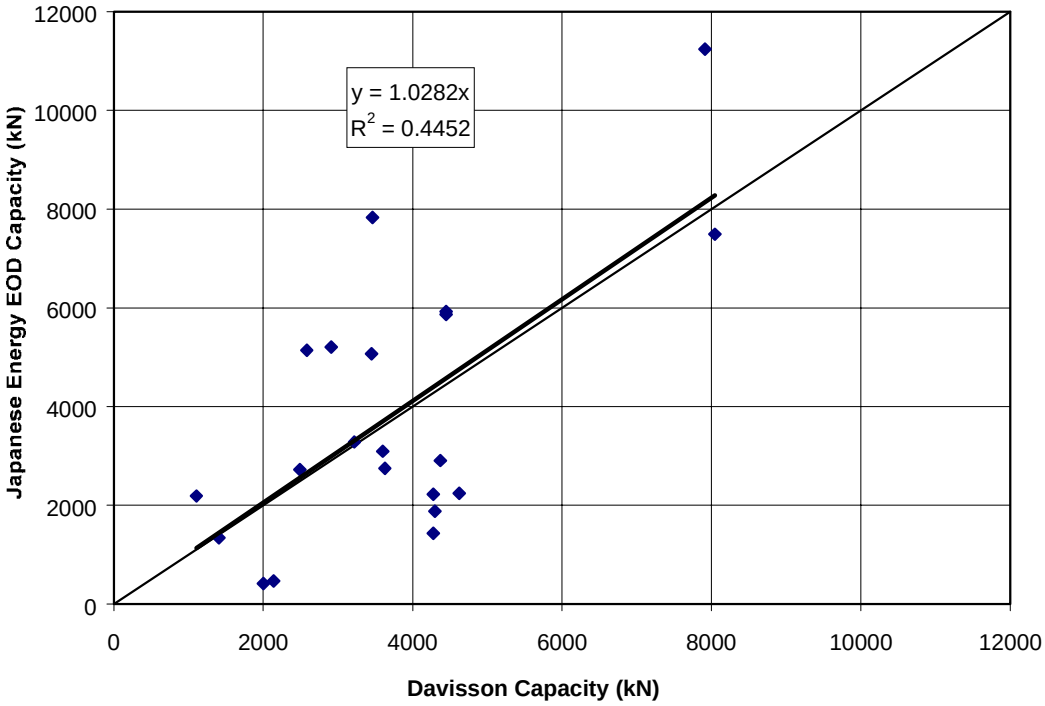

Figure D-1. Davisson Capacity vs. Sakai Method EOD Capacity

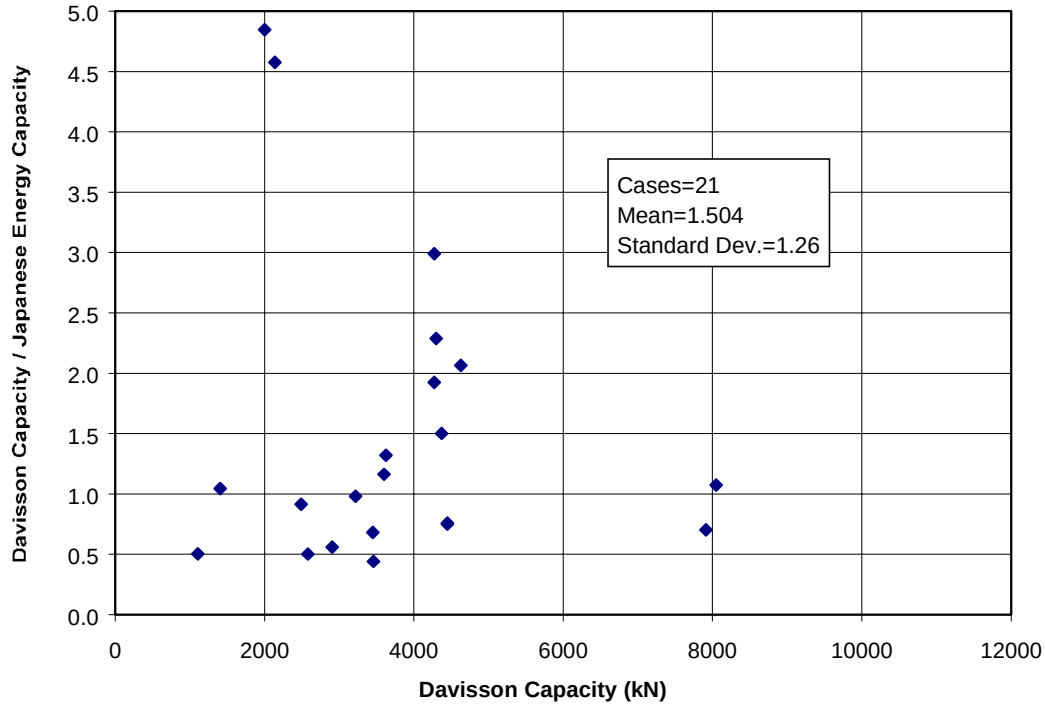

Figure D-2. Measured Over Predicted Capacity for Sakai Method at EOD

Table D-1. ϕ Values Evaluated for Sakai Method (EOD)

Span length (m)	Q_D/Q_L	Failure Probability p_f / Reliability Index β_T			
		2.50E-02	6.22E-03	1.22E-03	1.79E-04
		1.96	2.5	3.03	3.57
9	0.52	0.374	0.248	0.166	0.110
15	1.00	0.359	0.238	0.159	0.106
18	1.06	0.358	0.237	0.159	0.105
27	1.58	0.348	0.231	0.154	0.102
36	2.12	0.341	0.226	0.151	0.100
45	2.64	0.337	0.223	0.149	0.099
50	3.00	0.334	0.222	0.148	0.098
60	3.53	0.331	0.220	0.147	0.098

Table D-2. ASD Design Safety Factor Values Evaluated for Sakai Method (EOD)

Span length (m)	Q_D/Q_L	Failure Probability p_f / Reliability Index β_T			
		2.50E-02	6.22E-03	1.22E-03	1.79E-04
		1.96	2.5	3.03	3.57
9	0.52	4.221	6.361	9.515	14.341
15	1.00	4.179	6.299	9.422	14.201
18	1.06	4.175	6.293	9.413	14.188
27	1.58	4.150	6.254	9.355	14.100
36	2.12	4.132	6.228	9.316	14.041
45	2.64	4.120	6.210	9.289	14.000
50	3.00	4.114	6.200	9.274	13.978
60	3.53	4.106	6.188	9.257	13.952

Table D-3. ϕ Factors for Safety Factor = 2.50 – Sakai Method (EOD)

Span length (m)	Q_D/Q_L	ϕ	β_T	p_f
9	0.52	0.632	1.271	0.10195
15	1.00	0.600	1.284	0.09966
18	1.06	0.597	1.285	0.09948
27	1.58	0.578	1.293	0.09809
36	2.12	0.564	1.299	0.09706
45	2.64	0.555	1.302	0.09654
50	3.00	0.550	1.305	0.09603
60	3.53	0.544	1.307	0.09569

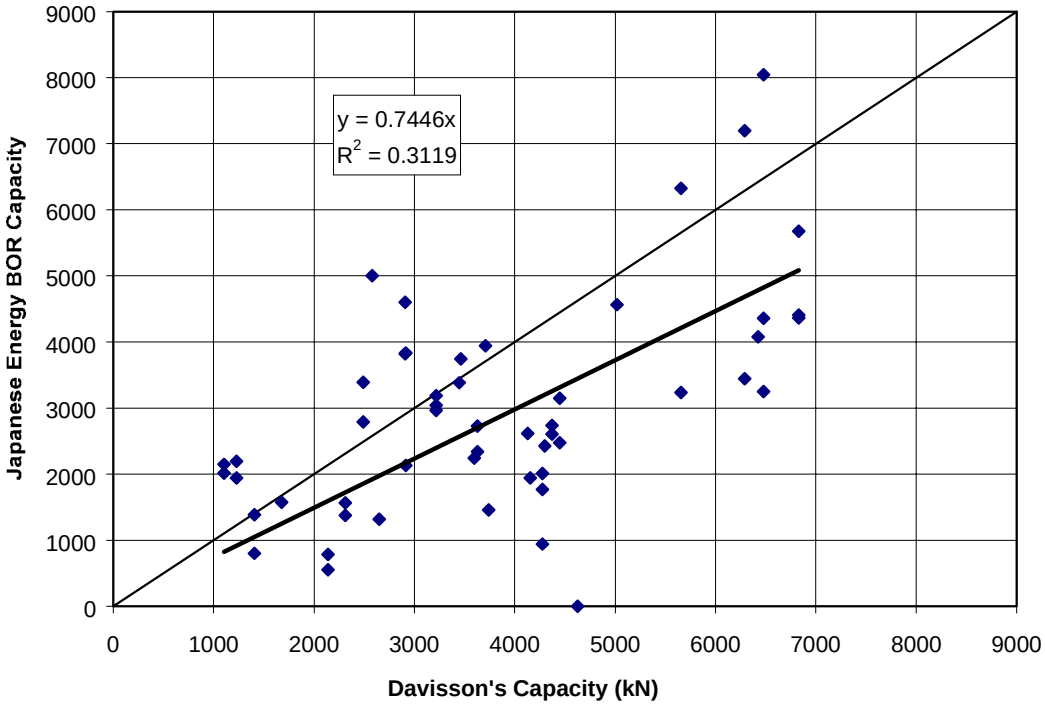

Figure D-3. Davisson Capacity vs. Sakai Method BOR

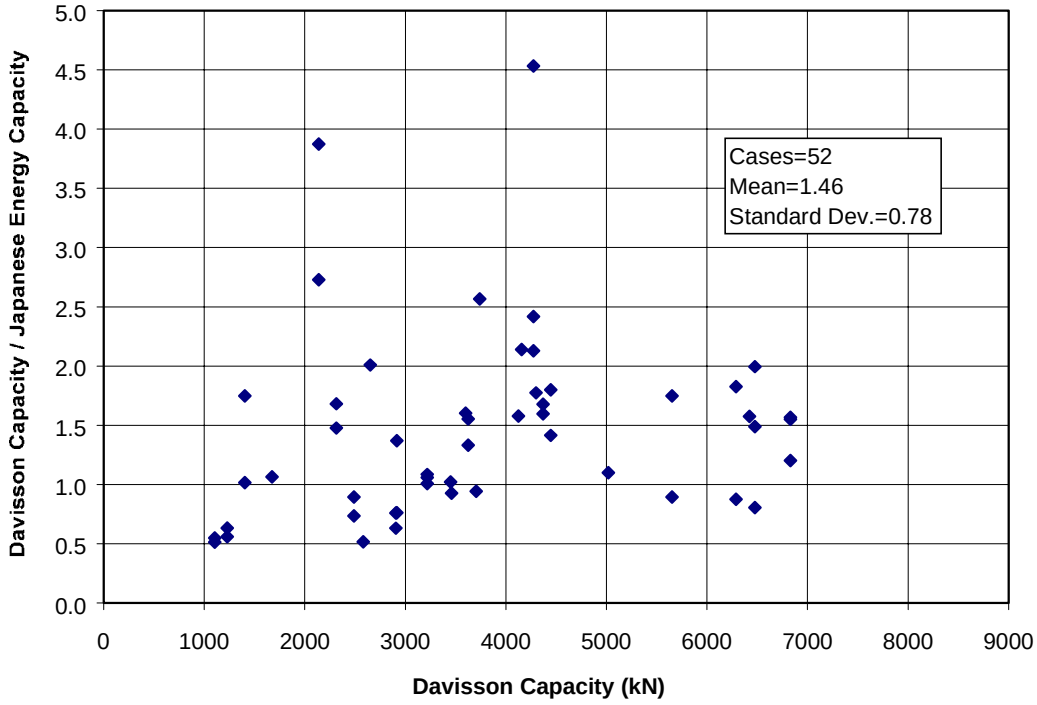

Figure D-4. Measured Over Predicted Capacity for Sakai Method at BOR

Table D-4. ϕ Values Evaluated for Sakai Method (BOR)

Span length (m)	Q_D/Q_L	Failure Probability p_f / Reliability Index β_T			
		2.50E-02	6.22E-03	1.22E-03	1.79E-04
		1.96	2.50	3.03	3.57
9	0.52	0.627	0.466	0.348	0.258
15	1.00	0.601	0.447	0.334	0.248
18	1.06	0.599	0.445	0.332	0.247
27	1.58	0.583	0.433	0.323	0.240
36	2.12	0.572	0.425	0.317	0.236
45	2.64	0.564	0.419	0.313	0.233
50	3.00	0.560	0.416	0.311	0.231
60	3.53	0.555	0.412	0.308	0.229

Table D-5. ASD Design Safety Factor Values Evaluated for Sakai Method (BOR)

Span length (m)	Q_D/Q_L	Failure Probability p_f / Reliability Index β_T			
		2.50E-02	6.22E-03	1.22E-03	1.79E-04
		1.96	2.50	3.03	3.57
9	0.52	2.520	3.391	4.540	6.110
15	1.00	2.495	3.358	4.495	6.050
18	1.06	2.493	3.355	4.491	6.044
27	1.58	2.477	3.334	4.463	6.007
36	2.12	2.467	3.320	4.444	5.982
45	2.64	2.460	3.311	4.431	5.964
50	3.00	2.456	3.305	4.424	5.955
60	3.53	2.451	3.299	4.416	5.944

Table D-6. ϕ Factors for Safety Factor = 2.50 – Sakai Method (BOR)

Span length (m)	Q_D/Q_L	ϕ	β	p_f
9	0.52	0.632	1.946	0.02586
15	1.00	0.600	1.964	0.02479
18	1.06	0.597	1.965	0.02474
27	1.58	0.578	1.976	0.02411
36	2.12	0.564	1.984	0.02366
45	2.64	0.555	1.990	0.02332
50	3.00	0.550	1.992	0.02321
60	3.53	0.544	1.996	0.02299

APPENDIX E

LRFD ANALYSIS RESULTS – FDOT METHOD

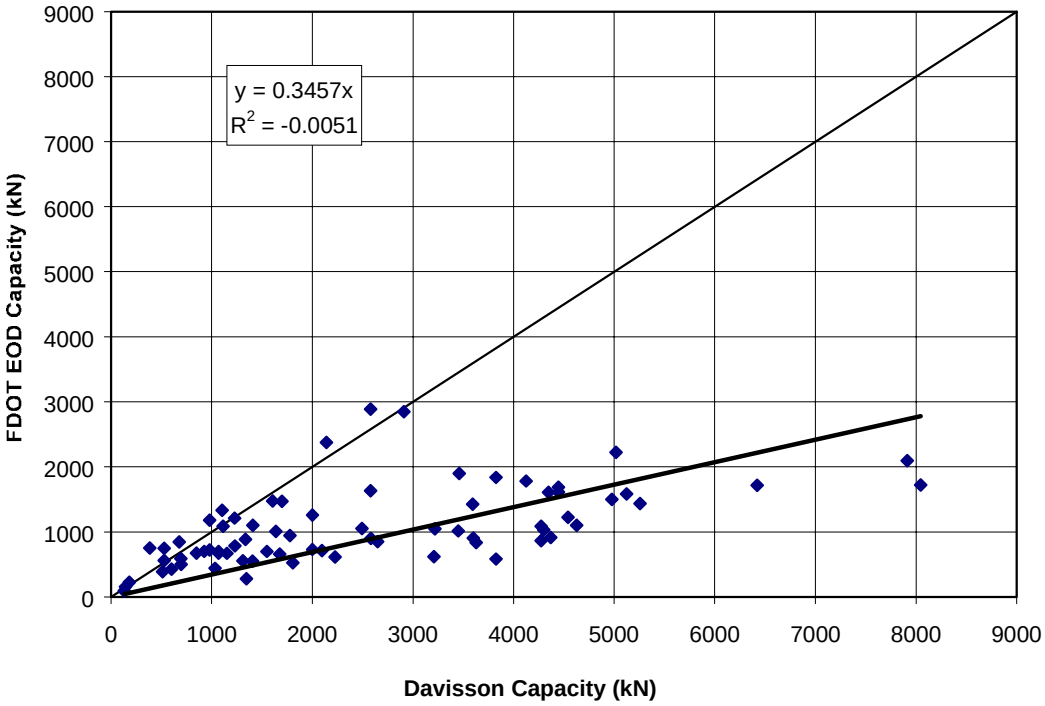

Figure E-1. Davisson Capacity vs. FDOT Method EOD Capacity

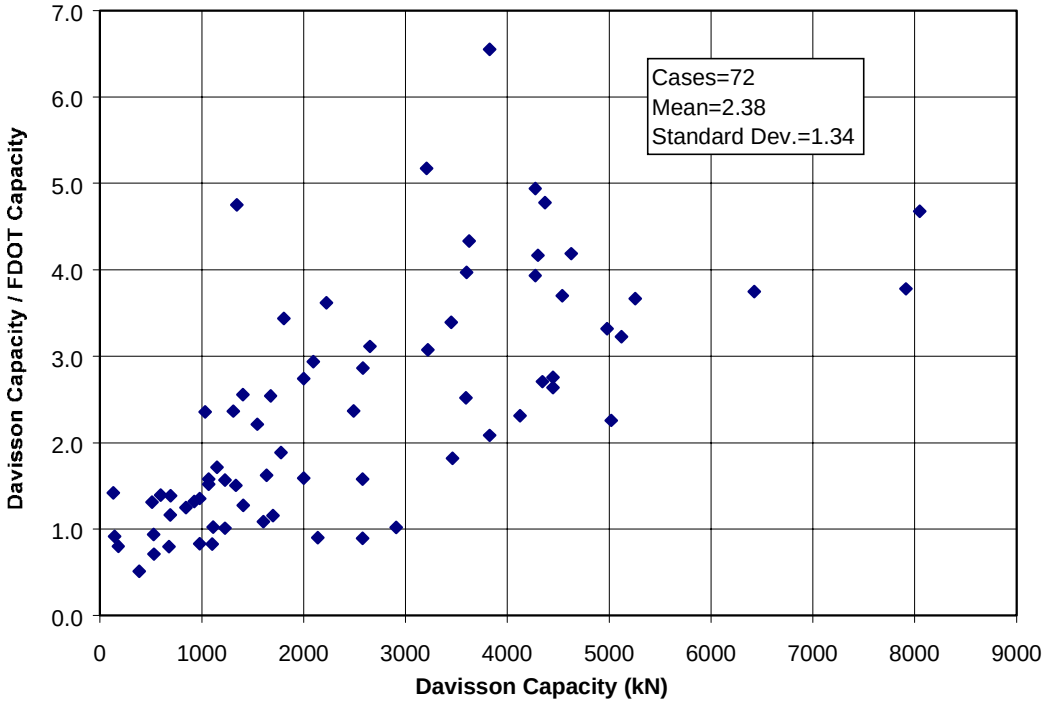

Figure E-2. Measured Over Predicted Capacity for FDOT Method at EOD

Table E-1. ϕ Values Evaluated for FDOT – Overall (EOD)

Span length (m)	Q_D/Q_L	Failure Probability p_f / Reliability Index β_T			
		2.50E-02	6.22E-03	1.22E-03	1.79E-04
		1.96	2.5	3.03	3.57
9	0.52	0.977	0.719	0.532	0.391
15	1.00	0.938	0.690	0.510	0.375
18	1.06	0.934	0.687	0.508	0.374
27	1.58	0.909	0.669	0.495	0.364
36	2.12	0.892	0.656	0.485	0.357
45	2.64	0.880	0.647	0.479	0.352
50	3.00	0.873	0.642	0.475	0.349
60	3.53	0.866	0.637	0.471	0.346

Table E-2. ASD Design Safety Factor Values Evaluated for FDOT – Overall (EOD)

Span length (m)	Q_D/Q_L	Failure Probability p_f / Reliability Index β_T			
		2.50E-02	6.22E-03	1.22E-03	1.79E-04
		1.96	2.5	3.03	3.57
9	0.52	1.616	2.196	2.969	4.037
15	1.00	1.600	2.175	2.940	3.997
18	1.06	1.598	2.173	2.937	3.994
27	1.58	1.588	2.160	2.919	3.969
36	2.12	1.582	2.150	2.907	3.952
45	2.64	1.577	2.144	2.899	3.941
50	3.00	1.575	2.141	2.894	3.934
60	3.53	1.572	2.137	2.889	3.927

Table E-3. ϕ Factors for Safety Factor = 1.00 – FDOT – Overall (EOD)

Span length (m)	Q_D/Q_L	ϕ	β_T	P_f
9	0.52	1.579	1.117	0.13210
15	1.00	1.500	1.134	0.12850
18	1.06	1.493	1.136	0.12808
27	1.58	1.444	1.146	0.12600
36	2.12	1.410	1.154	0.12435
45	2.64	1.387	1.159	0.12333
50	3.00	1.375	1.162	0.12272
60	3.53	1.360	1.165	0.12211

Table E-4. ϕ Values Evaluated for FDOT < 1779 kN (EOD)

Span length (m)	Q_D/Q_L	Failure Probability p_f / Reliability Index β_T			
		2.50E-02	6.22E-03	1.22E-03	1.79E-04
		1.96	2.5	3.03	3.57
9	0.52	0.657	0.491	0.369	0.276
15	1.00	0.631	0.471	0.354	0.264
18	1.06	0.628	0.469	0.352	0.263
27	1.58	0.611	0.457	0.343	0.256
36	2.12	0.600	0.448	0.336	0.251
45	2.64	0.592	0.442	0.332	0.248
50	3.00	0.587	0.439	0.330	0.246
60	3.53	0.582	0.435	0.327	0.244

Table E-5. ASD Design Safety Factor Values Evaluated for FDOT < 1779 kN (EOD)

Span length (m)	Q_D/Q_L	Failure Probability p_f / Reliability Index β_T			
		2.50E-02	6.22E-03	1.22E-03	1.79E-04
		1.96	2.5	3.03	3.57
9	0.52	2.402	3.215	4.281	5.730
15	1.00	2.378	3.184	4.239	5.674
18	1.06	2.376	3.181	4.235	5.669
27	1.58	2.362	3.161	4.209	5.634
36	2.12	2.352	3.148	4.191	5.610
45	2.64	2.345	3.139	4.179	5.594
50	3.00	2.341	3.134	4.172	5.585
60	3.53	2.337	3.128	4.164	5.575

Table E-6. ϕ Factors for Safety Factor = 1.00 – FDOT <1779 kN (EOD)

Span length (m)	Q_D/Q_L	ϕ	β_T	p_f
9	0.52	1.579	0.338	0.36787
15	1.00	1.500	0.356	0.36111
18	1.06	1.493	0.358	0.36036
27	1.58	1.444	0.369	0.35625
36	2.12	1.410	0.377	0.35327
45	2.64	1.387	0.382	0.35142
50	3.00	1.375	0.385	0.35030
60	3.53	1.360	0.389	0.34882

Table E-7. ϕ Values Evaluated for FDOT > 1779 kN (EOD)

Span length (m)	Q_D/Q_L	Failure Probability p_f / Reliability Index β_T			
		2.50E-02	6.22E-03	1.22E-03	1.79E-04
		1.96	2.5	3.03	3.57
9	0.52	1.783	1.406	1.114	0.878
15	1.00	1.710	1.349	1.068	0.843
18	1.06	1.703	1.343	1.064	0.839
27	1.58	1.658	1.307	1.036	0.817
36	2.12	1.626	1.283	1.016	0.801
45	2.64	1.604	1.265	1.002	0.791
50	3.00	1.593	1.256	0.995	0.785
60	3.53	1.579	1.245	0.986	0.778

Table E-8. ASD Design Safety Factor Values Evaluated for FDOT > 1779 kN (EOD)

Span length (m)	Q_D/Q_L	Failure Probability p_f / Reliability Index β_T			
		2.50E-02	6.22E-03	1.22E-03	1.79E-04
		1.96	2.5	3.03	3.57
9	0.52	0.886	1.123	1.418	1.798
15	1.00	0.877	1.112	1.404	1.780
18	1.06	0.876	1.111	1.403	1.778
27	1.58	0.871	1.104	1.394	1.767
36	2.12	0.867	1.100	1.388	1.760
45	2.64	0.865	1.096	1.384	1.755
50	3.00	0.863	1.095	1.382	1.752
60	3.53	0.862	1.093	1.379	1.749

Table E-9. ϕ Factors for Safety Factor = 1.00 – FDOT >1779 kN (EOD)

Span length (m)	Q_D/Q_L	ϕ	β_T	p_f
9	0.52	1.579	2.236	0.01269
15	1.00	1.500	2.258	0.01199
18	1.06	1.493	2.260	0.01193
27	1.58	1.444	2.274	0.01150
36	2.12	1.410	2.284	0.01120
45	2.64	1.387	2.291	0.01100
50	3.00	1.375	2.294	0.01091
60	3.53	1.360	2.299	0.01077

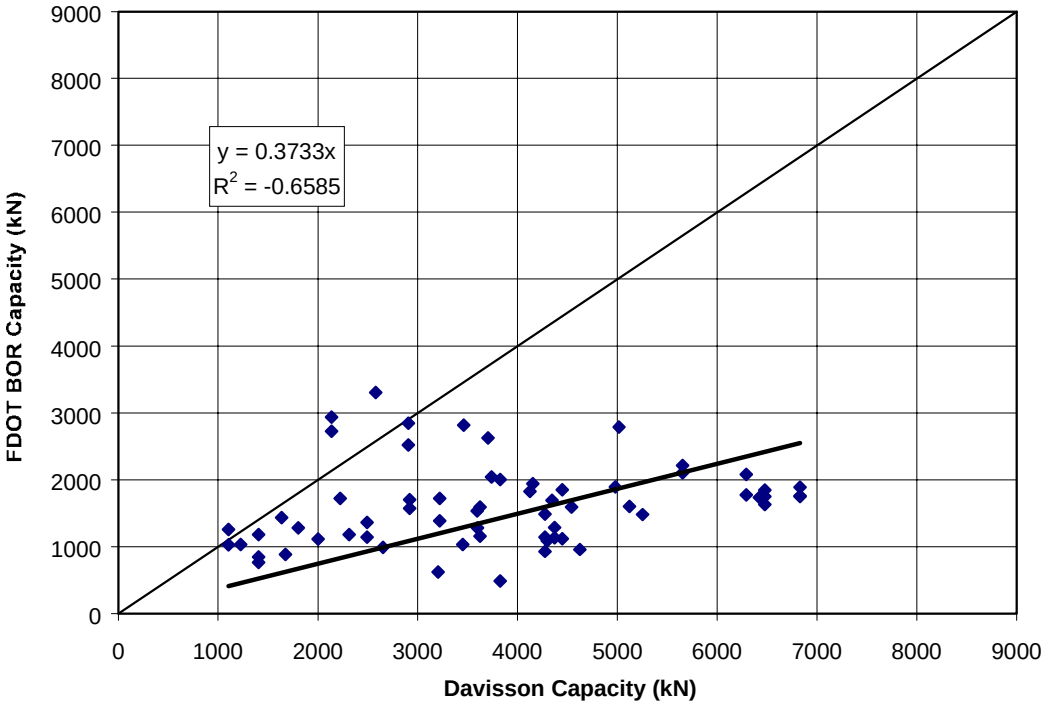

Figure E-3. Davisson Capacity vs. FDOT Method BOR

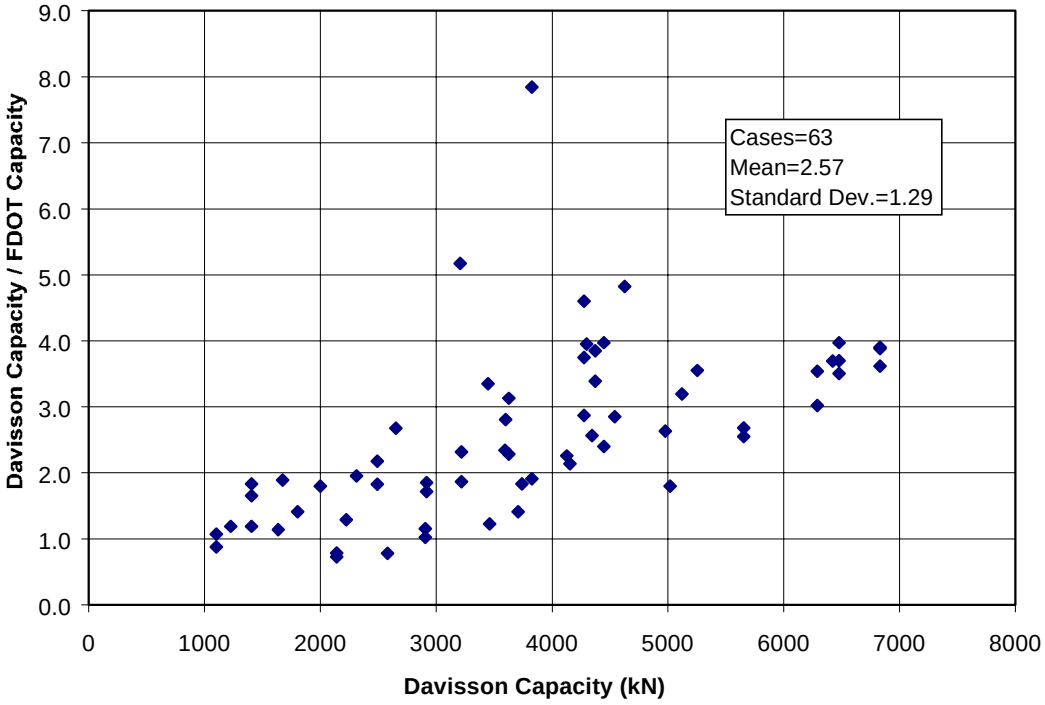

Figure E-4. Measured Over Predicted Capacity for FDOT Method at BOR

Table E-10. ϕ Values Evaluated for FDOT – Overall (BOR)

Span length (m)	Q_D/Q_L	Failure Probability p_f / Reliability Index β_T			
		2.50E-02	6.22E-03	1.22E-03	1.79E-04
		1.96	2.50	3.03	3.57
9	0.52	1.186	0.895	0.678	0.511
15	1.00	1.138	0.858	0.651	0.491
18	1.06	1.134	0.855	0.648	0.489
27	1.58	1.103	0.832	0.631	0.476
36	2.12	1.082	0.816	0.619	0.467
45	2.64	1.068	0.805	0.610	0.460
50	3.00	1.060	0.799	0.606	0.457
60	3.53	1.051	0.792	0.601	0.453

Table E-11. ASD Design Safety Factor Values Evaluated for FDOT – Overall (BOR)

Span length (m)	Q_D/Q_L	Failure Probability p_f / Reliability Index β_T			
		2.50E-02	6.22E-03	1.22E-03	1.79E-04
		1.96	2.50	3.03	3.57
9	0.52	1.331	1.765	2.328	3.087
15	1.00	1.318	1.748	2.305	3.057
18	1.06	1.317	1.746	2.303	3.054
27	1.58	1.309	1.735	2.289	3.035
36	2.12	1.303	1.728	2.279	3.023
45	2.64	1.299	1.723	2.273	3.014
50	3.00	1.297	1.720	2.269	3.009
60	3.53	1.295	1.717	2.265	3.003

Table E-12. ϕ Factors for Safety Factor = 1.00 – FDOT – Overall (BOR)

Span length (m)	Q_D/Q_L	ϕ	β	p_f
9	0.52	1.579	1.413	0.07890
15	1.00	1.500	1.432	0.07614
18	1.06	1.493	1.433	0.07600
27	1.58	1.444	1.445	0.07430
36	2.12	1.410	1.453	0.07318
45	2.64	1.387	1.459	0.07235
50	3.00	1.375	1.462	0.07194
60	3.53	1.360	1.466	0.07139

Table E-13. ϕ Values Evaluated for FDOT < 1779 kN (BOR)

Span length (m)	Q_D/Q_L	Failure Probability p_f / Reliability Index β_T			
		2.50E-02	6.22E-03	1.22E-03	1.79E-04
		1.96	2.50	3.03	3.57
9	0.52	0.941	0.778	0.646	0.534
15	1.00	0.903	0.747	0.620	0.512
18	1.06	0.899	0.744	0.617	0.510
27	1.58	0.875	0.724	0.601	0.497
36	2.12	0.858	0.710	0.589	0.487
45	2.64	0.847	0.700	0.581	0.481
50	3.00	0.841	0.695	0.577	0.477
60	3.53	0.833	0.689	0.572	0.473

Table E-14. ASD Design Safety Factor Values Evaluated for FDOT < 1779 kN (BOR)

Span length (m)	Q_D/Q_L	Failure Probability p_f / Reliability Index β_T			
		2.50E-02	6.22E-03	1.22E-03	1.79E-04
		1.96	2.50	3.03	3.57
9	0.52	1.678	2.029	2.445	2.956
15	1.00	1.662	2.009	2.421	2.927
18	1.06	1.660	2.007	2.419	2.925
27	1.58	1.650	1.995	2.404	2.907
36	2.12	1.643	1.987	2.394	2.894
45	2.64	1.638	1.981	2.387	2.886
50	3.00	1.636	1.978	2.383	2.881
60	3.53	1.633	1.974	2.378	2.876

Table E-15. ϕ Factors for Safety Factor = 1.00 – FDOT <1779 kN (BOR)

Span length (m)	Q_D/Q_L	ϕ	β	p_f
9	0.52	1.579	0.488	0.3130
15	1.00	1.500	0.516	0.3031
18	1.06	1.493	0.519	0.3021
27	1.58	1.444	0.536	0.2962
36	2.12	1.410	0.548	0.2920
45	2.64	1.387	0.557	0.2889
50	3.00	1.375	0.561	0.2876
60	3.53	1.360	0.566	0.2859

Table E-16. ϕ Values Evaluated for FDOT > 1779 kN (BOR)

Span length (m)	Q_D/Q_L	Failure Probability p_f / Reliability Index β_T			
		2.50E-02	6.22E-03	1.22E-03	1.79E-04
		1.96	2.50	3.03	3.57
9	0.52	1.357	1.039	0.799	0.611
15	1.00	1.302	0.996	0.766	0.587
18	1.06	1.297	0.992	0.763	0.584
27	1.58	1.262	0.966	0.743	0.569
36	2.12	1.238	0.947	0.729	0.558
45	2.64	1.221	0.935	0.719	0.550
50	3.00	1.212	0.928	0.714	0.546
60	3.53	1.202	0.920	0.708	0.542

Table E-17. ASD Design Safety Factor Values Evaluated for FDOT > 1779 kN (BOR)

Span length (m)	Q_D/Q_L	Failure Probability p_f / Reliability Index β_T			
		2.50E-02	6.22E-03	1.22E-03	1.79E-04
		1.96	2.50	3.03	3.57
9	0.52	1.164	1.520	1.976	2.582
15	1.00	1.152	1.505	1.957	2.557
18	1.06	1.151	1.504	1.955	2.555
27	1.58	1.144	1.495	1.943	2.539
36	2.12	1.139	1.488	1.935	2.528
45	2.64	1.136	1.484	1.929	2.521
50	3.00	1.134	1.482	1.926	2.517
60	3.53	1.132	1.479	1.923	2.512

Table E-18. ϕ Factors for Safety Factor = 1.00 – FDOT >1779 kN (BOR)

Span length (m)	Q_D/Q_L	ϕ	β	p_f
9	0.52	1.579	1.654	0.0491
15	1.00	1.500	1.674	0.0471
18	1.06	1.493	1.676	0.0469
27	1.58	1.444	1.688	0.0458
36	2.12	1.410	1.697	0.0449
45	2.64	1.387	1.703	0.0443
50	3.00	1.375	1.706	0.0441
60	3.53	1.360	1.710	0.0437

APPENDIX F

LRFD ANALYSIS RESULTS – ENGINEERING NEWS RECORD (ENR)

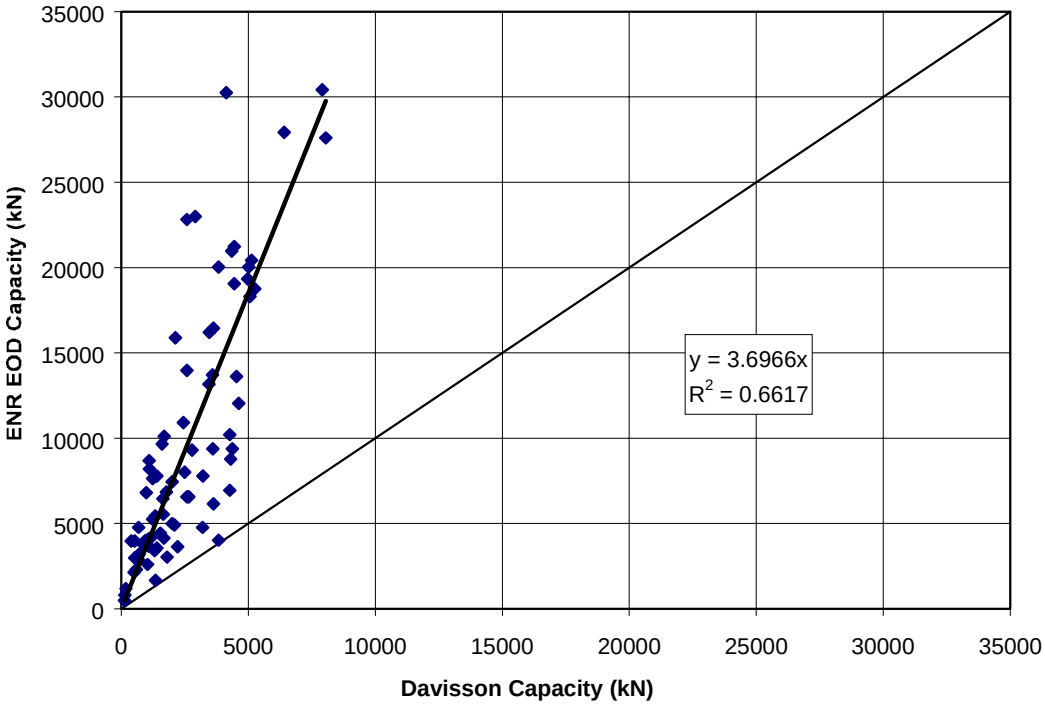

Figure F-1. Davisson Capacity vs. ENR EOD Capacity

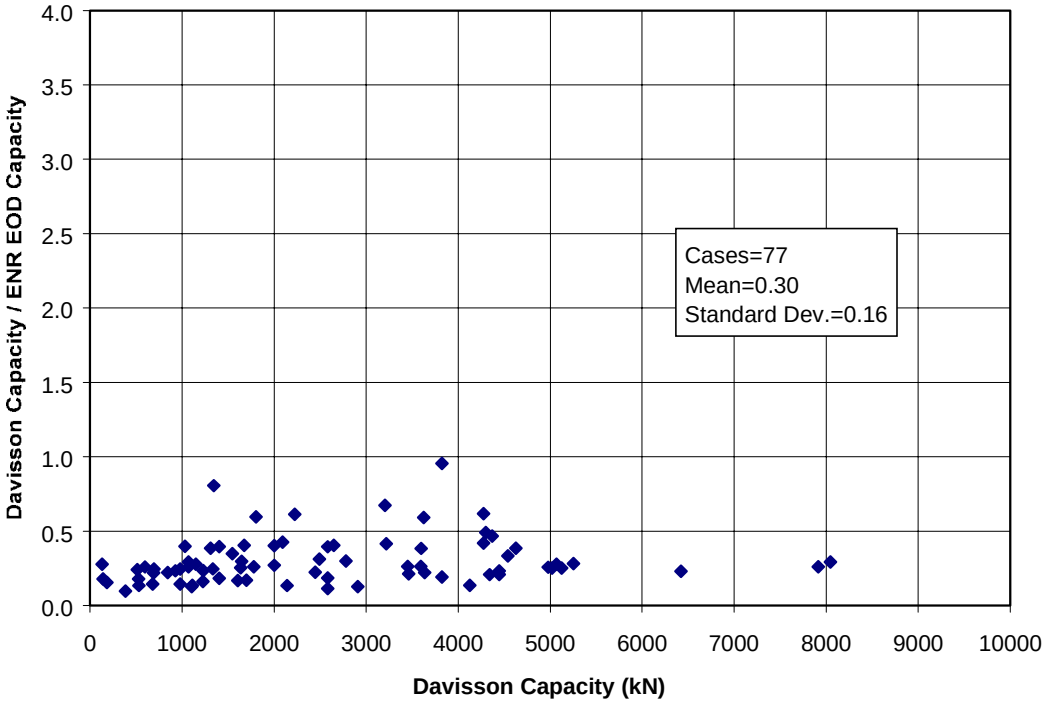

Figure F-2. Measured Over Predicted Capacity for ENR Method at EOD

Table F-1. ϕ Values Evaluated for ENR – Overall (EOD)

Span length (m)	Q_D/Q_L	Failure Probability p_f / Reliability Index β_T			
		2.50E-02	6.22E-03	1.22E-03	1.79E-04
		1.96	2.5	3.03	3.57
9	0.52	0.130	0.097	0.073	0.054
15	1.00	0.125	0.093	0.070	0.052
18	1.06	0.124	0.093	0.069	0.052
27	1.58	0.121	0.090	0.067	0.050
36	2.12	0.119	0.088	0.066	0.049
45	2.64	0.117	0.087	0.065	0.049
50	3.00	0.116	0.087	0.065	0.048
60	3.53	0.115	0.086	0.064	0.048

Table F-2. ASD Design Safety Factor Values Evaluated for ENR – Overall (EOD)

Span length (m)	Q_D/Q_L	Failure Probability p_f / Reliability Index β_T			
		2.50E-02	6.22E-03	1.22E-03	1.79E-04
		1.96	2.5	3.03	3.57
9	0.52	12.139	16.298	21.763	29.220
15	1.00	12.020	16.138	21.549	28.933
18	1.06	12.009	16.123	21.530	28.906
27	1.58	11.935	16.024	21.397	28.729
36	2.12	11.884	15.956	21.307	28.607
45	2.64	11.850	15.910	21.245	28.524
50	3.00	11.831	15.885	21.211	28.479
60	3.53	11.809	15.855	21.172	28.425

Table F-3. ϕ Factors for Safety Factor = 6.00 – ENR – Overall (EOD)

Span length (m)	Q_D/Q_L	ϕ	β_T	p_f
9	0.52	0.263	0.669	0.2519
15	1.00	0.250	0.687	0.2462
18	1.06	0.249	0.688	0.2459
27	1.58	0.241	0.700	0.2421
36	2.12	0.235	0.707	0.2399
45	2.64	0.231	0.713	0.2381
50	3.00	0.229	0.716	0.2372
60	3.53	0.227	0.719	0.2362

Table F-4. ϕ Values Evaluated for ENR < 1779 kN (EOD)

Span length (m)	Q_D/Q_L	Failure Probability p_f / Reliability Index β_T			
		2.50E-02	6.22E-03	1.22E-03	1.79E-04
		1.96	2.5	3.03	3.57
9	0.52	0.112	0.084	0.064	0.048
15	1.00	0.108	0.081	0.061	0.046
18	1.06	0.107	0.081	0.061	0.046
27	1.58	0.105	0.078	0.059	0.044
36	2.12	0.103	0.077	0.058	0.044
45	2.64	0.101	0.076	0.057	0.043
50	3.00	0.101	0.075	0.057	0.043
60	3.53	0.100	0.075	0.056	0.042

Table F-5. ASD Design Safety Factor Values Evaluated for ENR < 1779 kN (EOD)

Span length (m)	Q_D/Q_L	Failure Probability p_f / Reliability Index β_T			
		2.50E-02	6.22E-03	1.22E-03	1.79E-04
		1.96	2.5	3.03	3.57
9	0.52	14.037	18.709	24.806	33.063
15	1.00	13.899	18.526	24.562	32.739
18	1.06	13.886	18.509	24.540	32.709
27	1.58	13.801	18.395	24.389	32.508
36	2.12	13.742	18.317	24.285	32.370
45	2.64	13.702	18.264	24.215	32.276
50	3.00	13.681	18.235	24.177	32.225
60	3.53	13.655	18.201	24.131	32.165

Table F-6. ϕ Factors for Safety Factor = 6.00 – ENR <1779 kN (EOD)

Span length (m)	Q_D/Q_L	ϕ	β_T	p_f
9	0.52	0.263	0.363	0.3585
15	1.00	0.250	0.381	0.3518
18	1.06	0.249	0.383	0.3510
27	1.58	0.241	0.395	0.3466
36	2.12	0.235	0.403	0.3437
45	2.64	0.231	0.408	0.3418
50	3.00	0.229	0.411	0.3407
60	3.53	0.227	0.415	0.3393

Table F-7. ϕ Values Evaluated for ENR > 1779 kN (EOD)

Span length (m)	Q_D/Q_L	Failure Probability p_f / Reliability Index β_T			
		2.50E-02	6.22E-03	1.22E-03	1.79E-04
		1.96	2.5	3.03	3.57
9	0.52	0.154	0.116	0.088	0.066
15	1.00	0.148	0.111	0.084	0.063
18	1.06	0.147	0.111	0.084	0.063
27	1.58	0.143	0.108	0.082	0.061
36	2.12	0.141	0.106	0.080	0.060
45	2.64	0.139	0.104	0.079	0.059
50	3.00	0.138	0.104	0.078	0.059
60	3.53	0.136	0.103	0.078	0.058

Table F-8. ASD Design Safety Factor Values Evaluated for ENR > 1779 kN (EOD)

Span length (m)	Q_D/Q_L	Failure Probability p_f / Reliability Index β_T			
		2.50E-02	6.22E-03	1.22E-03	1.79E-04
		1.96	2.5	3.03	3.57
9	0.52	10.247	13.616	17.999	23.918
15	1.00	10.146	13.483	17.822	23.683
18	1.06	10.137	13.470	17.806	23.662
27	1.58	10.074	13.388	17.697	23.516
36	2.12	10.032	13.331	17.622	23.417
45	2.64	10.003	13.292	17.570	23.348
50	3.00	9.987	13.271	17.543	23.312
60	3.53	9.968	13.246	17.510	23.268

Table F-9. ϕ Factors for Safety Factor = 6.00 – ENR >1779 kN (EOD)

Span length (m)	Q_D/Q_L	ϕ	β_T	p_f
9	0.52	0.263	0.944	0.1727
15	1.00	0.250	0.962	0.1682
18	1.06	0.249	0.964	0.1676
27	1.58	0.241	0.976	0.1647
36	2.12	0.235	0.984	0.1627
45	2.64	0.231	0.989	0.1615
50	3.00	0.229	0.992	0.1607
60	3.53	0.227	0.996	0.1597

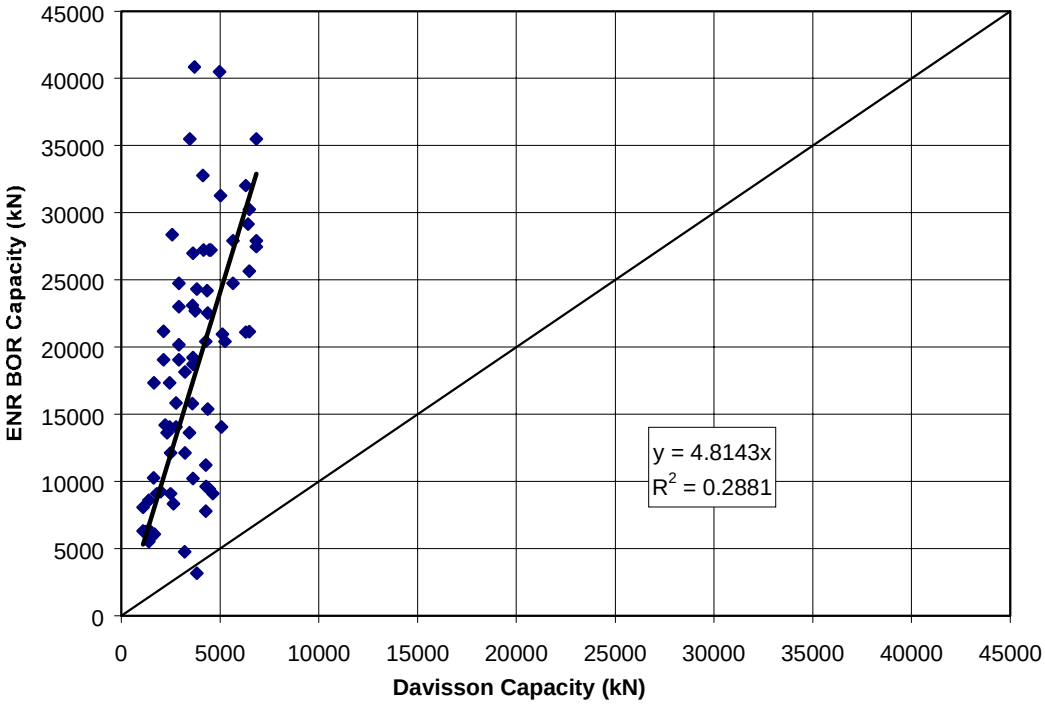

Figure F-3. Davisson Capacity vs. ENR BOR Capacity

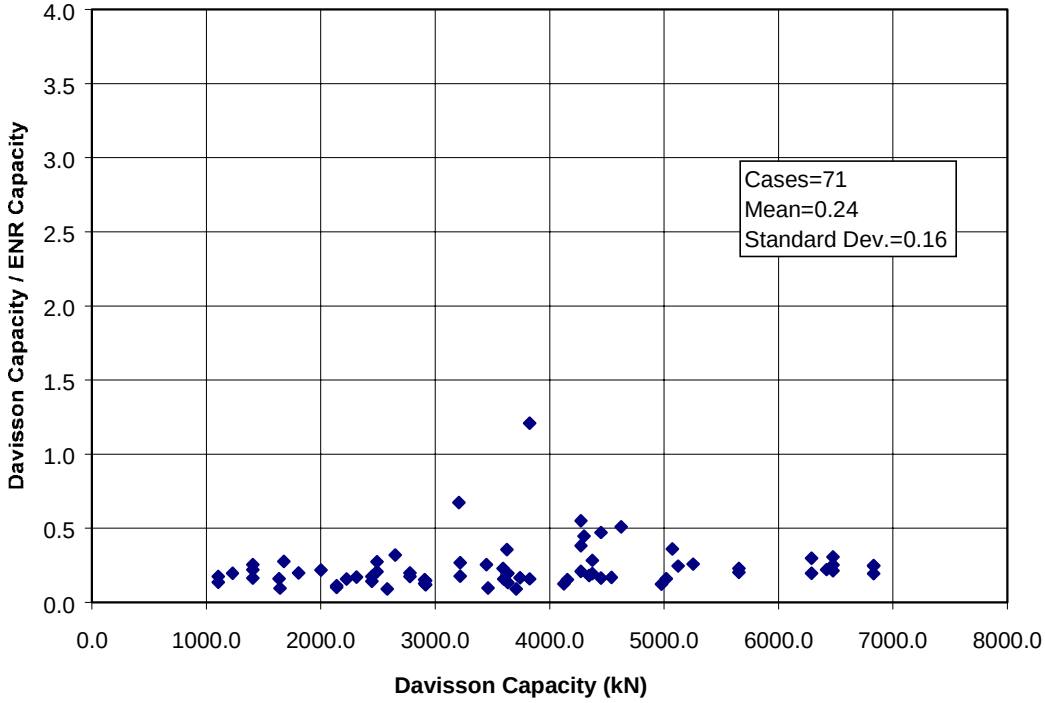

Figure F-4. Measured Over Predicted Capacity for ENR Method at BOR

Table F-10. ϕ Values Evaluated for ENR – Overall (BOR)

Span length (m)	Q_D/Q_L	Failure Probability p_f / Reliability Index β_T			
		2.50E-02	6.22E-03	1.22E-03	1.79E-04
		1.96	2.50	3.03	3.57
9	0.52	0.077	0.054	0.038	0.027
15	1.00	0.074	0.052	0.037	0.026
18	1.06	0.074	0.052	0.037	0.026
27	1.58	0.072	0.050	0.036	0.025
36	2.12	0.071	0.050	0.035	0.025
45	2.64	0.070	0.049	0.035	0.024
50	3.00	0.069	0.049	0.034	0.024
60	3.53	0.068	0.048	0.034	0.024

Table F-11. ASD Design Safety Factor Values Evaluated for ENR – Overall (BOR)

Span length (m)	Q_D/Q_L	Failure Probability p_f / Reliability Index β_T			
		2.50E-02	6.22E-03	1.22E-03	1.79E-04
		1.96	2.50	3.03	3.57
9	0.52	20.423	29.086	41.153	58.608
15	1.00	20.223	28.800	40.749	58.033
18	1.06	20.204	28.774	40.712	57.980
27	1.58	20.080	28.597	40.461	57.623
36	2.12	19.995	28.476	40.290	57.379
45	2.64	19.937	28.393	40.172	57.212
50	3.00	19.905	28.348	40.109	57.122
60	3.53	19.868	28.296	40.034	57.015

Table F-12. ϕ Factors for Safety Factor = 6.00 – ENR – Overall (BOR)

Span length (m)	Q_D/Q_L	ϕ	β	p_f
9	0.52	0.263	0.089	0.46474
15	1.00	0.250	0.104	0.45878
18	1.06	0.249	0.106	0.45799
27	1.58	0.241	0.115	0.45442
36	2.12	0.235	0.122	0.45165
45	2.64	0.231	0.126	0.45006
50	3.00	0.229	0.129	0.44888
60	3.53	0.227	0.131	0.44809

Table F-13. ϕ Values Evaluated for ENR < 1779 kN (BOR)

Span length (m)	Q_D/Q_L	Failure Probability p_f / Reliability Index β_T			
		2.50E-02	6.22E-03	1.22E-03	1.79E-04
		1.96	2.50	3.03	3.57
9	0.52	0.124	0.101	0.083	0.068
15	1.00	0.119	0.097	0.080	0.065
18	1.06	0.118	0.097	0.079	0.065
27	1.58	0.115	0.094	0.077	0.063
36	2.12	0.113	0.092	0.076	0.062
45	2.64	0.111	0.091	0.075	0.061
50	3.00	0.110	0.090	0.074	0.061
60	3.53	0.109	0.090	0.074	0.060

Table F-14. ASD Design Safety Factor Values Evaluated for ENR < 1779 kN (BOR)

Span length (m)	Q_D/Q_L	Failure Probability p_f / Reliability Index β_T			
		2.50E-02	6.22E-03	1.22E-03	1.79E-04
		1.96	2.50	3.03	3.57
9	0.52	12.777	15.610	19.002	23.217
15	1.00	12.651	15.457	18.816	22.989
18	1.06	12.640	15.443	18.798	22.968
27	1.58	12.562	15.348	18.683	22.827
36	2.12	12.509	15.283	18.604	22.730
45	2.64	12.472	15.239	18.549	22.664
50	3.00	12.453	15.215	18.520	22.628
60	3.53	12.429	15.186	18.486	22.586

Table F-15. ϕ Factors for Safety Factor = 6.00 – ENR <1779 kN (BOR)

Span length (m)	Q_D/Q_L	ϕ	β	p_f
9	0.52	0.263	-0.078	0.5313
15	1.00	0.250	-0.051	0.5205
18	1.06	0.249	-0.048	0.5193
27	1.58	0.241	-0.032	0.5130
36	2.12	0.235	-0.020	0.5082
45	2.64	0.231	-0.013	0.5054
50	3.00	0.229	-0.008	0.5034
60	3.53	0.227	-0.003	0.5014

Table F-16. ϕ Values Evaluated for ENR > 1779 kN (BOR)

Span length (m)	Q_D/Q_L	Failure Probability p_f / Reliability Index β_T			
		2.50E-02	6.22E-03	1.22E-03	1.79E-04
		1.96	2.50	3.03	3.57
9	0.52	0.077	0.054	0.038	0.026
15	1.00	0.074	0.052	0.036	0.025
18	1.06	0.074	0.051	0.036	0.025
27	1.58	0.072	0.050	0.035	0.025
36	2.12	0.070	0.049	0.034	0.024
45	2.64	0.069	0.048	0.034	0.024
50	3.00	0.069	0.048	0.034	0.024
60	3.53	0.068	0.048	0.033	0.023

Table F-17. ASD Design Safety Factor Values Evaluated for ENR > 1779 kN (BOR)

Span length (m)	Q_D/Q_L	Failure Probability p_f / Reliability Index β_T			
		2.50E-02	6.22E-03	1.22E-03	1.79E-04
		1.96	2.50	3.03	3.57
9	0.52	20.463	29.334	41.770	59.877
15	1.00	20.263	29.046	41.360	59.289
18	1.06	20.244	29.019	41.323	59.235
27	1.58	20.120	28.841	41.068	58.871
36	2.12	20.034	28.719	40.894	58.621
45	2.64	19.976	28.635	40.775	58.451
50	3.00	19.945	28.590	40.711	58.359
60	3.53	19.907	28.537	40.635	58.250

Table F-18. ϕ Factors for Safety Factor = 6.00 – ENR >1779 kN (BOR)

Span length (m)	Q_D/Q_L	ϕ	β	p_f
9	0.52	0.263	0.120	0.4524
15	1.00	0.250	0.135	0.4465
18	1.06	0.249	0.136	0.4461
27	1.58	0.241	0.146	0.4422
36	2.12	0.235	0.152	0.4398
45	2.64	0.231	0.156	0.4382
50	3.00	0.229	0.159	0.4370
60	3.53	0.227	0.162	0.4358

APPENDIX G

LRFD ANALYSIS RESULTS – MODIFIED ENR

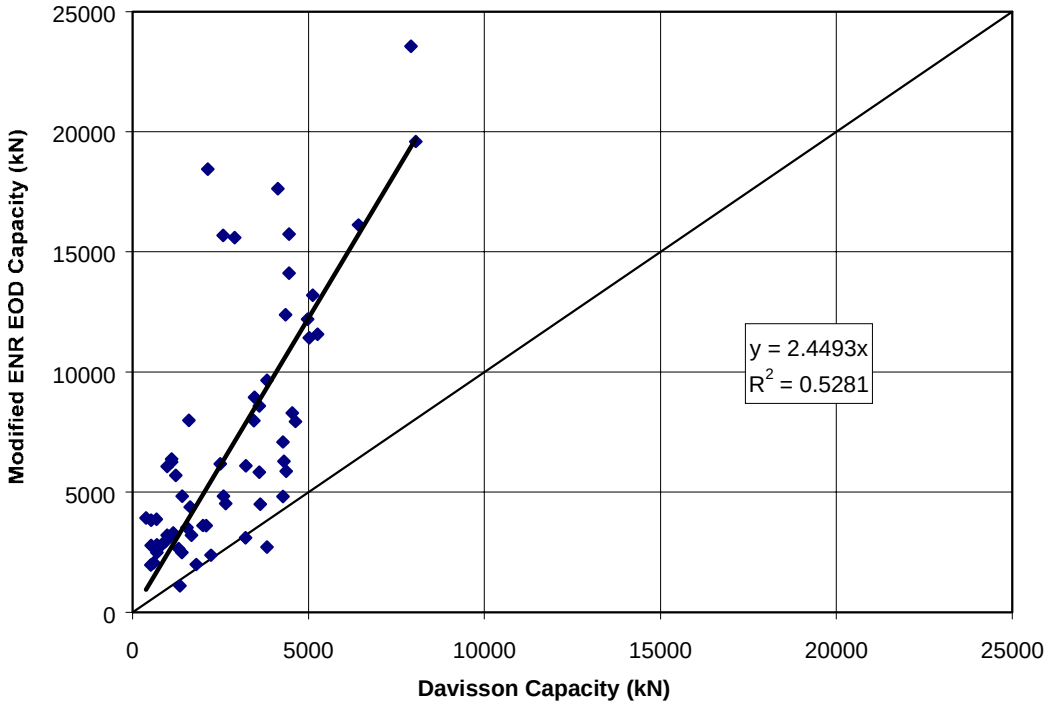

Figure G-1. Davisson Capacity vs. Modified ENR EOD Capacity

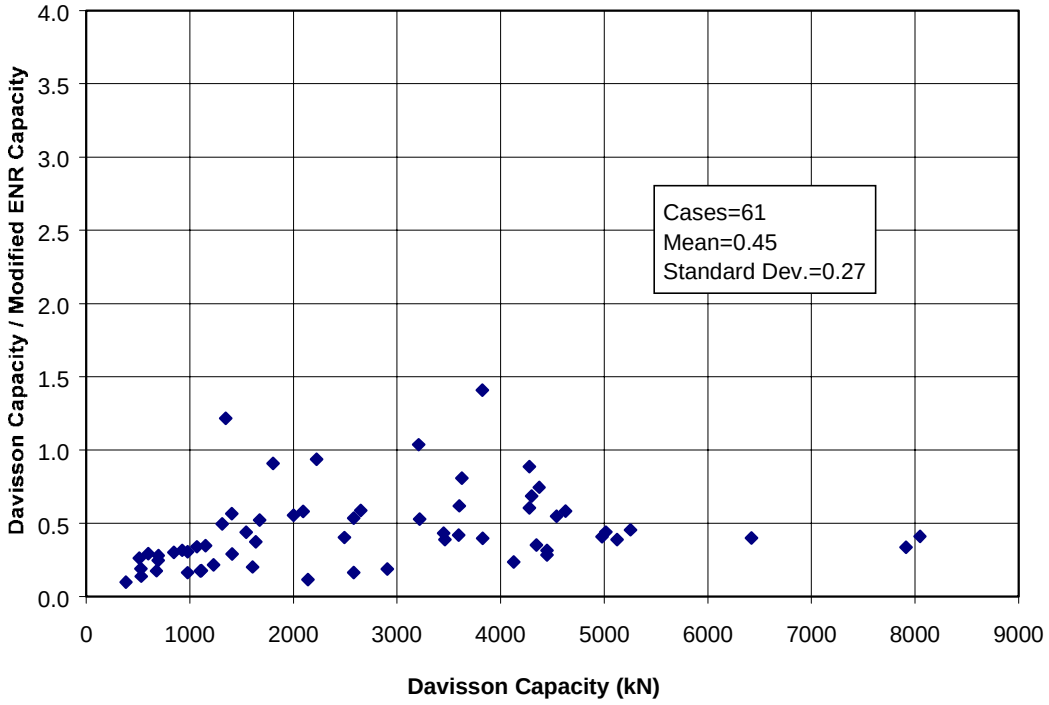

Figure G-2. Measured Over Predicted Capacity for Modified ENR Method at EOD

Table G-1. ϕ Values Evaluated for Modified ENR – Overall (EOD)

Span length (m)	Q_D/Q_L	Failure Probability p_f / Reliability Index β_T			
		2.50E-02	6.22E-03	1.22E-03	1.79E-04
		1.96	2.5	3.03	3.57
9	0.52	0.171	0.124	0.090	0.065
15	1.00	0.164	0.119	0.087	0.063
18	1.06	0.163	0.118	0.086	0.063
27	1.58	0.159	0.115	0.084	0.061
36	2.12	0.156	0.113	0.082	0.060
45	2.64	0.154	0.111	0.081	0.059
50	3.00	0.153	0.111	0.081	0.059
60	3.53	0.151	0.110	0.080	0.058

Table G-2. ASD Design Safety Factor for Modified ENR – Overall (EOD)

Span length (m)	Q_D/Q_L	Failure Probability p_f / Reliability Index β_T			
		2.50E-02	6.22E-03	1.22E-03	1.79E-04
		1.96	2.5	3.03	3.57
9	0.52	9.241	12.747	17.480	24.111
15	1.00	9.151	12.622	17.308	23.875
18	1.06	9.142	12.611	17.292	23.853
27	1.58	9.086	12.533	17.186	23.706
36	2.12	9.047	12.480	17.113	23.606
45	2.64	9.021	12.444	17.063	23.537
50	3.00	9.007	12.424	17.036	23.500
60	3.53	8.990	12.401	17.005	23.456

Table G-3. ϕ Factors for Safety Factor = 6.00 – Modified ENR – Overall (EOD)

Span length (m)	Q_D/Q_L	ϕ	β_T	p_f
9	0.52	0.263	1.235	0.1085
15	1.00	0.250	1.251	0.1056
18	1.06	0.249	1.253	0.1052
27	1.58	0.241	1.263	0.1034
36	2.12	0.235	1.270	0.1021
45	2.64	0.231	1.275	0.1012
50	3.00	0.229	1.278	0.1007
60	3.53	0.227	1.281	0.1002

Table G-4. ϕ Values Evaluated for Modified ENR < 1779 kN (EOD)

Span length (m)	Q_D/Q_L	Failure Probability p_f / Reliability Index β_T			
		2.50E-02	6.22E-03	1.22E-03	1.79E-04
		1.96	2.5	3.03	3.57
9	0.52	0.106	0.075	0.053	0.037
15	1.00	0.102	0.072	0.051	0.035
18	1.06	0.102	0.071	0.050	0.035
27	1.58	0.099	0.069	0.049	0.034
36	2.12	0.097	0.068	0.048	0.034
45	2.64	0.096	0.067	0.047	0.033
50	3.00	0.095	0.067	0.047	0.033
60	3.53	0.094	0.066	0.047	0.033

Table G-5. ASD Design Safety Factor for Modified ENR < 1779 kN (EOD)

Span length (m)	Q_D/Q_L	Failure Probability p_f / Reliability Index β_T			
		2.50E-02	6.22E-03	1.22E-03	1.79E-04
		1.96	2.5	3.03	3.57
9	0.52	14.853	21.174	29.986	42.746
15	1.00	14.708	20.966	29.692	42.327
18	1.06	14.694	20.947	29.665	42.288
27	1.58	14.604	20.818	29.482	42.028
36	2.12	14.542	20.730	29.357	41.850
45	2.64	14.500	20.670	29.272	41.728
50	3.00	14.477	20.637	29.226	41.662
60	3.53	14.450	20.599	29.171	41.584

Table G-6. ϕ Factors for Safety Factor = 6.00 – Modified ENR <1779 kN (EOD)

Span length (m)	Q_D/Q_L	ϕ	β_T	p_f
9	0.52	0.263	0.579	0.2815
15	1.00	0.250	0.594	0.2764
18	1.06	0.249	0.596	0.2758
27	1.58	0.241	0.605	0.2728
36	2.12	0.235	0.612	0.2704
45	2.64	0.231	0.616	0.2691
50	3.00	0.229	0.618	0.2685
60	3.53	0.227	0.621	0.2675

Table G-7. ϕ Values Evaluated for Modified ENR > 1779 kN (EOD)

Span length (m)	Q_D/Q_L	Failure Probability p_f / Reliability Index β_T			
		2.50E-02	6.22E-03	1.22E-03	1.79E-04
		1.96	2.5	3.03	3.57
9	0.52	0.200	0.145	0.105	0.076
15	1.00	0.192	0.139	0.101	0.073
18	1.06	0.191	0.138	0.101	0.073
27	1.58	0.186	0.135	0.098	0.071
36	2.12	0.183	0.132	0.096	0.069
45	2.64	0.180	0.130	0.095	0.069
50	3.00	0.179	0.129	0.094	0.068
60	3.53	0.177	0.128	0.093	0.067

Table G-8. ASD Design Safety Factor for Modified ENR > 1779 kN (EOD)

Span length (m)	Q_D/Q_L	Failure Probability p_f / Reliability Index β_T			
		2.50E-02	6.22E-03	1.22E-03	1.79E-04
		1.96	2.5	3.03	3.57
9	0.52	7.881	10.903	14.993	20.742
15	1.00	7.804	10.796	14.846	20.538
18	1.06	7.797	10.786	14.833	20.519
27	1.58	7.749	10.720	14.741	20.393
36	2.12	7.716	10.675	14.679	20.307
45	2.64	7.694	10.644	14.636	20.248
50	3.00	7.682	10.627	14.613	20.216
60	3.53	7.667	10.607	14.586	20.178

Table G-9. ϕ Factors for Safety Factor = 6.00 – Modified ENR >1779 kN (EOD)

Span length (m)	Q_D/Q_L	ϕ	β_T	p_f
9	0.52	0.263	1.506	0.0661
15	1.00	0.250	1.523	0.0639
18	1.06	0.249	1.524	0.0638
27	1.58	0.241	1.534	0.0626
36	2.12	0.235	1.541	0.0617
45	2.64	0.231	1.546	0.0611
50	3.00	0.229	1.549	0.0608
60	3.53	0.227	1.552	0.0604

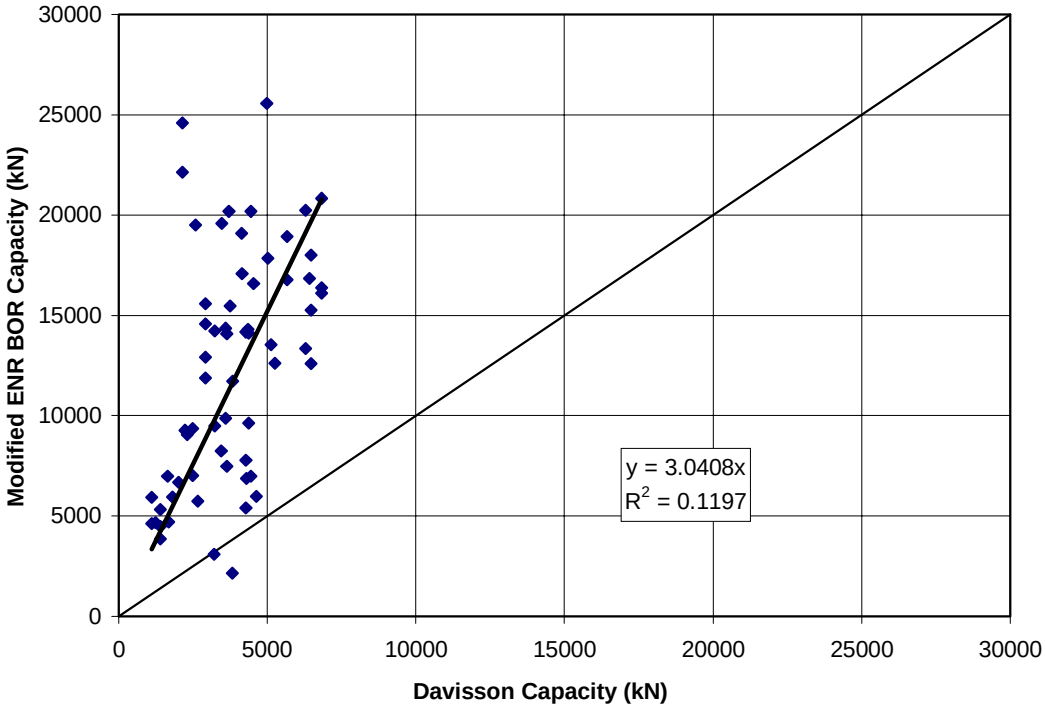

Figure G-3. Davisson Capacity vs. Modified ENR BOR Capacity

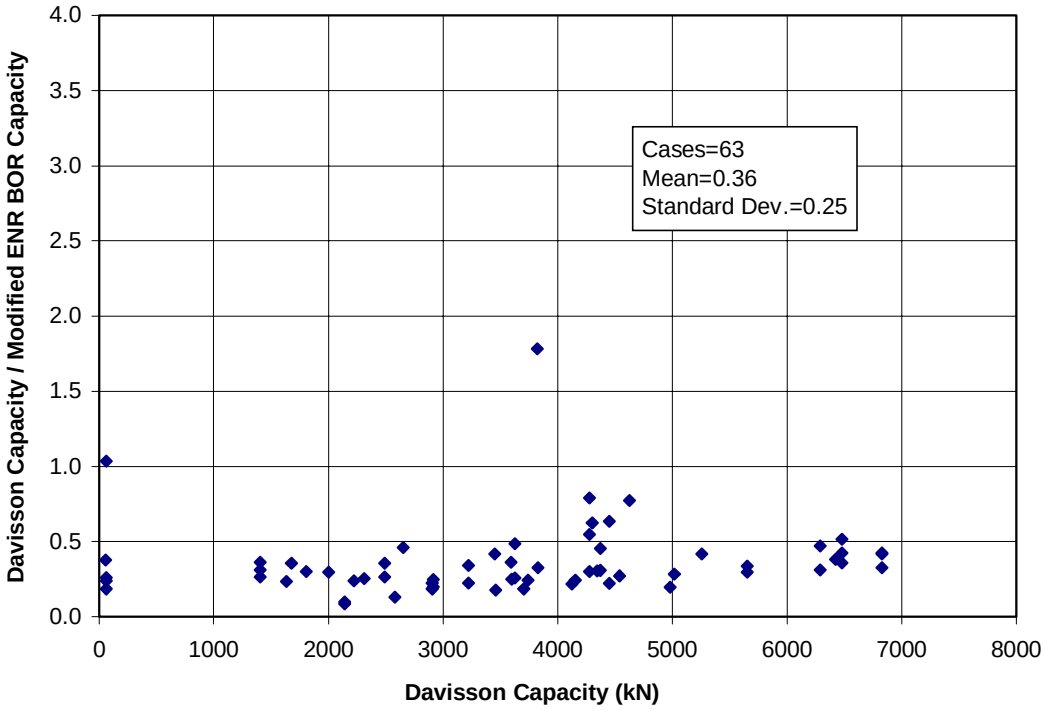

Figure G-4. Measured Over Predicted Capacity for Modified ENR Method at BOR

Table G-10. ϕ Values Evaluated for Modified ENR – Overall (BOR)

Span length (m)	Q_D/Q_L	Failure Probability p_f / Reliability Index β_T			
		2.50E-02	6.22E-03	1.22E-03	1.79E-04
		1.96	2.50	3.03	3.57
9	0.52	0.121	0.085	0.060	0.042
15	1.00	0.116	0.081	0.058	0.040
18	1.06	0.115	0.081	0.057	0.040
27	1.58	0.112	0.079	0.056	0.039
36	2.12	0.110	0.077	0.055	0.039
45	2.64	0.108	0.076	0.054	0.038
50	3.00	0.108	0.076	0.054	0.038
60	3.53	0.107	0.075	0.053	0.037

Table G-11. ASD Design Safety Factor for Modified ENR – Overall (BOR)

Span length (m)	Q_D/Q_L	Failure Probability p_f / Reliability Index β_T			
		2.50E-02	6.22E-03	1.22E-03	1.79E-04
		1.96	2.50	3.03	3.57
9	0.52	13.101	18.627	26.313	37.413
15	1.00	12.972	18.445	26.055	37.046
18	1.06	12.960	18.428	26.031	37.012
27	1.58	12.881	18.314	25.871	36.784
36	2.12	12.826	18.237	25.761	36.628
45	2.64	12.789	18.184	25.686	36.522
50	3.00	12.769	18.155	25.646	36.464
60	3.53	12.745	18.121	25.598	36.396

Table G-12. ϕ Factors for Safety Factor = 6.00 – Modified ENR – Overall (BOR)

Span length (m)	Q_D/Q_L	ϕ	β	p_f
9	0.52	0.263	0.762	0.2232
15	1.00	0.250	0.777	0.2187
18	1.06	0.249	0.778	0.2184
27	1.58	0.241	0.788	0.2155
36	2.12	0.235	0.794	0.2137
45	2.64	0.231	0.799	0.2123
50	3.00	0.229	0.801	0.2117
60	3.53	0.227	0.804	0.2108

Table G-13. ϕ Values Evaluated for Modified ENR < 1779 kN (BOR)

Span length (m)	Q_D/Q_L	Failure Probability p_f / Reliability Index β_T			
		2.50E-02	6.22E-03	1.22E-03	1.79E-04
		1.96	2.50	3.03	3.57
9	0.52	0.211	0.178	0.151	0.128
15	1.00	0.202	0.171	0.145	0.123
18	1.06	0.202	0.170	0.144	0.122
27	1.58	0.196	0.166	0.141	0.119
36	2.12	0.193	0.163	0.138	0.117
45	2.64	0.190	0.161	0.136	0.115
50	3.00	0.189	0.159	0.135	0.114
60	3.53	0.187	0.158	0.134	0.113

Table G-14. ASD Design Safety Factor for Modified ENR < 1779 kN (BOR)

Span length (m)	Q_D/Q_L	Failure Probability p_f / Reliability Index β_T			
		2.50E-02	6.22E-03	1.22E-03	1.79E-04
		1.96	2.50	3.03	3.57
9	0.52	7.482	8.853	10.442	12.356
15	1.00	7.408	8.766	10.340	12.235
18	1.06	7.401	8.758	10.330	12.223
27	1.58	7.356	8.704	10.267	12.148
36	2.12	7.325	8.667	10.223	12.097
45	2.64	7.303	8.642	10.194	12.062
50	3.00	7.292	8.628	10.178	12.043
60	3.53	7.278	8.612	10.159	12.020

Table G-15. ϕ Factors for Safety Factor = 6.00 – Modified ENR <1779 kN (BOR)

Span length (m)	Q_D/Q_L	ϕ	β	p_f
9	0.52	0.263	1.252	0.1054
15	1.00	0.250	1.283	0.0998
18	1.06	0.249	1.286	0.0993
27	1.58	0.241	1.306	0.0959
36	2.12	0.235	1.320	0.0935
45	2.64	0.231	1.329	0.0920
50	3.00	0.229	1.334	0.0912
60	3.53	0.227	1.340	0.0902

Table G-16. ϕ Values Evaluated for Modified ENR > 1779 kN (BOR)

Span length (m)	Q_D/Q_L	Failure Probability p_f / Reliability Index β_T			
		2.50E-02	6.22E-03	1.22E-03	1.79E-04
		1.96	2.50	3.03	3.57
9	0.52	0.121	0.085	0.060	0.042
15	1.00	0.116	0.081	0.057	0.040
18	1.06	0.116	0.081	0.057	0.040
27	1.58	0.113	0.079	0.055	0.039
36	2.12	0.111	0.077	0.054	0.038
45	2.64	0.109	0.076	0.054	0.038
50	3.00	0.108	0.076	0.053	0.037
60	3.53	0.107	0.075	0.053	0.037

Table G-17. ASD Design Safety Factor for Modified ENR > 1779 kN (BOR)

Span length (m)	Q_D/Q_L	Failure Probability p_f / Reliability Index β_T			
		2.50E-02	6.22E-03	1.22E-03	1.79E-04
		1.96	2.50	3.03	3.57
9	0.52	13.029	18.635	26.475	37.864
15	1.00	12.901	18.452	26.215	37.493
18	1.06	12.890	18.435	26.191	37.458
27	1.58	12.810	18.321	26.030	37.228
36	2.12	12.756	18.244	25.920	37.070
45	2.64	12.719	18.191	25.844	36.962
50	3.00	12.699	18.162	25.804	36.904
60	3.53	12.675	18.128	25.756	36.835

Table G-18. ϕ Factors for Safety Factor = 6.00 – Modified. ENR >1779 kN (BOR)

Span length (m)	Q_D/Q_L	ϕ	β	p_f
9	0.52	0.263	0.790	0.2149
15	1.00	0.250	0.805	0.2106
18	1.06	0.249	0.806	0.2103
27	1.58	0.241	0.815	0.2077
36	2.12	0.235	0.822	0.2057
45	2.64	0.231	0.826	0.2045
50	3.00	0.229	0.828	0.2040
60	3.53	0.227	0.831	0.2031

APPENDIX H

LRFD ANALYSIS RESULTS – GATES FORMULA

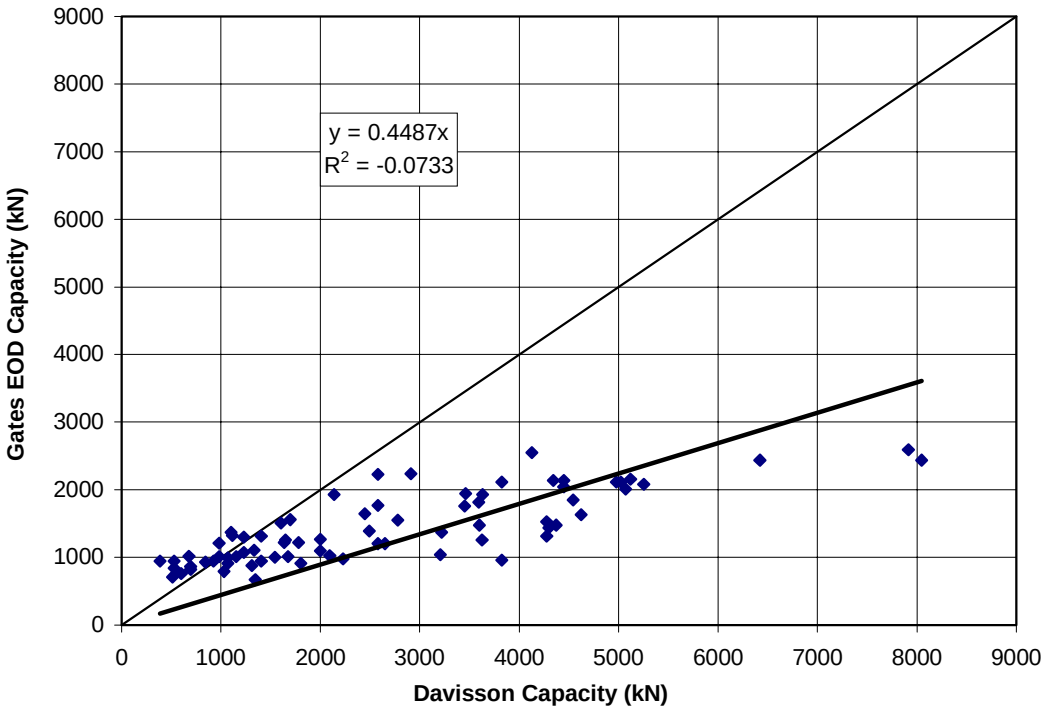

Figure H-1. Davisson Capacity vs. Gates EOD Capacity

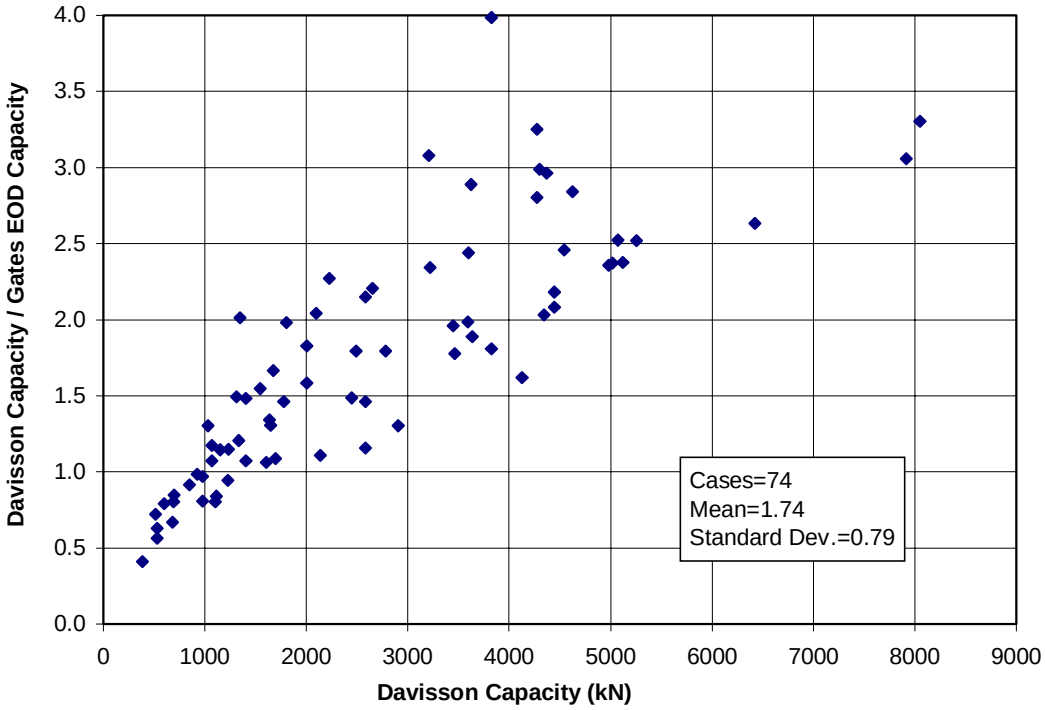

Figure H-2. Measured Over Predicted Capacity for Gates Method at EOD

Table H-1. ϕ Values Evaluated for Gates – Overall (EOD)

Span length (m)	Q_D/Q_L	Failure Probability p_f / Reliability Index β_T			
		2.50E-02	6.22E-03	1.22E-03	1.79E-04
		1.96	2.5	3.03	3.57
9	0.52	0.884	0.681	0.527	0.406
15	1.00	0.848	0.653	0.505	0.389
18	1.06	0.845	0.651	0.503	0.388
27	1.58	0.822	0.633	0.490	0.377
36	2.12	0.806	0.621	0.481	0.370
45	2.64	0.796	0.613	0.474	0.365
50	3.00	0.790	0.608	0.471	0.363
60	3.53	0.783	0.603	0.467	0.359

Table H-2. ASD Design Safety Factor for Gates – Overall (EOD)

Span length (m)	Q_D/Q_L	Failure Probability p_f / Reliability Index β_T			
		2.50E-02	6.22E-03	1.22E-03	1.79E-04
		1.96	2.5	3.03	3.57
9	0.52	1.786	2.319	2.997	3.891
15	1.00	1.769	2.297	2.967	3.853
18	1.06	1.767	2.294	2.965	3.849
27	1.58	1.756	2.280	2.946	3.826
36	2.12	1.749	2.271	2.934	3.809
45	2.64	1.744	2.264	2.925	3.798
50	3.00	1.741	2.260	2.921	3.792
60	3.53	1.738	2.256	2.915	3.785

Table H-3. ϕ Factors for Safety Factor = 3.00 – Gates – Overall (EOD)

Span length (m)	Q_D/Q_L	ϕ	β_T	p_f
9	0.52	0.526	3.032	0.00122
15	1.00	0.500	3.053	0.00113
18	1.06	0.498	3.054	0.00113
27	1.58	0.481	3.067	0.00108
36	2.12	0.470	3.076	0.00105
45	2.64	0.462	3.082	0.00103
50	3.00	0.458	3.085	0.00102
60	3.53	0.453	3.089	0.00101

Table H-4. ϕ Values Evaluated for Gates < 1779 kN (EOD)

Span length (m)	Q_D/Q_L	Failure Probability p_f / Reliability Index β_T			
		2.50E-02	6.22E-03	1.22E-03	1.79E-04
		1.96	2.5	3.03	3.57
9	0.52	0.683	0.554	0.451	0.366
15	1.00	0.655	0.532	0.433	0.351
18	1.06	0.653	0.529	0.431	0.350
27	1.58	0.635	0.515	0.420	0.340
36	2.12	0.623	0.505	0.412	0.334
45	2.64	0.615	0.499	0.406	0.329
50	3.00	0.610	0.495	0.403	0.327
60	3.53	0.605	0.491	0.400	0.324

Table H-5. ASD Design Safety Factor for Gates < 1779 kN (EOD)

Span length (m)	Q_D/Q_L	Failure Probability p_f / Reliability Index β_T			
		2.50E-02	6.22E-03	1.22E-03	1.79E-04
		1.96	2.5	3.03	3.57
9	0.52	2.311	2.850	3.500	4.316
15	1.00	2.289	2.822	3.466	4.273
18	1.06	2.286	2.819	3.463	4.269
27	1.58	2.272	2.802	3.441	4.243
36	2.12	2.263	2.790	3.427	4.225
45	2.64	2.256	2.782	3.417	4.213
50	3.00	2.253	2.777	3.411	4.206
60	3.53	2.248	2.772	3.405	4.198

Table H-6. ϕ Factors for Safety Factor = 3.00 – Gates <1779 kN (EOD)

Span length (m)	Q_D/Q_L	ϕ	β_T	p_f
9	0.52	0.526	2.632	0.00425
15	1.00	0.500	2.658	0.00394
18	1.06	0.498	2.660	0.00391
27	1.58	0.481	2.676	0.00373
36	2.12	0.470	2.687	0.00361
45	2.64	0.462	2.695	0.00352
50	3.00	0.458	2.699	0.00348
60	3.53	0.453	2.704	0.00343

Table H-7. ϕ Values Evaluated for Gates > 1779 kN (EOD)

Span length (m)	Q_D/Q_L	Failure Probability p_f / Reliability Index β_T			
		2.50E-02	6.22E-03	1.22E-03	1.79E-04
		1.96	2.5	3.03	3.57
9	0.52	1.464	1.192	0.974	0.793
15	1.00	1.404	1.144	0.935	0.761
18	1.06	1.399	1.139	0.931	0.758
27	1.58	1.361	1.109	0.906	0.738
36	2.12	1.335	1.087	0.889	0.724
45	2.64	1.318	1.073	0.877	0.714
50	3.00	1.308	1.065	0.871	0.709
60	3.53	1.296	1.056	0.863	0.703

Table H-8. ASD Design Safety Factor for Gates > 1779 kN (EOD)

Span length (m)	Q_D/Q_L	Failure Probability p_f / Reliability Index β_T			
		2.50E-02	6.22E-03	1.22E-03	1.79E-04
		1.96	2.5	3.03	3.57
9	0.52	1.079	1.325	1.620	1.990
15	1.00	1.068	1.312	1.605	1.970
18	1.06	1.067	1.310	1.603	1.969
27	1.58	1.061	1.302	1.593	1.956
36	2.12	1.056	1.297	1.586	1.948
45	2.64	1.053	1.293	1.582	1.943
50	3.00	1.051	1.291	1.579	1.939
60	3.53	1.049	1.289	1.576	1.936

Table H-9. ϕ Factors for Safety Factor = 3.00 – Gates >1779 kN (EOD)

Span length (m)	Q_D/Q_L	ϕ	β_T	p_f
9	0.52	0.526	4.649	0.00000167
15	1.00	0.500	4.675	0.00000147
18	1.06	0.498	4.678	0.00000145
27	1.58	0.481	4.694	0.00000134
36	2.12	0.470	4.705	0.00000127
45	2.64	0.462	4.713	0.00000122
50	3.00	0.458	4.717	0.00000120
60	3.53	0.453	4.722	0.00000117

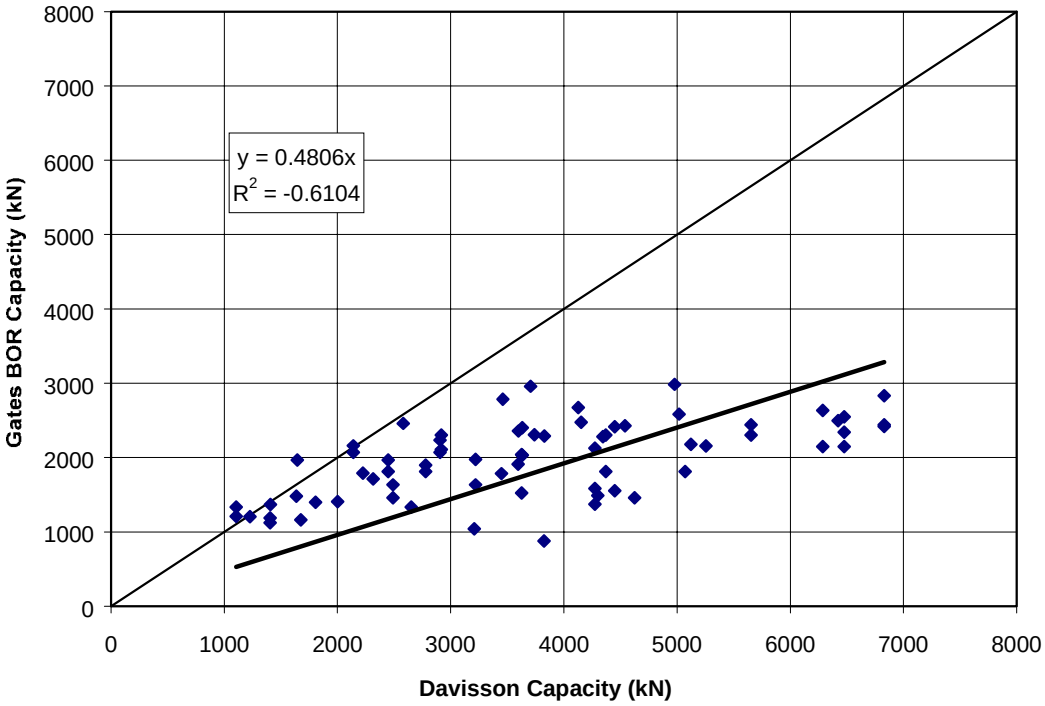

Figure H-3. Davisson Capacity vs. Gates BOR Capacity

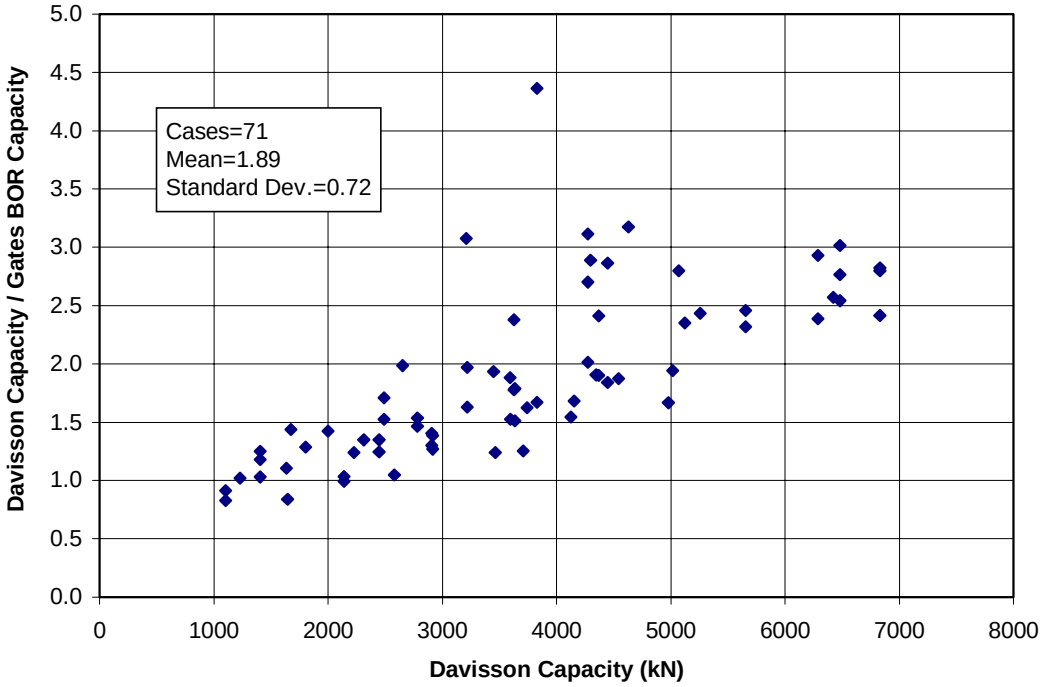

Figure H-4. Measured Over Predicted Capacity for Gates Method at BOR

Table H-10. ϕ Values Evaluated for Gates – Overall (BOR)

Span length (m)	Q_D/Q_L	Failure Probability p_f / Reliability Index β_T			
		2.50E-02	6.22E-03	1.22E-03	1.79E-04
		1.96	2.50	3.03	3.57
9	0.52	1.097	0.871	0.694	0.551
15	1.00	1.052	0.835	0.666	0.529
18	1.06	1.048	0.832	0.664	0.527
27	1.58	1.020	0.810	0.646	0.513
36	2.12	1.000	0.794	0.633	0.503
45	2.64	0.987	0.784	0.625	0.496
50	3.00	0.980	0.778	0.620	0.493
60	3.53	0.971	0.771	0.615	0.488

Table H-11. ASD Design Safety Factor for Gates – Overall (BOR)

Span length (m)	Q_D/Q_L	Failure Probability p_f / Reliability Index β_T			
		2.50E-02	6.22E-03	1.22E-03	1.79E-04
		1.96	2.50	3.03	3.57
9	0.52	1.440	1.813	2.274	2.864
15	1.00	1.426	1.796	2.252	2.836
18	1.06	1.424	1.794	2.250	2.833
27	1.58	1.416	1.783	2.236	2.816
36	2.12	1.410	1.775	2.226	2.804
45	2.64	1.406	1.770	2.220	2.796
50	3.00	1.403	1.767	2.216	2.791
60	3.53	1.401	1.764	2.212	2.786

Table H-12. ϕ Factors for Safety Factor = 3.00 – Gates – Overall (BOR)

Span length (m)	Q_D/Q_L	ϕ	β	p_f
9	0.52	0.526	3.679	0.0001173
15	1.00	0.500	3.702	0.0001072
18	1.06	0.498	3.704	0.0001063
27	1.58	0.481	3.718	0.0001006
36	2.12	0.470	3.728	0.0000967
45	2.64	0.462	3.735	0.0000940
50	3.00	0.458	3.739	0.0000926
60	3.53	0.453	3.743	0.0000911

Table H-13. ϕ Values Evaluated for Gates < 1779 kN (BOR)

Span length (m)	Q_D/Q_L	Failure Probability p_f / Reliability Index β_T			
		2.50E-02	6.22E-03	1.22E-03	1.79E-04
		1.96	2.50	3.03	3.57
9	0.52	0.855	0.732	0.628	0.538
15	1.00	0.821	0.702	0.603	0.516
18	1.06	0.817	0.700	0.600	0.514
27	1.58	0.796	0.681	0.584	0.500
36	2.12	0.780	0.668	0.573	0.491
45	2.64	0.770	0.659	0.566	0.484
50	3.00	0.764	0.654	0.561	0.480
60	3.53	0.758	0.648	0.556	0.476

Table H-14. ASD Design Safety Factor for Gates < 1779 kN (BOR)

Span length (m)	Q_D/Q_L	Failure Probability p_f / Reliability Index β_T			
		2.50E-02	6.22E-03	1.22E-03	1.79E-04
		1.96	2.50	3.03	3.57
9	0.52	1.846	2.157	2.513	2.936
15	1.00	1.828	2.136	2.488	2.908
18	1.06	1.826	2.134	2.486	2.905
27	1.58	1.815	2.121	2.471	2.887
36	2.12	1.807	2.112	2.460	2.875
45	2.64	1.802	2.105	2.453	2.866
50	3.00	1.799	2.102	2.449	2.862
60	3.53	1.796	2.098	2.445	2.857

Table H-15. ϕ Factors for Safety Factor = 3.00 – Gates <1779 kN (BOR)

Span length (m)	Q_D/Q_L	ϕ	β	p_f
9	0.52	0.526	3.644	0.0001345
15	1.00	0.500	3.679	0.0001173
18	1.06	0.498	3.682	0.0001159
27	1.58	0.481	3.703	0.0001067
36	2.12	0.470	3.718	0.0001006
45	2.64	0.462	3.728	0.0000967
50	3.00	0.458	3.733	0.0000948
60	3.53	0.453	3.740	0.0000922

Table H-16. ϕ Values Evaluated for Gates > 1779 kN (BOR)

Span length (m)	Q_D/Q_L	Failure Probability p_f / Reliability Index β_T			
		2.50E-02	6.22E-03	1.22E-03	1.79E-04
		1.96	2.50	3.03	3.57
9	0.52	1.250	1.008	0.817	0.659
15	1.00	1.199	0.967	0.783	0.632
18	1.06	1.194	0.963	0.780	0.629
27	1.58	1.162	0.938	0.759	0.613
36	2.12	1.140	0.920	0.745	0.601
45	2.64	1.125	0.907	0.735	0.593
50	3.00	1.117	0.901	0.730	0.589
60	3.53	1.107	0.893	0.723	0.583

Table H-17. ASD Design Safety Factor for Gates > 1779 kN (BOR)

Span length (m)	Q_D/Q_L	Failure Probability p_f / Reliability Index β_T			
		2.50E-02	6.22E-03	1.22E-03	1.79E-04
		1.96	2.50	3.03	3.57
9	0.52	1.263	1.566	1.934	2.397
15	1.00	1.251	1.551	1.915	2.374
18	1.06	1.250	1.549	1.913	2.371
27	1.58	1.242	1.540	1.901	2.357
36	2.12	1.237	1.533	1.893	2.347
45	2.64	1.233	1.529	1.888	2.340
50	3.00	1.231	1.526	1.885	2.336
60	3.53	1.229	1.524	1.881	2.332

Table H-18. ϕ Factors for Safety Factor = 3.00 – Gates >1779 kN (BOR)

Span length (m)	Q_D/Q_L	ϕ	β	p_f
9	0.52	0.526	4.134	0.0000179
15	1.00	0.500	4.159	0.0000160
18	1.06	0.498	4.161	0.0000159
27	1.58	0.481	4.177	0.0000148
36	2.12	0.470	4.187	0.0000142
45	2.64	0.462	4.195	0.0000137
50	3.00	0.458	4.199	0.0000134
60	3.53	0.453	4.203	0.0000132

APPENDIX I

FORCE AND VELOCITY TRACES FROM PDA SIGNAL

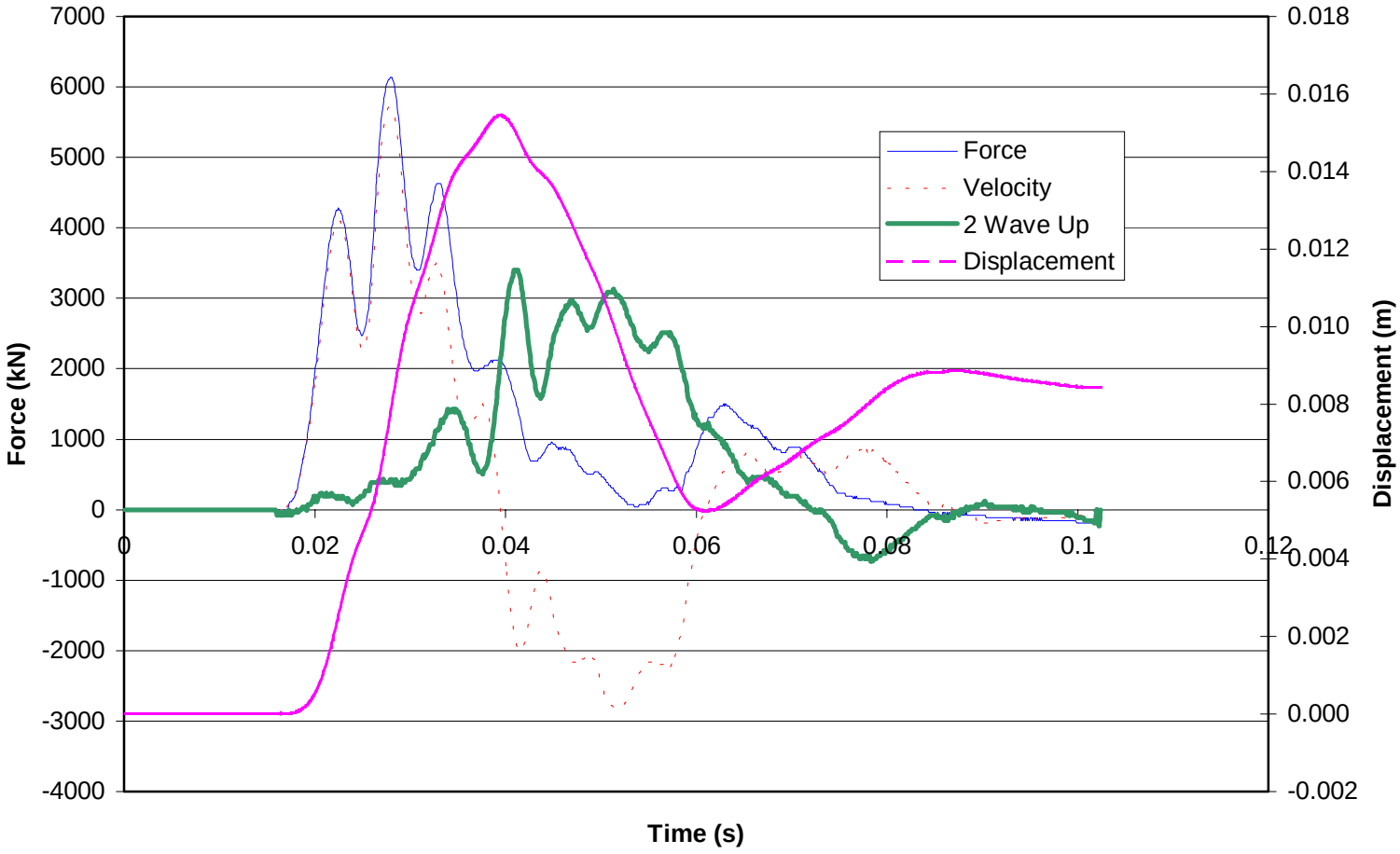

Figure I-1. Force, Velocity, Double Wave Up, and Displacement Traces for TS4I (Pascagoula Bridge)

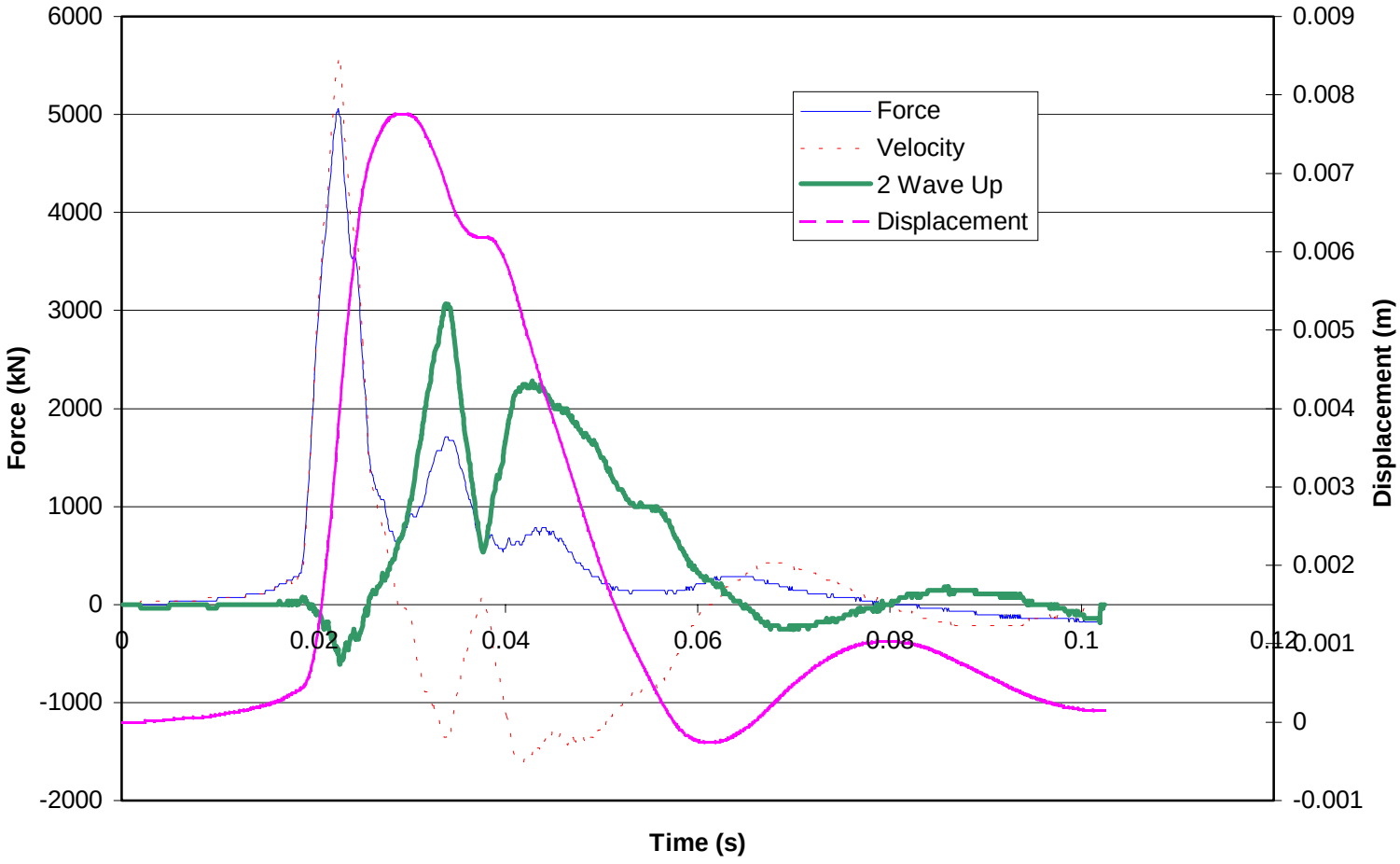

Figure I-2. Force, Velocity, Double Wave Up, and Displacement Traces for TS1B102 (Vilano Bridge)

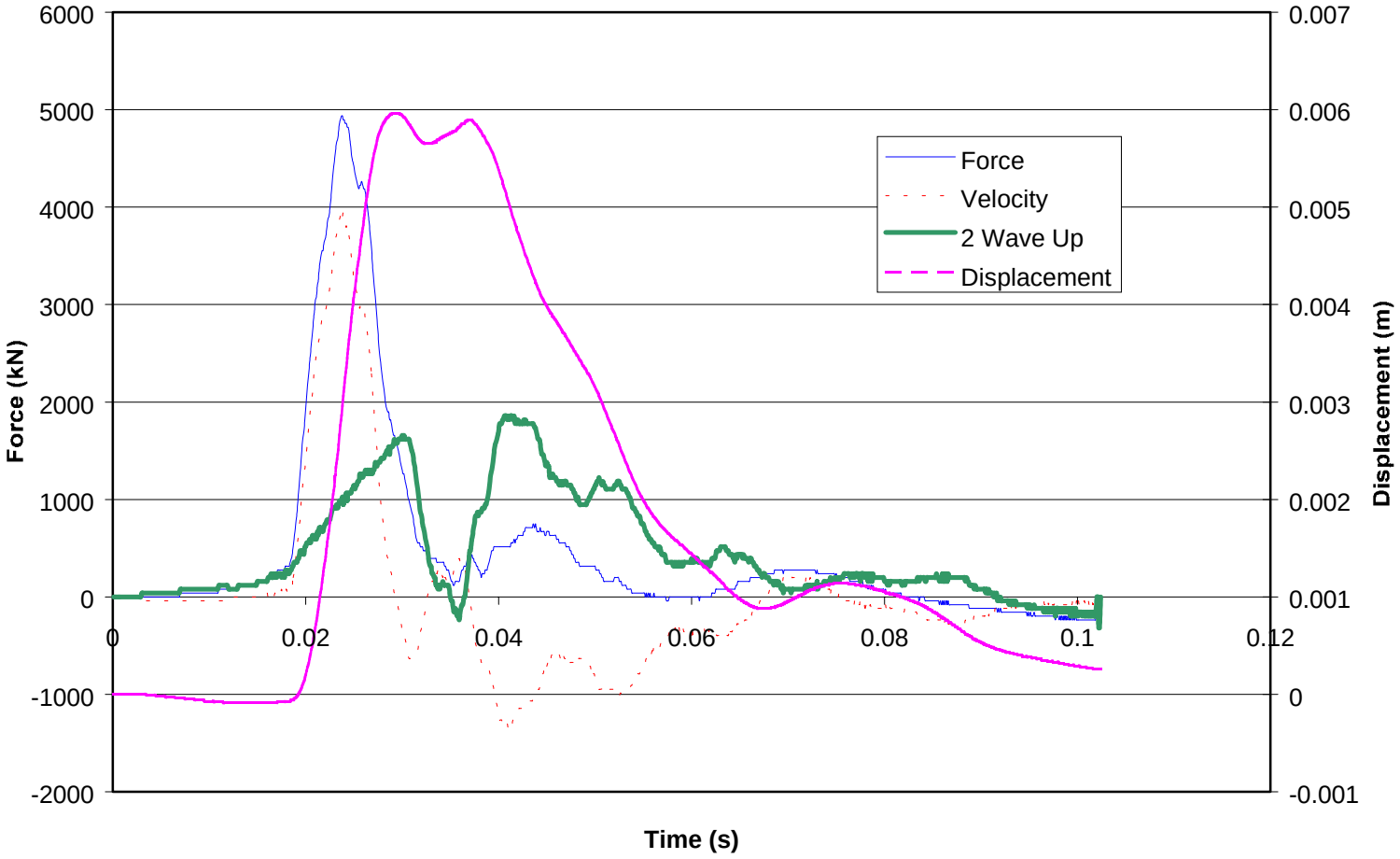

Figure I-3. Force, Velocity, Double Wave Up, and Displacement Traces for B5RS2 (Escambria Bridge)

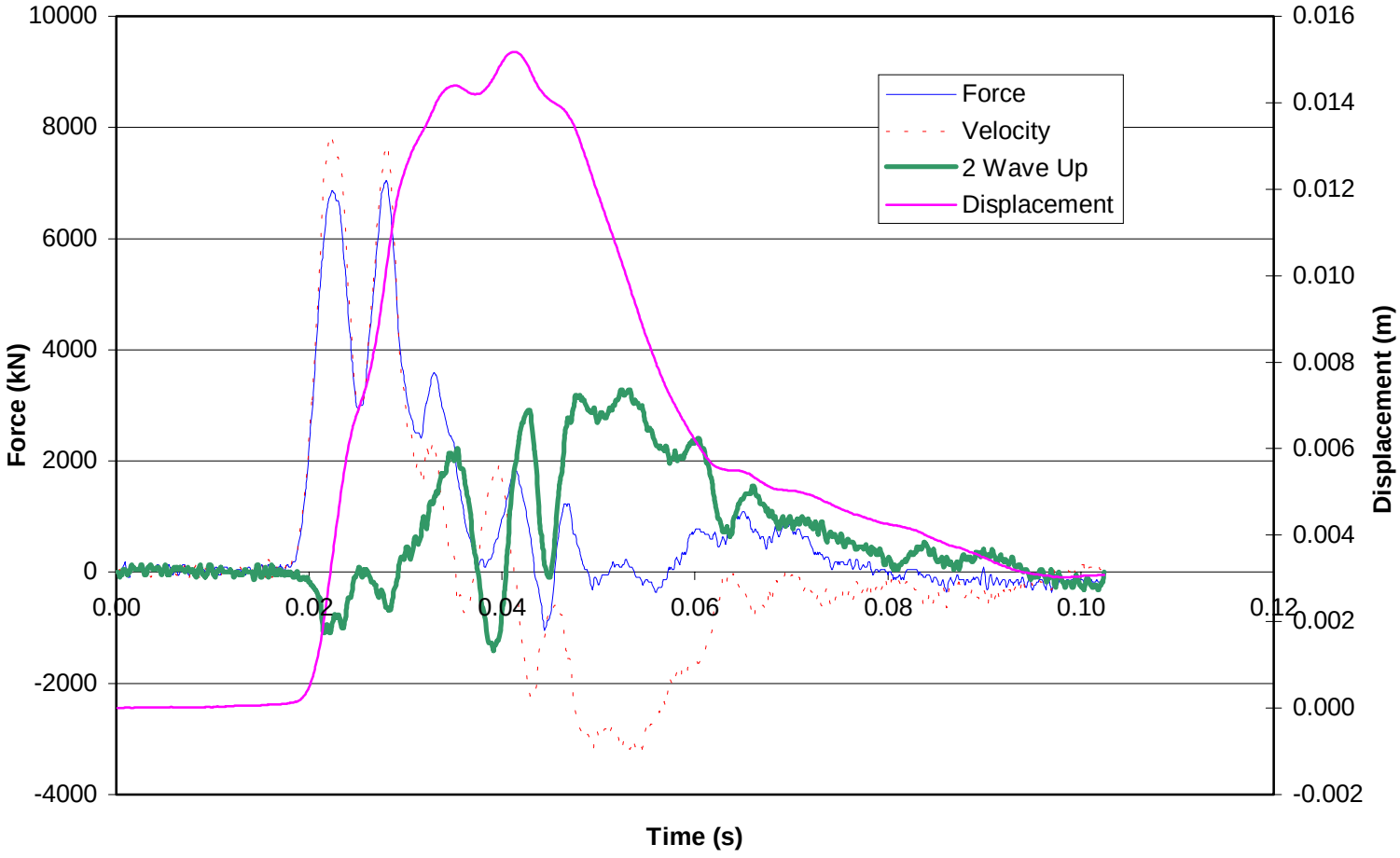

Figure I-4. Force, Velocity, Double Wave Up, and Displacement Traces for TS13A1-A (Buckman Bridge)

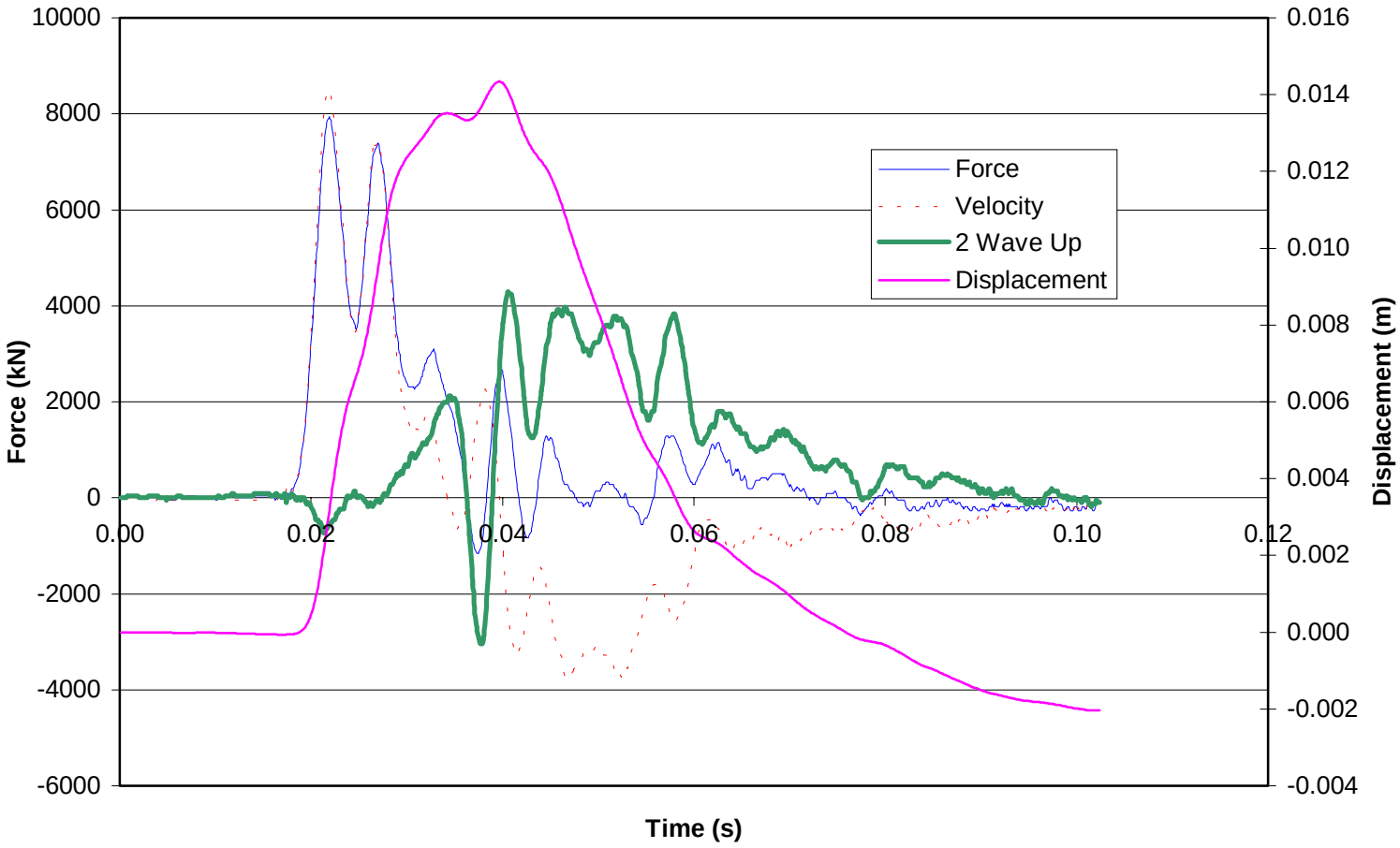

Figure I-5. Force, Velocity, Double Wave Up, and Displacement Traces for TS19FRCB (Buckman Bridge)

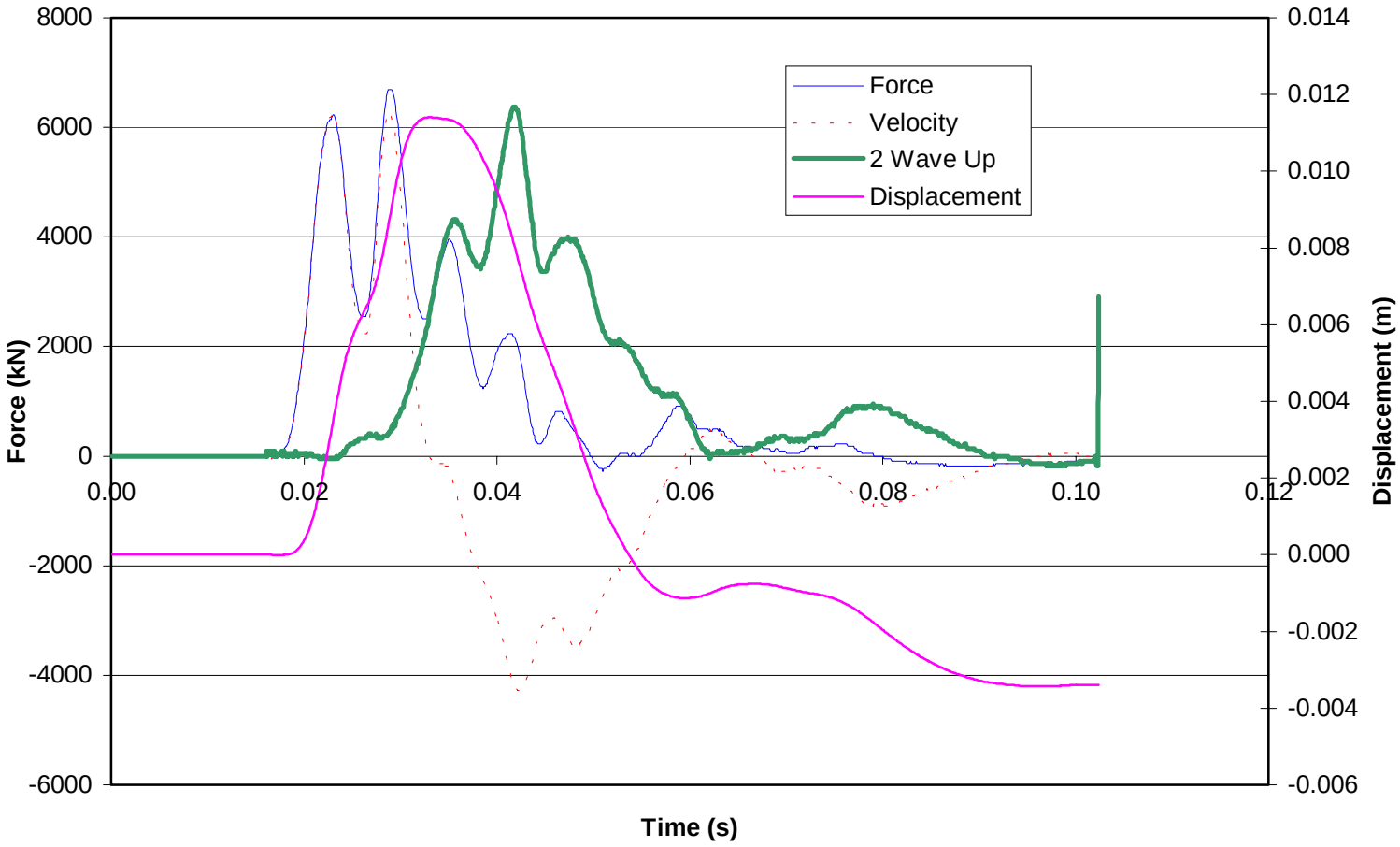

Figure I-6. Force, Velocity, Double Wave Up, and Displacement Traces for TS24ALTA (Buckman Bridge)

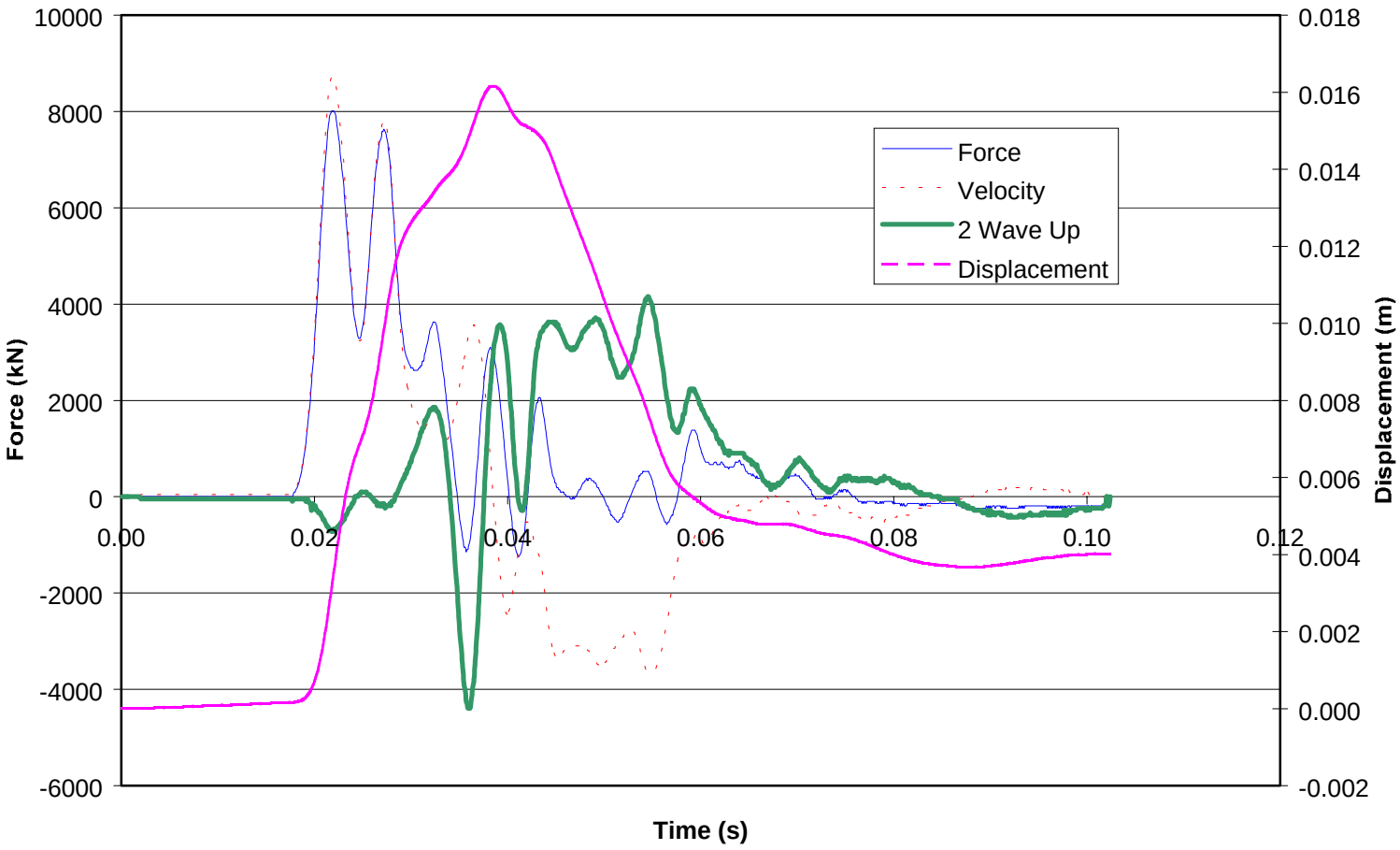

Figure I-7. Force, Velocity, Double Wave Up, and Displacement Traces for TS29RC (Buckman Bridge)

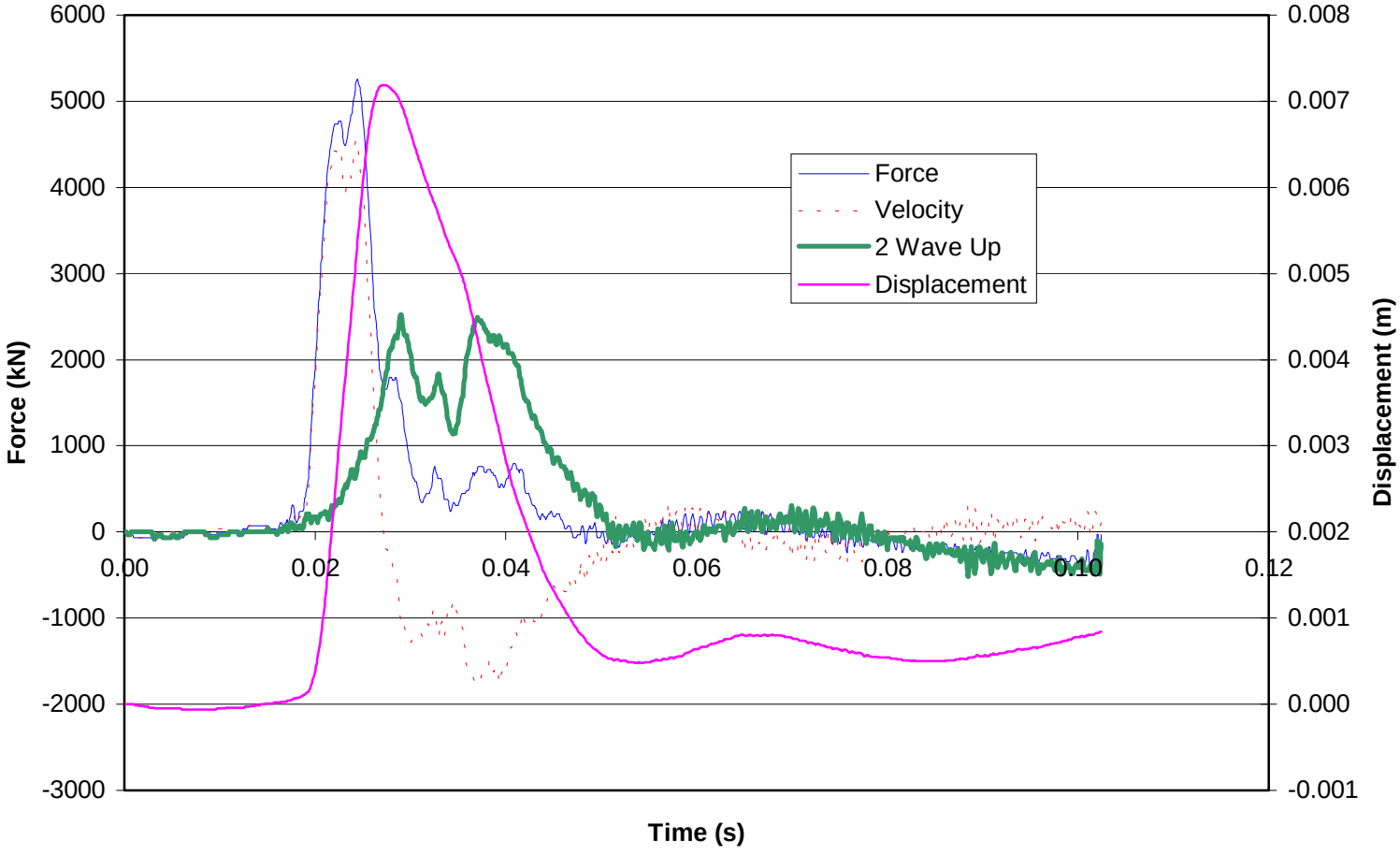

Figure I-8. Force, Velocity, Double Wave Up, and Displacement Traces for F6-58A (Acosta Bridge)

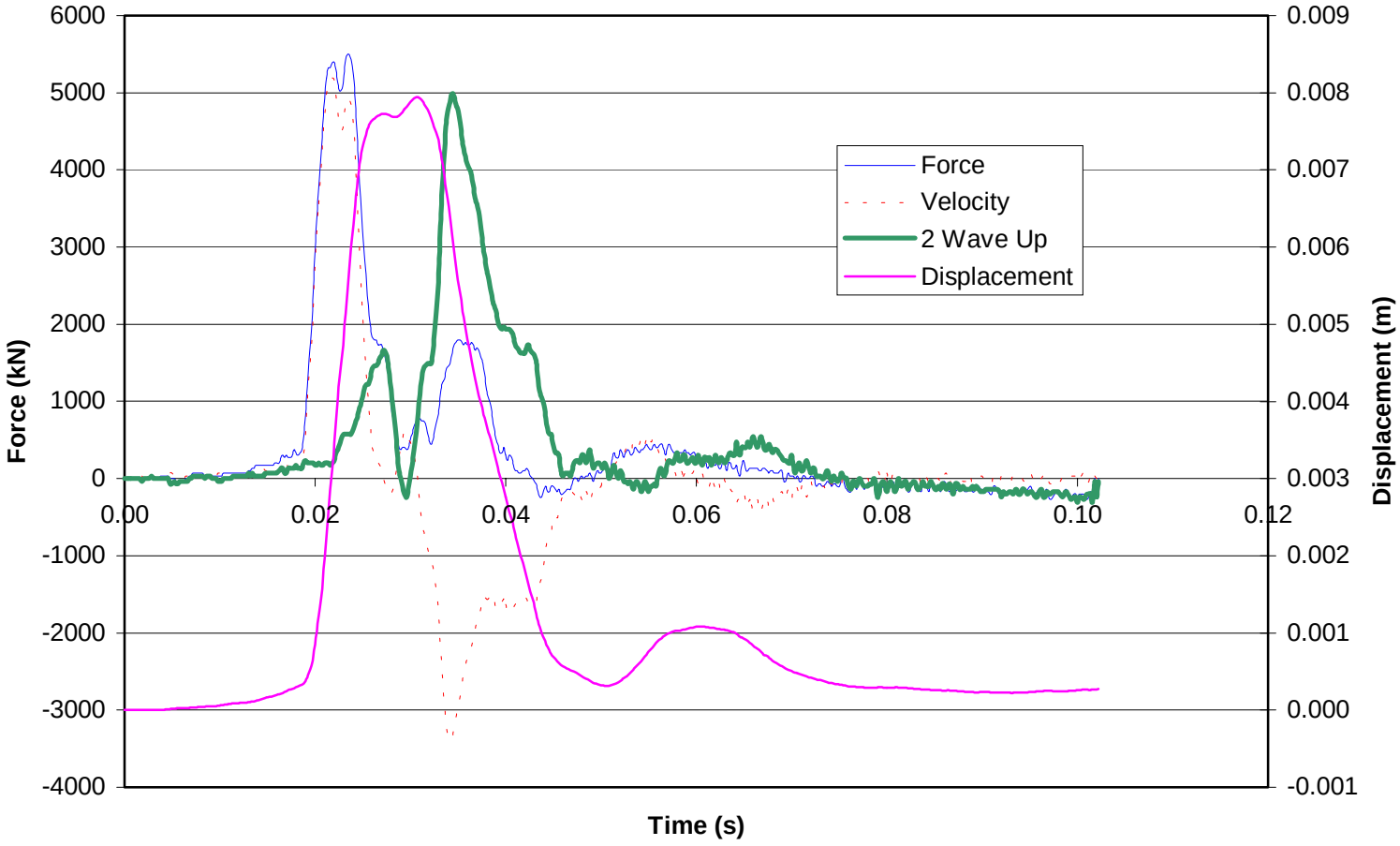

Figure I-9. Force, Velocity, Double Wave Up, and Displacement Traces for G13-37 (Acosta Bridge)

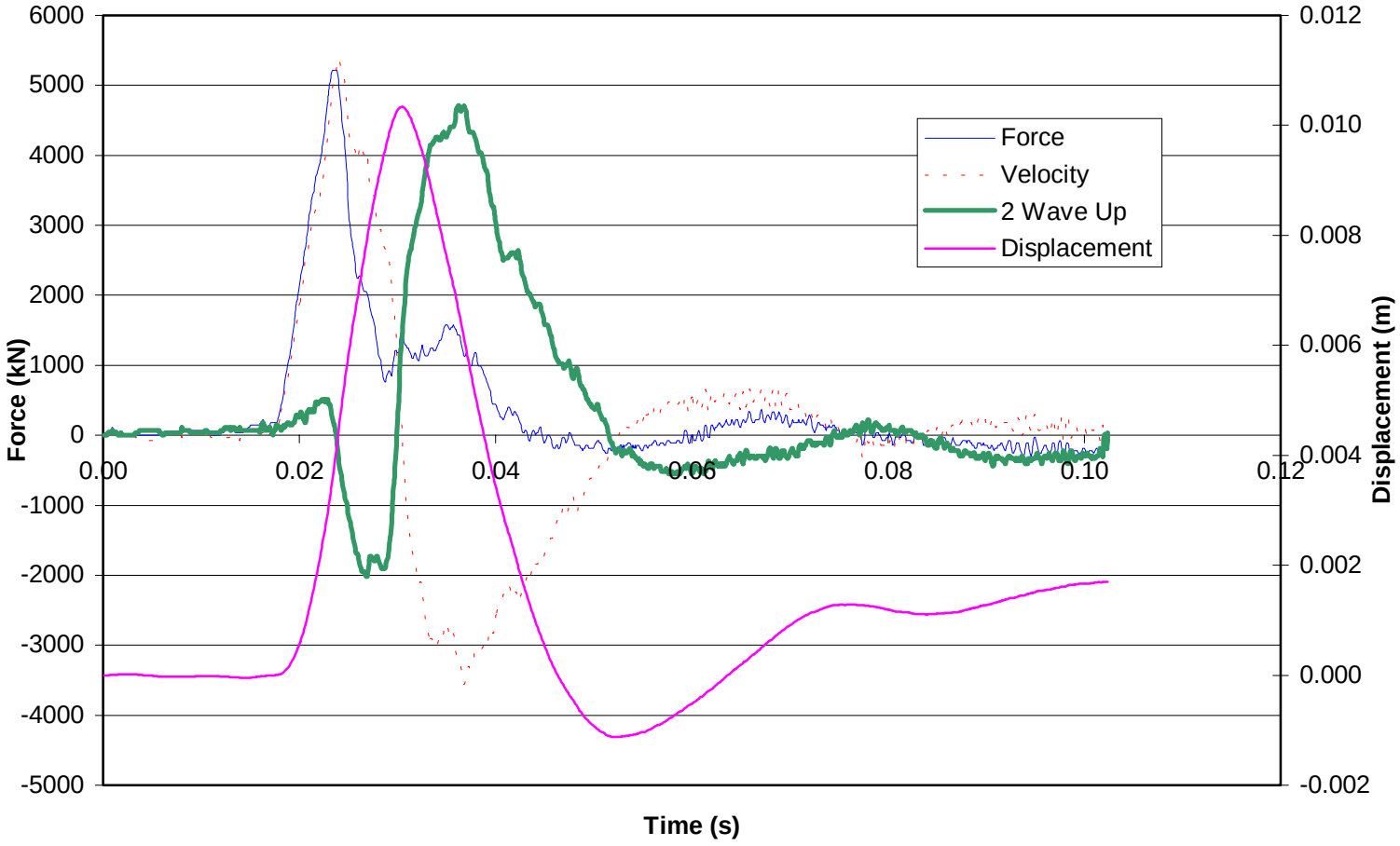

Figure I-10. Force, Velocity, Double Wave Up, and Displacement Traces for H2-27B (Acosta Bridge)

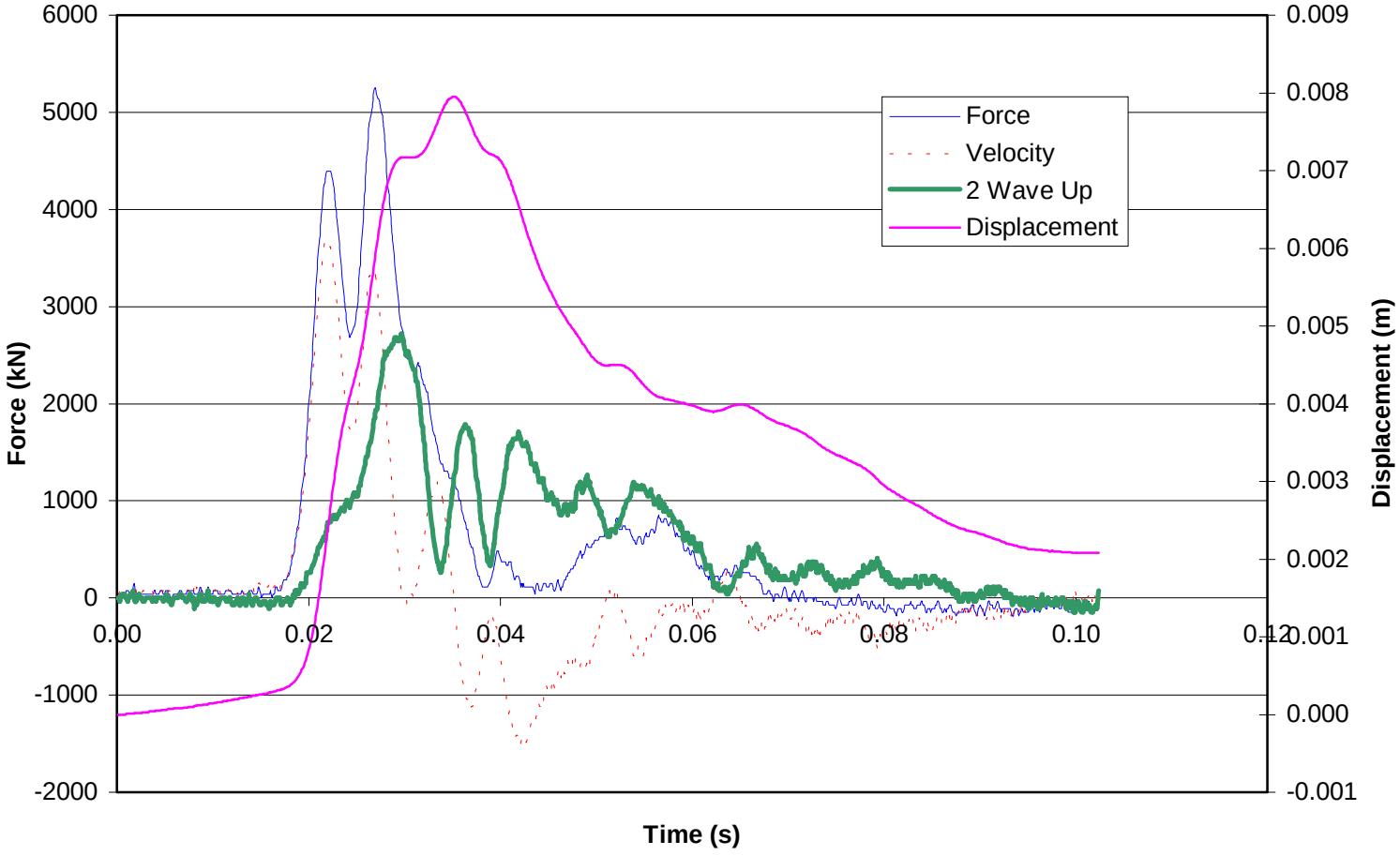

Figure I-11. Force, Velocity, Double Wave Up, and Displacement Traces for B1-76F (Choctawhatche Bridge)

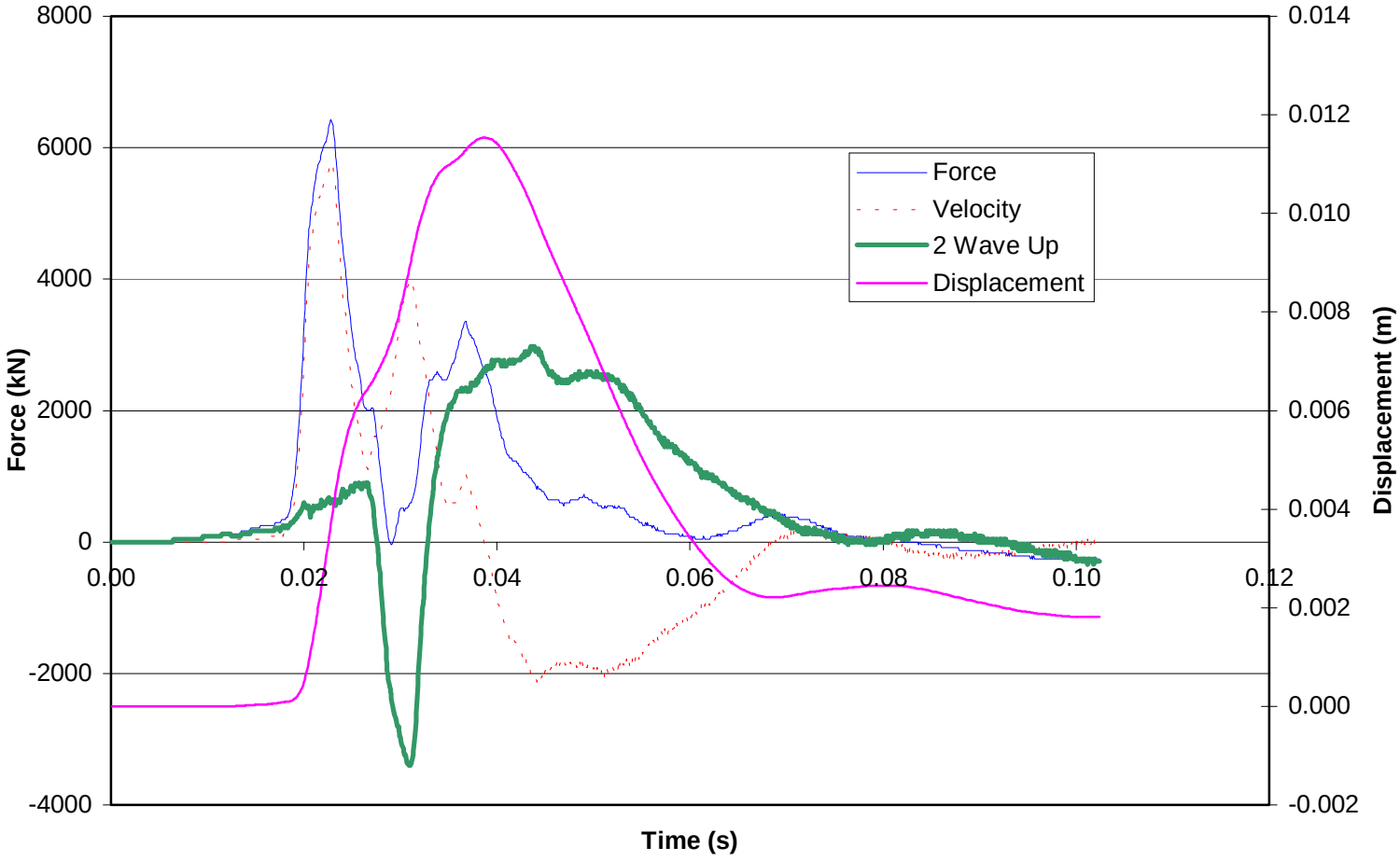

Figure I-12. Force, Velocity, Double Wave Up, and Displacement Traces for PR5R2 (Choctawhatche Bridge)

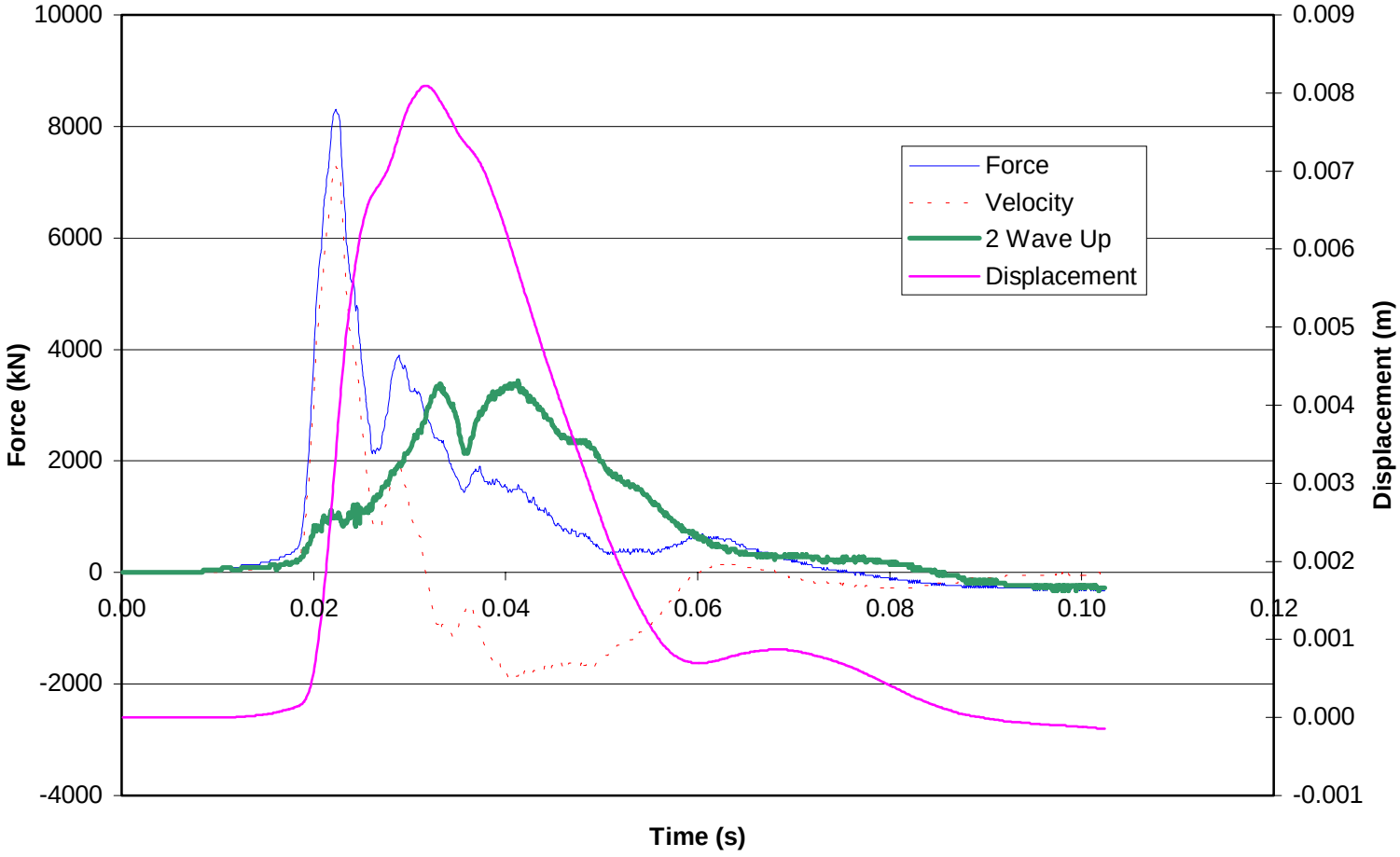

Figure I-13. Force, Velocity, Double Wave Up, and Displacement Traces for B8-97R2 (Choctawhatche Bridge)

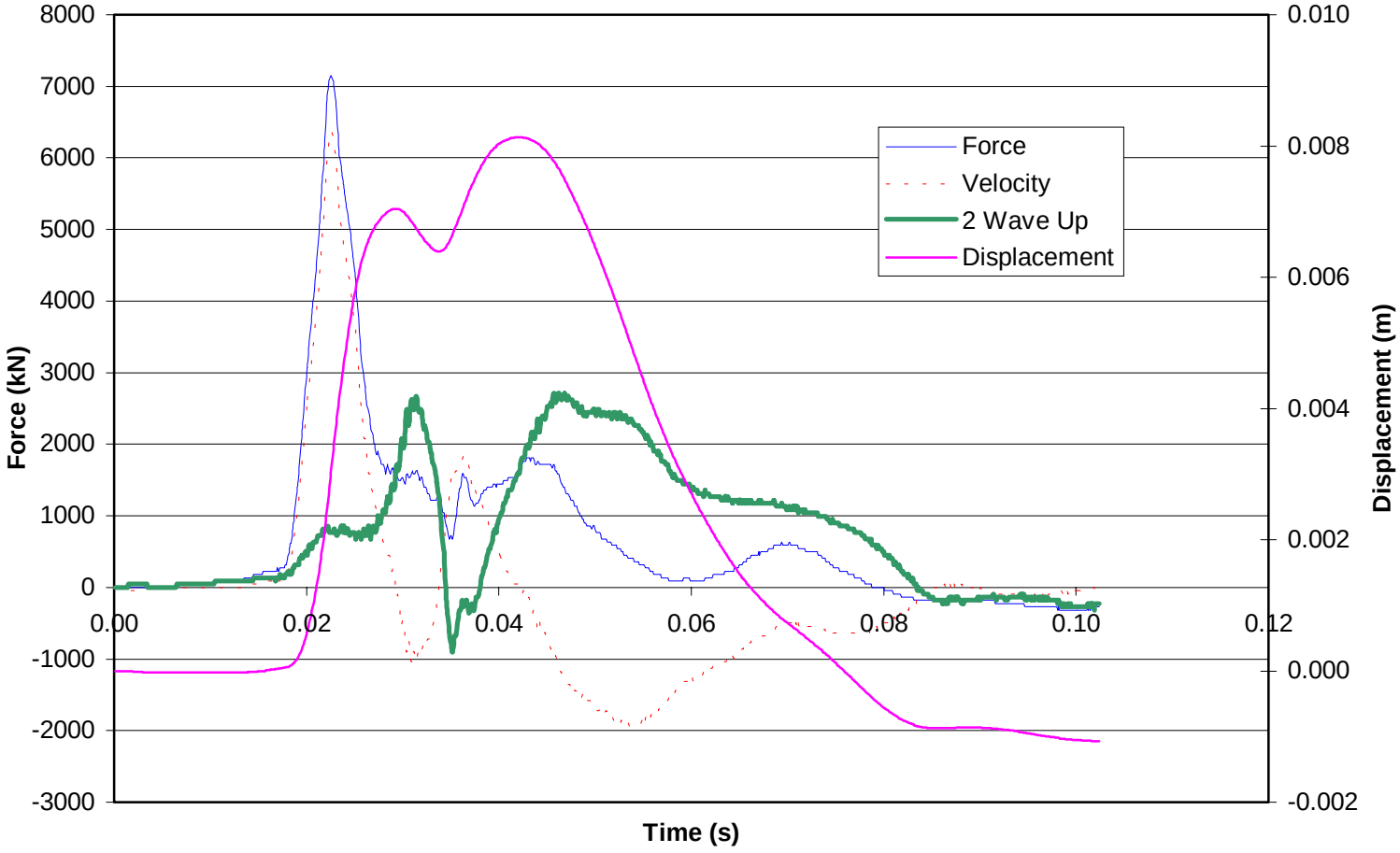

Figure I-14. Force, Velocity, Double Wave Up, and Displacement Traces for B14-89R2 (Choctawhatche Bridge)

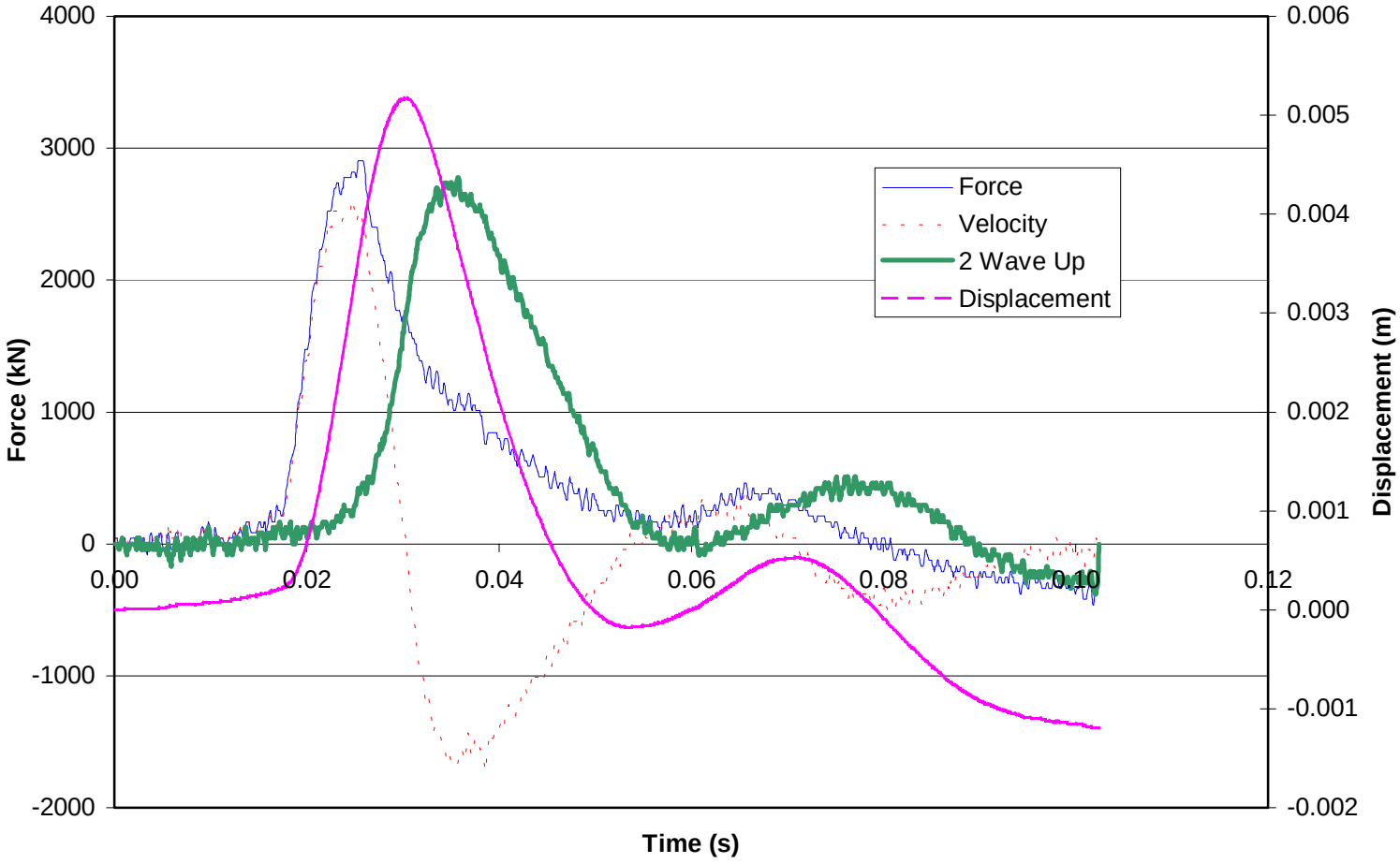

Figure I-15. Force, Velocity, Double Wave Up, and Displacement Traces for B17-94R2 (Choctawhatche Bridge)

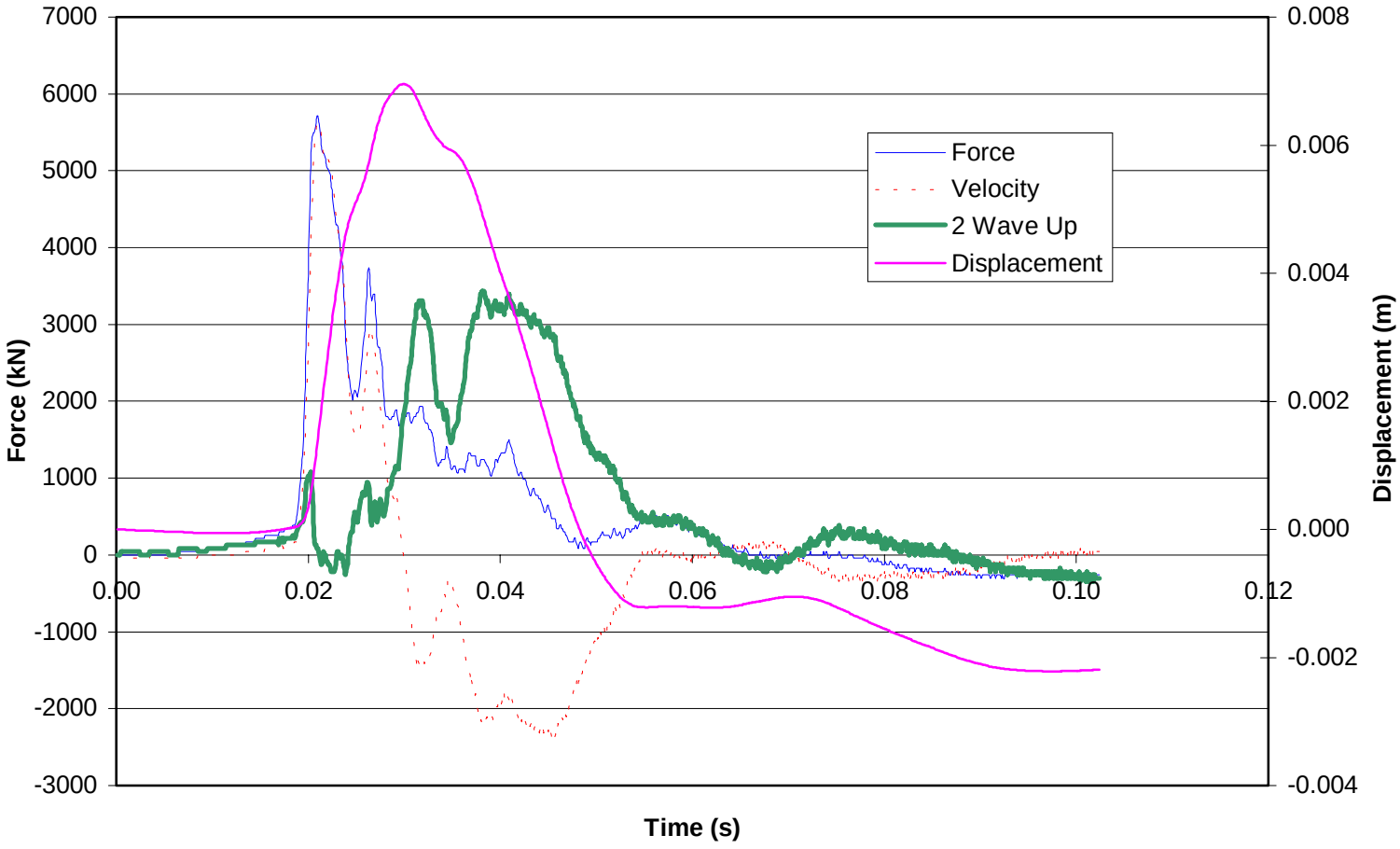

Figure I-16. Force, Velocity, Double Wave Up, and Displacement Traces for PR35FIN (Choctawhatche Bridge)

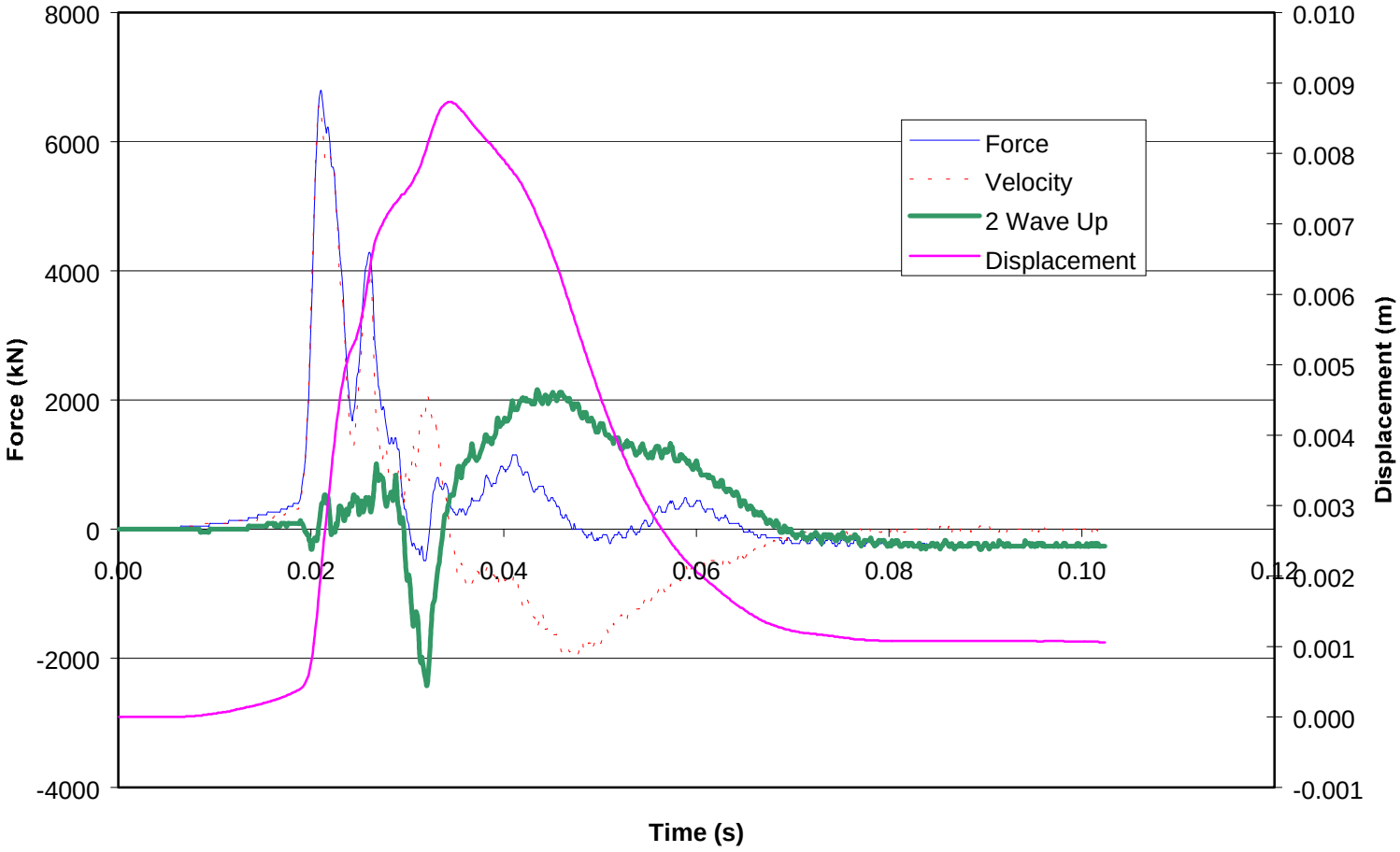

Figure I-17. Force, Velocity, Double Wave Up, and Displacement Traces for B23-76F2 (Choctawhatche Bridge)

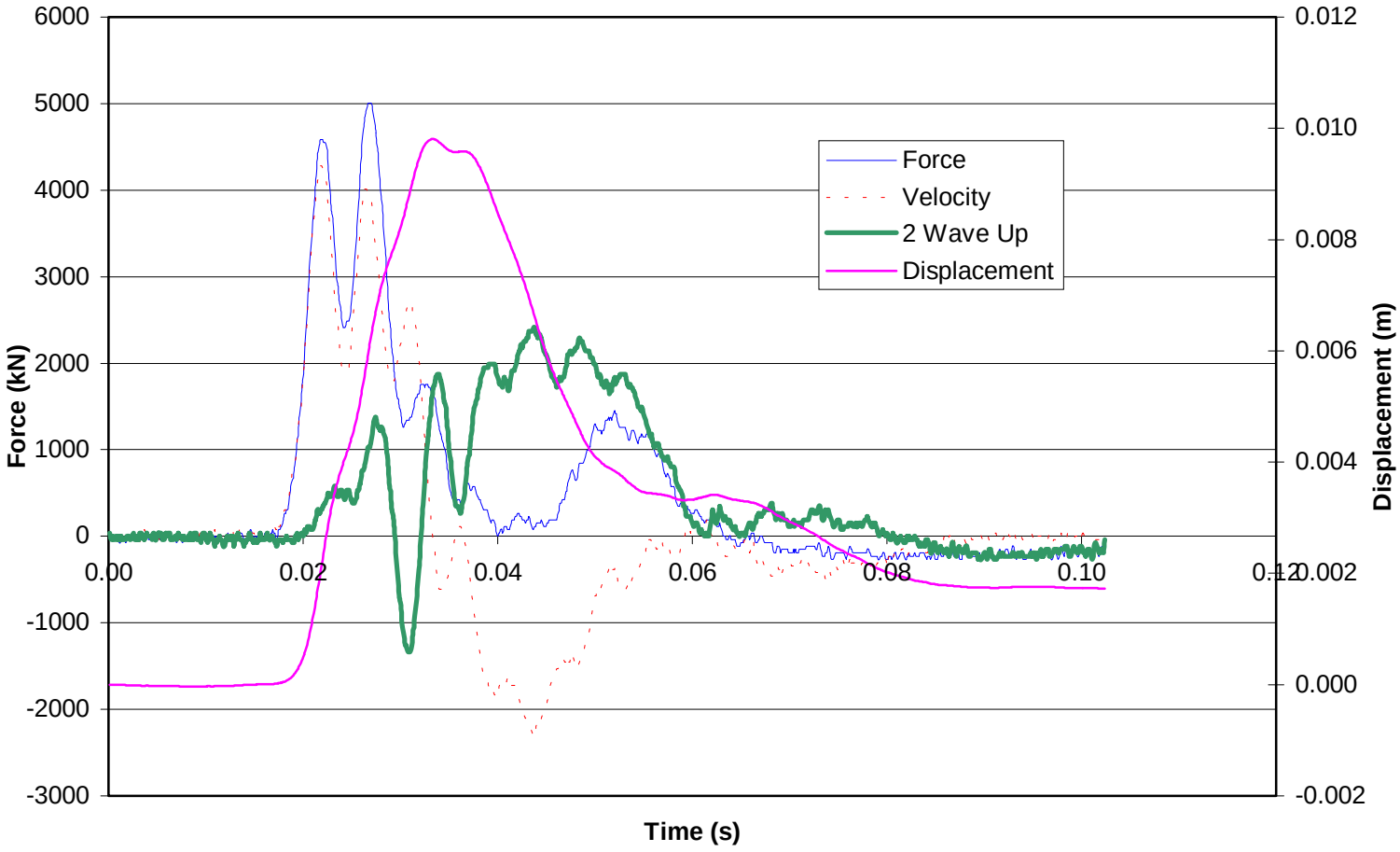

Figure I-18. Force, Velocity, Double Wave Up, and Displacement Traces for B27-63F (Choctawhatche Bridge)

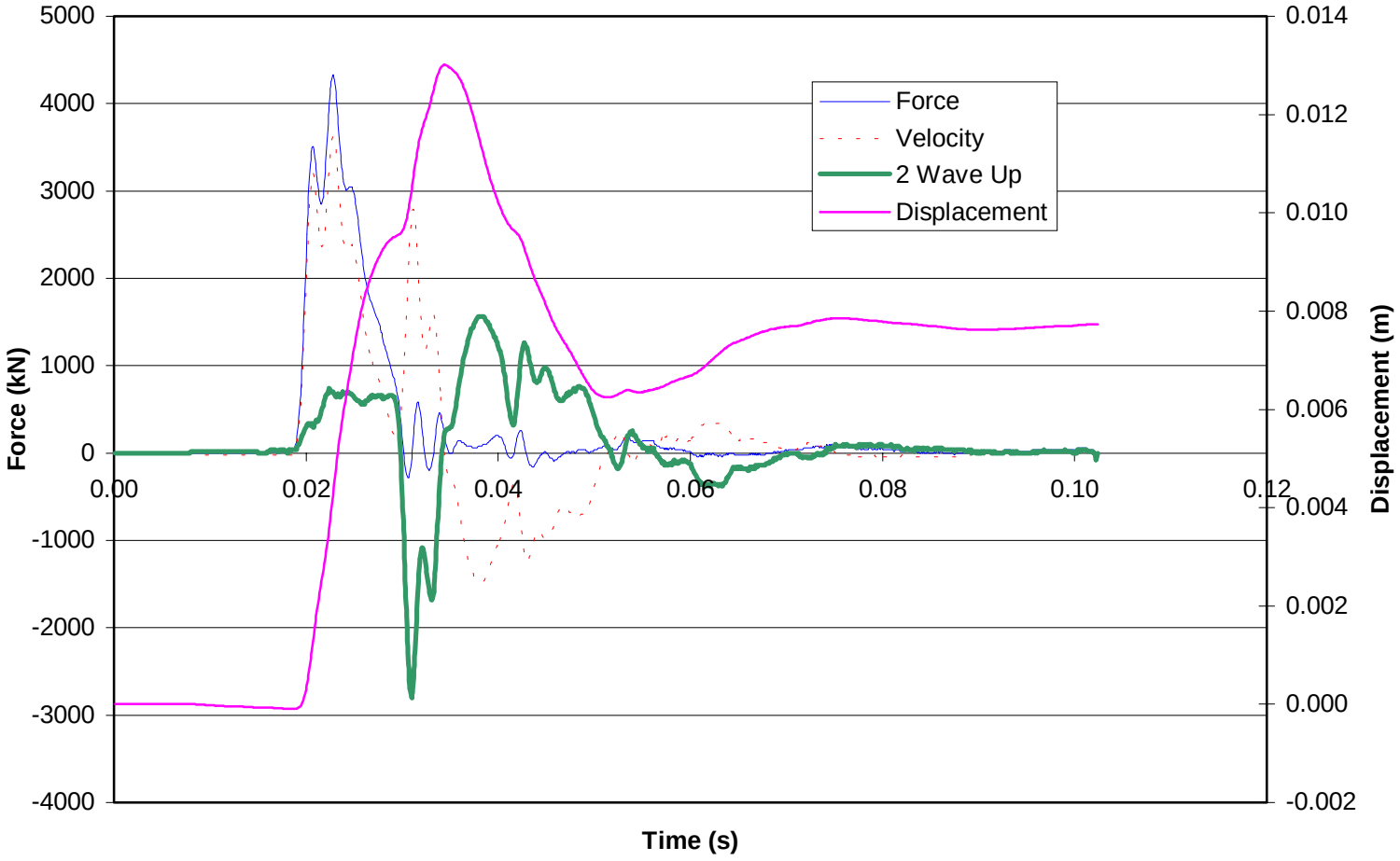

Figure I-19. Force, Velocity, Double Wave Up, and Displacement Traces for AUC63K (Aucilla Bridge)

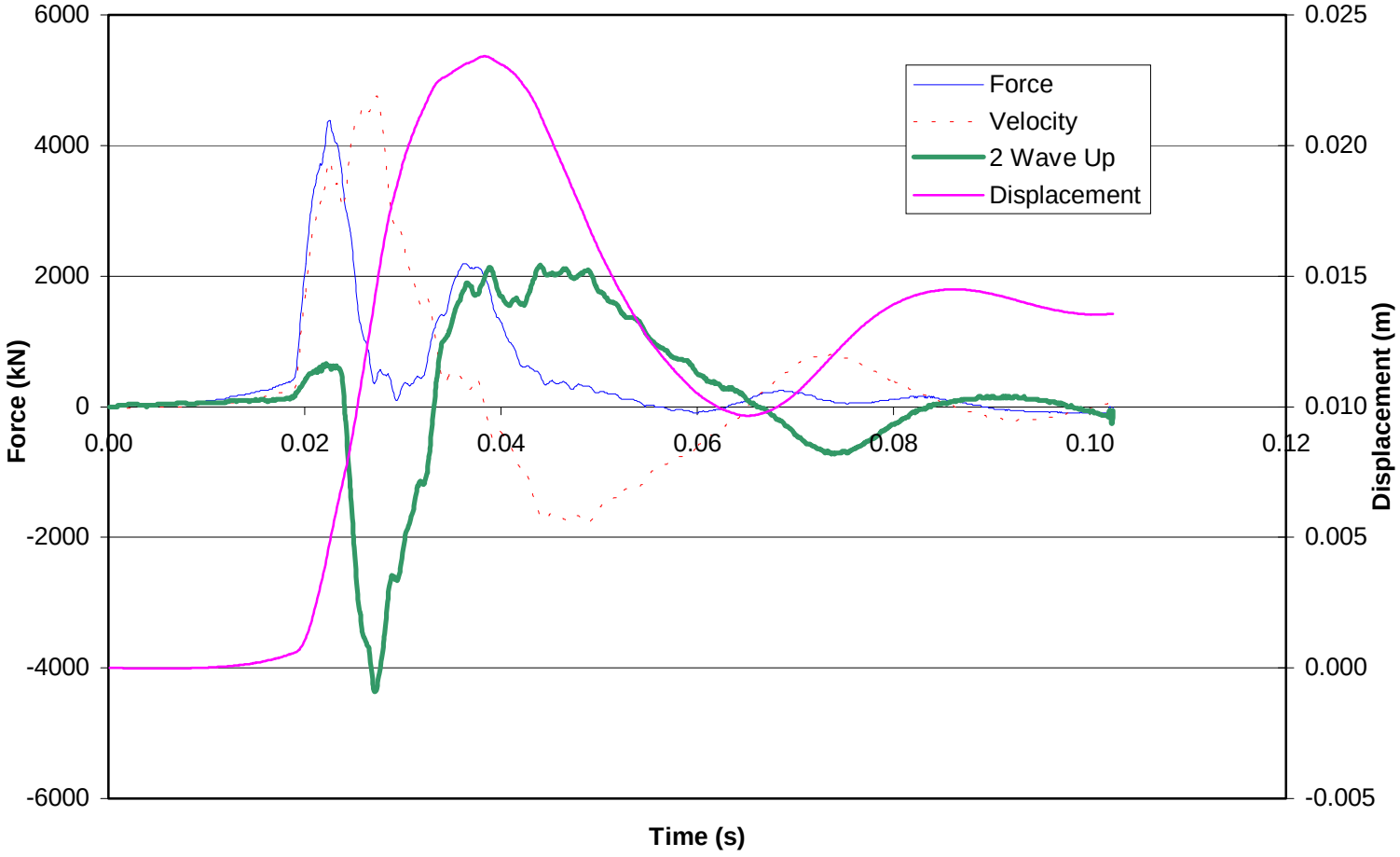

Figure I-20. Force, Velocity, Double Wave Up, and Displacement Traces for BKM30J (Buckman Bridge)

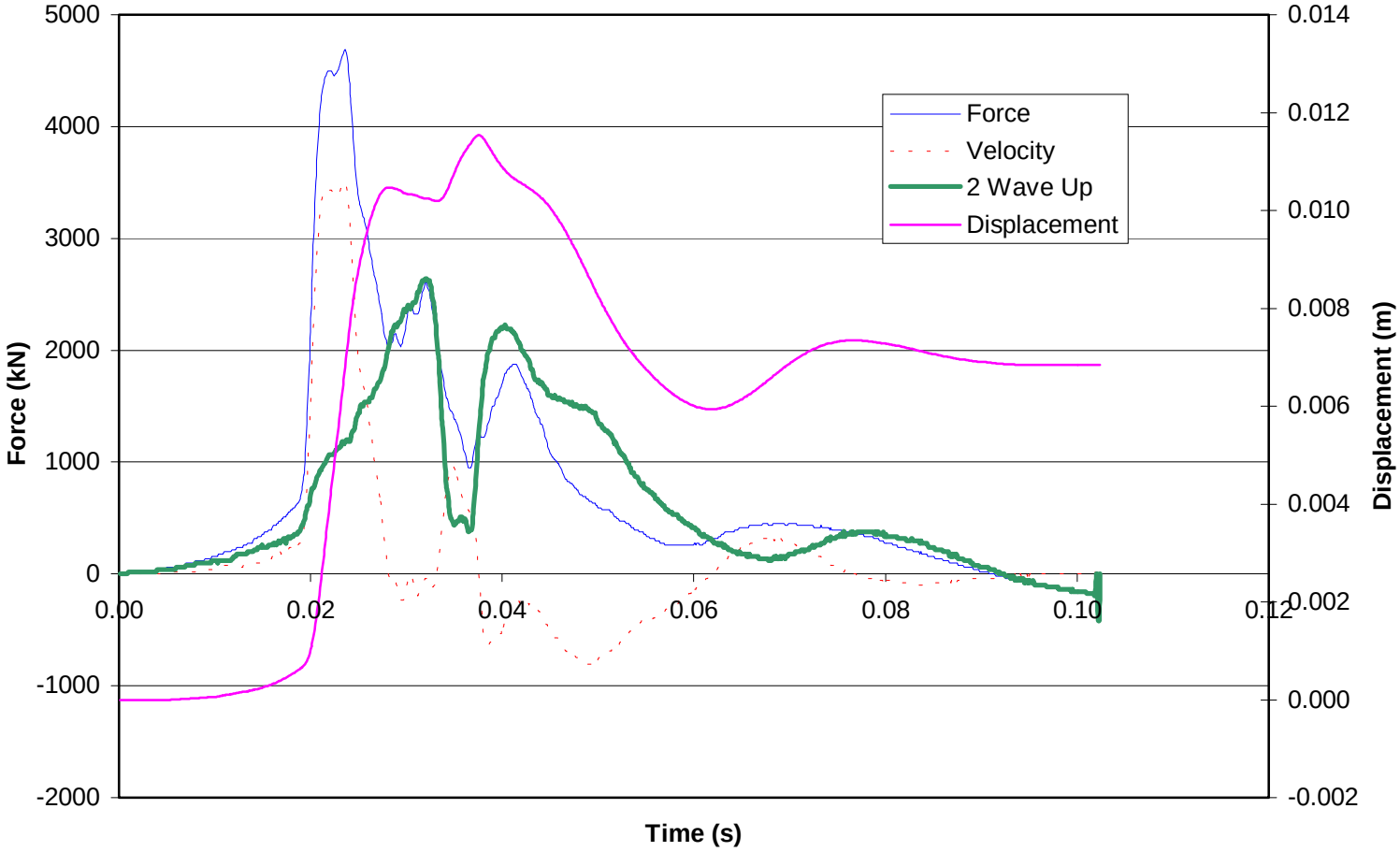

Figure I-21. Force, Velocity, Double Wave Up, and Displacement Traces for SBZ83N (Seabreeze Bridge)

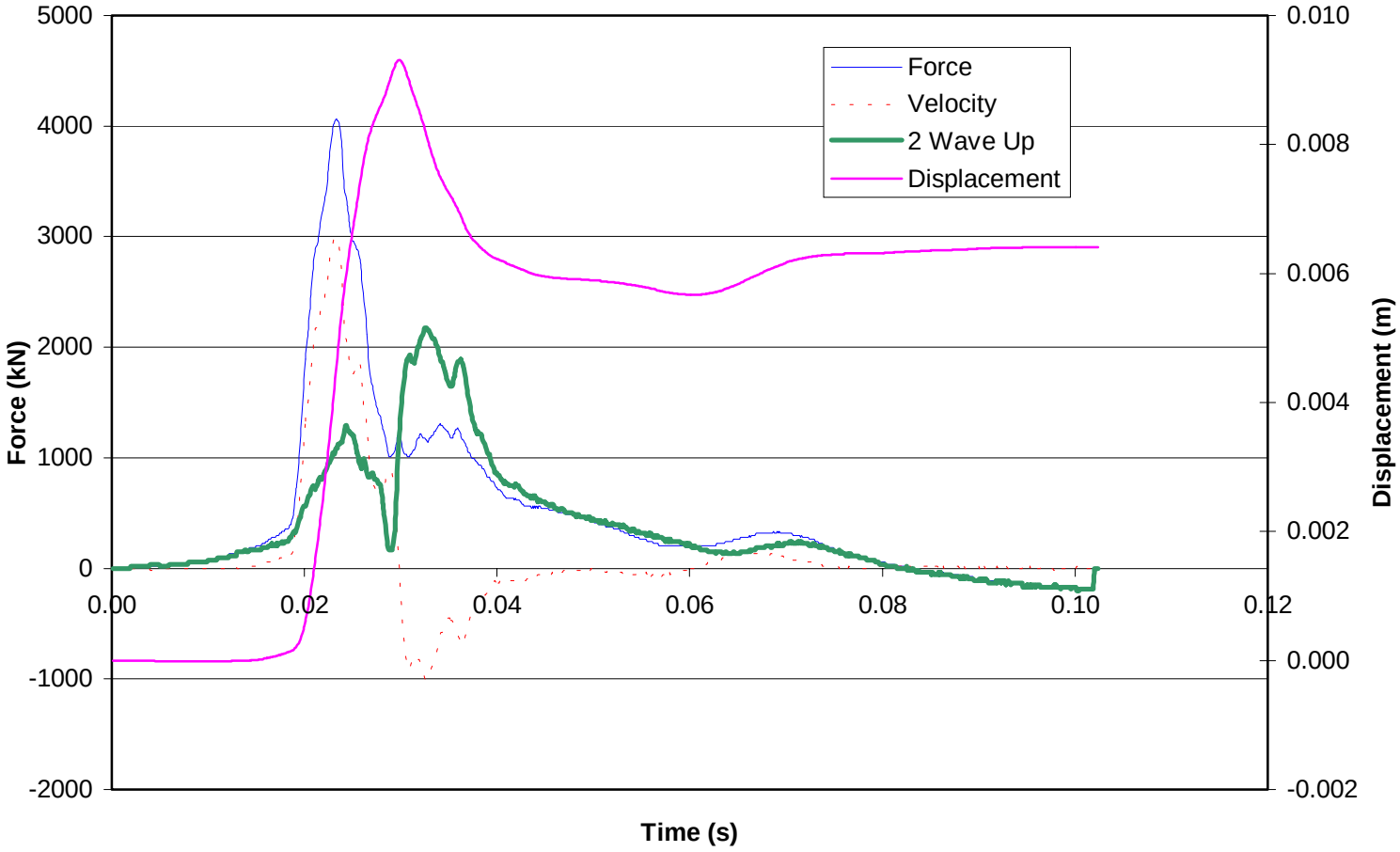

Figure I-22. Force, Velocity, Double Wave Up, and Displacement Traces for VLE-32C (Vilano East Bridge)

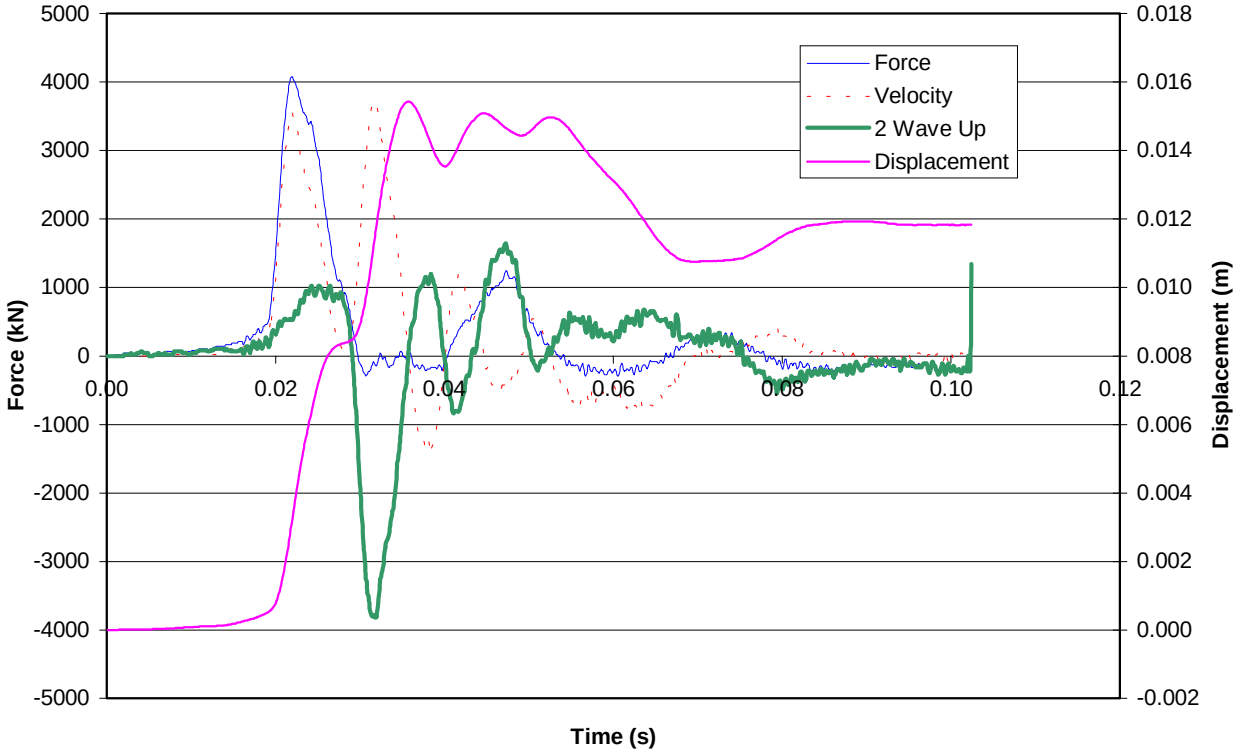

Figure I-23. Force, Velocity, Double Wave Up, and Displacement Traces for VLWA-61D (Vilano West Bridge)

APPENDIX J

OUTPUT FILE FOR SUGGESTED METHOD & GRL PROCEDURE (FORTRAN)

****

```
**********   FLORIDA DEPARTMENT OF TRANSPORTATION  **********
**********                                         **********
**********SUGGESTED METHOD FOR DETERMINE SKIN & TIP**********
**********       CAPACITIES / METHOD 1             **********
************************************************************


<<<<< PILE INFORMATION >>>>>

LENGTH    =        29.76 m
WAVESPEED =      4643.00 m/s
MODU      =  51750160.00 kN/m2
AREA      =          .42 m2
DT TIME   =       .00010 s

      TIME       VEL       FOR      ZVEL      DISP    2 WAVE UP
       (s)     (m/s)      (kN)      (kN)       (m)      (kN)

     .0001      .000      .000      .000    .00000      .000
     .0002      .000      .000      .000    .00000      .000
     .0003      .000      .000      .000    .00000      .000
     .0004      .000      .000      .000    .00000      .000
     .0005      .000      .000      .000    .00000      .000
     .0006      .000      .000      .000    .00000      .000
     .0007      .000      .000      .000    .00000      .000
     .0008      .000      .000      .000    .00000      .000
     .0009      .000      .000      .000    .00000      .000
     .0010      .000      .000      .000    .00000      .000
     .0011      .000      .000      .000    .00000      .000
     .0012      .000      .000      .000    .00000      .000
     .0013      .000      .000      .000    .00000      .000
     .0014      .000      .000      .000    .00000      .000
     .0015      .000      .000      .000    .00000      .000
     .0016      .000      .000      .000    .00000      .000
     .0017      .000      .000      .000    .00000      .000
     .0018      .000      .000      .000    .00000      .000
     .0019      .000      .000      .000    .00000      .000
     .0020      .000      .000      .000    .00000      .000
     .0021      .000      .000      .000    .00000      .000
     .0022      .000      .000      .000    .00000      .000
     .0023      .000      .000      .000    .00000      .000
     .0024      .000      .000      .000    .00000      .000
     .0025      .000      .000      .000    .00000      .000
     .0026      .000      .000      .000    .00000      .000
     .0027      .000      .000      .000    .00000      .000
     .0028      .000      .000      .000    .00000      .000
     .0029      .000      .000      .000    .00000      .000
     .0030      .000      .000      .000    .00000      .000
     .0031      .000      .000      .000    .00000      .000
     .0032      .000      .000      .000    .00000      .000
     .0033      .000      .000      .000    .00000      .000
     .0034      .000      .000      .000    .00000      .000
     .0035      .000      .000      .000    .00000      .000
     .0036      .000      .000      .000    .00000      .000
     .0037      .000      .000      .000    .00000      .000
     .0038      .000      .000      .000    .00000      .000
     .0039      .000      .000      .000    .00000      .000
```

.0040	.000	.000	.000	.00000	.000
.0041	.000	.000	.000	.00000	.000
.0042	.000	.000	.000	.00000	.000
.0043	.000	.000	.000	.00000	.000
.0044	.000	.000	.000	.00000	.000
.0045	.000	.000	.000	.00000	.000
.0046	.000	.000	.000	.00000	.000
.0047	.000	.000	.000	.00000	.000
.0048	.000	.000	.000	.00000	.000
.0049	.000	.000	.000	.00000	.000
.0050	.000	.000	.000	.00000	.000
.0051	.000	.000	.000	.00000	.000
.0052	.000	.000	.000	.00000	.000
.0053	.000	.000	.000	.00000	.000
.0054	.000	.000	.000	.00000	.000
.0055	.000	.000	.000	.00000	.000
.0056	.000	.000	.000	.00000	.000
.0057	.000	.000	.000	.00000	.000
.0058	.000	.000	.000	.00000	.000
.0059	.000	.000	.000	.00000	.000
.0060	.000	.000	.000	.00000	.000
.0061	.000	.000	.000	.00000	.000
.0062	.000	.000	.000	.00000	.000
.0063	.000	.000	.000	.00000	.000
.0064	.000	.000	.000	.00000	.000
.0065	.000	.000	.000	.00000	.000
.0066	.000	.000	.000	.00000	.000
.0067	.000	.000	.000	.00000	.000
.0068	.000	.000	.000	.00000	.000
.0069	.000	.000	.000	.00000	.000
.0070	.000	.000	.000	.00000	.000
.0071	.000	.000	.000	.00000	.000
.0072	.000	.000	.000	.00000	.000
.0073	.000	.000	.000	.00000	.000
.0074	.000	.000	.000	.00000	.000
.0075	.000	.000	.000	.00000	.000
.0076	.000	.000	.000	.00000	.000
.0077	.000	.000	.000	.00000	.000
.0078	.000	.000	.000	.00000	.000
.0079	.000	.000	.000	.00000	.000
.0080	.000	.000	.000	.00000	.000
.0081	.000	.000	.000	.00000	.000
.0082	.000	.000	.000	.00000	.000
.0083	.000	.000	.000	.00000	.000
.0084	.000	.000	.000	.00000	.000
.0085	.000	46.440	.000	.00000	46.440
.0086	.000	46.440	.000	.00000	46.440
.0087	.000	46.440	.000	.00000	46.440
.0088	.000	46.440	.000	.00000	46.440
.0089	.000	46.440	.000	.00000	46.440
.0090	.000	46.440	.000	.00000	46.440
.0091	.000	46.440	.000	.00000	46.440
.0092	.000	46.440	.000	.00000	46.440
.0093	.000	46.440	.000	.00000	46.440
.0094	.000	46.440	.000	.00000	46.440
.0095	.000	46.440	.000	.00000	46.440
.0096	.000	46.440	.000	.00000	46.440

.0097	.000	46.440	.000	.00000	46.440
.0098	.000	46.440	.000	.00000	46.440
.0099	.000	46.440	.000	.00000	46.440
.0100	.000	46.440	.000	.00000	46.440
.0101	.000	46.440	.000	.00000	46.440
.0102	.000	46.440	.000	.00000	46.440
.0103	.000	46.440	.000	.00000	46.440
.0104	.000	46.440	.000	.00000	46.440
.0105	.000	92.881	.000	.00000	92.881
.0106	.000	92.881	.000	.00000	92.881
.0107	.000	92.881	.000	.00000	92.881
.0108	.000	92.881	.000	.00000	92.881
.0109	.000	92.881	.000	.00000	92.881
.0110	.000	92.881	.000	.00000	92.881
.0111	.000	92.881	.000	.00000	92.881
.0112	.000	92.881	.000	.00000	92.881
.0113	.000	92.881	.000	.00000	92.881
.0114	.000	92.881	.000	.00000	92.881
.0115	.010	92.881	46.440	.00000	46.440
.0116	.010	92.881	46.440	.00000	46.440
.0117	.010	92.881	46.440	.00000	46.440
.0118	.010	92.881	46.440	.00000	46.440
.0119	.010	92.881	46.440	.00000	46.440
.0120	.010	92.881	46.440	.00001	46.440
.0121	.010	92.881	46.440	.00001	46.440
.0122	.010	92.881	46.440	.00001	46.440
.0123	.010	92.881	46.440	.00001	46.440
.0124	.010	92.881	46.440	.00001	46.440
.0125	.010	139.321	46.440	.00001	92.881
.0126	.010	139.321	46.440	.00001	92.881
.0127	.010	139.321	46.440	.00001	92.881
.0128	.010	139.321	46.440	.00001	92.881
.0129	.010	139.321	46.440	.00001	92.881
.0130	.010	139.321	46.440	.00002	92.881
.0131	.010	139.321	46.440	.00002	92.881
.0132	.010	139.321	46.440	.00002	92.881
.0133	.010	139.321	46.440	.00002	92.881
.0134	.010	139.321	46.440	.00002	92.881
.0135	.010	139.321	46.440	.00002	92.881
.0136	.010	139.321	46.440	.00002	92.881
.0137	.010	139.321	46.440	.00002	92.881
.0138	.010	139.321	46.440	.00002	92.881
.0139	.010	139.321	46.440	.00002	92.881
.0140	.010	139.321	46.440	.00003	92.881
.0141	.010	139.321	46.440	.00003	92.881
.0142	.010	139.321	46.440	.00003	92.881
.0143	.010	139.321	46.440	.00003	92.881
.0144	.010	139.321	46.440	.00003	92.881
.0145	.020	185.761	92.881	.00003	92.881
.0146	.020	185.761	92.881	.00003	92.881
.0147	.020	185.761	92.881	.00003	92.881
.0148	.020	185.761	92.881	.00004	92.881
.0149	.020	185.761	92.881	.00004	92.881
.0150	.020	185.761	92.881	.00004	92.881
.0151	.020	185.761	92.881	.00004	92.881
.0152	.020	185.761	92.881	.00004	92.881
.0153	.020	185.761	92.881	.00005	92.881

.0154	.020	185.761	92.881	.00005	92.881
.0155	.020	232.201	92.881	.00005	139.321
.0156	.020	232.201	92.881	.00005	139.321
.0157	.020	232.201	92.881	.00005	139.321
.0158	.020	232.201	92.881	.00006	139.321
.0159	.020	232.201	92.881	.00006	139.321
.0160	.020	232.201	92.881	.00006	139.321
.0161	.040	232.201	185.761	.00006	46.440
.0162	.030	232.201	139.321	.00007	92.881
.0163	.030	232.201	139.321	.00007	92.881
.0164	.030	232.201	139.321	.00007	92.881
.0165	.030	278.642	139.321	.00008	139.321
.0166	.030	278.642	139.321	.00008	139.321
.0167	.030	278.642	139.321	.00008	139.321
.0168	.030	278.642	139.321	.00009	139.321
.0169	.030	278.642	139.321	.00009	139.321
.0170	.030	278.642	139.321	.00009	139.321
.0171	.030	325.082	139.321	.00009	185.761
.0172	.030	325.082	139.321	.00010	185.761
.0173	.030	325.082	139.321	.00010	185.761
.0174	.040	325.082	185.761	.00010	139.321
.0175	.040	325.082	185.761	.00011	139.321
.0176	.040	325.082	185.761	.00011	139.321
.0177	.040	371.522	185.761	.00012	185.761
.0178	.040	371.522	185.761	.00012	185.761
.0179	.040	371.522	185.761	.00012	185.761
.0180	.040	371.522	185.761	.00013	185.761
.0181	.050	417.963	232.201	.00013	185.761
.0182	.040	417.963	185.761	.00014	232.201
.0183	.050	417.963	232.201	.00014	185.761
.0184	.050	464.403	232.201	.00015	232.201
.0185	.060	510.843	278.642	.00015	232.201
.0186	.070	557.283	325.082	.00016	232.201
.0187	.080	650.164	371.522	.00017	278.642
.0188	.100	743.044	464.403	.00017	278.642
.0189	.140	928.806	650.164	.00019	278.642
.0190	.150	1114.567	696.604	.00020	417.963
.0191	.200	1300.328	928.806	.00022	371.522
.0192	.230	1439.649	1068.126	.00024	371.522
.0193	.280	1671.850	1300.328	.00027	371.522
.0194	.310	1950.492	1439.649	.00030	510.843
.0195	.360	2182.693	1671.850	.00033	510.843
.0196	.420	2461.335	1950.492	.00037	510.843
.0197	.480	2832.857	2229.133	.00041	603.724
.0198	.530	3111.499	2461.335	.00046	650.164
.0199	.600	3436.581	2786.417	.00052	650.164
.0200	.640	3808.103	2972.178	.00058	835.925
.0201	.740	4179.625	3436.581	.00065	743.044
.0202	.800	4551.147	3715.222	.00073	835.925
.0203	.880	4829.789	4086.745	.00081	743.044
.0204	.920	5108.431	4272.506	.00090	835.925
.0205	.980	5340.632	4551.147	.00100	789.485
.0206	1.020	5526.393	4736.909	.00110	789.485
.0207	1.060	5712.154	4922.670	.00120	789.485
.1006	-.010	-278.642	-46.440	-.00013	-232.201
.1007	-.010	-278.642	-46.440	-.00013	-232.201
.1008	-.010	-278.642	-46.440	-.00013	-232.201

.1009	-.010	-278.642	-46.440	-.00013	-232.201
.1010	-.010	-325.082	-46.440	-.00013	-278.642
.1011	-.010	-278.642	-46.440	-.00013	-232.201
.1012	-.010	-325.082	-46.440	-.00013	-278.642
.1013	-.010	-278.642	-46.440	-.00013	-232.201
.1014	-.010	-325.082	-46.440	-.00013	-278.642
.1015	-.010	-278.642	-46.440	-.00013	-232.201
.1016	-.010	-325.082	-46.440	-.00014	-278.642
.1017	.000	-278.642	.000	-.00014	-278.642
.1018	.000	-325.082	.000	-.00014	-325.082
.1019	.000	-278.642	.000	-.00014	-278.642
.1020	-.010	-325.082	-46.440	-.00014	-278.642
.1021	-.010	-325.082	-46.440	-.00014	-278.642
.1022	-.010	-325.082	-46.440	-.00014	-278.642
.1023	-.010	-325.082	-46.440	-.00014	-278.642
.1024	-.010	-325.082	-46.440	-.00014	-278.642

MAX FORCE TIME (T1) = .02230 s
TIME AT 2L/c (T2) = .03512 s
SKIN TIME (T3) = .03320 s
FORCE STARTING TIME = .01870 s
RISE TIME = .00360 s
MAXIMUM FORCE = 8312.81 kN
MAXIMUM VELOCITY = 1.57 m/s

<<<<< SUGGESTED METHOD >>>>>

T/S RATIO = .327
J_c = .377
RST = 6618.246 kN = 1487.915 kips
SKINCAP = 4986.349 kN = 1121.032 kips
TIPCAP = 1631.896 kN = 366.883 kips
EQUIV DAMP= 1.391

***** METHOD 1 *****

METHOD 1 RATIO = 1.444
TOTAL CAPACITY = 9079.075 kN = 2041.159 kips
TOTAL TIP CAP = 5363.852 kN = 1205.902 kips
TOTAL SKIN CAP = 3715.222 kN = 835.257 kips